SYNTHESIS AND APPLICATIONS OF *β*- AND *MESO*-SUBSTITUTED PORPHYRINS

Ph.D. THESIS

by

RAVI KUMAR

DEPARMENT OF CHEMISTRY
INDIAN INSTITUTE OF TECHNOLOGY ROORKEE
ROORKEE-247 667 (INDIA)
JUNE, 2015

SYNTHESIS AND APPLICATIONS OF *β*- AND *MESO*-SUBSTITUTED PORPHYRINS

A THESIS

*Submitted in partial fulfilment of the
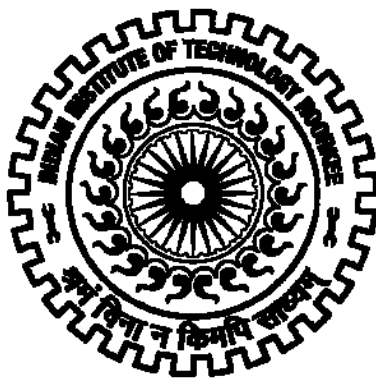requirements for the award of the degree
of*

DOCTOR OF PHILOSOPHY

in

Chemistry

by

RAVI KUMAR

**DEPARMENT OF CHEMISTRY
INDIAN INSTITUTE OF TECHNOLOGY ROORKEE
ROORKEE-247 667 (INDIA)
JUNE, 2015**

INDIAN INSTITUTE OF TECHNOLOGY ROORKEE
ROORKEE

CANDIDATE'S DECLARATION

I hereby certify that the work which is being presented in the thesis entitled **"SYNTHESIS AND APPLICATIONS OF *β*- AND *MESO*-SUBSTITUTED PORPHYRINS"** in partial fulfilment of the requirements for the award of the Degree of Doctor of Philosophy and submitted in the Department of Chemistry of the Indian Institute of Technology Roorkee, Roorkee is an authentic record of my own work carried out during a period from January, 2012 to June, 2015 under the supervision of Dr. M. Sankar, Assistant Professor, Department of Chemistry, Indian Institute of Technology Roorkee, Roorkee.

The matter presented in the thesis has not been submitted by me for the award of any other degree of this or any other Institute.

(Ravi Kumar)

This is to certify that the above statement made by the candidate is correct to the best of my knowledge.

Dated: **(Dr. M. Sankar)**

Supervisor

Dedicated

To

My Parents and Teachers

ACKNOWLEDGEMENTS

my abounding feelings to younger brother, Mr. Pawan Kumar for his constant support, encouragement and affection throughout my life.

The financial assistance provided by Ministry of Human Resourse Development (MHRD), New Delhi that made my research work very smooth and prompt, is greatfully acknowledged.

I am extremely thankful to those people, whose names have been unknowingly left, thank you very much for your prayers. It had really helped a lot. I apologize and believe that they will be always with me as they were during the times of need.

Last but not the least I feel privileged for my stay at IIT Roorkee and providing a great work culture and a wonderful ambience. I fare-a-diu to the prestigious Institute fully satisfied and take an oath to serve for the mankind of my nation and the whole world with whatever the knowledge and wisdom I possess and will acquire in future by virtue of furtherance of my research work and results thereof.

<div align="right">

Ravi Kumar

</div>

ABSTRACT

Substituted porphyrins have unique electronic and optical properties that empower their use as model compounds of biological importance and potential material applications. The advantage of using porphyrin ligands is that they are conformationally flexible and can adopt a range of nonplanar conformations needed for a variety of biological functions. The structural, spectral and electrochemical redox properties of porphyrins can be tuned by peripheral functionalization of porphyrin ring. Particularly, the *β*-functionalization of *meso*-tetraphenylporphyrins exerts much larger steric and electronic effects on the porphyrin π-system. Further, the substituted porphyrins with appropriate binding pockets have been the subject of intensive research to design anion receptors with high selectivity owing to their potential applications in environmental, clinical, chemical and biological sectors.

Meso- or *β*-Substituted 'push-pull' porphyrins have been utilised as sensitizers in porphyin-sensitised solar cells (PSSC) and photodynamic therapy (PDT), as chemosensors in anion sensing, as non-linear optical (NLO) material and as catalysts for oxidative transformation of organic substrates due to their outstanding properties such as strong absorption in visible region, flexible architectural modification to tailor physicochemical and optoelectronic parameters and high thermal and chemical stability. The thesis consists of eight different Chapters.

First Chapter 1 is introductory one which deals with the recent chemical literature on the *meso*- and *β*-pyrrole functionalised porphyrins and their potential applications in the arena of PSSC, PDT, NLO, anion sensing and catalysis.
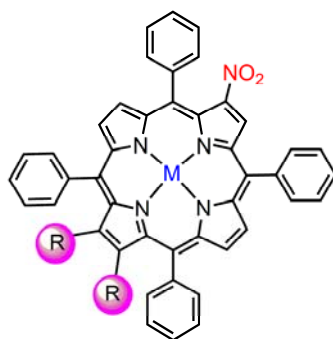
R = Br, Ph, CN, 2-Thienyl, ─═─Ph
M = 2H, Co(II), Ni(II), Cu(II)and Zn(II)
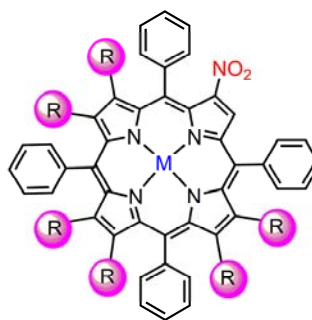
R = Br, Ph, 2-Thienyl, ─═─Ph
M = 2H, Co(II), Ni(II), Cu(II)and Zn(II)

Chapter 2 describes about the synthesis, characterization and tunable electrochemical redox properties of two new families of porphyrins with mixed substituent pattern viz. 2-nitro-12,13-disubstituted-*meso*-tetraphenylporphyrins (H$_2$TPP(NO$_2$)X$_2$, X = Ph, phenylethynyl (PE), 2-thienyl (Th), Br and CN) and 2-nitro-7,8,12,13,17,18-hexasubstituted-*meso*-tetraphenylporphyrins (H$_2$TPP(NO$_2$)X$_6$, X = Br, Ph, PE and Th) and their metal (Co(II), Ni(II), Cu(II) and Zn(II)) complexes. Remarkable red-shift in the Soret band (45 - 70 nm) and longest wavelength band, Q$_x$(0,0) (65 - 90 nm) are exhibited by H$_2$TPP(NO$_2$)X$_6$ as compared to H$_2$TPP(NO$_2$). The single crystal structures of MTPP(NO$_2$)X$_2$ (M = Zn(II) and Ni(II); X = Br, Ph and PE) showed quasi-planar conformation whereas H$_2$TPP(NO$_2$)Th$_2$ and NiTPP(NO$_2$)Br$_6$ exhibited moderate and highly nonplanar saddle shape conformations, respectively. The imino proton resonances of H$_2$TPP(NO$_2$)X$_6$ are significantly downfield shifted ($\Delta\delta$ = 1.10 - 1.80 ppm) relative to H$_2$TPP(NO$_2$). Mixed substituted highly nonplanarporphyrins exhibited higher protonation and deprotonation constants relative to H$_2$TPPX$_8$ (X = Cl and Br). The redox tunability was achieved by introducing electron donors (Ph and Th) and acceptor groups (PE, Br and CN) on MTPP(NO$_2$) back bone. The unusual variation in spectral and electrochemical redox properties of mixed substituted porphyrins are interpreted in terms of both an inductive and resonance interactions of susbtituents on porphyrin π-system as well as nonplanarity of the macrocycle.

R = H, NiTPP(CN)$_4$ (**1**)
R = ^{t}But, NiT(^{t}But-Ph)P(CN)$_4$ (**2**)
R = OMe, NiT(*p*-OMe-Ph)P(CN)$_4$ (**3**)

X = NO$_2$, NiTPP(NO$_2$)Cl$_7$ (**4**)
X = Cl, NiTPPCl$_8$ (**5**)
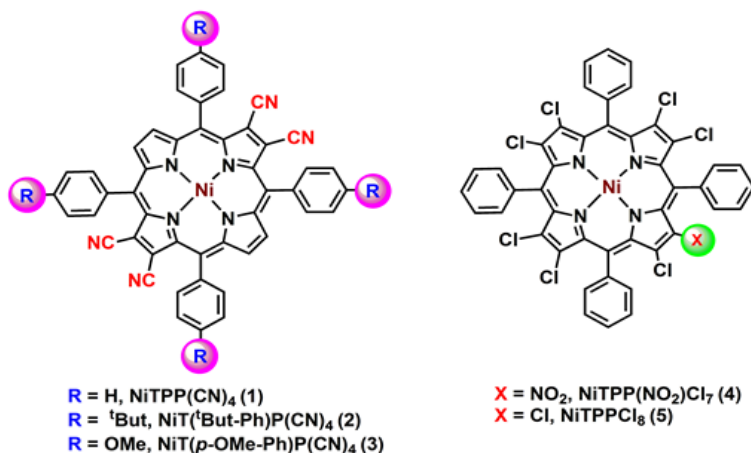
Chapter 3 deals with the synthesis of highly electron deficient β-substitutedNi(II) porphyrins (**1-5**) and their utilization asnovel sensors for selective rapid visual detection of CN⁻ions. This chapter describesthe single crystal X-ray structures, electronic spectraland electrochemical redox properties of these sensors. The ratiometric and

colorimetric responses of these porphyrins were monitored by change in optical absorption spectra. These sensors were found to be highly selective for cyanide ions with extremely high binding constants (10^{16}- 10^{8}M^{-2}) through axial ligation of CN$^-$ ions and are able to detect < 0.11 ppm of CN$^-$ ions. **1-5** were recovered from **1-5•2CN$^-$** adduct by acid treatment and reused without loss of their sensing ability. CN$^-$ binding strongly perturbs the redox properties of parent porphyrin π-system. The applicability of **1-5** as a practical visible colorimetric test kits for CN$^-$ ions in an aqueous and non-aqueous media have also been explored.Single crystal X-ray, spectroscopic studies and DFT calculations were used to establish the mode of binding of CN- ions to these sensors.

Chapter 4 considers the photophysical, electrochemical redox, solvatochromism and anion sensing properties exhibited by β-tetra and octa-phenylethynyl substituted *meso*-tetraphenyl- porphyrins and their metal complexes (Co(II), Ni(II), Cu(II) and Zn(II)). H$_2$TPP(PE)$_8$ exhibite

X = H, MTPP(PE)$_4$
X = PE, MTPP(PE)$_8$
M = 2H, Co(II), Cu(II), Ni(II), and Zn(II)

Charge Transfer in H$_2$TPP(PE)$_8$

Toluene DCM Dioxane THF Pyridine o-DCB DMF DMSO
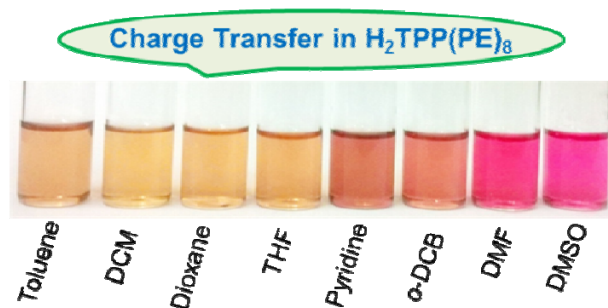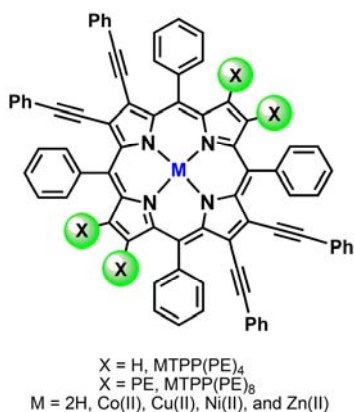
remarkable red shift in the Soret ($\Delta\lambda_{max}$= 92 nm) band and longest wavelength band, Q$_x$(0,0) ($\Delta\lambda_{max}$ = 117 nm), as compared to H$_2$TPP. Interestingly, MTPP(PE)$_8$ exhibited 450-500 mV anodic shift in first ring reduction potentials as compared to MTPP which is ascribed to electron accepting nature of phenylethynyl groups and extended π-conjugation whereas the first ring oxidation potentials remain unaltered. Free base and Zn(II) porphyrinsexhibits 10-20 times lower fluorescence quantum yields and 2-6 timeslower lifetime valuesthan that of MTPPs. These porphyrins display a strong solvatochromism as reflected by a large red-shift in their absorption and emission maxima upon increasing the solvent polarity. These porphyrins exhibited lower radiative

rate constants (k_r) and enhanced nonradiative rate constants (k_{nr}) as compared to MTPP. The decrement in fluorescenece lifetime values, quantum yields, radiative rate constants(k_r) and profound solvatochromism with enhanced nonradiative rate constants (k_{nr}) have been interpreted in terms of intramolecular charge transfer (ICT) from porphyrin core to phenyethynylmoities. Further, ZnTPP(PE)$_8$ was utilized for the colorimetric "naked-eye" detection of CN^-, F^-, Cl^-, Br^-, $H_2PO_4^-$ and CH_3COO^- ions through axial coordination of anionsto Zn(II) metal centre.The electron deficient nature of Zn(II) centre of ZnTPP(PE)$_n$ was established by axial ligation studies with anions in dichloromethane.

Chapter 5 deals with a novel series of 'push-pull' Zn(II) porphyrin dyes containing various electron donors such as pyrenyl, 2-thienyl, phenyl, 4′-bromophenyl and 4′-^{t}butylphenyl and 4′-carboxyphenyl acceptor moieties have been designed and synthesized (in two steps). Their optical absorption spectra, electrochemical redox and photovoltaic properties have been investigated in detail. The overall power conversion efficiencies (η) of DSSCs based on these dyes are in the range of 2.2 to 4.3% and highly dependent upon their donor moiety. The incorporation of 10,20-dimesityl groups is highly beneficial to prevent close π-π aggregation, thus favorably suppressing charge recombination and intermolecular interaction.
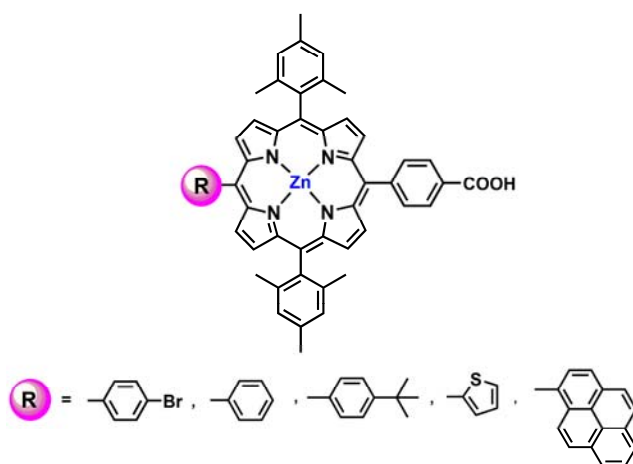
Among all, pyrenyl appended Zn(II) porphyrin has exhibited higher power conversion efficiencies of 4.3% under 1 sun illumination due to electron donating ability of pyrenyl moiety and extended π-conjugation.

Chapter 6 describes the synthesis and characterization of 2,3,7,8,12,13,17,18-octachloro-*meso*-tetraphenylporphyrinato oxovanadium(IV) (VOTPPCl$_8$). VOTPPCl$_8$ exhibited dramatic anodic shift 0.5 V in first ring reduction potential whereas 0.22 V anodic shift in first ring oxidation as compared to VOTPP indicating the electron deficient nonplanar conformation of the porphyrin core. We have optimized the catalytic conditions and found VOTPPCl$_8$ is more selective towards epoxidation with very high yield and turnover frequency (TOF) due to highly electron deficient nature and robust structure.

0.002 mol% VOTPPCl$_8$, 2 equiv. 30% H$_2$O$_2$

0.4 equiv. NaHCO$_3$, CH$_3$CN/H$_2$O, 60 °C, 0.5 h

Olefins

Epoxides

85 - 100% Conversion

100% Selectivity

VOTPPCl$_8$
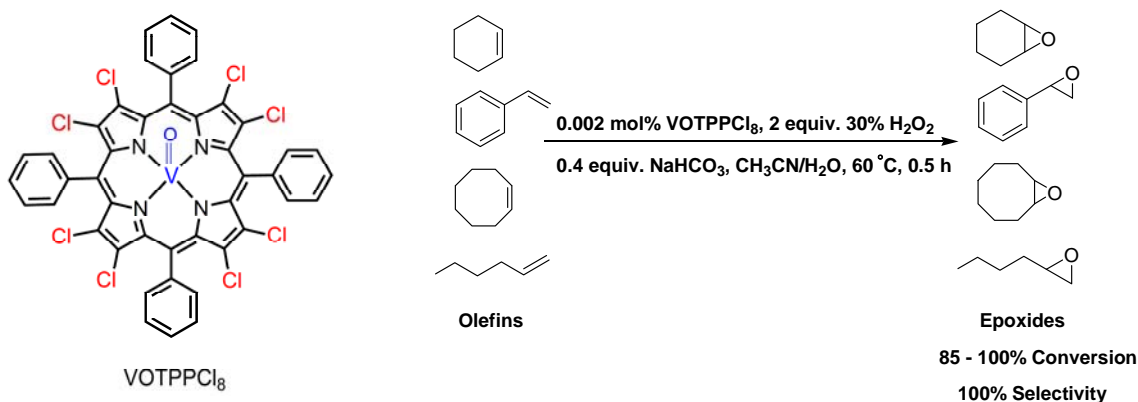
Chapter 7 considers the facile synthesis of *Meso-tetrakis*(4'-diethoxyphosphorylphenyl) porphyrin (H$_2$TPhPP) and its metal complexes MTPhPP (M = Cu(II), Ni(II) and Zn(II)) *via* modified Lindsey method with higher yield (50%) as compared to literature methods. H$_2$TPhPP exhibited 120-140 mV anodic shift in first ring redox potentials as compared to H$_2$TPP. Similarly, MTPhPP (M = Ni(II), Cu(II) and Zn(II)) exhibited 70-210 mV anodic shift in first ring oxidation potentials and 80-120 mV in first ring reduction potentials as compared to corresponding MTPPs due to strong electron withdrawing nature of diethoxyphosphoryl substituents.

PO(OEt)$_2$

(EtO)$_2$OP—

—PO(OEt)$_2$

PO(OEt)$_2$

M = 2H, H$_2$TPhPP   M = Cu(II), CuTPhPP
M = Ni(II), NiTPhPP   M = Zn(II), ZnTPhPP
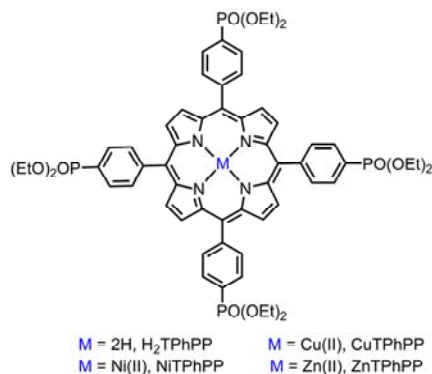
Chapter 8 summarizes the results and conclusions of the present study

LIST OF PAPERS
PUBLISHED/ACCEPTED/COMMUNICATED

1. **R. Kumar** and M. Sankar, "Synthesis, spectral and electrochemical studies of electronically tunable β-substituted porphyrins with mixed substituent pattern", *Inorg. Chem.* **2014**, *53*, 12706-12719.

2. **R. Kumar**, N. Chaudhri, and M. Sankar, "Ratiometric and colorimetric "naked eye" selective detection of CN^- ions by electron deficient Ni(II) porphyrins and their reversibility studies", *Dalton Trans.*, **2015**, *44*, 9149-9156.

3. **R. Kumar,** P. Yadav, A. Kumar and M. Sankar, "Facile synthesis and electrochemical studies of diethoxyphosphorylphenyl substituted porphyrin and its metal complexes", *Chem. Lett.*, **2015**, DOI: 10.1246/cl.150233.

4. **R. Kumar,** P. Yadav, P. Rathi and M. Sankar, "Photophysical, electrochemical redox, solvatochromism and anion sensing properties of β-tetra- and -octaphenylethynyl substituted *meso*-tetraphenylporphyrins" (*Revised and Submitted*).

5. **R. Kumar,** N. Choudhary, M. Sankar and M. R. Maurya, "Electron Deficient Nonplanar β-Octachlorovanadylporphyrin as Highly Efficient and Selective Epoxidation Catalyst for Olefins" (*Submitted for Publication*).

6. **R. Kumar**, V. Sudhakar Nesan, M. Sankar and K. Krishnamoorthy, "Simple Cost-effective *Trans*-A$_2$BC-porphyrins with Various Donor Groups for Dye-Sensitized Solar Cells" (*Manuscript under preparation*).

7. K. Praksh**, R. Kumar** and M. Sankar, "Mono- and Tri-β-Substituted Unsymmetrical Metalloporphyrins: Synthesis, Spectral and Electrochemical Properties**"** (*Submitted for Publication*).

PRESENTATION IN INTERNATIONAL/NATIONAL CONFERENCES

1. **R. Kumar**, N. Grover, N. Chaudhri, K. Praksh and M. Sankar, "Asymmetrically β-Substituted Porphyrins: Synthesis, Photophysical and Electrochemical Redox Properties"

oral presentation at the **227**[th] **Electrochemical Society (ECS) meeting** held at Chicago, USA during May 25-28, 2015.

2. **R. Kumar**, N. Grover and M. Sankar "Synthesis and Studies on β-Substituted Novel Push-Pull Porphyrins" oral presentation at the **8**[th] **International Conference on Porphyrins and Phthalocyanines (ICPP-8)** held at Istanbul, Turkey during June 22-27, 2014.

3. **R. Kumar,** N. Grover and M. Sankar, "Synthesis and Studies on β-Substituted Novel 'Push-Pull' Porphyrins for Nonlinear Optical (NLO) Applications" poster presentation at the **8**[th] **International Conference on Porphyrins and Phthalocyanines (ICPP-8**) held at Istanbul, Turkey during June 22-27, 2014.

4. **R. Kumar,** N. Chaudhri and M. Sankar "Selective Cyanide ion Detection by β-Substituted Electron Deficient Metalloporphyrins" poster presented at the **17**[th] **National Symposium in Chemistry organized by Chemical Research Society of India (CRSI),** February 6-8, 2015 at NCL, Pune.

5. **R. Kumar,** N. Chaudhri and M. Sankar "β-Substituted Porphyrins as Cyanide Sensors" presented at **Royal Society Chemistry (RSC) India Roadshow** held at IIT Delhi on 5th Nov 2014.

6. **R. Kumar** and M. Sankar, M. "Synthesis of β-substituted 'Push-pull' Porphyrins for Nonlinear Optical (NLO) Applications" poster presented at the 15th national symposium on **Modern Trends in Inorganic Chemistry (MTIC-XV),** December 13-16, 2013 at IIT Roorkee, India.

*****

TABLE OF CONTENTS

Title	Page No

List of schemes

List of Figures

addition of 2 equiv. of CN⁻ and 10 equiv of other anions.

List of Tables

CHAPTER 1

INTRODUCTION

Photodynamic Therapy (PDT)

Nonlinear Optical Applications (NLO)

Dye-Sensitized Solar Cells (DSSCs)

Sensors

Porphyrin

Sorbents

Catalysis

CHAPTER 1

INTRODUCTION

1.1 GENERAL INTRODUCTION TO TETRAPYRROLES

Tetrapyrroles contain four pyrrole rings which are joined together by methine carbons or methylene bridge to give cyclic tetrapyrrole ring system. They are vital for life, serving as pigments and cofactors in many biological functions. They are present throughout the biological kingdom from archaebacteria to plants and animals and participate in a broad spectrum of essential biological reactions [1-2]. They are highly colored and exhibit varying degrees of π-conjugation leading to different non-planar conformation of the tetrapyrrole macrocycle. The interior pyrrole nitrogens are positioned at the four corners of the square and are ideal for coordination to various metal ions. There are at least four different types of tetrapyrrole skeletons such as porphyrin, chlorin, corrin and methanocorphin are present in biological system (Figure 1.1). These tetrapyrrole skeletons in association with appropriate metal ions and suitable protein matrix serve as active sites in metalloproteins and bring about a variety of biological functions [3]. Some examples of metalloproteins bearing porphyrins are hemoglobin, myoglobin, cytochromes [1], chlorin in chlorophylls [4], corrin in vitamin B_{12} [5] and methanocorphin in coenzyme F_{430} [3]. The selective function of the metalloprotein is influenced by the choice of the skeleton, metal ion and the ligated fifth or sixth group to the core metal ion from the protein matrix. The protein matrix controls and regulates the active site structure and function of metalloprotein [1-5].

Heme-containing proteins are involved in oxygen transport (hemoglobin) and storage (myoglobin), electron transfer (cyctochromes), respiration and detoxification of reactive oxygen species (various oxidases, peroxidases and catalases), nitrogen fixation (nitrogenase) and protection mechanism against xenobiotics (cyctochrome P450 enzymes). In photosynthesis, chlorophyll plays a crucial role in the conversion of light energy to chemical energy. B_{12} coenzymes act as cofactors in a series of essential enzymatic reactions (e.g. methyl transfer) related to nucleic acid, protein and lipid synthesis. Coenzyme F_{430} is involved in the production of methane in methanogenic bacteria.
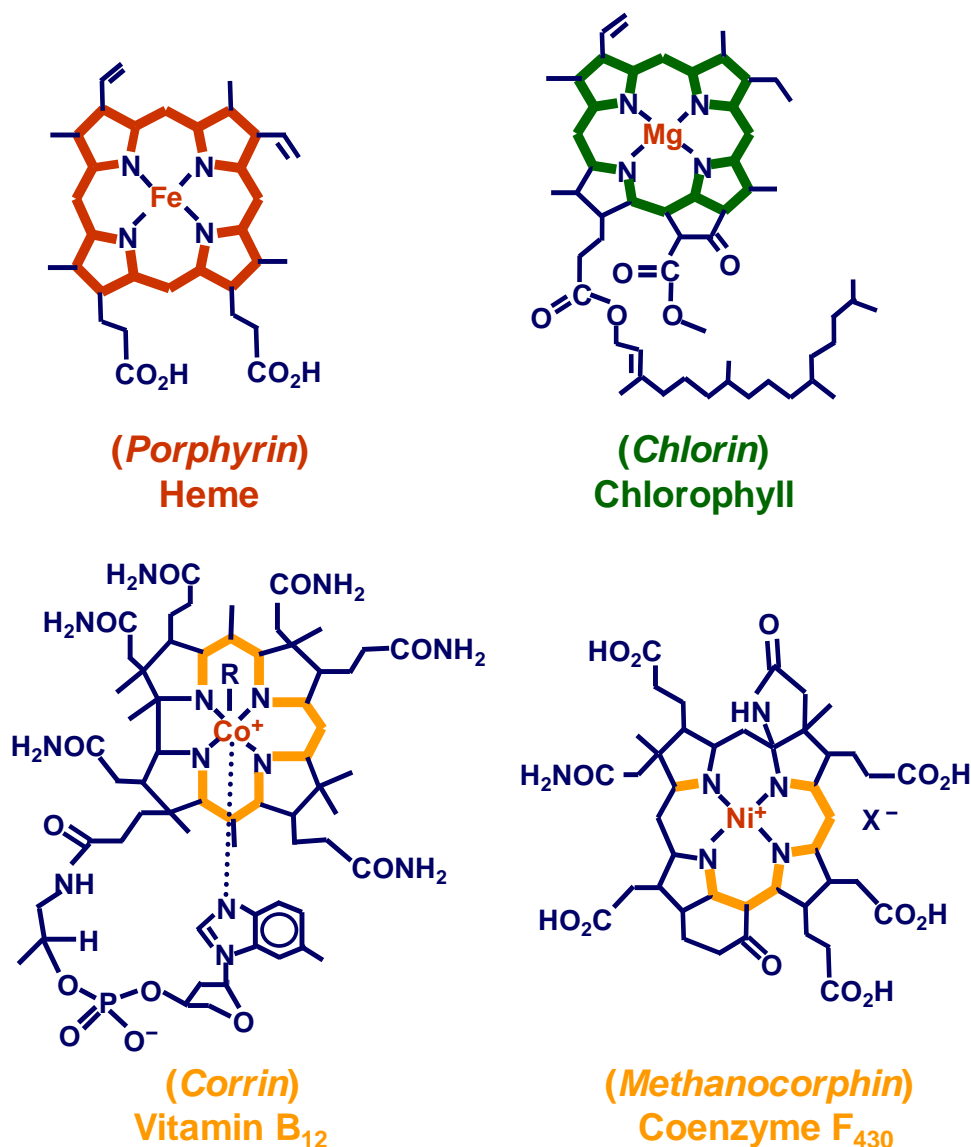
Figure 1. Chemical structures of various tetrapyrroles found in nature. Heavy lines denote π-bonds/conjugated π-bonds.

1.2 SYNTHETIC ANALOGUES OF TETRAPYRROLES

The diverse functions of tetrapyrroles prompted the laboratory synthesis of porphyrinoids (i.e. porphyrins and their analogues) [6]. Naturally occurring porphyrinoids bear only substituents at the β-pyrrole positions and devoid of *meso*-positions as shown in Figure 1.1. Among the synthesized porphyrins, 5,10,15,10-tetraphenylporphyrin, H_2TPP (Figure 1.2) and its metal complexes were studied extensively due to their ease of synthesis and facile functionalization.

3

Further, they are potential precursors for *β*- and/or *meso*-phenyl functionalized porphyrins since these positions are available for substitution. Functionalized porphyrins are useful biomimetic model compounds and also exhibit interesting physicochemical properties. In the late 1970's Dolphin has edited a series of volumes entitled "*The Porphyrins*" on the synthesis, mechanism and properties of wide range of tetrapyrrole pigments [7]. In these volumes, the individual aspects of tetrapyrrole pigments are described in detail. In the early 2000's, Kadish, Smith and Guilard have edited 20 volumes of "*The Porphyrin Handbook*" on various aspects of tetrapyrrole pigments [8]. Recently, the same editors have edited 35 volumes of "*Handbook of Porphyrin Science*" with applications of tetrapyrroles to chemistry, material science, biology, physics, medicine and engineering with updated literature [9]. The advantage of using porphyrin ligands is that they are conformationally flexible and can adopt a range of nonplanar conformations needed for a variety of biological functions [10-12]. In this introductory chapter, a review of porphyrin literature on the *meso*-phenyl and *β*-pyrrole functionalized porphyrins and their utilization in dye-sensitized solar cells (DSSCs), catalysis, photodynamic therapy (PDT), anion sensing and nonlinear optics have been discussed.
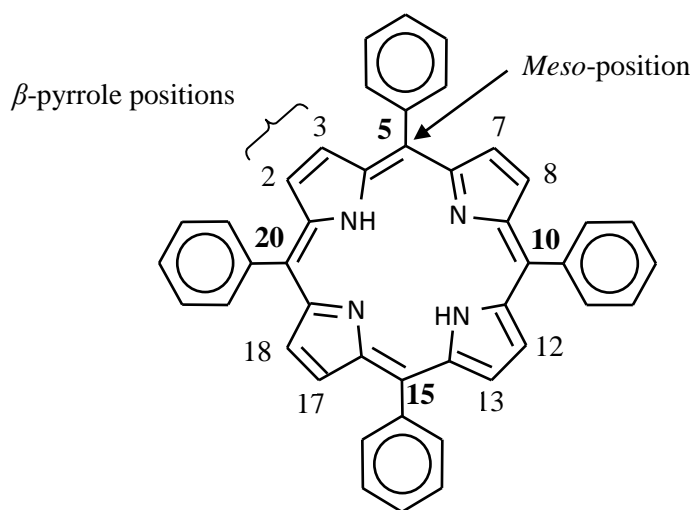
Figure 2 Molecular Structure and numbering scheme for H_2TPP.

1.3 PORPHYRINS FOR DSSC APPLICATIONS

Development of a sustainable society and growing global energy consumption demand clean and renewable energy resources. Several environmental issues aroused by large consumption of

fossil fuel. Artificial photosynthesis and photovoltaic technologies are desirable to harvest substantially inexhaustible solar energy. Dye-sensitized solar cells (DSSCs), [13-19] have proven their potentials as feasible energy device for solar energy conversion and are having following advantages such as low cost, easy production, flexibility, and transparency relative to traditional silicon solar cells. **The sensitizer is a crucial element in DSSC, exerting significant influence on the power conversion efficiency as well as the stability of the devices. They should be panchromatic and robust in terms of chemical as well as photochemical stability**.

(a)   (b)
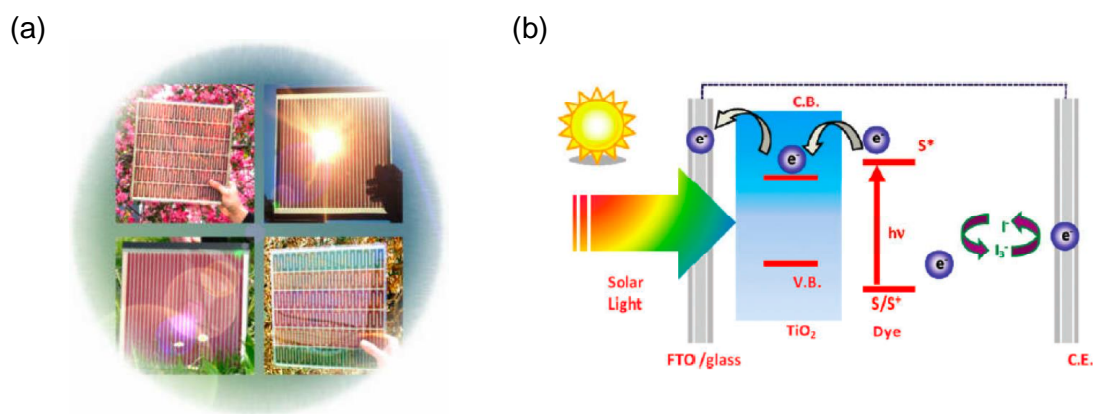
Figure 3. (a) A selection of dye-sensitized solar cells (DSSCs). (b) Schematic representation of the fundamental processes in DSSC.

1.3.1 The Working Principle of DSSC:

Figure 1.3a represents a set of dye-sensitized solar cells (DSSCs). The TiO_2 or SnO_2 coated conducting films (anode), photosensitizer (dye), I^-/I_3^- (Iodide/triiodide) electrolyte and Pt counter electrode (cathode) are the important components of DSSC. The COOH group is essential to attach a dye on the TiO_2 or SnO_2 surface *via* chemisorption process. The schematic representation of the electron transfer pathway is shown in Figure 1.3b. Dye should have lower excited-state oxidation potentials to perform fast electron transfer (electron injection) to conduction band of TiO_2 or SnO_2 surface resulting charge in separation (dye radical cation $(dye^{+\bullet})$ and a negative charge within in the Titania or SnO_2 phase) in pico- to femtoseconds $(10^{-12}$ to 10^{-15} s) time-scale. The injected electrons diffuse through the nano-network of particles until they reaches electrically conductive surface for current collection. The electric charge thus extracted from photoanode as current can be utilized to provide useful electric power. The oxidized dye $(dye^{+\bullet}$ is then reduced rapidly (within nanoseconds) by iodide anion present in the

electrolyte system. In order to close the electric circuit, the negative charges are directed to the surface of a counter electrode (C.E) where I_3^- is reduced to I^-. **Thus no net chemical reaction occurs within DSSC**. The DSSC operation is much closer to photosynthetic processes.

In DSSCs, polypyridyl ruthenium complexes [20-23] have been utilized to achieve electric power conversion efficiency (η) up to 11% due to their broad absorption spectrum through metal-to-ligand charge transfer (MLCT), the longer exciton lifetime, and their long-term chemical stability [20-23]. Despite their overwhelming performance, Ru-polypyridyl sensitizers encounter several drawbacks such as the high cost of noble metal ruthenium, the requirement for careful synthesis, hefty purification steps, toxicity to environment and low molar extinction coefficients in the red region of visible spectrum which hampers their large-scale applications [20,21]. Organic dyes such as coumarin, indoline, oligoene, thiophene, triarylamine, perylene, cyanine, fluorine, merocyanine and hemicyanine derivatives are of great interest owing to their modest cost, ease of synthesis and structural modification, large molar absorption coefficients, and satisfactory stability [24-28]. Some organic dyes with the conversion efficiencies in a range of 5-9% have been prepared. Most of the organic dyes don't absorb longer wavelength (red and NIR region) which limit their wide applications.

YD2-*o*-C8 **Y123**
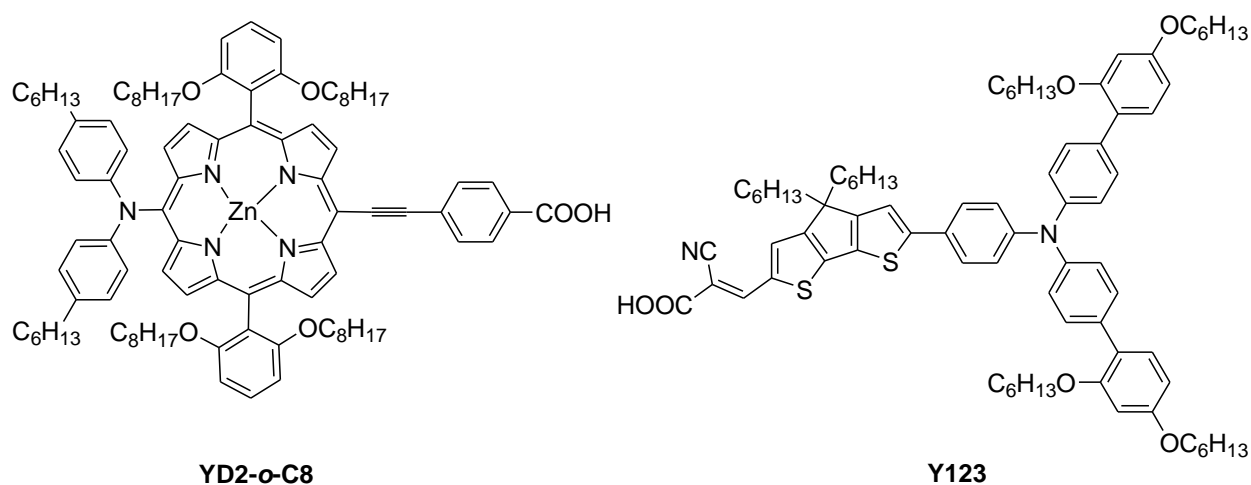
Figure 4 Porphyrin dye with co-sensitizer showing photon-to-current efficiency of 12.3%.

Recently reported porphyrins and phthalocyanine dyes are the best due to their high thermal and photochemical stability, strong absorption in visible region as well as their optical, photophysical and electrochemical properties can be tuned by peripheral substitutions [13-19,29-31]. The most efficient porphyrin sensitizer features push–pull D–π–A structures and/or π-extensions that make

porphyrins panchromatic in visible and even near-infrared regions. Consequently, porphyrin sensitizers have exhibited power conversion efficiencies that are comparable to or even higher than those of well-established highly efficient DSSCs based on ruthenium complexes. The synthetic flexibility of D–π–A dyes has enabled the engineering of enhanced compatibility toward these alternative redox couples by introducing steric bulk into the donor component and π-system, minimizing the unfavourable recombination between the electrolyte and the TiO_2 surface. For example, remarkable power conversion efficiency (η) of 12.3%, was achieved by zinc porphyrin sensitizer (YD2-*o*-C8) co-sensitized with an organic dye (Y123) using a cobalt-based electrolyte which is superior to those based on Ru complexes [32]. Recently, a class of push–pull porphyrins with an electron-donating diarylamino group and an electron-withdrawing carboxyphenylethynyl anchoring group, **GY50** and **SM315** (Figure 1.5) have revealed remarkably high efficiencies of 12% and 13% with cobalt electrolyte under standard one sun illumination [33].
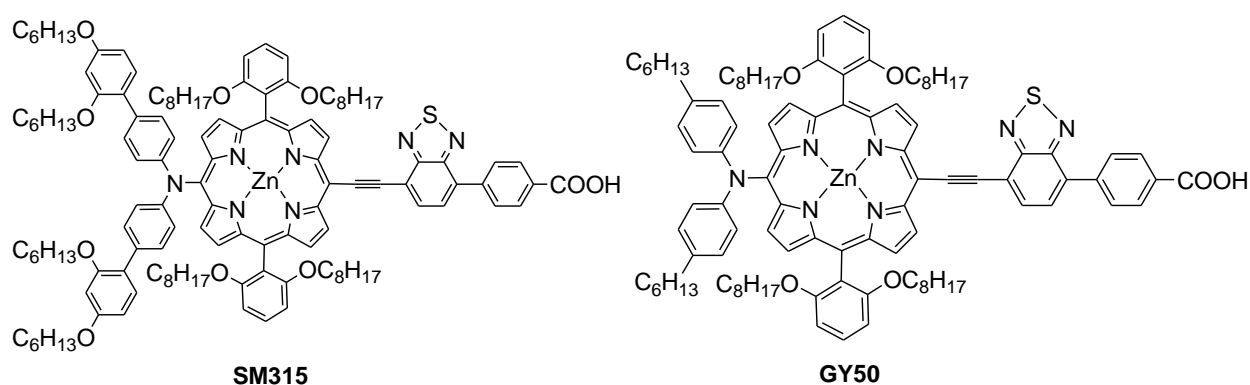
Figure 5 Highly efficient porphyrin sensitizers with reported efficiency of approx. 13%.

These results were the outcome of fine tuning of the HOMO-LUMO levels and the intrinsic intense absorption bands of porphyrin π-system with extended conjugation. Thus, it can be safely believed that these porphyrinic dyes will shape the future for highly efficient DSSCs.

1.4 PORPHYRINS AS ANION SENSORS

Porphyrins are having rich spectroscopic and electrochemical redox properties which can be utilized for anion sensing application. The design of anion host containing responsive functional group(s) as an integral part of host macrocyclic framework is an active area of research [34-37].

Recently, there is a quest to develop methods for selective anion detection, extraction and transportation which will be applied for environmental monitoring. In order to achieve an enhanced sensitivity and selectivity towards a particular anion, a fine tuning of binding sites is mandatory which is often difficult due to their wide range of geometries, high solvation energies, larger size and accessibility in a very narrow pH range as compared to their cationic counterparts.

CN^- is extremely toxic to living organisms, it binds strongly to iron center in heme and the active site of cytochrome c which completely stops the O_2 transport in the blood and the mitochondrial electron transport chain, thus inhibiting cellular respiration [38]. The selective recognition of F^- ions is of great importance for monitoring F^- ion metabolism in nature, the analysis of drinking water and in the treatment of osteoporosis [39,40]. Phosphate ions are playing a crucial role in biological processes such as signaling, energy transduction, information storage and expression [41]. The OAc^- ions are the most common building blocks in biosynthesis and a critical component of various metabolic processes. The rate of OAc^- production and oxidation has been often used an indicator of organic decomposition in marine sediments [42].

Calixpyrroles [43-46], phlorins [47], corroles [48,49], sapphyrins [50,51], N-confused porphyrins [52,53], oxoporphyrinogens [54,55] and porphyrins [56] are excellent multifunctional candidates for a great variety of anion sensor applications *via* N-H groups of the pyrrole units through hydrogen bonding interactions. Several porphyrins bearing N-H groups at the *ortho*-positions of the *meso*-aryl substituents have been utilized as effective anion sensors [57,58]. Recently, porphyrins bearing NH groups at the *para*-positions of the *meso*-phenyl ring have been demonstrated for $H_2PO_4^-$ ion sensing [59].

Notably, metalloporphyrinoids have been utilized for the detection of CN^- ions due to intrinsic affinity of cyanide for many metals such as zinc [60-64] rhodium [65], and copper [66] coordinated to porphyrins. Recently, cyanide sensing through chemodosimetric method by a new calix[4]pyrrole derivative [67], Pd-calixphyrin [68], cobalt corrins [69-71], and subphthalocyanine dye [72] have been reported in literature. In all cases, cyanide binds irreversibly to porphyrinoids. Even though they achieved selectivity for cyanide ions but extremely lower detection limits (in ppm or ppb range) and recyclability of the sensor after

detection is questionable. Hence the synthesis of highly selective and recyclable cyanide sensors is still challenging.

Chemodosimeters

(a)   (b)   (c)

R = H, COOH

Chemosensors

(d)   (e)

6-MET: M = 2H, R = S-MET
6-PEG$_{1000}$: M = 2H, R = S-PEG$_{1000}$

6Zn-PEG$_{1000}$: M = Zn(II), R = S-PEG$_{1000}$

6Pt-MET: M = Pt(II), R = S-MET
6Pt-PEG$_{1000}$: M = Pt(II), R =S-PEG$_{1000}$

6Ga-MET: M = Ga(III)Cl, R = S-MET
6Ga-PEG$_{1000}$: M = Ga(III)Cl, R =S-PEG$_{1000}$

With S-MET =

S-PEG$_{1000}$ =
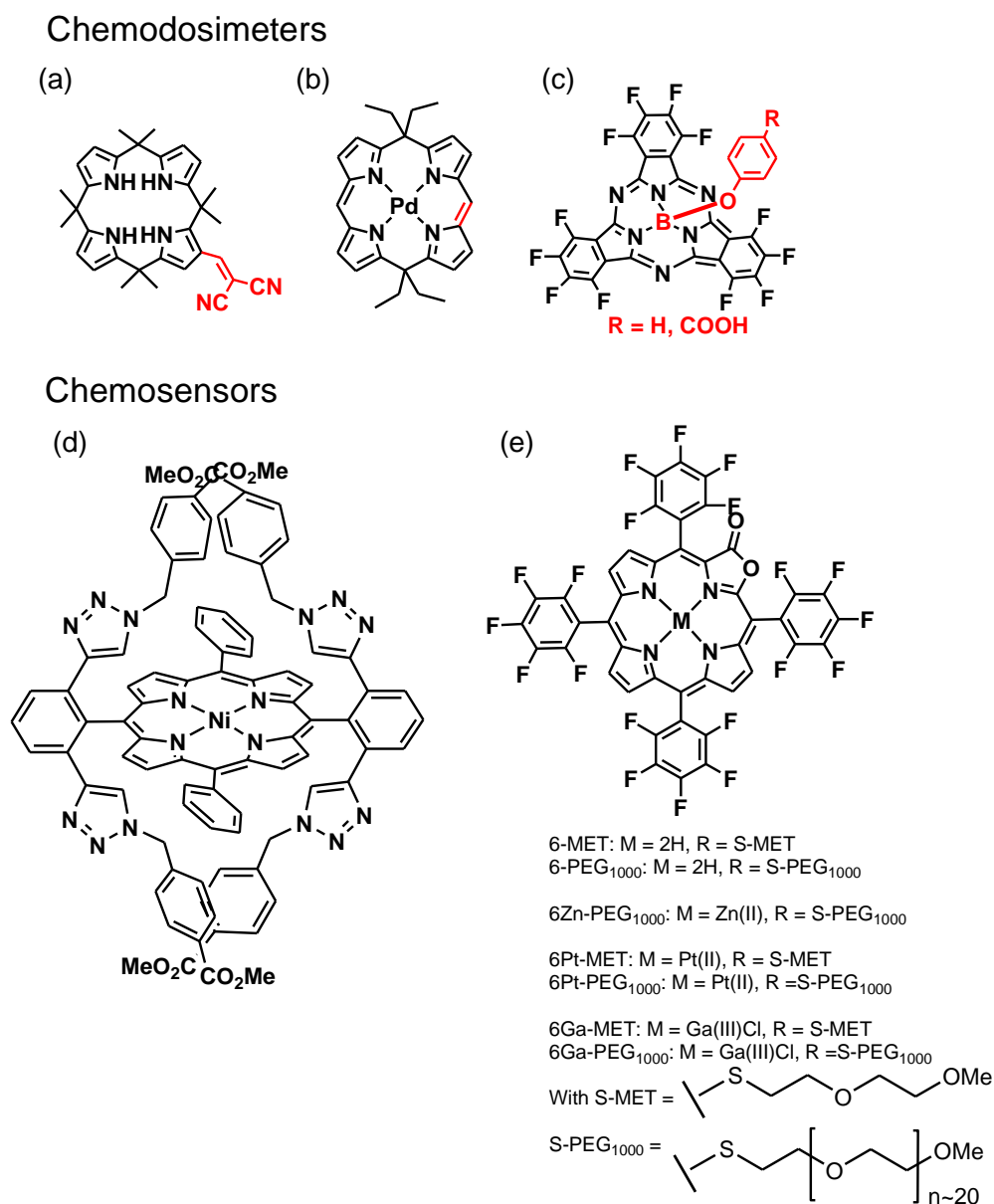
Figure 6. Molecular Structures of chemodosimeters and chemosensors for cyanide ions.

1.5 METALLOPORPHYRINS AS CATALYSTS

The active center of the cytochromes is having *heme* group. It consists of porphyrin ring chelated to the iron atom. Cyctochrome P-450 enzyme catalyses the oxidation of harmful organic substrates into water-soluble products [73-75]. These water-soluble products are excreted

through urine. Superoxide dismutase, catalase and peroxidase are enzymes that are involved in H_2O_2 metabolism. They are also involved in detoxification of harmful reactive species into water-soluble products. Inspired from the nature, researchers have synthesized several metalloporphyrin derivatives as efficient catalysts for oxidation reactions [73-84]. Iron and manganese porphyrin complexes were widely utilized as effective homogenous catalysts for such oxygenation reactions in last few decades. These porphyrins have shown very high turnover numbers (TON) with good yields [79]. It is proven that these metalloporphyrins form high valent metaloxo species which is the active intermediate and react with organic substrates and transfers oxygen to substrates. Also the sterically hindered electron deficient perhaloporphyrins and pernitroporphyrins (Figure 1.7) are found to be highly efficient robust catalysts [79,81]. In these porphyrins, oxidative degradation through bimolecular attack is prevented due to steric hindrance provided by *β*-pyrrole substituents and electron deficient nature of porphyrin π-system increases stability.

R = Pentafluorophenyl, Mesityl, Phenyl, 2,6-Dichlorophenyl

M = Mn(III)Cl, Fe(III)Cl
R = 2,6-Dichlorophenyl
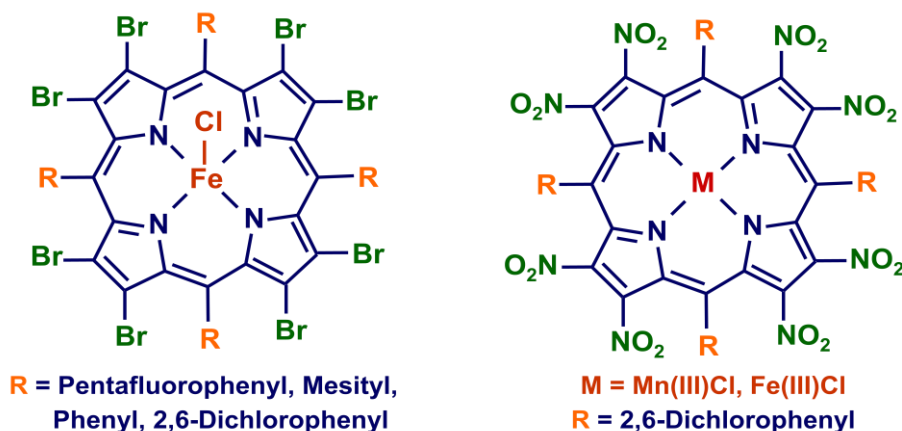
Figure 7 Highly efficient sterically hindered metalloporphyin catalysts.

Oxidation of olefins to epoxy compounds has always been an interesting area of research for the chemists owing to their great importance in the production of highly valued commodity chemicals such as polyurethanes, unsaturated resins, glycols, surfactants, and other products [85]. Metalloporphyrins have been found to be efficient catalysts for various oxidation reactions using variety of oxygen atom donors [73-84]. The major drawbacks of homogenous MTPP-based catalysts are the macrocyclic ring is liable for oxidative self-destruction, aggregation of metalloporphyrins through π-π interactions and poor product selectivity. Recently, highly efficient and stable Mn[III]-porphyrinic framework (MOF) was demonstrated for selective

epoxidation of olefins in quantitative yield in heterogeneous media [86-88]. The great advantage of these MOF catalysts is that the catalyst can be recovered by simple filtration or centrifugation and reused for several cycles.

1.6 PORPHYRIN SENSITIZERS IN PHOTODYNAMIC THERAPHY

Nowadays people are getting cancer disease very easily due to the gene mutation by various exposures such as toxic chemical vapors, ionizing radiation or by natural mutation which occurs in our body, but always our immune system works effectively to destroy these mutant cells to avoid their adverse effects. In some cases, these mutant cells survive by overcoming the immune system and divide uncontrollably and form tumor which undergo metastasis by which it spreads to other parts of the body. Many methods such as radiation therapy, chemotherapy and hypothermia were followed to treat cancer by which healthy cells also get destroyed due to these non-selective harsh treatments. Recently, photodynamic therapy (PDT) has been developed to treat this efficiently to avoid healthy cell damage by targeting selectively cancerous cells.

Figure 8. Photodynamic therapy (PDT) is given to a patient (Pictorial representation).

Photodynamic therapy is a medicinal treatment which employs the combination of light and drug as shown in Figure 1.8. This therapy is used for the treatment of cancer. Recently, many porphyrin derivatives were utilized in photodynamic therapy. Preferably, porphyrin should have absorbance in the range of 750-900 nm (therapeutic window). Herein, porphyrin molecule absorbs light energy and goes into the excited state from where this molecule goes in to the triplet state through intersystem crossing (ISC). From triplet state, porphryin will come back to the ground state by transferring its energy to the oxygen molecule. By this energy, O_2 molecule changes its spin from triplet state to singlet state. In singlet state, O_2 is highly reactive and it causes the death of tumor. This is called type II mechanism. Apart from energy transfer, the electron transfer also can occur (type I mechanism) which leads to the formation of radicals and radical ions, after the interaction with oxygen, can produce oxygenated products such as superoxide ion, O_2^- which will destroy cancer cells.
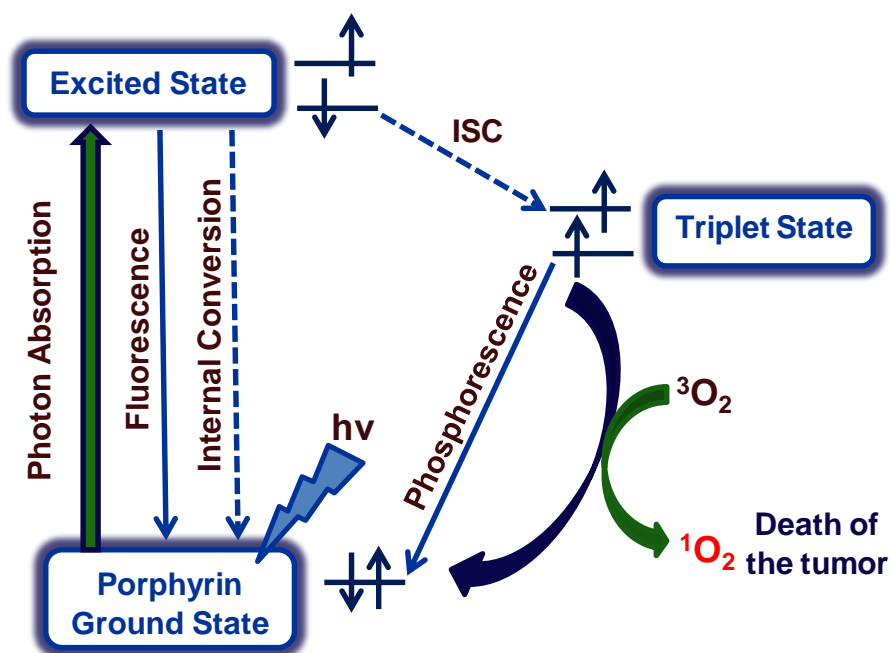
Figure 9 Representation of photophysical processes occur in photodynamic therapy (PDT).

The advantages of using porphyrin derivatives as sensitizers are: (i) there is no long-term side effect, (ii) highly specific (iii) short exposure time, (iv) unlike radiation therapy, it can be repeated many times, (v) little or no-scarring after operation, (vi) highly cheap as compared other methods.

There are only two drawbacks: (i) This PDT treatment is only applicable to areas where light can reach. This problem can be solved using laser guided surgery by endoscopic method. (ii) The common drugs being currently employed leave people very sensitive to light for some time. So they should not expose to light for some days. PDT can't be used to people who have certain blood diseases (e.g. *porphyrias* (a rare group of diseases that affect the skin or nervous system) or people who are allergic to porphyrins).
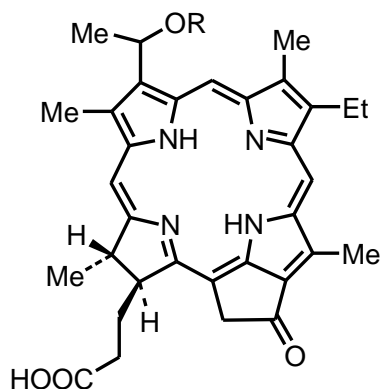
Figure 10. Chemical structure of photochlor (effective PDT drug) reported by Pandey *et al*.

Dolphin *et al* are the pioneer to work on porphyrin derivatives for PDT applications [89]. Recently, Pandey *et al.* have reported the application of pyropheophorbide-a derivatives (HPPH) or photochlor for PDT applications [90-93]. Dougherty *et al*. have carried the pharmacokinetics studies of photofrin and photochlor [94]. HPPHs are derived from chlorophyll-a and are excellent PDT agent with limited skin phototoxicity. At present, it is in advanced clinical trials for various indications such as lung, esophagus, including Barrett's and head and neck cancer. The clinical results are very promising as compared to commercially available Photofrin or Foscan. Actually, none of the patients treated with phorochlor showed any significant long-term skin phototoxicity. The animal and human clinical data of photochlor-PDT shows its enormous potential in treating certain types of cancers. Recently, Kumar *et al* reported the triazole-linked cationic porphyrins-carboline conjugate as potential agent for cancer treatment with very high phototoxicity [95]. Further, Král *et al* have reported porphyrin-pentamethinium conjugate for PDT applications [96].

1.7 PORPHYRINS IN NLO MATERIAL APPLICATIONS

Nonlinear optical materials are essential in modern photonic technologies. They are used to fabricate optoelectronic sensors, optical switches and connectors, components of telecommunication systems and computer, new high-density information-storage devices, and image processing systems. A lot of effort is being expended to develop modern photonic devices based on organic compounds including porphyrins with considerable nonlinear optical (NLO) properties [97-118]. Among all, Senge *et al.* and Therien *et al.* have reported wide variety of unsymmetrical 'push-pull' porphyrins for NLO applications [97,99,103-106].

NLO deals mainly with various new optical effects and phenomena that arise from the interactions of intense coherent radiation with matter. In general, the nonlinearity is only observed at very high light intensities, e.g. radiation using lasers. The optical properties of a medium are defined by the optical susceptibility (χ) which is related to the refractive index (η) and the dielectric constant (ε) [97].

The molecular polarization is given by

$$\mathbf{P} = \alpha\mathbf{E} + \beta\mathbf{EE} + \gamma\mathbf{EEE}$$

where α is the linear polarizability, β is the quadratic or second order hyperpolarizability and γ is the cubic hyperpolarizability and E is the applied electric field.

When a molecule is subjected to an intense electric field by laser pulse, the 2nd and 3rd terms become important, which are neglected otherwise and the NLO behavior can be observed [97].

Pioneer work on 'push-pull' porphyrins was developed by Suslick *et al.* using aminophenyl donors and nitrophenyl acceptors [98]. Later Krishnan *et al.* have reported functionalized fluoroaryl porphyrins bearing a β-nitro group and *N,N*-dimethylamino moieties (**1**) (at the *para* positions of *meso*-aryl groups) [115]. In 2005, Mussini *et al.* have reported some pseudo-linear chromophores based on TPP core [116]. Actually, 2-nitroporphyrins can be prepared easily using Menke reaction conditions using $Cu(NO_3)_2$ in presence of acetic acid and acetic anhydride. Further, 2-cyanoporphyrin (**3a**) also was used for NLO study which was prepared from 2-bromoporphyrin by reacting with CuCN. Sonogashira coupling of copper 2-bromoporphyrin with 4-nitrophenylacetylene followed by demetallation afforded the corresponding free base

(a)

(c)

1a R^1 = H, R^2 = F
1b R^1 = H, R^2 = NMe$_2$
1c R^1 = NO$_2$, R^2 = F
1d R^1 = NO$_2$, R^2 = NMe$_2$

(b)

M = 2H, Cu(II), Zn(II)
2a R = H, MTPP(CHO)
2b R = Br, MTPP(CHO)Br$_2$
2c R = 2-Thienyl, MTPP(CHO)(2-Thienyl)$_2$
2d R = Ph, MTPP(CHO)(Ph)$_2$
2e R = PE, MTPP(CHO)(PE)$_2$

3a R = CN

3b R = NO$_2$

3c R =

3d R =

3e R =

3d R =

3e R =

3f R =

3g R =

3h R =
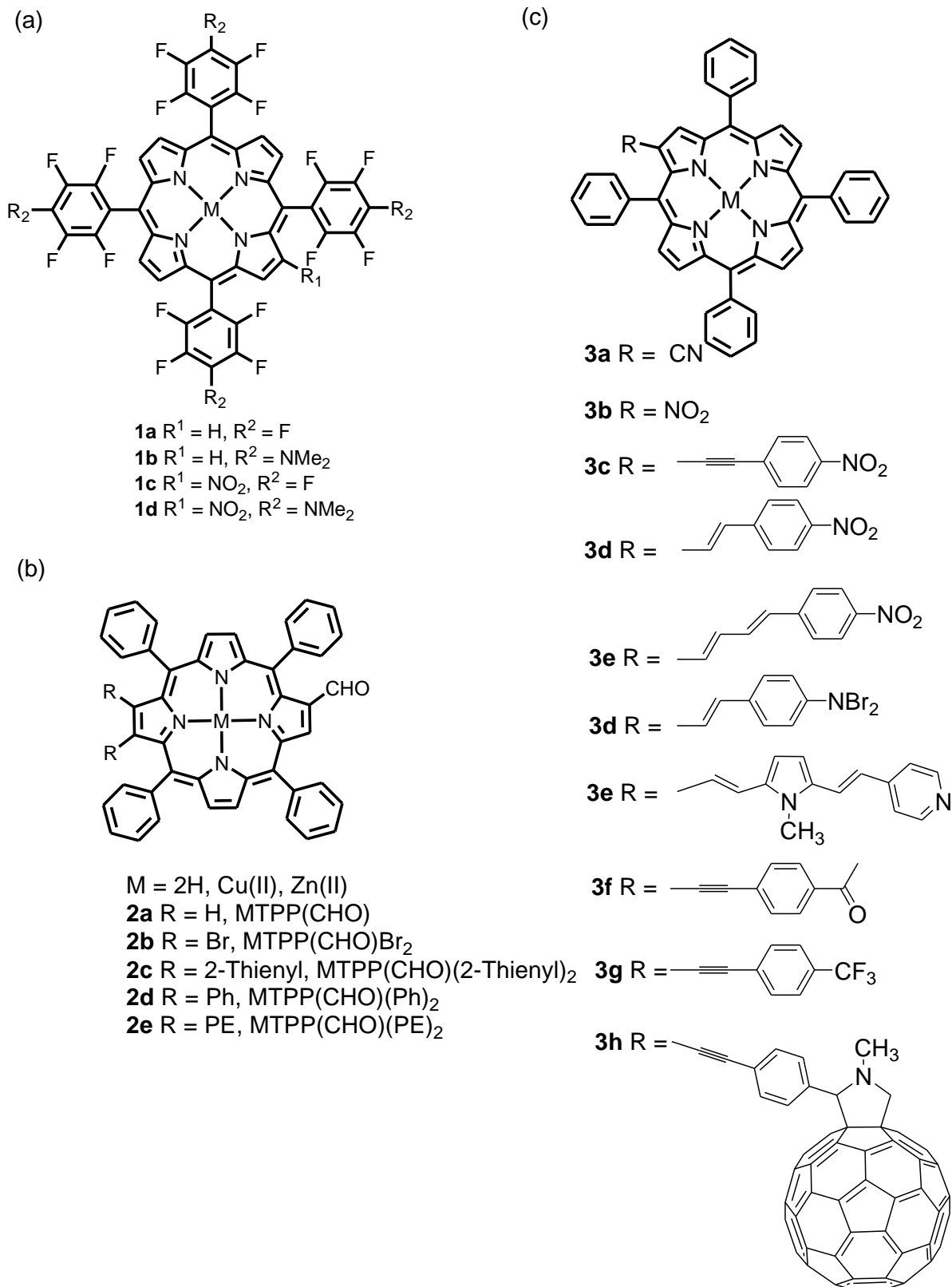
Figure 11 Chemical structures of *β*-substituted porphyrins for NLO applications.

15

Porphyrin (**3c**). 2-formyl porphyrin was utilized for Wittig reactions (**3d**-**3e**) and further functioanlization led to new type of *β*-substituted porphyrins (**2a**-**2e**) which were utilized for NLO studies [117]. A wide variety of arylethynyl groups have been introduced to modify the *β*-position of the porphyrins (**3f,3g**) using Pd(dba)$_2$/AsPh$_3$ without CuI as a catalyst to suppress the homocoupling **3g** and heating with N-methylglycine/fullerene (C$_{60}$) afforded the desired porphyrin (**3h**) in a good yield. Recently, Mongin *et al*. have reported the synthesis and photophysical properties of new multiporphyrin assemblies having ocupolar and quadrupolar cores [118]. They have utilized smooth electronic disconnection approach between two-photon absorbing conjugated systems and peripheral porphyrin sensitizers. They have achieved striking (non-resonant) TPA enhancement in the NIR region while retaining excellent fluorescence and photosensitization properties. These molecular systems pave a way for two-photon imaging and photodynamic therapy.

1.8 OBJECTIVES AND SCOPE OF THE PRESENT WORK

β-Pyrrole functionalized 'push-pull' porphyrins are of growing interest for their use as nonlinear optical materials, sensitizers in DSSC and PDT, anion sensors, catalysts and model compounds of biological nonplanar tetrapyrroles. Further, these highly substituted porphyrins exhibit unique photophysical, electrochemical redox and stereochemical properties. Of the porphyrins, *β*-brominated 2-nitroporphyrins, viz. H$_2$TPP(NO$_2$)Br$_n$ (n = 2 and 6) served as precursors for the synthesis of new porphyrins with mixed substituents pattern, viz. MTPP(NO$_2$)R$_n$ (n = 2 and 6; R = Ph, PE, 2-thienyl and CN; M = Co(II), Ni(II), Cu(II) and Zn(II)) that are preparatively difficult. Introduction of appropriate substituents (by varying in shape, size and electronic nature of substituents) at the pyrrole positions of the porphyrin could provide tunable shape, symmetry and electronic properties of the porphyrin macrocycle. Synthesis and studies on such porphyrins are largely limited. The present thesis reports the facile synthesis, unique photophysical and tunable electrochemical redox properties of newly synthesized porphyrins having mixed substituents pattern.

Generally, the electronic absorption spectra of Ni(II) complexes of tetraphenylporphyrin derivatives are largely independent of ligating nitrogenous bases and anions. Herein, a series of highly electron deficient Ni(II) porphyrins, viz. NiTPP(CN)$_4$ derivatives, NiTPP(NO$_2$)Cl$_7$ and

NiTPPCl$_8$ are utilized for selective cyanide ion sensing which was confirmed by various spectroscopic studies and single crystal X-ray structures.

Although a variety of *meso*-phenylethynyl substituted 'push-pull' porphyrins have been investigated extensively, the photophysical, electrochemical redox, solvatochromism and anion sensing properties of tetra- and octa-β-phenylethynyl substituted tetraphenylporphyrins have not been studied so far.

A large number of porphyrinic dyes are known in the literature. Generally, they were prepared by multistep synthetic routes *via* expensive Pd-catalyzed coupling reactions. Herein we are reporting two-step synthesis of novel 'push-pull' porphyrins (*trans*-A$_2$BC type) in very good yields and their photovoltaic properties.

Numerous reports on Fe(III) and Mn(III) porphyrins for catalytic applications in homogeneous and heterogeneous media are available. Often the stability, recyclability and product selectivity of these catalysts are questionable. Herein, we are reporting the selective epoxidation of olefins by stable β-octachlorovanadylporphyrin (VOTPPCl$_8$) with very high turnover frequency (TOF).

Meso-tetrakis(4'-phosphonicacidphenyl)porphyrin is known for DSSC and other material applications. Herein, we have developed a simple one-step synthetic procedure for *Meso-terakis* (4'-phosphorylphenyl)porphyrin and their metal complexes. Further, we explored their spectroscopic and electrochemical redox properties.

The thesis of consists of eight different chapters

Chapter 1 deals with the chemical literature on the *meso*-phenyl and β-pyrrole functionalized porphyrins and their applications in DSSC, anion sensing, catalysis, PDT and NLO. Further we have discussed about the importance tetrapyrroles in biological systems.

Chapter 2 describes the synthesis, spectral and electrochemical studies of electronically tunable β-substituted porphyrins with mixed substituents pattern.

Chapter 3 describes the ratiometric and colorimetric "naked eye" selective detection of CN⁻ ions by electron deficient Ni(II) porphyrins and their reversibility studies.

Chapter 4 includes the synthesis, spectroscopic, electrochemical redox, solvatochromism and anion binding properties of *β*-tetra and -octaphenylethynyl substituted *meso*-tetraphenyl-porphyrins.

Chapter 5 involves with cost-effective *trans*-A_2BC porphyrins containing various donor groups for dye-sensitized solar cells.

Chapter 6 describes about the electron deficient nonplanar *β*-octachlorovanadylporphyrin as highly efficient and selective epoxidation catalyst for olefins

Chapter 7 deals with the facile synthesis and electrochemical studies of diethoxyphosphoryl-phenyl substituted porphyrin and its metal complexes.

Chapter 8 summarizes the results obtained in the present study.

1.9 REFERENCES

1.   Lippard, S. J.; Berg, J. M.,"Principles of Bioinorganic Chemistry", University Science Books, Mill Valley, California, **1994**.

2.   Eichhorn, G. L.,"Inorganic Biochemistry", Elsevier, Amsterdam, **1973**.

3.   Kaim, W.; Schwederski, B.,"Bioinorganic Chemistry: Inorganic Elements in the Chemistry of Life: An Introduction and Guide", John Wiley & Sons, **1987.**

4.   Katz, J. J.;Shipman, L. L.;Norris, J. R., "Chlorophyll organization and energy transfer in photosynthesis", Ciba Foundation Symposium, **1979**.

5.   Dolphin, D.,"B_{12}", John Wiley, New York, **1982**.

6. Fuhrhop, J.-H.; Smith, K. M.,"Laboratory methods". pp. 757-870. In K.M. Smith, Ed., Porphyrins and metalloporphyrins, Elsevier, Amsterdam, **1975**.

7. Dolphin, D., "The Porphyrins", Academic Press, New York, **1979**, Vol. 1-7.

8. Kadish, K. M.; Smith, K. M.;Guilard, R., Eds., "The Porphyrin Handbook", Academic Press, New York, Vol. 1-10, **2000** and Vol. 11-20, **2005.**

9. Kadish, K. M.; Smith,K. M.; Guilard, R., Eds., "Handbook of Porphyrin Science*"*, World Scientific Publishing Co. Inc., New Jersey, Vol. 1-25, **2012** and Vol. 25-35, **2014**.

10. Shelnutt, J. A.; Song, X.-Z.; Ma, J.-G.; Jia, S.-L; Jentzen, W.; Medforth, C. J., "Nonplanarporphyrins and their significance in proteins", *Chem. Soc. Rev.* **1998,** *27*, 31-42.

11. Senge, M. O., "Exercises in molecular gymnastics-bending, stretching and twisting porphyrins", *Chem. Commun*. **2006**, 243-256.

12. Ravikanth, M.; Chandrashekar, T. K., "Nonplanar porphyrins and their biological relevance; ground and excited state dynamics" *Struct. Bond.* **1995,** *82*, 1-83.

13. Hagfeldt, A.; Boschloo, G.; Sun, L.; Kloo, L.; Pettersson, H., "Dye-sensitized solar cells", *Chem. Rev*. **2010**, *110*, 6595-6663.

14. Subbaiyan, N. K.; D'Souza, F., "Light-to-electron converting panchromatic supramolecular solar cells of phthalocyanine-porphyrin heterodimers adsorbed onto nanocrystalline SnO_2 electrodes", *Chem. Commun.* **2012**, *48*, 3641-3643.

15. Higashino, T.; Imahori, H., "Porphyrins as excellent dyes for dye-sensitized solar cells: recent developments and insights", *Dalton Trans*. **2015**, *44*, 448-463.

16. Hardin, B. E.; Snaith , H. J.; McGehee, M. D., " The renaissance of dye-sensitized solar cells", *Nat. Photonics* **2012**, *6*, 162-169.

17. Zhang, S.; Yang, X.; Numata, Y.; Han, L., "Highly efficient dye-sensitized solar cells: progress and future challenges", *Energy Environ. Sci*. **2013**, *6*, 1443-1464.

18. Hart, A. S.; Chandra, B. K. C.; Gobeze, H. B.; Sequeira, L. R.; D'Souza, F., "Porphyrin-sensitized solar cells: effect of carboxyl anchor group orientation on the cell performance", *ACS Appl. Mater. Interfaces* **2013**, *5*, 5314-5323.

19. Urbani, M.; Gratzel, M.; Nazeeruddin, M. K.; Torres, T., "*Meso*-substituted porphyrins for dye-sensitized solar cells", *Chem. Rev.* **2014**, *114*, 12330-12396.

20. Nazeeruddin, M. K.; Angelis, F. D.; Fantacci, S.; Selloni, A.; Viscardi, G.; Liska, P.; Ito, S.; Takeru . B.; Grätzel, M, "Combined experimental and DFT-TDDFT computational study of photoelectrochemical cell ruthenium sensitizers", *J. Am. Chem. Soc*. **2005**, *127*, 16835-16847.

21. Han, L.; Islam, A.; Chen, H.; Malapaka, C.; Chiranjeevi, B.; Zhang, S.; Yang X.; Yanagida, M., "High-efficiency dye-sensitized solar cell with a novel co-adsorbent", *Energy Environ. Sci*. **2012**, *5*, 6057-6060.

22. Yu, Q.; Wang, Y.; Yi, Z.; Zu, N.; Zhang, J.; Zhang, M.; Wang, P., "High-efficiency dye-sensitized solar cells: The influence of lithium ions on exciton dissociation, charge recombination, and surface states", *ACS Nano* **2010,** *4*, 6032-6038.

23. Wang, P.; Zakeeruddin, S. M.; Moser, J. E.; Nazeeruddin, M. K.; Sekiguchi, T.; Gratzel, M., "A stable quasi-solid-state dye-sensitized solar cell with an amphiphilic ruthenium sensitizer and polymer gel electrolyte", *Nat. Mater*. **2003**, *2*, 402-407.

24. Liang, M.; Chen, J., "Arylamine oranic dyes for dye-sensitized solar cells", *Chem. Soc. Rev*. **2013**, *42*, 3453-3488 and references therein.

25. Lee, C.-P.; Lin, R. Y.-Y.; Lin, L.-Y.; Li, C.-T.; Chu, T.-C.; Sun, S.-S.; Lin, J. T.; Ho, K.-C., "Recent progress in organic sensitizers for dye sensitized solar cells", *RSC Adv.* **2015**, *5*, 23810-23825 and references therein.

26. Bai, Y.; Zhang, J.; Zhou, D.; Wang, Y.; Zhang, M.; Wang, P., "Engineering Organic sensitizers for iodine-free dye-sensitized solar cells: red-shifted current response concomitant with attenuated charge recombination", *J. Am. Chem. Soc.***2011,** *133*, 11442-11445.

27. Chen, Y.-S.; Li, C.; Zeng, Z.-H.; Wang, W.-B.; Wang, X.-S.; Zhang, B.-W., "Efficient electron injection due to a special adsorbing group's combination of carboxyl and hydroxyl: dye-sensitized solar cells based on new hemicyanine dyes", *J. Mater. Chem.* **2005**, *15*, 1654–1661.

28. Wu, Y.; Marszalek, M.; Zakeeruddin, S. M.; Zhang, Q.; Tian, H.; Gratzel, M.; Zhu, W., "High-conversion-efficiency organic dye-sensitized solar cells: molecular engineering on D-A-π-A featured organic indoline dyes", *Energy Environ. Sci.* **2012,** *5*, 8261-8272.

29. Campbell, W. M.; Burrell, A. K.; Officer, D. L.; Jolley, K. W., "Porphyrins as light harvesters in the dye-sensitised TiO$_2$ solar cell", *Coord. Chem. Rev.* **2004**, *248*, 1363–1379.

30. Martinez-Diaz, M. V.; de la Torre, G.; Torres, T., "Lighting porphyrins and phthalocyanines for molecular photovoltaics", *Chem. Commun.* **2010**, *46*, 7090–7108.

31. Griffith, M. J.; Sunahara, K.; Wagner, P.; Wagner, K.; Wallace, G. G.; Officer, D. L.; Furube, A.; Katoh, R.; Mori, S.; Mozer, A. J., "Porphyrins for dye-sensitized solar cells: new insights into efficiency-determining electron transfer steps", *Chem. Commun.* **2012**, *48,* 4145-4162.

32. Yella, A.; Lee, H. W.; Tsao, H. N.; Yi, C.; Chandiran, A. K.; Nazeeruddin, M. K.; Diau, E. W.-G.; Yeh, C. Y.; Zakeeruddin, S. M.; Grätzel, M., "Porphyrin-sensitized solar cells with cobalt (II/III)-based redox electrolyte exceed 12 percent efficiency", *Science* **2011**, *334*, 629-634.

33. Mathew, S.; Yella, A.; Gao, P.; Humphry-Baker, R.; CurchodBasile, F. E.; Ashari-Astani, N.; Tavernelli, I.; Rothlisberger, U.; Nazeeruddin, M. K.; Grätzel, M., "Dye-sensitized solar cells with 13% efficiency achieved through the molecular engineering of porphyrin sensitizers", *Nat. Chem.* **2014,** *6*, 242-247.

34. Kim, D. S.; Sessler, J. L., "Calix[4]pyrroles: versatile molecular containers with ion transport, recognition, and molecular switching functions", *Chem. Soc. Rev.* **2015**, *44*, 532-546.

35. Roznyatovskiy, V. V.; Lee, C.-H.; Sessler, J. L., "π-Extended isomeric and expanded porphyrins", *Chem. Soc. Rev.* **2013**, *42*, 1921-1933.

36. Beer, P. D.; Gale, P. A., "Anion recognition and sensing: The state of the art and future perspectives", *Angew. Chem. Int. Ed*. **2001**, *40*, 486-516.

37. Matthews, E.; Beer, P. D., "Calixarene-based Anion Receptors", *Supramol. Chem*. **2005**, *17*, 411-435.

38. Vennesland, B.; Comm, E. E.; Knownles, C. J.; Westly J.; Wissing, F., "Cyanide in Biology", Academic press, London, **1981**.

39. Frant, M. S.; Ross, J., "Electrode for sensing fluoride ion activity in solution", *Science* **1966**, *154*, 1533-1555.

40. Briancon, D., "Fluoride and osteoporosis: an overview", *Rev. Rheum.***1997**, *64*, 78-81.

41. Adams, R. L. P.; Knowler, J. T.; Leader, D. P., "The Biochemistry of the Nucleic Acids", Chapman and Hall, New York, 11th ed., **1992.**

42. Shang, X. F.; Xu, X. F., "The anion recognition properties of hydrazone derivatives containing anthracene", *BioSystems*, **2009**, *96*, 165-171.

43   Lee, C.-H.; Miyaji, H.; Yoon, D.-W.; Sessler, J. L., "Strapped and other topographically nonplanar calixpyrrole analogues. Improved anion receptors", *Chem. Commun.* **2008**, 24-34.

44. Kim, S. K.; Sessler, J. L., "Calix[4]pyrrole-based ion pair receptors", *Acc. Chem. Res.* **2014**, *47*, 2525-2536.

45. Anzenbacher, P.; Nishiyabu, R.; Palacois, M. A., "N-confused calix[4]pyrroles", *Coord. Chem. Rev*. **2006**, *250*, 2929-2938.

46. Gale, P. A.; Lee, C.-H., "Calix[n]pyrroles as anion and ion-pair complexants", *Top. Heterocycl. Chem.* **2010**, *24*, 39-73.

47. Pistner, A. J.; Lutterman, D. A.; Ghidiu, M. J.; Ma Y.-Z.; Rosenthal, J., "Synthesis, electrochemistry, and photophysics of a family of phlorin macrocycles that display cooperative fluoride binding", *J. Am. Chem. Soc.* **2013**, *135*, 6601-6607.

48.　Santos, C. I.; Oliveira, M. E.; Barata, J. F. B.; Faustino, M. A. F.; Cavaleiro, J. A. S.; Neves M. G.; Lodeiro, C., "Corroles as anion chemosensors: exploiting their fluorescence behaviour from solution to solid-supported devices", *J. Mater. Chem.* **2012**, *22*, 13811-13819.

49.　Yadav, P.; Sankar, M., "Synthesis, spectroscopic and electrochemical studies of phosphoryl and carbomethoxyphenyl substituted corroles, and their anion detection properties", *Dalton Trans.* **2014**, *43*, 14680-14688.

50.　Sessler, J. L.; Davis, J. M., "Sapphyrins: Versatile Anion Binding Agents", *Acc. Chem. Res.* **2001**, *34*, 989-997.

51.　Cho, D. G., "Syntheses and studies of sapphyrins and anion receptors", Umi Dissertation Publishing, **2012**.

52.　Won, D. H.; Toganoh, M.; Uno H.; Furuta, H., "Pt(II) N-confused porphyrin: An expanded pyrrole that affords a stable π-anion", *Dalton Trans*. **2009**, 6151-6158.

53.　Xie, Y.; Marimoto T.; Furuta, H., "Sn^{IV} complexes of N-confused porphyrins and oxoporphyrins-unique fluorescence "switch-on" halide receptors", *Angew. Chem. Int. Ed*. **2006**, *45*, 6907-6910.

54.　D'Souza, F.; Subbaiyan, N. K.; Xie, Y.; Hill, J. P.; Ariga, K.; Ohkubo, K.; Fukuzumi, S., "Anion-complexation-induced stabilization of charge separation", *J. Am. Chem. Soc*. **2009**, *131*, 16138-16146.

55.　Hill, J. P.; Schumacher, A. L.; D'Souza, F.; Labuta, J.; Redshaw, C.; Elsegood, M. R. J.; Aoyagi, M.; Nakanishi, T.; Ariga, K., "Chromogenic indicator for anion reporting based on an N-substituted oxoporphyrinogen", *Inorg. Chem.* **2006**, *45*, 8288-8296.

56.　Takeuci, M.; Shioya, T; Swager, T. M., "Allosteric Fluoride Anion Recognition by a Doubly Strapped Porphyrin", *Angew. Chem. Int. Ed*. **2001**, *40*, 3372-3376.

57.　Cormode, D. P.; Drew, M. G. B.; Jagessar R.; Beer, P. D., "Metalloporphyrin anion sensors: the effect of the metal centre on the anion binding properties of amide-functionalised and tetraphenyl metalloporphyrins", *Dalton Trans.* **2008**, 6732-6741.

58. Beer, P. D.; Cormode D. P.; Davis, J. J., "Zinc metalloporphyrin-functionalised nanoparticle anion sensors", *Chem. Commun*. **2004**, 414-415.

59. Rodrigues, J. M. M.; Farinha, A. S.; Muteto, P. V.; Woranovicz-Barreira, S. M.; Paz, F. A. A.; Neves, M. G.; Cavaleiro, J. A. S.; Tome, A. C.; Gomes, M. T.; Sessler, J. L.; Tome, J. P. C., "New porphyrin derivatives for phosphate anion sensing in both organic and aqueous media", *Chem. Commun*., **2014**, *50*, 1359-1361.

60. Chen, L. D.; Zou, X. U.; Buhlmann, P., "Cyanide-selective electrode based on Zn(II) tetraphenylporphyrin as ionophore", *Anal. Chem.* **2012**, *84*, 9192-9198.

61. Yoon, H.; Lee, C.-H.; Jeong, Y.-H.; Gee H.-C.; Jang, W.-D., "A zinc porphyrin-based molecular probe for the determination of contamination in commercial acetonitrile", *Chem. Commun*. **2012**, *48*, 5109-5111.

62. Kim Y.-H.; Hong, J.-I., "Ion pair recognition by Zn–porphyrin/crown ether conjugates: v isible sensing of sodium cyanide", *Chem. Commun*. **2002**, 512-513.

63. Liu, H.; Shao, X. B.; Jia, M. X.; Jiang, X. K.; Li Z. T.; Chen, G. J., "Selective recognition of sodium cyanide and potassium cyanide by diaza-crown ether-capped Zn-porphyrin receptors in polar solvents", *Tetrahedron* **2005**, *61*, 8095-8100.

64. Worlinsky, J. L.; Halepas S.; Brukner, C., "PEGylated meso-arylporpholactone metal complexes as optical cyanide sensors in water", *Org. Biomol. Chem.* **2014**, *12*, 3991-4001.

65. Hambright, P.; Langley, R., "Cyanide scavengers: Kinetics of the reaction of rhodium(III)-tetrakis(4-sulfonatophenyl)porphyrin with cyanide and hydrogen cyanide", *Inorg. Chim. Acta* **1987**, *137*, 209-212.

66. Legako, J. A.; White B. J.; Harmon, H. J., "Detection of cyanide using immobilized porphyrin and myoglobin surfaces", *Sens. Actuators, B* **2003**, *91*, 128-132.

67. Hong, S.-J.; Yoo, J.; Kim, S.-H.; Kim, J. S.; Yoon J.; Lee, C.-H., "*β*-Vinyl substituted calix[4]pyrrole as a selective ratiometric sensor for cyanide anion", *Chem. Commun.* **2009**, 189-191.

68. Holaday, M. G. D.; Tarafdar, G.; Adinarayana, B.; Reddy M. L. P.; Srinivasan, A., "Chemodosimetric cyanide sensing in a 5,15-porphodimethene Pd(II) complex", *Chem. Commun*. **2014**, *50*, 10834-10836.

69. Mannel-Croise, C.; Meister, C.; Zelder, F., "Naked-Eye screening of metal-based chemosensors for biologically important anions", *Inorg. Chem*. **2010**, *49*, 10220-10222.

70. Mannel-Croise, C.; Probst B.; Zelder, F., "A straightforward method for the colorimetric detection of endogenous biological cyanide", *Anal. Chem.* **2009**, *81*, 9493-9498.

71. Mannel-Croise C.; Zelder, F., "Complex samples cyanide detection with immobilized corrinoids", *ACS Appl. Mater. Interfaces* **2012**, *4*, 725-729.

72. Palomares, E.; Martinez-Diaz, M. V.; Torres, T.; Coronado, E., "A highly sensitive hybrid colorimetric and fluorometric molecular probe for cyanide sensing based on a subphthalocyanine dye", *Adv. Funct. Mater*. **2006**, *16*, 1166-1170.

73 Sheldon, R. A., "Metalloporphyrins in Catalytic Oxidations", Marcel Dekker, Inc., New York, **1994**.

74 Meunier, B., "Biomimetic Oxidation Catalyzed by Transition Metal Complexes", Imperial College Press, London, **1999**.

75 Montanari F.; Casella L., "Metalloporphyrin Catalyzed Oxidations", Kluwer Academic Publishers, Boston, **1994**.

76. Bartoli, J. F.; Mansuy, O.; Le, B.-O.; Ozette, K. L. B.; Palacio, M.; Manusy, D., "New manganese *β*-polynitroporphyrins as particularly efficient catalysts for biomimetic hydroxylation of aromatic compounds with H_2O_2", *J. Chem. Soc., Chem. Commun.* **2000**, 827-828.

77. Bartoli, J. F.; Battioni, P.; De Foor, W. R.; Mansuy, D., "Synthesis and remarkable properties of iron β-polynitroporphyrins as catalysts for monooxygenation reactions", *J. Chem. Soc., Chem. Commun.* **1994**, 23-24.

78. Ellis Jr., P. E.; Lyons, J. E., "Selective air oxidation of light alkanes catalysed by activated metalloporphyrins-The search for a suprabiotic system", *Coord. Chem. Rev.* **1990**, *105*, 181-193.

79. Grinstaff, M. W.; Hill, M. G.; Labinger, L. A.; Gray H. B., "Mechanism of catalytic oxygenation of alkanes by halogenated iron porphyrins", *Science* **1994**, *264*, 1311-1313.

80. Groves, J. T.; Neumann, R., "Regioselective oxidation catalysis in synthetic phospholipid vesicles. Membrane-spanning steroidal metallo-porphyrins", *J. Am. Chem. Soc*. **1989,** *111*, 2900-2909.

81. Dolphin, D.; Traylor, T. G.; Xie, L. Y., "Polyhaloporphyrins: Unusual ligands for metals and metal-catalyzed oxidations", *Acc. Chem. Res*. **1997**, *30*, 251-259.

82. Meunier, B., "Metalloporphyrins as versatile catalysts for oxidation reactions and oxidative DNA Cleavage", *Chem. Rev*. **1992**, *92*, 1411-1456.

83. Sono, M.; Roach, M. P.; Coulter E. D.; Dawson, J. H., "Heme-containing oxygenases", *Chem. Rev*. **1996**, *96*, 2841-2887.

84. Suslick, K. S., "Shape-selective oxidation by metalloporphyrins" pp. 41-63. In: Kadish, K. M.; Smith, K. M.; Guilard, R., Eds., The porphyrin handbook, Academic Press, New York, **2000**.

85. Weissemel K.; Arpe, H. J., "Industrial Organic Chemistry", 3rd ed., VCH: Weinheim, Germany, **1997**.

86. Araghi, M.; Mirkhani, V.; Moghadam, M.; Tangestaninejad, S.; Mohammdpoor-baltork, I., "Synthesis and characterization of a new porphyrin-polyoxometalate hybrid material and investigation of its catalytic activity", *Dalton Trans*. **2012**, *41*, 3087-3094.

87. Zhang, W.; Jiang, P.; Wang, Y.; Zhang, J.; Zhang, P., "Bottom-up approach to engineer two covalent porphyrinic frameworks as effective catalysts for selective oxidation", *Catal. Sci. Technol.* **2015**, *5*, 101-104.

88. Zhang, K.; Yu, Y.; Nguyen, S. T.; Hupp, J. T.; Broadbelt, L. J.; Farha, O. K., "Epoxidation of the commercially relevant divinylbenzene with [tetrakis-(pentafluorophenyl)porphyrinato]iron(III) chloride and its derivatives", *Ind. Eng. Chem. Res.* **2015**, *54*, 922-927.

89. Dolphin, D.; Sternberg, E., "Medical applications of dyes: A review of photodynamic therapy", Chemistry of functional dyes, Eds. Yoshida, Z.; Kitao, T., Mita Press, Tokyo, Japan, **1989**, Ch. 12, 587-597.

90. Ethirajan, M.; Chen, Y.; Joshi P.; Pandey, R. K., "The role of porphyrin chemistry in tumor imaging and photodynamic therapy", *Chem. Soc. Rev.* **2011**, *40*, 340-362.

91. Pandey, R. K.; Sumlin, A. B.; Potter, W. R.; Bellnier, D. A.; Henderson, B. W.; Aoudia, M.; Rodgers, M. R.; Smith K. M.; Dougherty, T. J., "Alkyl ether analogs of chlorophyll-*a* derivatives: Part 1. Synthesis, photophysical properties and photodynamic efficacy", *Photochem. Photobiol.* **1996**, *64*,194-204.

92. Loewen, G. M.; Pandey, R. K.; Bellnier, D.; Henderson B. W.; Dougherty, T. J., "Endobronchial photodynamic therapy for lung cancer", *Lasers Surg. Med.* **2006,** *38*, 364-370.

93. Gryshuk, A.; Graham, A.; Pandey, R. K.; Potter, W. R.; Missert, J. R.; Oseroff, A.; Dougherty, T. J.; Pandey, R. K., "A First Comparative Study of Purpurinimide-based Fluorinated *vs.* Nonfluorinated Photosensitizers for Photodynamic Therapy", *Photochem. Photobiol.* **2002**, *76*, 555-559.

94. Bellnier, D. A.; Greco, W. R.; Loewen, G. M.; Nava, H.; Oseroff A. R.; T. Dougherty, J., "Clinical pharmacokinetics of the PDT photosensitizers porfimer sodium (photofrin), 2-[1-Hexyloxyethyl]-2-devinyl pyropheophorbide-a (Photochlor) and 5-ALA-induced protoporphyrin IX", *Lasers Surg. Med.* **2006**, *38*, 439-444.

95. Kumar, D.; Mishra, B. A.; Shekar, K. P. C.; Kumar, A.; Akamatsu, K.; Kusaka E.; Ito, T., "Remarkable photocytotoxicity of a novel triazole-linked cationic porphyrin-*β*-carboline conjugate", *Chem. Commun.* **2013**, *49*, 683-685.

96. Bříza, T.; Králová, J.; Cígler, P.; Kejík, Z.; Poučková, P.; Vašek, P.; Moserová, I.; Martásek, P.; Král, V., "Combination of two chromophores: Synthesis and PDT application of porphyrin–pentamethinium conjugate" *Bioorg. Med. Chem. Lett.,* **2012**, *1*, 82-84.

97. Senge, M. O.; Fazekas, M.; Notaras, E. G. A.; Blau, W. J.; Zaeadzka, M.; Locos, O. B.; Mhuircheartaigh, E. M. N., "Non linear optical properties of porphyrins", *Adv. Mater.* **2007**, *19*, 2737–2774.

98. Suslick, K. S.; Chen, C. T.; Meredith, G. R.; Cheng, L. T.; "Push-pull porphyrins for nonlinear materials" *J. Am. Chem. Soc.* **1992**, *114*, 6928-6930.

99. Zawadzka, M.; Wang, J.; Blau W. J.; Senge, M. O., "Nonlinear absorption properties of 5, 10-A$_2$B$_2$ porphyrins-correlation of molecular structure with the nonlinear responses", *Photochem. Photobiol. Sci.* **2013**, *12*, 996-1007.

100. Morone, M.; Beverina, L.; Abbotto, A.; Silvestri, F.; Collini, E.; Ferrante, C.; Bozio, R.; Pagani, G. A., "Enhancement of two-photon absorption cross-section and singlet-oxygen generation in porphyrins upon β-functionalization with donor-acceptor substituents", *Org. Lett.* **2006,** *8*, 2719-2722.

101. Lembo, A.; Tagliatesta, P.; Guldi, D. M., "Synthesis and photophysical investigation of new porphyrin derivatives with β-pyrrole ethynyl linkage and corresponding dyad with [60] fullerene *J. Phys. Chem. A* **2006**, *110*, 11424-11434.

102. Qin, J.; Wada, T.; Sasabe, H., "Asymmetric porphyrins and metalloporphyrins for nonlinear optics", *Mol. Cryst. Liq. Cryst. A* **1992**, *217*, 47-51.

103. Priyadarshy, S.; Therien, M. J.; Beratan, D. N., "Acetylenyl-linked, porphyrin-bridged, donor-acceptor molecules: A theoretical analysis of the molecular first hyperpolarizability in highly conjugated push-pull chromophore structures", *J. Am. Chem. Soc.* **1996**, *118*, 1504-1510.

104. Karki, L.; Vance, F. W.; Hupp, J. T.; Le-Cours, S. M.; Therien, M. J., "Electronic stark effect studies of a porphyrin-based push-pull chromophore displaying a large first hyperpolarizability: State-specific contributions to β", *J. Am. Chem. Soc.* **1998**, *120*, 2606-2611.

105. Jiang, N.; Zuber, G.; Keinan, S.; Nayak, A.; Yang, W.; Therien, M. J.; Beratan, D. N., "Design of Coupled Porphyrin Chromophores with Unusually Large Hyperpolarizability", *J. Phys. Chem. C.* **2012**, *116*, 9724–9733.

106. LeCours, S. M.; Guan, H. W.; DiMagno, S. G.; Wang C. H.; Therien, M. J., "Push-Pull arylethynyl porphyrins: New chromophores that exhibit large molecular first-order hyperpolarizabilities", *J. Am. Chem. Soc.* **1996**, *118*, 1497-1503.

107. LeCours, S. M.; DiMagno, S. G.; Therien, M. J., "Exceptional electronic modulation of porphyrins through *meso*-arylethynyl groups. Electronic spectroscopy, electronic structure, and electrochemistry of [5,15-Bis[(aryl)ethynyl]-10,20-diphenylporphinato]zinc(II) complexes. X-ray crystal structures of [5,15-Bis[(4'-fluorophenyl)ethynyl]-10,20-diphenylporphinato]zinc(II) and 5,15-bis[(4'-methoxyphenyl)ethynyl]-10,20-diphenylporphyrin", *J. Am. Chem. Soc.* **1996**, *118*, 11854-11864.

108. Albert, I. D. L.; Marks,T. J.; Ratner, M. A., "Large molecular hyperpolarizabilities in "push-pull" porphyrins. Molecular planarity and auxiliary donor-acceptor effects", *Chem. Mater.* **1998**, *10*, 753-762.

109. Yamamoto, S.; Diercksen, G. H. F.; Karelson, M., "An ab initio CI study of electronic spectra of substituted free-base porphyrins", *Chem. Phys. Lett.* **2000**, *318*, 590-596.

110. Salek, P.; Vahtras, O.; Helgaker, T.; Agren, H., "Density-functional theory of linear and nonlinear time-dependent molecular properties", *J. Chem. Phys.* **2002,** *117*, 9630-9645.

111. Misra, R.; Kumar, R.; PrabhuRaja, V.; Chandrashekar, T. K., "Modified push–pull expanded corroles: Syntheses, structure and nonlinear optical properties", *J. Photochem. Photobiol. A* **2005**, *175*, 108-117.

112. Ray, P. C.; Leszczynski, J., "Nonlinear optical properties of highly conjugated push–pull porphyrin aggregates: Role of intermolecular interaction", *Chem. Phys. Lett.* **2006**, *419*, 578-583.

113. Monnereau, C.; Blart, E.; Montembault, V.; Fontaine, L.; Odobel, F., "Synthesis of new crosslinkable co-polymers containing a push-pull zinc porphyrin for non-linear optical applications" *Tetrahedron* **2005**, *61*, 10113-10121.

114. Wang, A.; Long, L.; Meng, S.; Li, X.; Zhao, W.; Song, Y.; Cifuentes, M. P.; Humphrey, M. G.; Zhang, C., "Cooperative enhancement of optical nonlinearities in a porphyrin derivative bearing a pyrimidine chromophore at the periphery", *Org. Biomol. Chem.* **2013**, *11*, 4250-4257.

115. Sen, A.; Ray, P. C.; Das, P. K.; Krishnan, V., "Metalloporphyrins for quadratic nonlinear optics", *J. Phys. Chem.* **1996**, *100*, 19611-19613.

116. Annoni, E.; Pizzotti, M.; Ugo, R.; Quici, S.; Morotti, T.; Bruschi, M.; Mussini, P., "Synthesis, electronic characterisation and significant second-order non-linear optical responses of meso-tetraphenylporphyrins and their Zn^{II} complexes carrying a push or pull group in the *β* pyrrolic position", *Eur. J. Inorg. Chem.* **2005**, 3857-3874.

117. Kalnoor, B. S.; Bist, P. B.; Jena, K. C.; Velkannan, V.; Bhyrappa, P., "Mixed *β*-pyrrole substituted *meso*-tetraphenylporphyrins and their metal complexes: Optical nonlinearity using degenerate four wave mixing technique", *J. Phys. Chem. A* **2013**, *117*, 8216−8221.

118. Mongin, O.; Sankar, M.; Charlot, M.; Mir Y.; Blanchard-Desce, M., "Strong enhancement of two-photon absorption properties in synergic 'semi-disconnected' multiporphyrin assemblies designed for combined imaging and photodynamic therapy", *Tetrahedron Lett.* **2013**, *54*, 6474-6478.

CHAPTER 2

Synthesis, Spectral and Electrochemical Properties of Electroincally Tunable β-Substituted Porphyrins with Mixed Substituent Pattern
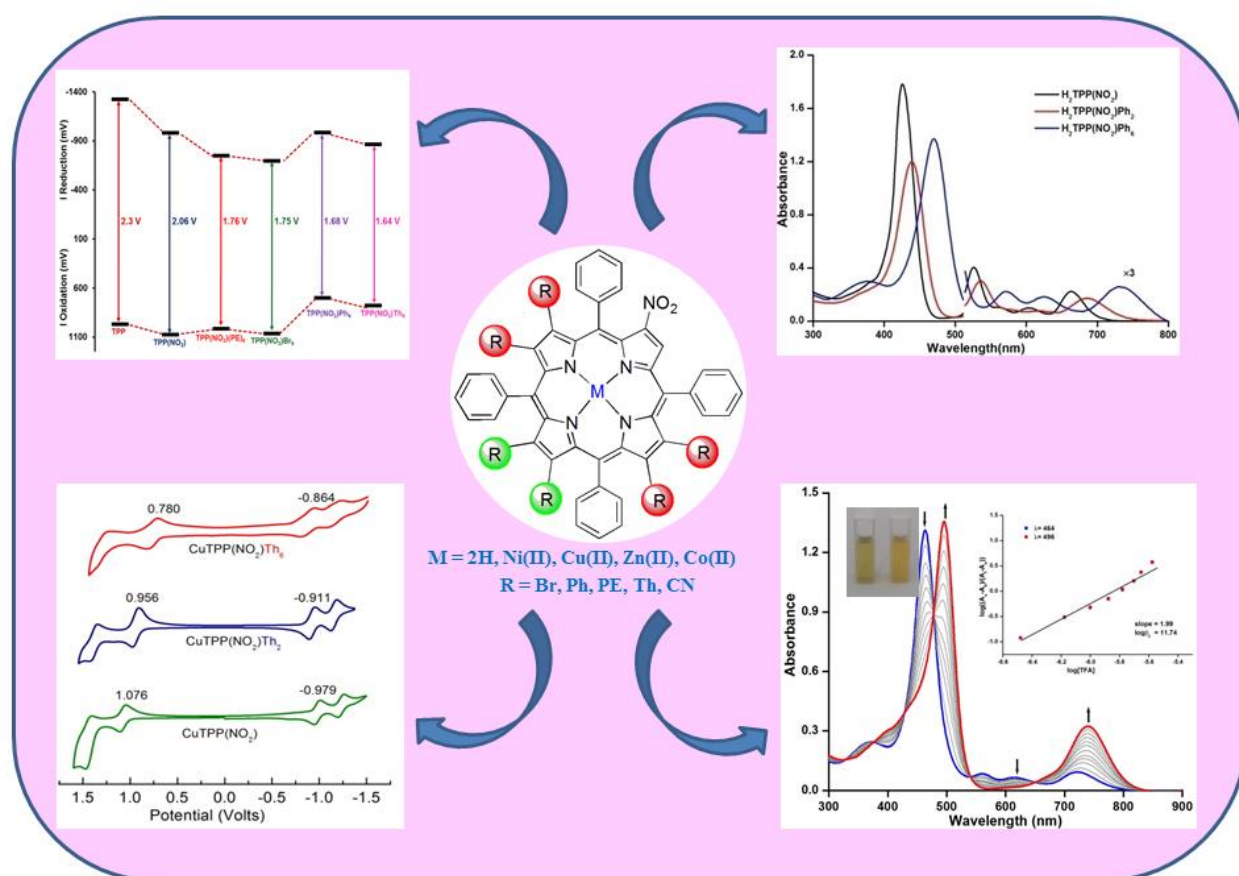
CHAPTER 2

SYNTHESIS, SPECTRAL AND ELECTROCHEMICAL PROPERTIES OF ELECTROINCALLY TUNABLE *β*-SUBSTITUTED PORPHYRINS WITH MIXED SUBSTITUENT PATTERN

2.1 INTRODUCTION

Porphyrinoids play a crucial role in the biological systems, and their synthesis arouses continuing interests in biological, material and inorganic chemistry [1]. The *β*-functionalization of *meso*-tetraphenylporphyrins is of great interest since the electronic properties of the porphyrin macrocycle can be altered by small changes in the substituents [2]. Moreover, the substituents at the *β*-pyrrole positions of the porphyrins exert much larger steric and electronic effects on the porphyrin π-system [2,3] than substituents at the *meso*-aryl positions. The *β*-nitration of the porphyrin ring is of special interest since the nitro groups are versatile and can be converted into several other functional groups [4-5]. *β*-Nitroporphyrins exhibited interesting catalytic [6], photophysical [7] and nonlinear optical properties [8]. Further, *β*-bromosubstituted tetraarylporphyrins are useful substrates for nucleophilic aromatic substitutions and palladium mediated cross-coupling reactions [2]. The *meso*-substituted push-pull porphyrins have been widely explored due to their relative ease of synthesis whereas the studies on *β*-pyrrole mixed substituted or push-pull porphyrins are very much limited due to lack of synthetic methodologies.

Herein, we focused to synthesize the mixed substituted porphyrins in order to tune the electronic spectral and electrochemical redox properties of the porphyrin π-system. In general, the syntheses and properties of porphyrins bearing mixed antipodal *β*-substituents are largely unexamined [9-12]. With these objectives, we report the syntheses, structural, physicochemical and electrochemical redox properties of two new families of porphyrins with mixed substituent pattern viz. 2-nitro-12,13-disubstituted-5,10,15,20-tetraphenylporphyrins ($H_2TPP(NO_2)X_2$, X = Ph, phenylethynyl (PE), 2-thienyl (Th), Br and CN) and 2-nitro-7,8,12,13,17,18-hexasubstituted-5,10,15,20-tetraphenylporphyrins ($H_2TPP(NO_2)X_6$, X = Br, Ph, PE and Th) and their metal (Co(II), Ni(II), Cu(II) and Zn(II)) complexes (Chart 1). To the best of our knowledge, the

protonation and deprotonation studies, ^{1}H NMR spectral features and electrochemical redox properties of *β*-pyrrole tri- and hepta-substituted *meso*-TPPs with mixed substituent pattern and their metal complexes have not been studied so far.

R = Br, Ph, CN, 2-thienyl, ═══ Ph
M = 2H, Co(II), Ni(II), Cu(II), Zn(II)

R = Br, Ph, 2-thienyl, ═══ Ph
M = 2H, Co(II), Ni(II), Cu(II), Zn(II)
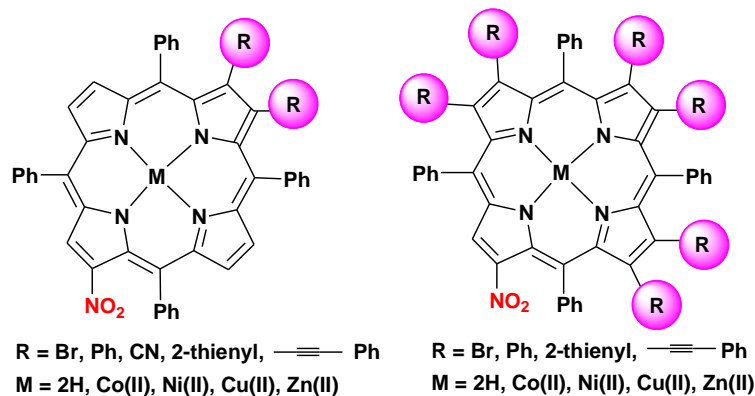
Chart 1. Molecular structures of porphyrins with mixed substituent pattern.

2.2 EXPERIMENTAL SECTION

2.2.1 Reagent and methods

All commercially available chemicals were purchased from appropriate sources and used as received unless otherwise mentioned. Freshly recrystallised N-bromosuccinimide was used for bromination reactions. 2-nitro-12,13-dibromo-*meso*-tetraphenylporphyrin, 2-nitro-7,8,12,13,17,18-hexabromo-*meso*-tetraphenylporphyrinato copper(II) and its free base were synthesized by modified literature methods [10]. Mixed substituted porphyrins, $ZnTPP(NO_2)(PE)_2$, $ZnTPP(NO_2)Br_2$, and $H_2TPP(NO_2)(Th)_2$ were crystallized by the direct diffusion of CH_3OH to a saturated porphyrin solution in $CHCl_3$ over a period of 10 - 15 days. X-ray quality single crystals of $NiTPP(NO_2)Ph_2$ was obtained by direct diffusion of hexane to a saturated porphyrin solution in $CHCl_3$ containing a few drops of pyridine over a period of seven days. Crystal of $NiTPP(NO_2)Br_6$ were obtained by vapor diffusion of hexane into the saturated solution of porphyrin in 1,2-dichloroethane containing a few drops of pyridine. The single crystals obtained were mounted on mounting loops. All diffraction data were collected using a Bruker APEXII diffractometer at 25 °C equipped with graphite-monochromated Mo *Kα* (λ = 0.71073 Å) by the ω-2θ scan. The structures were solved by direct methods using SIR97 and SHELX-97 [13]. Crystallographic data for these compounds are summarized in Table A1 in the Appendix 1. CCDC- 1018319 ($NiTPP(NO_2)Ph_2$), -1018393 ($ZnTPP(NO_2)(PE)_2$), - 1018509

($H_2TPP(NO_2)(Th)_2$), - 1019075 ($ZnTPP(NO_2)Br_2$), and -1019824 ($NiTPP(NO_2)Br_6$ contain the supplementary crystallographic data. The ground state geometries of mixed substituted free base porphyrins ($H_2TPP(NO_2)X_6$ and $H_2TPP(NO_2)X_2$) were optimized in the gas phase by DFT calculations with B3LYP functional and LANL2DZ basis set using Gaussian 09.

UV-Vis absorption spectra were measured in distilled dichloromethane using Shimadzu UV-1800 spectrometer at 298 K. The fluorescence spectra were carried out using Hitachi F-4600 spectroflurometer in CH_2Cl_2. All ^1H NMR measurements were performed using Bruker AVANCE 500 spectrometer in $CDCl_3$. MALDI-TOF-MS spectra were measured using a Bruker UltrafleXtreme-TN MALDI-TOF/TOF spectrometer using dithranol as a matrix and ESI mass spectra were recorded using Bruker Daltanics-microTOF. The elemental analysis was carried out on Elementarvario EL III instrument. Cyclic voltammetric measurements were carried out using BAS Epsilon and CH 620E electrochemical workstation. A three electrode system was used and consisted of a Pt button working electrode (0.2 mm diameter), Ag/AgCl reference electrode and a Pt-wire counter electrode. The concentrations of all porphyrins employed were ~1 mM. All measurements were performed in triple distilled CH_2Cl_2 solution which was purged with Ar gas, using 0.1 M $TBAPF_6$ as the supporting electrolyte.

The stoichiometry and binding constants for protonation were analyzed by Hill equation [14].

$\log[(A_n-A_0)/(A_f-A_n)] = \log\beta_2 + n\log[TFA]$

The Hill plot was constructed by plotting $\log[(A_n-A_0)/(A_f-A_n)]$ versus $\log[TFA]$ where A_0 and A_n are the absorbance values of porphyrin employed and protonated species, respectively at a given concentration of the TFA added. A_f denotes the absorbance of the diprotonated species at a particular wavelength. The slope of the line (n) was found to be two for one-to-two stoichiometry between the porphyrin and the added TFA. The value of $\log\beta_2$ is evaluated from the intercept of the line at $\log[(A_n-A_0)/(A_f-A_n)] = 0.0$. In the present study, the $\log\beta_2$ values were evaluated by using a minimum of two wavelengths and an average value of n and $\log\beta_2$ is reported. The similar methodology was employed for deprotonation studies also.

2.2.2 Synthesis of $MTPP(NO_2)X_2$ (X = Br, Ph, Th, PE and CN) derivatives:

(a) Synthesis of 2-nitro-12,13-dibromo-*meso*-tetraphenylporphyrin and its metal complexes
2-nitro-*meso*-tetraphenylporphyrin (0.220 g, 0.447 mmol, 1 equiv.) was taken in 45 mL of distilled $CHCl_3$. To this, freshly recrystallized NBS (0.148 g, 1.119 mmol) was added and

refluxed for 72 hrs. Solvent was rotary evaporated to dryness under vacuum. The crude porphyrin was purified on silica column using $CHCl_3$ as eluent. Yield was found to be 81% (0.220 g).

H₂TPP(NO₂)Br₂: ^{1}H NMR in $CDCl_3$: δ (ppm) 8.97 (s, 1H, β-pyrrole-H), 8.84 (t, 3H, J = 5 Hz, β-pyrrole-H), 8.78 (d, 1H, J = 4.5 Hz, β-pyrrole-H), 8.28 (d, 2H, J = 7 Hz, *meso-o*-phenyl-H), 8.22 (d, 2H, J = 7 Hz *meso-o*-phenyl-H), 8.16 (t, 4H, J = 8.5 Hz, *meso-o*-phenyl-H),7.85-7.70 (m, 12H, *meso-m*- and *p*-phenyl-H), -2.63 (bs, 1H, imino-H), -2.68 (bs, 1H, imino-H). ESI-MS (m/z): found 818.10 $[M+H]^+$, calcd. 818.22. Anal. Calcd for $C_{44}H_{27}N_5O_2Br_2$•0.5 $CHCl_3$: C, 60.93; H, 3.16; N, 7.98%. Found: C, 60.69; H, 3.34; N, 7.66%.

H₂TPP(NO₂)Br₂ (0.0183mmol) was dissolved in 10 mL of $CHCl_3$. To this, 10 equiv. of $M(OAc)_2$•nH_2O (M = Cu(II), Zn(II), Co(II), 10 equiv.) in 2 mL of methanol was added and refluxed for 40 minutes and then cooled to room temperature, washed with water, dried over anhydrous sodium sulphate. The crude product was purified by column chromatography on silica column using $CHCl_3$ as eluent. Further, Ni(II) complexes were prepared by refluxing $H_2TPP(NO_2)Br_2$ and $Ni(OAc)_2$•$4H_2O$ (10 equiv.) in DMF for 2 hours followed by the precipitation with water. The crude product was purified on silica column using $CHCl_3$ as eluent. Yield was found to be 80 - 90%.

NiTPP(NO₂)Br₂: ^{1}H NMR in $CDCl_3$: δ (ppm) 8.90 (s, 1H, β-pyrrole-H), 8.64 (d, 1H, J = 5 Hz, β-pyrrole-H), 8.58 (d, 1H, J = 5 Hz, β-pyrrole-H), 8.51 (d, 1H, J = 4.5 Hz, β-pyrrole-H), 8.45 (d, 1H, J = 5 Hz, β-pyrrole-H), 8.02-7.92 (m, 4H, *meso-o*-phenyl-H), 7.85 (d, 4H, J = 6.5 Hz, *meso-o*-phenyl-H), 7.75-7.59 (m, 12H, *meso-m*- and *p*-phenyl-H). MALDI-TOF-MS (m/z): found 874.54 $[M^+]$, calcd. 874.22. Anal. Calcd for $C_{44}H_{25}N_5O_2Br_2Ni$•$2H_2O$: C, 58.38; H, 2.67; N, 7.73%. Found: C, 58.11; H, 2.80; N, 7.47%. **CuTPP(NO₂)Br₂**: MALDI-TOF-MS (m/z): found 879.48 $[M^+]$, calcd., 879.07. **ZnTPP(NO₂)Br₂:** ^{1}H NMR in $CDCl_3$: δ (ppm) 9.14 (s, 1H, β-pyrrole-H), 8.85 (dd, 2H, Ja = 8 Hz, Jb = 4.5 Hz β-pyrrole-H), 8.81-8.75 (m, 2H, β-pyrrole-H), 8.16 (t, 4H, J = 6 Hz, *meso-o*-phenyl-H), 8.03 (d, 4H, J = 6.5 Hz, *meso-o*-phenyl-H), 7.84-7.64 (m, 12H, *meso-m*- and *p*-phenyl-H). MALDI-TOF-MS (m/z): found 881.25 $[M^+]$, calcd. 880.91. **CoTPP(NO₂)Br₂:** ESI-MS (m/z): found 873.99 $[M^+]$, calcd. 874.46.

(b) Synthesis of 2-nitro-12,13-diphenyl-*meso*-tetraphenylporphyrin and its metal complexes

Two-way stoppered RB flask was charged with $H_2TPP(NO_2)Br_2$ (0.16 g, 0.196 mmol), phenyl boronic acid (0.284 g, 2.33 mmol) and K_2CO_3 (0.648 g, 4.68 mmol). To this, 50 mL of distilled

toluene was added and purged with Ar gas for 10 minutes. Then Pd(PPh$_3$)$_4$(0.045 g, 0.039 mmol) was added under Ar and heated to 100 ℃ for 18 hrs. After completion of the reaction, the solvent was removed by rotary evaporation. The residue was redissolved in CHCl$_3$ (50 mL) and washed with saturated NaHCO$_3$ (50 ml) followed by 30% NaCl solution (50 ml). Finally, the organic layer was dried over anhydrous Na$_2$SO$_4$. The crude product was purified on silica column using variant polarity from CHCl$_3$/hexane mixture (3:1, v/v) to 100% CHCl$_3$ as eluent. The desired product was recrystallised from CHCl$_3$/CH$_3$OH mixture (1:3, v/v). The yield was found to be 0.130 g (71%).

H$_2$TPP(NO$_2$)Ph$_2$: ^{1}H NMR in CDCl$_3$: δ (ppm) 8.98 (s, 1H, β-pyrrole-H), 8.81 (d, 1H, J = 5 Hz, β-pyrrole-H), 8.78 (d, 1H, J = 5 Hz, β-pyrrole-H), 8.58 (t, 2H, J = 5 Hz, β-pyrrole-H), 8.30 (dd, 2H, J = 7.5 Hz, J = 1.5 Hz, *meso-o*-phenyl-H), 8.23 (dd, 2H, J = 7.5 Hz, J = 1.5 Hz, *meso-o*-phenyl-H), 7.85 (d, 2H, J = 6.5 Hz, *meso-o*-phenyl-H), 7.80 (t, 5H, J = 8.0 Hz, *meso-o and m*-phenyl-H), 7.74 (d, 3H, J = 7.5 Hz, *meso-o* and *m*-phenyl-H), 7.33-7.21 (m, 6H, *meso-m-* and *p*-phenyl-H), 6.90-6.80 (m, 10H, β-pyrrolePh-H), -2.31 (bs, 1H, imino-H). ESI-MS (m/z): found 812.34 [M$^+$], calcd. 812.39. Anal. Calcd for C$_{56}$H$_{37}$N$_5$O$_2$: C, 82.84; H, 4.59; N, 8.62%. Found: C, 82.98; H, 4.27; N, 8.34%.

The metal complexes were prepared with similar procedures of the corresponding metal complexes of MTPP(NO$_2$)Br$_2$. The yield was found to be 85 - 95%. **NiTPP(NO$_2$)Ph$_2$:** ^{1}H NMR in CDCl$_3$: δ (ppm) 8.92 (s, 1H, β-pyrrole-H), 8.54 (d, 1H, J = 5 Hz, β-pyrrole-H), 8.42 (d, 1H, J = 5 Hz, β-pyrrole-H), 8.29 (d, 1H, J = 5 Hz, β-pyrrole-H), 8.23 (d, 1H, J = 5 Hz, β-pyrrole-H), 8.00-7.94 (m, 4H, *meso-o*-phenyl-H), 7.73-7.58 (m, 6H, *meso-m*-phenyl-H), 7.48 (d, 2H, J = 7.0 Hz, *meso-o*-phenyl-H), 7.42 (d, 2H, J = 7.0 Hz, *meso-o*-phenyl-H), 7.19 (AB quartet, 2H, J = 8.0 Hz, *meso-m*-phenyl-H), 7.09 (t, 4H, J = 7.5 Hz, *meso-p*-phenyl-H), 6.95-6.76 (m, 10H, β-pyrrolePh-H). MALDI-TOF-MS (m/z): found 868.98 [M$^+$], calcd. 868.62. Anal. Calcd for C$_{56}$H$_{35}$N$_5$O$_2$Ni•0.5CH$_3$OH: C, 76.71; H, 4.22; N, 4.52%. Found: C, 76.98; H, 4.36; N, 4.74%.

ZnTPP(NO$_2$)Ph$_2$: ^{1}H NMR in CDCl$_3$: δ (ppm) 9.12 (s, 1H, β-pyrrole-H), 8.80 (d, 1H, J = 5 Hz, β-pyrrole-H), 8.755 (d, 1H, J = 4.5 Hz, β-pyrrole-H), 8.53-8.51 (m, 2H, β-pyrrole-H), 8.21 (d, 2H, J = 7 Hz, *meso-o*-phenyl-H), 8.18 (d, 2H, J = 6.5 Hz, *meso-o*-phenyl-H), 7.80-7.70 (m, 8H, *meso-o*-phenyl-H), 7.67 (at, 2H, J = 7.5 Hz, *meso-m*-phenyl-H), 7.24-7.22 (m, 2H, *meso-m*-phenyl-H), 7.15 (dt, 4H, J = 7.5Hz, J = 2.5Hz, *meso-p*-phenyl-H), 6.93 (d, 4H, J = 7.5 H, β-pyrrolePh-*o*-H), 6.90-6.80 (m, 6H, β-pyrrolePh-*m-* and *p*-H). MALDI-TOF-MS (m/z): found

875.51 [M$^+$], calcd. 875.32. Anal. Calcd for $C_{56}H_{35}N_5O_2Zn$: C, 76.84; H, 4.03; N, 8.00%. Found: C, 76.69; H, 4.04; N, 7.78%. **CuTPP(NO$_2$)Ph$_2$:** Anal. Calcd for $C_{56}H_{35}N_5O_2Cu$: C, 75.61; H, 4.34; N, 7.73%. Found: C, 75.52; H, 4.26; N, 7.44%. MALDI-TOF-MS (m/z): found 873.91 [M$^+$], calcd. 873.47. **CoTPP(NO$_2$)Ph$_2$:** ESI-MS (m/z): found 868.23 [M$^+$], calcd., 868.86.

(c) Synthesis of 2-nitro-12,13-diphenylethynyl-*meso*-tetraphenylporphyrin and its metal complexes

H$_2$TPP(NO$_2$)Br$_2$ (0.3 g, 0.366 mmol), Pd(PPh$_3$)$_4$ (0.084 g, 0.073 mmol) were dissolved in distilled 1,4-dioxane (90 mL) and purged with argon gas for 15 minutes. To this, tributyl(phenylethynyl)stannane (0.406 mL, 1.158 mmol) in 42 mL of degassed dioxane was added and heated to 80℃ for 3 hrs under argon atmosphere. After completion of the reaction, the solvent was removed by vacuum distillation. The crude porphyrin was redissolved in CHCl$_3$ (20 mL) and purified on silica column using variant polarity from CHCl$_3$/hexane mixture (3:2, v/v) to 100% CHCl$_3$ as eluent. The desired product was recrystallised from CHCl$_3$/CH$_3$OH mixture (1:3, v/v) containing one drop of Et$_3$N. The yield was found to be 0.210 g (73%).

H$_2$TPP(NO$_2$)(PE)$_2$: ^{1}H NMR in CDCl$_3$: δ (ppm) 8.99 (s, 1H, β-pyrrole-H), 8.90 (d, 1H, J = 4.5 Hz, β-pyrrole-H), 8.86 (d, 1H, J = 5 Hz, β-pyrrole-H), 8.77 (d, 1H, J = 5.5 Hz, β-pyrrole-H), 8.76 (d, 1H, J = 5 Hz, β-pyrrole-H), 8.30-8.18 (m, 8H, *meso-o*-phenyl-H), 7.85-7.68 (m, 12H, *meso-m and p*-phenyl-H), 7.38-7.26 (m, 10H, β-pyrrole-PE-H), -2.51 (s, 1H, imino-H), -2.54 (s, 1H, imino-H). ESI-MS (m/z): found 860.27 [M$^+$], calcd. 859.99. Anal. Calcd for $C_{60}H_{37}N_5O_2 \bullet 2H_2O$: C, 80.43; H, 4.61; N, 7.82%. Found: C, 80.83; H, 4.37; N, 7.83%. The metal complexes were prepared with similar procedures of the corresponding metal complexes of MTPP(NO$_2$)Br$_2$ and the yields were found to be 80 - 85%.

NiTPP(NO$_2$)(PE)$_2$: ^{1}H NMR in CDCl$_3$: δ (ppm) 8.91 (s, 1H, β-pyrrole-H), 8.61 (d, 1H, J = 5 Hz, β-pyrrole-H), 8.60 (d, 1H, J = 5.5 Hz, β-pyrrole-H), 8.52 (d, 1H, J = 5 Hz, β-pyrrole-H), 8.45 (d, 1H, J = 5 Hz, β-pyrrole-H), 8.02-7.94 (m, 8H, *meso-o*-phenyl-H), 7.75-7.58 (m, 12H, *meso-m and p*-phenyl-H), 7.33-7.26 (m, 10H, β-pyrrole-PE-H). MALDI-TOF-MS (m/z): found 917.02 [M$^+$], calcd. 916.66. Anal. Calcd for $C_{60}H_{35}N_5O_2Ni$: C, 78.62; H, 3.85; N, 7.64%. Found: C, 78.58; H, 3.94; N, 7.47%. **ZnTPP(NO$_2$)(PE)$_2$:** ^{1}H NMR in CDCl$_3$: δ (ppm) 9.14 (s, 1H, β-pyrrole-H), 8.88 (d, 1H, J = 5 Hz, β-pyrrole-H), 8.85 (d, 1H, J = 5 Hz, β-pyrrole-H), 8.74 (d, 1H, J = 4.5 Hz, β-pyrrole-H), 8.73 (d, 1H, J = 4.5 Hz, β-pyrrole-H), 8.21-8.13 (m, 8H, *meso-o*-phenyl-H), 7.82-7.64 (m, 12H, *meso-m and p*-phenyl-H), 7.40-7.34 (m, 4H, β-pyrrole-*o*-PE-H),

7.31-7.26 (m, 6H, *β*-pyrrole-*m and p*-PE-H). MALDI-TOF-MS (m/z): found 923.46 [M$^+$], calcd. 923.36. Anal. Calcd for $C_{60}H_{35}N_5O_2Zn \bullet H_2O$: C, 76.55; H, 3.96; N, 7.44%. Found: C, 76.24; H, 3.79; N, 7.29%. **CuTPP(NO$_2$)(PE)$_2$:** MALDI-TOF-MS (m/z): found 921.98 [M$^+$], calcd. 921.52. Anal. Calcd. for $C_{60}H_{35}N_5O_2Cu$: C, 78.42; H, 3.92; N, 7.51%. Found: C, 78.20; H, 3.83; N, 7.60%. **CoTPP(NO$_2$)(PE)$_2$:** ESI-MS (m/z): found 916.25 [M$^+$], calcd., 916.90. Anal. Calcd. for $C_{60}H_{35}N_5O_2Co \bullet 2H_2O$: C, 75.62; H, 4.13; N, 7.35%. Found: C, 75.45; H, 3.87; N, 7.31%.

(d) Synthesis of 2-nitro-12,13-dithienyl-*meso*-tetraphenylporphyrin and its metal complexes:

$H_2TPP(NO_2)Br_2$ (0.15 g, 0.183 mmol), thiophene-2-boronic acid (0.117 g, 0.914 mmol) and K_2CO_3 (0.609 g, 4.40 mmol) were taken in a two-way stoppered RB flask. To this, 60 mL of distilled toluene was added and purged with Ar gas for 10 minutes. Then Pd(PPh$_3$)$_4$ (0.042 g, 0.036 mmol) was added under Ar and heated to 90°C for 10 hrs. After completion of the reaction, the solvent was removed by rotary evaporation. The crude porphyrin was redissolved in CHCl$_3$ (50 mL) and washed with saturated NaHCO$_3$ (50 mL) followed by 30% NaCl solution (50 mL). Finally, the organic layer was dried over anhydrous Na$_2$SO$_4$. The crude product was purified on silica column using variant polarity from CHCl$_3$ to 2% EtOAc/CHCl$_3$ as eluent. The desired product was recrystallised from CHCl$_3$/CH$_3$OH mixture (1:3, v/v). The yield was found to be 0.085 g (56%).

H$_2$TPP(NO$_2$)Th$_2$: ^{1}H NMR in CDCl$_3$: δ (ppm) 8.96 (s, 1H, *β*-pyrrole-H), 8.77 (t, 2H, *J* = 5.5 Hz, *β*-pyrrole-H), 8.68-8.59 (m, 2H, *β*-pyrrole-H), 8.30 (d, 2H, *J* = 6.5 Hz, *meso-o*-phenyl-H) , 8.24 (d, 2H, *J* = 7 Hz, *meso-o*-phenyl-H), 7.99 (d, 2H, *J* = 7 Hz, *meso-o*-phenyl-H), 7.95 (d, 2H, *J* = 7 Hz, *meso-o*-phenyl-H), 7.84-7.70 (m, 6H, *meso-m and p*-phenyl-H), 7.46- 7.35 (m, 6H, *meso-m and p*-phenyl-H), 6.98 (s, 2H, *β*-pyrroleTh-H), 6.64-6.57 (m , 3H, *β*-pyrroleTh-H), 6.56 (s, 1H, *β*-pyrroleTh-H), -2.24 (s, 2H, imino-H). ESI-MS (m/z): found 824.23 [M$^+$], calcd. 824.00. Anal. Calcd for $C_{52}H_{33}N_5O_2S_2 \bullet 2H_2O$: C, 72.62; H, 4.34; N, 8.14; S, 7.46%. Found: C, 72.94; H, 4.22; N, 7.91; S, 7.16%.

The metal complexes were prepared with similar procedures of the corresponding metal complexes of MTPP(NO$_2$)Br$_2$ and the yields were found to be almost quantitative.

NiTPP(NO$_2$)Th$_2$: ^{1}H NMR in CDCl$_3$: δ (ppm) 8.90 (s, 1H, *β*-pyrrole-H), 8.53 (d, 1H, *J* = 5 Hz, *β*-pyrrole-H), 8.43 (d, 1H, *J* = 5 Hz, *β*-pyrrole-H), 8.36 (d, 1H, *J* = 5 Hz, *β*-pyrrole-H), 8.29 (d, 1H, *J* = 5 Hz, *β*-pyrrole-H), 8.02-7.96 (m, 4H, *meso-o*-phenyl-H), 7.74-7.55 (m, 10H, *meso-o*-

and m-phenyl-H), 7.37-7.26 (m, 3H, *meso-m- and p*-phenyl-H), 7.24-7.21 (m, 3H, *meso-p*-phenyl-H), 7.06 (d, 1H, *J* = 4.5 Hz, *β*-pyrroleTh-H), 7.02 (d, 1H, *J* = 5 Hz, *β*-pyrroleTh-H), 6.60 (t, 1H, *J* = 4.5 Hz, *β*-pyrroleTh-H), 6.53 (t, 1H, *J* = 4 Hz, *β*-pyrroleTh-H), 6.47 (d, 1H, *J* = 2.5 Hz, *β*-pyrroleTh-H), 6.36 (d, 1H, *J* = 2.5 Hz, *β*-pyrroleTh-H). MALDI-TOF-MS (m/z): found 880.94 [M$^+$], calcd. 880.68. **ZnTPP(NO$_2$)Th$_2$:** ^{1}H NMR in CDCl$_3$: δ (ppm) 9.15 (s, 1H, *β*-pyrrole-H), 8.82 (d, 1H, *J* = 4.5 Hz, *β*-pyrrole-H), 8.79 (d, 1H, *J* = 4.5 Hz, *β*-pyrrole-H), 8.60 (t, 2H, *J* = 5 Hz, *β*-pyrrole-H), 8.18 (t, 4H, *J* = 8.5 Hz, *meso-o*-phenyl-H), 7.86 (t, 4H, *J* = 8 Hz *meso-o*-phenyl-H), 7.81-7.72 (m, 4H, *meso-m*-phenyl-H), 7.68 (t, 2H, *J* = 7.5 Hz *meso-m*-phenyl-H), 7.42-7.35 (m, 2H, *meso-m*-phenyl-H), 7.33- 7.28 (m, 4H, *meso-p*-phenyl-H), 7.04 (d, 2H, *J* = 5 Hz, *β*-pyrroleTh-H), 6.66-6.56 (m, 4H, *β*-pyrroleTh-H). MALDI-TOF-MS (m/z): found 887.59 [M$^+$], calcd. 887.37. **CuTPP(NO$_2$)Th$_2$:** MALDI-TOF-MS (m/z): found 885.89 [M$^+$], calcd. 885.53. Anal. Calcd for C$_{52}$H$_{31}$N$_5$O$_2$S$_2$Cu: C, 70.53; H, 3.53; N, 7.91; S, 7.24%. Found: C, 70.64; H, 3.56; N, 7.97; S, 7.51%. **CoTPP(NO$_2$)Th$_2$:** ESI-MS (m/z): found 880.16 [M$^+$], calcd. 880.13. Anal. Calcd for C$_{52}$H$_{31}$N$_5$O$_2$S$_2$Co•0.5CHCl$_3$: C, 67.34; H, 3.38; N, 7.45; S, 6.82%. Found: C, 67.46; H, 3.42; N, 7.41; S, 6.55%.

(e) Synthesis of 2-nitro-12,13-dicyano-*meso*-tetraphenylporphyrinato Nickel(II)

NiTPP(NO$_2$)Br$_2$ (0.15 g, 0.172 mmol) and copper(I)cyanide (0.307 g, 3.43 mmol) was taken in 100 mL two neck RB and to it was added 10 mL of quinoline. The reaction mixture was refluxed at 200°C for 2 hours. At the end of this period the reaction mixture was cooled and filtered through G-4 crucible to remove excess copper cyanide. 30 mL of CHCl$_3$ was added and organic phase was washed with 10% HCl (3 × 50 mL), water (2 times), dried over Na$_2$SO$_4$ and then evaporated to dryness. The crude product was loaded on silica column and purified using CHCl$_3$ as eluent. NiTPP(NO$_2$)CN was obtained as first fraction in 24% yield followed by NiTPP(NO$_2$)(CN)$_2$ in 61% yield.

NiTPP(NO$_2$)(CN)$_2$: ^{1}H NMR in CDCl$_3$: δ (ppm) 9.22 (s, 1H, *β*-pyrrole-H), 8.84-8.69 (m, 3H, *β*-pyrrole-H), 8.62 (d, 1H, *J* = 5 Hz, *β*-pyrrole-H), 7.92-7.81 (m, 11H, *meso-o- and m*-phenyl-H), 7.76-7.67 (m, 9H, *meso-m- and p*-phenyl-H). MALDI-TOF-MS (m/z): found 766.82 [M$^+$], calcd. 766.44.

(f) Synthesis of 2-nitro-12,13-dicyano-*meso*-tetraphenylporphyrin and it metal complexes

NiTPP(NO$_2$)(CN)$_2$ (0.07 g, 0.091 mmol) was taken in 20 mL of CHCl$_3$ and to it was added 0.1 mL of conc. H$_2$SO$_4$ dropwise, stirred vigorously at 0°C for 2 hours. At the end of this period,

distilled water (40 mL) was added dropwise to the reaction mixture with constant stirring. The organic layer was separated and washed with water (2×30 mL) followed by neutralization using 25% aqueous ammonia solution (20 mL). The organic layer was dried over anhydrous Na_2SO_4 and concentrated to small volume. This was purified by silica gel chromatograpy using $CHCl_3$ as eluent and the yield of the product was found to be 0.05 g (77%).

$H_2TPP(NO_2)(CN)_2$: ^1H NMR in $CDCl_3$: δ (ppm) 9.33 (s, 1H, β-pyrrole-H), 9.02-8.94 (m, 3H, β-pyrrole-H), 8.91 (d, 1H, J = 5 Hz, β-pyrrole-H), 8.20-8.10 (m, 8H, *meso-o*-phenyl-H), 7.99-7.91 (m, 3H, *meso-m-* and *p*-phenyl-H), 7.88-7.77 (m, 9H, *meso-m-* and *p*-phenyl-H), -2.52(s, 2H, imino-H). ESI-MS (m/z): found 711.00 [M+H]$^+$, calcd. 710.77. Anal. Calcd for $C_{46}H_{27}N_7O_2$: C, 77.84; H, 3.83; N, 13.81%. Found: C, 77.66; H, 4.13; N, 13.52%.

$MTPP(NO_2)(CN)_2$ (M = Co(II), Cu(II) and Zn(II)) were prepared with similar procedures of the corresponding metal complexes of $MTPP(NO_2)Br_2$ and the yields were found to be 80 - 90%.

$ZnTPP(NO_2)(CN)_2$: ^1H NMR in $CDCl_3$: δ (ppm) 9.35 (s, 1H, β-pyrrole-H), 8.89-8.79 (m, 3H, β-pyrrole-H), 8.77 (br s, 1H, β-pyrrole-H), 8.15-7.98 (m, 8H *meso-o*-phenyl-H), 7.92-7.69 (m, 12H, *meso-m-* and *p*-phenyl-H). MALDI-TOF-MS (m/z): found 773.36 [M$^+$], calcd., 773.14.

$CuTPP(NO_2)(CN)_2$: MALDI-TOF-MS (m/z): 710.02 (calcd.,771.30). $C_{46}H_{25}N_7O_2Cu \bullet 0.5H_2O$: C, 70.81; H, 3.36; N, 12.57%. Found: C, 70.92; H, 3.50; N, 12.69%. **$CoTPP(NO_2)(CN)_2$:** MALDI-TOF-MS (m/z): found 766.19 [M$^+$], calcd. 766.14. Anal. Calcd for $C_{46}H_{25}N_7O_2Co \bullet H_2O$: C, 70.41; H, 3.47; N, 12.50%. Found: C, 70.64; H, 3.25; N, 12.32%.

2.2.3 Synthesis of $MTPP(NO_2)X_6$ (X = Br, Ph, Th and PE) derivatives:

(a) Synthesis of 2-nitro-7,8,12,13,17,18-hexabromo-*meso*-tetraphenylporphyrinato Copper(II):[21c]

$CuTPP(NO_2)$ (0.3 g, 0.416 mmol) was taken in 40 mL of distilled 1,2-dichloroethane in a 100 mL RB. To this, recrystallized NBS (0.74 g, 4.16 mmol) was added and refluxed for 16 hrs at 80℃. At the end of the reaction, the solvent was removed by rotary evaporation and redissolved in $CHCl_3$ (25 mL). The crude product was purified on silica column using $CHCl_3$ as eluent and recrystallised from $CHCl_3/CH_3OH$ mixture (1:3, v/v). The yield was found to be 0.28 g (81%). MALDI-TOF-MS (m/z): found 1195.84 [M+H]$^+$, calcd. 1194.65. Anal. Calcd for $C_{44}H_{21}N_5Br_6O_2Cu \bullet 0.5H_2O$: C, 43.91; H, 1.84; N, 5.82%. Found: C, 43.76; H, 2.20; N, 5.28%.

(b) Synthesis of 2-nitro-7,8,12,13,17,18-hexabromo-*meso*-tetraphenylporphyrin and its metal complexes

CuTPP(NO$_2$)Br$_6$ (0.25 g, 0.209 mmol) was dissolved in 40 mL of CHCl$_3$. To this, 1.5 mL of conc. H$_2$SO$_4$ was added dropwise and stirred vigorously at 0°C for 1 hour. At the end of this period, distilled water (80 mL) was added dropwise to the reaction mixture with stirring. The organic layer was separated and washed with water (2 × 50 mL) followed by neutralization using aquous ammonia (25%) solution (20 mL). The organic layer was dried over anhydrous Na$_2$SO$_4$ and concentrated to small volume. This was purified by silica gel chromatography using CHCl$_3$ as eluent, and the yield of the product was found to be 92%.

H$_2$TPP(NO$_2$)Br$_6$: ^{1}H NMR in CDCl$_3$: δ (ppm) 8.59 (s, 1H, β-pyrrole-H), 8.24 (d, 4H, J = 7 Hz, *meso-o*-phenyl-H), 8.20 (ad, 4H, J = 7 Hz, *meso-o*-phenyl-H), 7.87-7.76 (m, 10H, J = 8.5 Hz, *meso-m*- and *p*-phenyl-H), 7.74 (t, 2H, J = 7.5 Hz, *meso-p*-phenyl-H). MALDI-TOF-MS (m/z): found 1133.51 [M[+]], calcd. 1133.12.

The metal complexes were prepared with similar procedures of the corresponding metal complexes of MTPP(NO$_2$)Br$_2$ and the yields were found to be 84 - 90%. **NiTPP(NO$_2$)Br$_6$:** ^{1}H NMR in CDCl$_3$: δ (ppm) 8.50 (s, 1H, β-pyrrole-H), 7.97 (d, 2H, J = 7 Hz, *meso-o*-phenyl-H), 7.96-7.89 (m, 6H, *meso-o*-phenyl-H), 7.79-7.62 (m, 12H, *meso-m*- and *p*-phenyl-H). MALDI-TOF-MS (m/z): found 1190.12 [M[+]], calcd. 1189.80. Anal. Calcd for C$_{44}$H$_{21}$Br$_6$N$_5$O$_2$Ni: C, 44.42; H, 1.78; N, 5.89%. Found: C, 44.12; H, 1.92; N, 5.66%. **ZnTPP(NO$_2$)Br$_6$:** ^{1}H NMR in CDCl$_3$: δ (ppm) 8.74 (s, 1H, β-pyrrole-H), 8.17 (t, 4H, J = 8 Hz, *meso-o*-phenyl-H), 8.11 (t, 4H, J = 8.5 Hz, *meso-o*-phenyl-H), 7.86-7.72 (m, 10H, *meso-m*- and *p*-phenyl-H), 7.69 (t, 2H, J = 7.5 Hz, *meso-p*-phenyl-H). MALDI-TOF-MS (m/z): found 1196.67 [M[+]], calcd. 1196.50. **CoTPP(NO$_2$)Br$_6$:** MALDI-TOF-MS (m/z): found 1190.57 [M[+]], calcd. 1190.04.

(b) Synthesis of 2-nitro-7,8,12,13,17,18-hexaphenyl-*meso*-tetraphenylporphyrin and its metal complexes:

H$_2$TPP(NO$_2$)Br$_6$ (0.3 g, 0.264 mmol), phenylboronic acid (0.774 g, 6.33 mmol) and K$_2$CO$_3$ (1.76 g, 12.67 mmol) were taken in a two-neck RB flask. To this, 120 mL of distilled toluene was added and purged with Ar gas for 15 minutes. Then Pd(PPh$_3$)$_4$ (0.061 g, 0.05 mmol) was added under Ar and heated to 100℃ for 15 hrs. After completion of the reaction, the solvent was removed by rotary evaporation. The crude porphyrin was redissolved in CHCl$_3$ (80 mL) and washed with saturated NaHCO$_3$ (70 mL) followed by 30% NaCl solution (50 mL). Finally, the

organic layer was dried over anhydrous Na_2SO_4. The crude product was purified on silica column using variant polarity from $CHCl_3$ to 5 - 8% EtOAc in $CHCl_3$ as eluent. The desired product was recrystallised from $CHCl_3/CH_3OH$ mixture (1:3, v/v). The yield was found to be 0.23 g (78%).

$H_2TPP(NO_2)Ph_6$: ^1H NMR in $CDCl_3$: δ (ppm) 8.31 (s, 1H, β-pyrrole-H), 8.03 (d, 2H, J = 7 Hz, *meso-o*-phenyl-H), 7.85 (d, 2H, J = 7 Hz, *meso-o*-phenyl-H), 7.58 (d, 2H, J = 7.5 Hz, *meso-o*-phenyl-H), 7.56 (d, 2H, J = 8 Hz, *meso-o*-phenyl-H), 7.39-7.18 (m, 5H, *meso-m*-phenyl-H), 6.96-6.58 (m, 33H, β-pyrrolePh-H, *meso-m*- and *p*-phenyl-H), 6.5 (d, 4H, J = 7 Hz, β-pyrrole Ph-H). ESI-MS (m/z): found 1176.38 [M•Na•K-H]$^+$, calcd. 1177.37. Anal. Calcd for $C_{80}H_{53}N_5O_2$: C, 86.07; H, 4.79; N, 6.27%. Found: C, 86.01; H, 4.93; N, 6.15%.

The metal complexes were prepared with similar procedures of the corresponding metal complexes of $MTPP(NO_2)Br_2$ and crude products were purified by silica gel (for Co (II), Ni(II) and Cu(II)) or alumina for $ZnTPP(NO_2)Ph_6$ column chromatography using $CHCl_3$/5 - 6% EtOAc in $CHCl_3$ as eluent. The desired product was recrystallised from $CHCl_3/CH_3OH$ mixture (1:3, v/v) containing a drop of Et_3N. The yield was found to be 80-86%.

$NiTPP(NO_2)Ph_6$: ^1H NMR in $CDCl_3$: δ (ppm) 8.37 (s, 1H, β-pyrrole-H), 7.60 (dd, 2H, J = 7Hz,J = 1 Hz, *meso-o*-phenyl-H), 7.57 (dd, 2H, J = 7Hz,J = 1 Hz, *meso-o*-phenyl-H), 7.25-7.12 (m, 4H, *meso-o*-phenyl-H), 7.06 (t, 2H, J = 7.5 Hz, *meso-m*-phenyl-H), 7.03 (t, 4H, J = 7.0 Hz, *meso-m*-phenyl-H), 6.88-6.50 (m, 36H, β-pyrrolePh-H, *meso-m*- and *p*-phenyl-H). MALDI-TOF-MS (m/z): found 1173.12 [M$^+$], calcd. 1173.01. **$ZnTPP(NO_2)Ph_6$:** ^1H NMR in $CDCl_3$: δ (ppm) 8.57 (s, 1H, β-pyrrole-H), 7.93 (d, 2H, J = 7 Hz, *meso-o*-phenyl-H), 7.78 (d, 2H, J = 7 Hz, *meso-o*-phenyl-H), 7.44 (d, 2H, J = 7 Hz, *meso-o*-phenyl-H), 7.42 (d, 2H, J = 7 Hz, *meso-o*-phenyl-H), 7.32-7.20 (m, 4H, J = 7.5 Hz, *meso-m*-phenyl-H), 7.16 (t, 2H, J = 8.0 Hz, *meso-m*-phenyl-H), 6.89-6.57 (m, 36H, β-pyrrolePh-H and *meso-m*- and *p*-phenyl-H). MALDI-TOF-MS (m/z): found 1179.62 [M$^+$], calcd. 1179.71. **$CuTPP(NO_2)Ph_6$:** MALDI-TOF-MS (m/z): found 1178.18 [M$^+$], calcd. 1177.86. Anal. Calcd for $C_{80}H_{51}N_5O_2Cu$: C, 78.13; H, 4.19; N, 5.66%. Found: C, 78.38; H, 4.30; N, 5.47%. **$CoTPP(NO_2)Ph_6$:** ESI-MS (m/z): found 1173.38 [M$^+$], calcd. 1173.25. Anal. Calcd for $C_{80}H_{51}N_5O_2Co$: C, 81.90; H, 4.38; N, 5.97%. Found: C, 81.98; H, 4.24; N, 5.74%.

(c) Synthesis of 2-nitro-7,8,12,13,17,18-hexaphenylethynyl-*meso*-tetraphenylporphyrin and its metal complexes

H$_2$TPP(NO$_2$)Br$_6$ (0.2 g, 0.176 mmol) and Pd(PPh$_3$)$_4$ (0.04 g, 0.035 mmol) were dissolved in distilled 1,4-dioxane and purged with Ar gas for 15 minutes. To this, tributyl(phenylethynyl)stannane (0.618 mL, 1.76 mmol) in 100 mL of degassed dioxane was added and heated to 80℃ for 40 minutes under Ar atmosphere. After completion of the reaction, the solvent was removed by vacuum distillation. The crude porphyrin was redissolved in CHCl$_3$ (20 mL) and purified on silica column using CHCl$_3$/hexane mixture (7:3, v/v) to 100% CHCl$_3$ as eluent. The desired product was recrystallised from CHCl$_3$/CH$_3$OH mixture (1:3, v/v) containing one drop of Et$_3$N. The yield was found to be 0.12 g (54%).

H$_2$TPP(NO$_2$)(PE)$_6$: ^{1}H NMR in CDCl$_3$: δ (ppm) 8.60 (bs, 1H, β-pyrrole-H), 8.44 (d, 2H, J = 6.5 Hz, *meso-o*-phenyl-H), 8.40 (d, 2H, J = 7.5 Hz, *meso-o*-phenyl-H), 8.28 (d, 2H, J = 7 Hz, *meso-o*-phenyl-H), 7.83-7.70 (m, 8H, *meso-m*-phenyl-H), 7.70-7.64 (m, 4H, *meso-p*-phenyl-H), 7.37-7.18 (m, 30H, β-pyrrole PE-H), -1.43 (bs, 2H, NH). ESI-MS (m/z): found 1261.47 [M+H]$^+$, calcd. 1261.47. Anal. Calcd for C$_{92}$H$_{53}$N$_5$O$_2$•1.5 H$_2$O: C, 85.83; H, 4.38; N, 5.44%. Found: C, 85.98; H, 4.33; N, 5.34%.

The metal complexes were prepared with similar procedures of the corresponding metal complexes of MTPP(NO$_2$)Br$_2$ and the yields were found to be 80 - 90%. **NiTPP(NO$_2$)(PE)$_6$:** ^{1}H NMR in CDCl$_3$: δ (ppm) 8.57 (s, 1H, β-pyrrole-H), 8.20 (d, 2H, J = 7 Hz, *meso-o*-phenyl-H), 8.17 (d, 2H, J = 7 Hz, *meso-o*-phenyl-H), 8.15-8.12 (m, 2H, *meso-o*-phenyl-H), 8.08 (d, 2H, J = 7 Hz, *meso-o*-phenyl-H), 7.75-7.64 (m, 10H, *meso-m-* and *p*-phenyl-H), 7.62-7.54 (m, 2H, *meso-p*-phenyl-H), 7.32-7.16 (m, 30H, β-pyrrole PE-H). MALDI-TOF-MS (m/z): found 1317.63 [M$^+$], calcd. 1317.14. Anal. Calcd for C$_{92}$H$_{51}$N$_5$O$_2$Ni: C, 83.89; H, 3.90; N, 5.32%. Found: C, 83.53; H, 4.04; N, 5.19%. **ZnTPP(NO$_2$)(PE)$_6$:** ^{1}H NMR in CDCl$_3$: δ (ppm) 8.81 (s, 1H, β-pyrrole-H), 8.34 (d, 2H, J = 7.5 Hz, *meso-o*-phenyl-H), 8.32-8.29 (m, 4H, *meso-o*-phenyl-H), 8.22 (d, 2H, J = 8.5 Hz, *meso-o*-phenyl-H), 7.78-7.66 (m, 10H, *meso-m-* and *p*-phenyl-H), 7.62 (dt, 2H, J = 5 Hz, J = 2 Hz, *meso-p*-phenyl-H), 7.40-7.18 (m, 30H, β-pyrrole PE-H). MALDI-TOF-MS (m/z): found 1324.17 [M$^+$], calcd. 1323.84. **CuTPP(NO$_2$)(PE)$_6$:** MALDI-TOF-MS (m/z): found 1322.38 [M$^+$], calcd. 1322.00. Anal. Calcd for C$_{92}$H$_{51}$N$_5$O$_2$Cu•1.5H$_2$O: C, 81.97; H, 4.19; N, 5.11%. Found: C, 81.79; H, 3.96; N, 5.12%. **CoTPP(NO$_2$)(PE)$_6$:** ESI-MS (m/z): found 1317.41 [M$^+$], calcd. 1317.38. Anal. Calcd for C$_{92}$H$_{51}$N$_5$O$_2$Co: C, 83.88; H, 3.90; N, 5.31%. Found: C, 83.74; H, 3.73; N, 5.44%.

(d) Synthesis of 2-nitro-7,8,12,13,17,18-hexa(2-thienyl)-*meso*-tetraphenylporphyrin

H$_2$TPP(NO$_2$)Br$_6$ (0.070 g, 0.0617 mmol), thiophene-2-boronic acid (0.189 g, 1.477 mmol) and K$_2$CO$_3$ (0.252 g, 1.823 mmol) were taken in two-neck RB flask. To this, 35 mL of distilled toluene was added and purged with Ar gas for 15 minutes. Then Pd(PPh$_3$)$_4$(0.014 g, 0.012 mmol) was added under Ar and heated to 90℃ for 15 hrs. After completion of the reaction, the solvent was removed by rotary evaporation. The crude porphyrin was redissolved in CHCl$_3$ (30 mL) and washed with saturated NaHCO$_3$ (25 mL) followed by 30% NaCl solution (25 mL). Finally, the organic layer was dried over anhydrous Na$_2$SO$_4$.The crude product was purified on silica column using variant polarity from CHCl$_3$ to 5-8% EtOAc in CHCl$_3$ as eluent. The desired product was recrystallised from CHCl$_3$/CH$_3$OH mixture (1:3, v/v). The yield was found to be 0.036 g (51%).

H$_2$TPP(NO$_2$)Th$_6$: ^{1}H NMR in CDCl$_3$: δ (ppm) 8.28 (s, 1H, β-pyrrole-H), 7.82 (d, 1H, J = 6.5 Hz, *meso-o*-phenyl-H), 7.98 (d, 1H, J = 6.5 Hz, *meso-o*-phenyl-H), 7.94 - 7.78 (m, 3H, *meso-o*-phenyl-H), 7.74 (s, 1H, *meso-o*-phenyl-H), 7.73 (s, 1H, *meso-o*-phenyl-H), 7.66 - 7.55 (m, 4H, *meso-o*-phenyl and *meso-m*-phenyl), 7.52 - 7.37 (m, 9H, *meso-m- and p*-phenyl), 7.37-7.27 (m, 2H, β-pyrroleTh-H), 7.15-6.96 (m, 6H, β-pyrroleTh-H), 6.95 - 6.84 (m, 2H, β-pyrroleTh-H), 6.80 - 6.25 (m, 8H, β-pyrroleTh-H). MALDI-TOF-MS (m/z): found 1152.21 [M$^+$], calcd. 1152.50. Anal. Calcd for C$_{68}$H$_{41}$N$_5$O$_2$S$_6$•0.5H$_2$O: C, 70.32; H, 3.64; N, 6.03; S, 16.56%. Found: C, 70.39; H, 3.80; N, 5.90; S, 16.55%.

The metal complexes were prepared with similar procedures of the corresponding metal complexes of MTPP(NO$_2$)Br$_2$ and the yields were found to be 80 - 90%. **NiTPP(NO$_2$)Th$_6$:** ^{1}H NMR in CDCl$_3$: δ (ppm) 8.39 (s, 1H, β-pyrrole-H), 7.82-7.63 (m, 6H, *meso-o*-phenyl-H), 7.41-7.28 (m, 8H, *meso-o- and m*-phenyl-H), 7.25-7.18 (m, 2H, *meso-m*-phenyl-H), 7.01-6.80 (m, 11H, *meso-p*-phenyl and β-pyrroleTh-H), 6.55- 6.17 (m, 11H, β-pyrroleTh-H). MALDI-TOF-MS (m/z): found 1209.50 [M$^+$], calcd. 1209.18. Anal. Calcd for C$_{68}$H$_{39}$N$_5$O$_2$S$_6$Ni•0.5H$_2$O: C, 64.84; H, 3.14; N, 5.52; S, 15.16%. Found: C, 64.69; H, 3.50; N, 5.20; S, 15.35%. **ZnTPP(NO$_2$)Th$_6$:** ^{1}H NMR in CDCl$_3$: δ (ppm) 8.50 (s, 1H, β-pyrrole-H), 8.09 (d, 2H, J = 7 Hz, *meso-o*-phenyl-H), 7.97 (d, 2H, J = 6.5 Hz, *meso-m*-phenyl-H), 7.84 - 7.73 (m, 4H, *meso-o*-phenyl-H), 7.44 - 7.28 (m, 6H, *meso-m*-phenyl), 7.08 - 6.89 (m, 8H, *meso-m*- and *p*-phenyl, β-pyrroleTh-H), 6.88 - 6.75 (m, 4H, β-pyrroleTh-H), 6.65 - 6.29 (m, 12H, β-pyrroleTh-H). MALDI-TOF-MS (m/z): found 1216.36 [M$^+$], calcd. 1215.88. **CuTPP(NO$_2$)Th$_6$:** MALDI-TOF-MS (m/z): found 1214.49 [M$^+$], calcd. 1214.03. Anal. Calcd for C$_{68}$H$_{39}$N$_5$O$_2$S$_6$Cu: C, 64.84; H, 3.24; N, 5.77; S, 15.85%. Found: C, 64.65; H, 3.50; N, 5.89; S, 15.67%. **CoTPP(NO$_2$)Th$_6$:** ESI-MS (m/z): found 1208.11 [M$^+$],

calcd. 1208.08. Anal. Calcd for $C_{68}H_{39}N_5O_2S_6Co$: C, 67.53; H, 3.25; N, 5.79; S, 15.91%. Found: C, 67.74; H, 3.42; N, 5.81; S, 15.45%.

2.3 RESULTS AND DISCUSSION

2.3.1 Synthesis and characterization
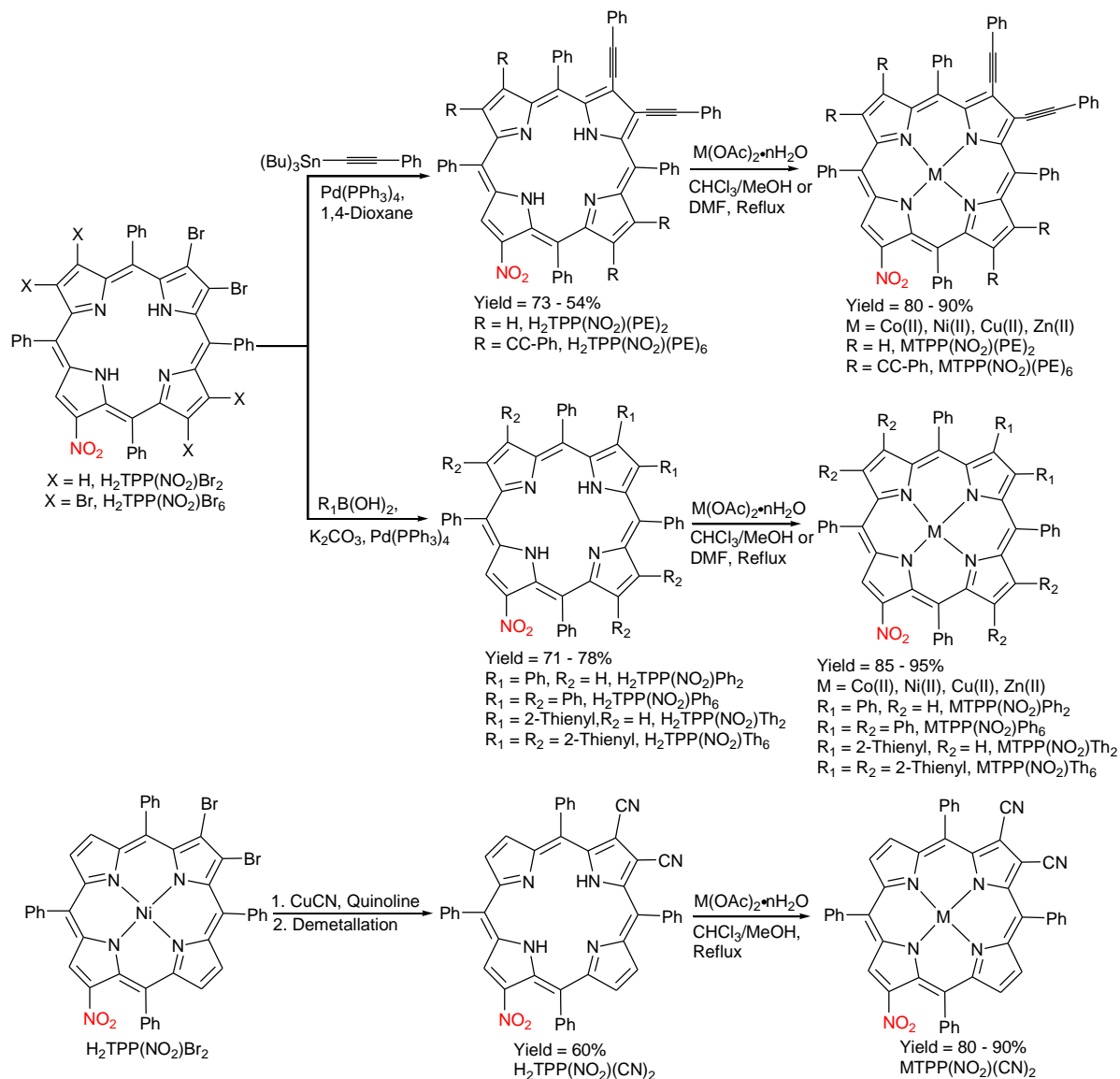
Scheme 1. Synthetic routes for various mixed substituted porphyrins.

Two new families of *β*-pyrrole mixed substituted porphyrins, viz. *β*-tri- and hepta-substituted *meso*-tetraphenylporphyrins (MTPP(NO$_2$)X$_n$, n = 2, 6) were synthesized and characterized. 2-Nitro-*meso*-TPPs are versatile precursors in porphyrin chemistry due to their excellent stability

towards demetallation/metallation sequences [10] and can be prepared in high yields (70-80%). The regioselective bromination of 2-nitro-*meso*-TPP afforded 2-nitro-12,13-dibromo-*meso*-TPP (H$_2$TPP(NO$_2$)Br$_2$) which was further utilized for Pd catalyzed coupling reactions.
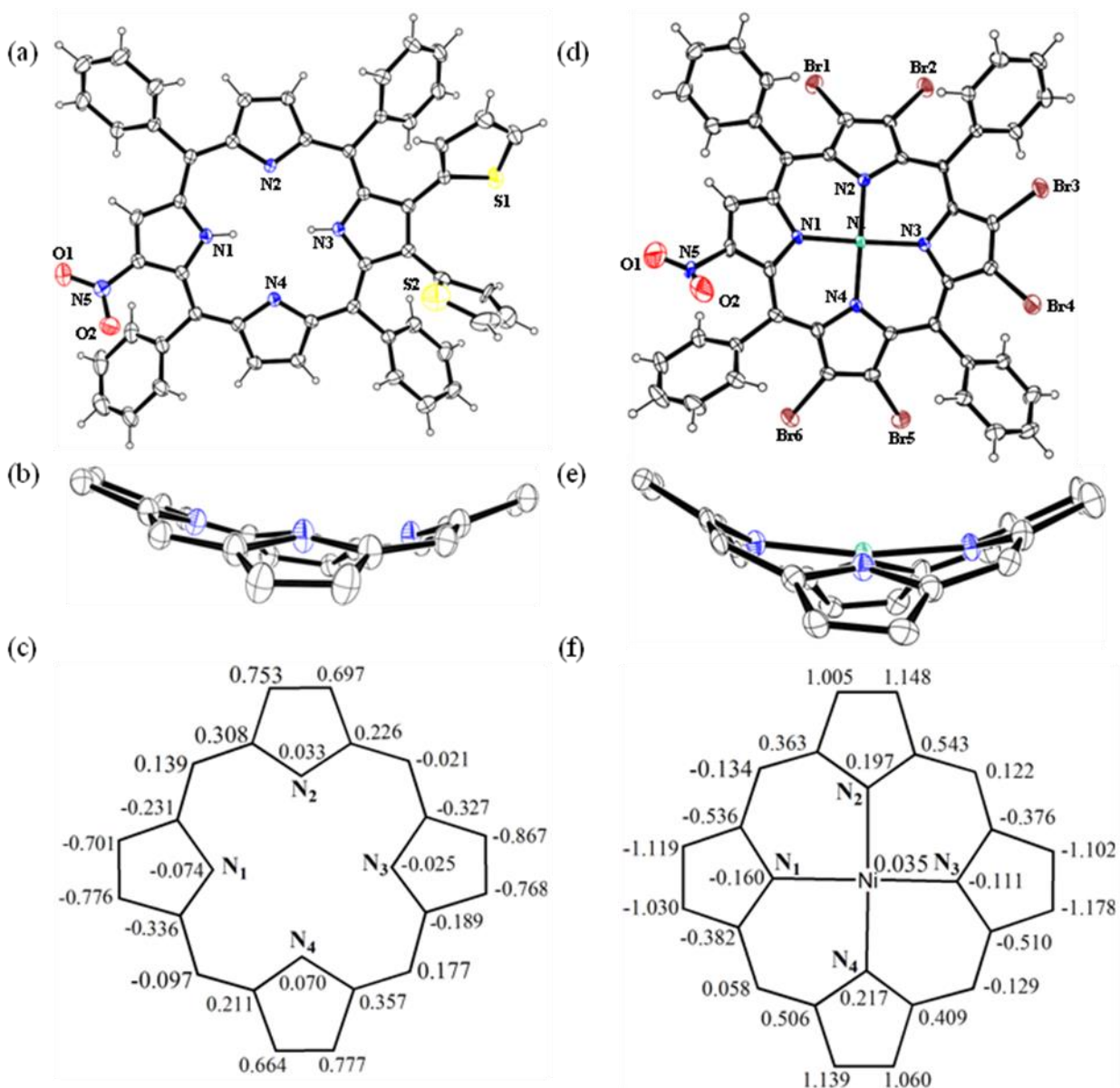
Figure 1. The ORTEP diagrams showing top and side views of H$_2$TPP(NO$_2$)(Th)$_2$ (1a and 1b) and NiTPP(NO$_2$)Br$_6$ (1d and 1e), respectively. The solvates are not shown for clarity, and in side view, the *β*-substituents and *meso*-phenyl groups are not shown for clarity. The displacement of porphyrin-core atoms in Å from the mean plane are shown in figures 1c and 1f for H$_2$TPP(NO$_2$)(Th)$_2$ and NiTPP(NO$_2$)Br$_6$, repectively.

$H_2TPP(NO_2)Br_2$ was subjected to Suzuki coupling using phenylboronic acid affording $H_2TPP(NO_2)Ph_2$ with 71% yield. In general, β-substituted 2-thienyl porphyrins were prepared using Stille coupling reactions by reacting bromoporphyrins with expensive tributylthienyl-stannane. We have synthesized the same *via* Suzuki coupling reaction using inexpensive 2-thienylboronic acid with the yields of 50-60%. $H_2TPP(NO_2)Br_2$ was subjected to Stille coupling reaction using tributylphenylethynylstannane in order to get $H_2TPP(NO_2)(PE)_2$. $NiTPP(NO_2)Br_2$ was also reacted with CuCN in quinoline to afford $NiTPP(NO_2)(CN)_2$ with 61% yield which was further demetallated using H_2SO_4 to get $H_2TPP(NO_2)(CN)_2$. The $CuTPP(NO_2)$ was hexabrominated using 10 equiv. of freshly recrystallized NBS by refluxing in 1,2-dichloroethane at 80℃ for 16 hrs with 80% yield [10]. Then $H_2TPP(NO_2)Br_6$ was obtained by acid demetallation of $CuTPP(NO_2)Br_6$ under mild conditions which was subjected to Suzuki cross coupling reactions to afford $H_2TPP(NO_2)Ph_6$ and $H_2TPP(NO_2)Th_6$ with good yields (60 - 70%). $H_2TPP(NO_2)(PE)_6$ was obtained *via* Stille coupling in 55% yield using a similar procedure of that of $H_2TPP(NO_2)(PE)_2$. The attempts to prepare $MTPP(NO_2)(CN)_6$ were failed by reacting $NiTPP(NO_2)Br_6$ with CuCN, and end up with degraded products. The metal complexes (Co(II), Cu(II) and Zn(II)) were prepared by reacting free base porphyrins with corresponding metal acetate hydrates (10 equiv.) in refluxing $CHCl_3/CH_3OH$ mixture for 30 minutes whereas Ni(II) complexes were synthesized using nickel acetate in refluxing DMF . The synthesized porphyrins were characterized by UV-Visible, fluorescence, ^{1}H NMR and mass spectroscopic techniques, elemental analysis and single crystal X-ray studies.

2.3.2 Crystal Structure Discussion

Crystallographic data of the $NiTPP(NO_2)Ph_2(Py)$, $ZnTPP(NO_2)(PE)_2(CH_3OH)$, $ZnTPP(NO_2)Br_2(CH_3OH)$, $NiTPP(NO_2)Br_6$ and $H_2TPP(NO_2)(Th)_2 \bullet CH_3OH \bullet H_2O$ are listed in Table A1 in Appendix 1. The ORTEP views (top and side) of $H_2TPP(NO_2)(Th)_2$ and $NiTPP(NO_2)Br_6$ are shown in figure 1. The top and side ORTEP views for $MTPP(NO_2)X_2$ (M = Ni(II) and Zn(II); X = Ph, PE, and Br) are shown in Figure A1 in Appendix 1. The selected average bond lengths and bond angles of these five porphyrins are listed in Table A2 in Appendix 2. The observed bond distances and bond angles in these porphyrins are similar to those reported in the literature [2,15,16]. The nonplanarity of the porphyrin core is induced by the steric repulsion among the peripheral substituents, which enforces the relief of the strain

through bond lengths and angles. The C-C bond distances of the β-pyrrole carbons (C_β-C_β bond lengths) bearing three β-substituents in these porphyrins are longer than that of $C_{\beta'}$-$C_{\beta'}$ distances where antipodal pyrroles bearing no substitution (Table A2 in Appendix 1). One would anticipate varying degrees of nonplanar conformations for porphyrins with mixed substituents pattern, since they bear substituents of different sizes which results in an increase in C_β-C_α-C_m angles with concomitant decrease in the N-C_α-C_m and M-N-C_α angles (Table S2 in Appendix 1). The pyrrole groups of the $H_2TPP(NO_2)(Th)_2$ are tilted alternatively up and down from the mean plane formed by porphyrin macrocycle and the β-substituents (nitro and 2-thienyl groups) on the opposite pyrrole units are tilted towards one face of the porphyrin. The 2-thienyl groups are oriented *trans* to each other in order to minimize the repulsions between the lone pairs. The displacement of atoms from the mean plane ($\Delta24$) clearly shows the saddle conformation of the core (Figure 1). This is evident from the mean plane displacement of the β-pyrrole carbons (ΔC_β) and the *meso*-carbons from the mean plane (Figure 1c). The magnitude of the displacement of the β-pyrrole carbons (ΔC_β) of $H_2TPP(NO_2)(Th)_2$ was found to be $\pm$ 0.75 Å which is significantly higher than that reported for H_2TPPBr_2 ($\Delta C_\beta = \pm$ 0.209 Å) but lower than that of H_2TPPBr_6 ($\Delta C_\beta = \pm$ 0.903 Å) [10]. Notably, the inner core imino protons (NH) are hydrogen bonded with pyrrole nitrogens which are evidenced from the distance between shortest N···N of 2.908 Å. The nitro group of $H_2TPP(NO_2)(Th)_2$ is interacting with the pyrrole moiety of another porphyrin unit with the distance of 3.217 Å exhibiting donor-acceptor interactions. Further, the oxygen of NO_2 group has van der Walls interactions with the aromatic CH of thienyl and phenyl groups (O···C distances of 3.3 to 3.6 Å). The steric crowding between the β-substituents and the *meso*-phenyl rings as well as the supramolecular interactions are responsible for the nonplanar conformation of the porphyrin macrocycle in $H_2TPP(NO_2)(Th)_2$. Notably, $NiTPP(NO_2)Br_6$ has shown severe saddle shape conformation (Figures 1d and 1e) with the displacement of the β-pyrrole carbons, ($\Delta C_\beta = \pm$ 1.10 Å). This is further supported by the increment in C_β-C_α-C_m angles (~ 127°) with concomitant decrement in the N-C_α-C_m (~ 123°) and M-N-C_α (~ 125°) angles along with larger C_β-C_β and $C_{\beta'}$-$C_{\beta'}$ bond lengths (1.34 - 1.35 Å). Ni(II) ion is in square planar geometry and is about 0.035 Å above the mean plane. The longer M-N bond length as compared to M-N′ in $MTPP(NO_2)X_n$ (Table S2 in Appendix 1) is possibly due to electron withdrawing effect of peripheral β-substitutents. It is known from the literature that $ZnTPPBr_4$, $ZnTPP(Ph)_4Br_4$, $NiTPPBr_4(CN)_4$ and $NiTPP(Ph)_4(CN)_4$ structures exhibited longer M-N

distances due to the presence of the electron withdrawing groups, which reduce the electron density on imino nitrogens [17,18]. The methyl group of the axially coordinated CH_3OH in $ZnTPP(NO_2)(PE)_2$ shows some positional disorder. It is noteworthy that the Zn(II) ion is about 0.295 Å above the mean plane which is higher than that of $ZnTPP(NO_2)Br_2 \bullet CH_3OH$ complex (0.237 Å). Notably, five coordinated Ni(II) ion in $NiTPP(NO_2)Ph_2(Py)$ is 0.397 Å above the mean plane of the porphyrin core. Moreover, the N-M-N and N′-M-N′ angles (161 - 170°) are deviated from 180° indicating the nonplanar conformation of $M-(N)_4$ core. The magnitude of the displacement of the β-pyrrole carbons ($\Delta C_\beta = \pm$ 0.16 Å) in $NiTPP(NO_2)Ph_2(Py)$ and $ZnTPP(NO_2)Br_2(CH_3OH)$ is slightly higher than that of $ZnTPP(NO_2)(PE)_2(CH_3OH)$ ($\Delta C_\beta = \pm 0.072$ Å). Hence the above-mentioned metalloporphyrins ($MTPP(NO_2)X_2$) show quasi-planar conformations. Moreover, $ZnTPP(NO_2)X_2(CH_3OH)$ (X = Br, PE) is showing dimeric structure through the hydrogen bonding interactions between the coordinated methanol with the nitro group of the another porphyrin units with the shortest O···O distance of 2.874 (5) Å. The closest distance between the metalloporphyrin units is more than 3.40 Å indicating that the steric crowding between the β-substituents and the *meso*-phenyl groups is responsible for the nonplanar conformation rather than the π-π interactions between the macrocyclic π-systems. From the single crystal structure analysis, it is observed that $H_2TPP(NO_2)Th_2$ and $ZnTPP(NO_2)Br_6$ exhibit moderate and severe nonplanar saddle shape conformations, repectively. Unfortunately, we were unable to crystallize other free bases and metal complexes of mixed substituted porphyrins and hence we carried out full geometry optimization using DFT studies.

2.3.3 DFT Calculations

The ground state geometries of mixed substituted free base porphyrins ($H_2TPP(NO_2)X_6$ and $H_2TPP(NO_2)X_2$) were optimized in the gas phase by DFT calculations using B3LYP functional and LANL2DZ basis set [19]. Figures 2 and A2 - A4 in Appendix represent the fully optimized geometries of these porphyrins (top and side views) as well as the deviation of core atoms from the porphyrin mean plane. The selected average bond lengths and bond angles of $H_2TPP(NO_2)X_2$ and $H_2TPP(NO_2)X_6$ are listed in the Tables A3 and A4 in Appendix 1, respectively. The observed bond lengths and bond angles in B3LYP/LanL2DZ optimized geometries of mixed substituted porphyrins are similar to those reported in the literature [2,15,16]. Nonplanar conformation of free base porphyrins arises by the tilting of the pyrrole rings to prevent repulsive

interactions among the substituents, and these results in the increment of bond lengths of C_β-C_β as well as in the bond angles of C_β-C_α-C_m with concomitant decrease in the bond angles of N-C_α-
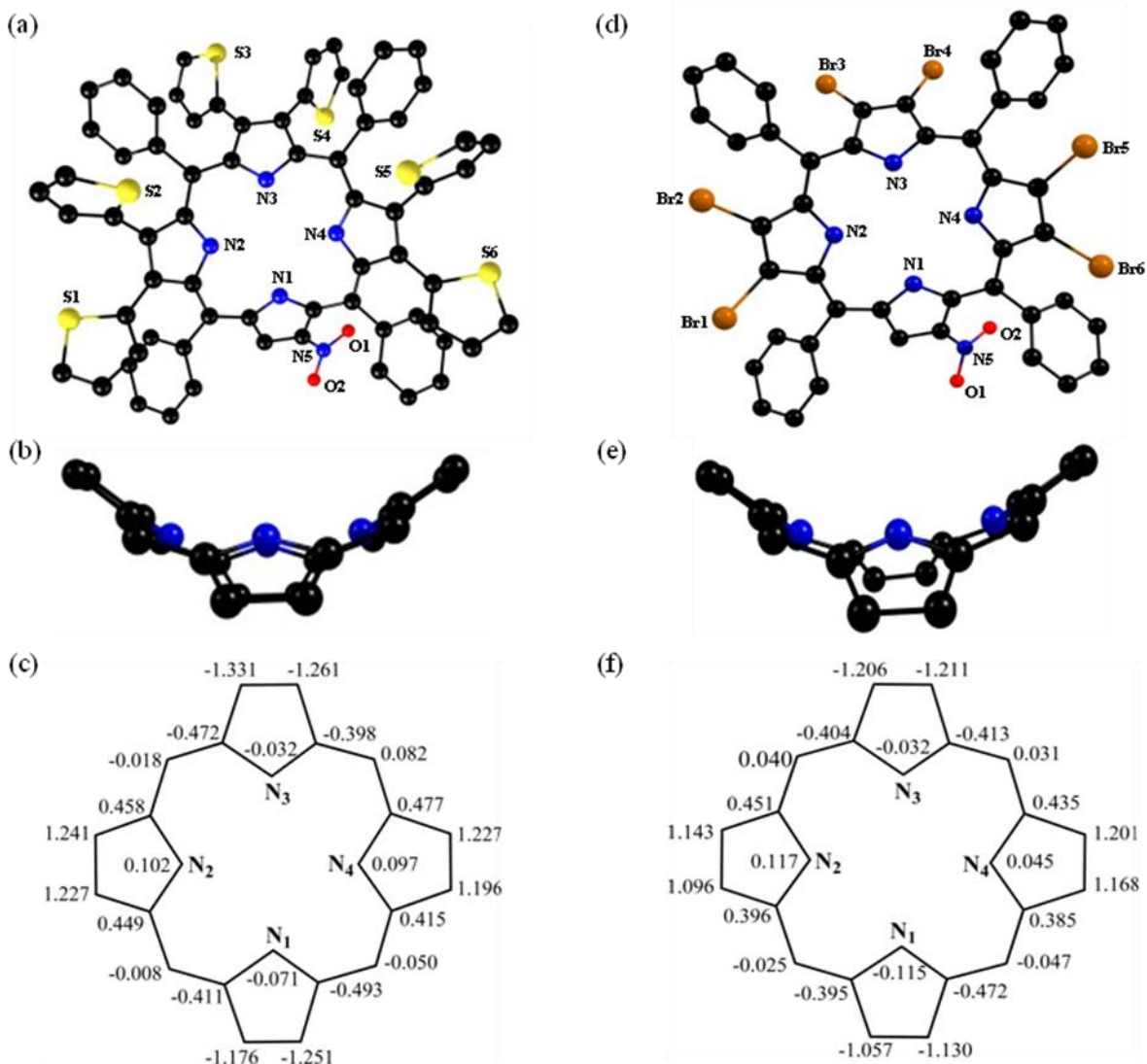
Figure 2. B3LYP/LANL2DZ optimised geometries showing top as well as side views of H$_2$TPP(NO$_2$)(Th)$_6$ (1a and 1b) and H$_2$TPP(NO$_2$)Br$_6$ (1d and 1e), respectively. In side view, the β-substituents and meso-phenyl groups are not shown for clarity. The displacement of porphyrin-core atoms in Å from the mean plane are shown in figures 1c and 1f for H$_2$TPP(NO$_2$)(Th)$_6$ and H$_2$TPP(NO$_2$)Br$_6$, repectively. Color codes for atoms: C (black), N (blue), O (red), S (yellow) and Br (brown).

C_m. Herein, H$_2$TPP(NO$_2$)X$_2$ systems exhibited about 2 - 4° change in these angles, and this change is comparable to that of the saddle shaped CuTPP(Ph)$_4$(CH$_3$)$_4$ and H$_2$TPPTh$_4$ structures

[18,20,21]. Notably, the $H_2TPP(NO_2)X_6$ (X = Ph, PE, Br and Th) exhibited highly nonplanar severe saddle-shape conformational features in comparison to $H_2TPP(NO_2)X_2$. The $C_{\beta'}-C_{\beta'}$ bond lengths (1.391 - 1.417 Å) of the pyrroles bearing four β-substituents in $H_2TPP(NO_2)X_6$ systems are longer than the $C_{\beta}-C_{\beta}$ distances (1.375 - 1.388 Å) of the antipodal pyrroles bearing three β-substituents (Table S4 in appendix 1). The increment in the bond angles of $C_{\beta}-C_{\alpha}-C_m$ with the concomitant decrement in the bond angles of $N-C_{\alpha}-C_m$ in $H_2TPP(NO_2)X_6$ systems were found to be significantly large (4 - 8º) in these angles which are comparable to that of H_2TPPX_8 (X = Br, Cl and Ph) [2] and H_2TPPBr_6 structures [10]. Among all, $H_2TPP(NO_2)Th_6$ exhibited higher nonplanarity ($\Delta C_{\beta} = \pm 1.240$ Å) as compared to all other porphyrins. The top and side views of $H_2TPP(NO_2)Th_6$ were shown in Figures 2a and 2b, respectively. Figure 2c represents the displacement of porphyrin-core atoms from the mean plane in Å indicating the severe saddle-shape conformation. The 2-thienyl groups substituted at the β-pyrrole carbons are oriented *trans* to each other in order to minimize the lone pair repulsions as seen in the crystal structures. The mean plane displacement of the β-pyrrole carbons (ΔC_{β}) and the *meso*-carbons from the mean plane follows the order: $H_2TPP(NO_2)(CN)_2$ < $H_2TPP(NO_2)(PE)_2$ < $H_2TPP(NO_2)Br_2$ ≈ $H_2TPP(NO_2)Ph_2$ < $H_2TPP(NO_2)(Th)_2$ < $H_2TPP(NO_2)(PE)_6$ < $H_2TPP(NO_2)Br_6$ ≈ $H_2TPP(NO_2)Ph_6$ < $H_2TPP(NO_2)(Th)_6$ indicating the varying degrees of nonplanarity in these mixed substituted porphyrins. The electronic effects of the substituents and the influence of nonplanarity (as evidenced from single crystal X-ray structures and DFT caluculations) on pophyrin π-system are further examined by spectroscopic and electrochemical redox studies.

2.3.4 Electronic Spectral Studies

Optical absorption spectra of porphyrins and their metal complexes are influenced by the presence of peripheral substituents and core metal ions. It is known that the nonplanar conformation of the macrocycle induces unusual red-shift in their spectral properties [2,22,23]. Table 1 lists the absorption spectral data of newly synthesized free base porphyrins in CH_2Cl_2 at 298 K. Representative absorption spectra of $H_2TPP(NO_2)Ph_n$ (n = 0, 2 and 6) and $NiTPP(NO_2)X_2$ are shown in figure 3a and 3b, respevctively. All free base derivatives ($H_2TPP(NO_2)X_n$ where n = 0, 2, 6) exhibited a characteristic Soret band (B band) and three Q bands whereas H_2TPP shows one B band and four Q bands. $H_2TPP(NO_2)$ exhibited red-shifts in Soret ($\Delta\lambda_{max}$ = 9 nm) and in $Q_x(0,0)$ band ($\Delta\lambda_{max}$ = 17 nm) relative to H_2TPP. $H_2TPP(NO_2)X_2$ (X

= Br, Ph, PE, Th and CN) showed further red-shifts in B band ($\Delta\lambda_{max}$ = 10 - 20 nm) and $Q_x(0,0)$ band ($\Delta\lambda_{max}$ = 20 - 30 nm) relative to $H_2TPP(NO_2)$ (Figure A5 in Appendix 1). This is possibly due to the inductive and/or conjugative interaction of the substituents with the π-system as well as the nonplanarity of the porphyrin macrocycle as evidenced from the crystal structure of $H_2TPP(NO_2)Th_2$ and the optimized geometries of $H_2TPP(NO_2)X_2$ (*vide supra*). Table A5 in Appendix 1 lists the UV-Vis spectral data of all the metal complexes. Although, the metal complexes, $MTPP(NO_2)X_2$ (M = Co(II), Ni(II), Cu(II) and Zn(II)) bear lower symmetry, they exhibited a B and two Q bands with molar extinction coefficients (ε) similar to those of their corresponding MTPPs (D_{4h}) [24].

$H_2TPP(NO_2)X_6$ (X = Br, Ph, PE and Th) exhibited large red-shifts in the Soret band ($\Delta\lambda_{max}$ = 40 - 70 nm) and $Q_x(0,0)$ band ($\Delta\lambda_{max}$ = 65 - 90 nm) relative to $H_2TPP(NO_2)$ due to the increase in the number of X, nonplanarity of the macrocycle and/or electronic nature of the substituents (Figure A6 in Appendix 1). The longest wavelength band ($Q_x(0,0)$) of free-base porphyrins showed an interesting trend in red-shift and aligns in the following order: $H_2TPP(NO_2)$ < $H_2TPP(NO_2)Br_2$ < $H_2TPP(NO_2)Ph_2$ < $H_2TPP(NO_2)(PE)_2$ < $H_2TPP(NO_2)(Th)_2$ < $H_2TPP(NO_2)(CN)_2$ < $H_2TPP(NO_2)Ph_6$ < $H_2TPP(NO_2)Br_6$ < $H_2TPP(NO_2)(PE)_6$ < $H_2TPP(NO_2)(Th)_6$.
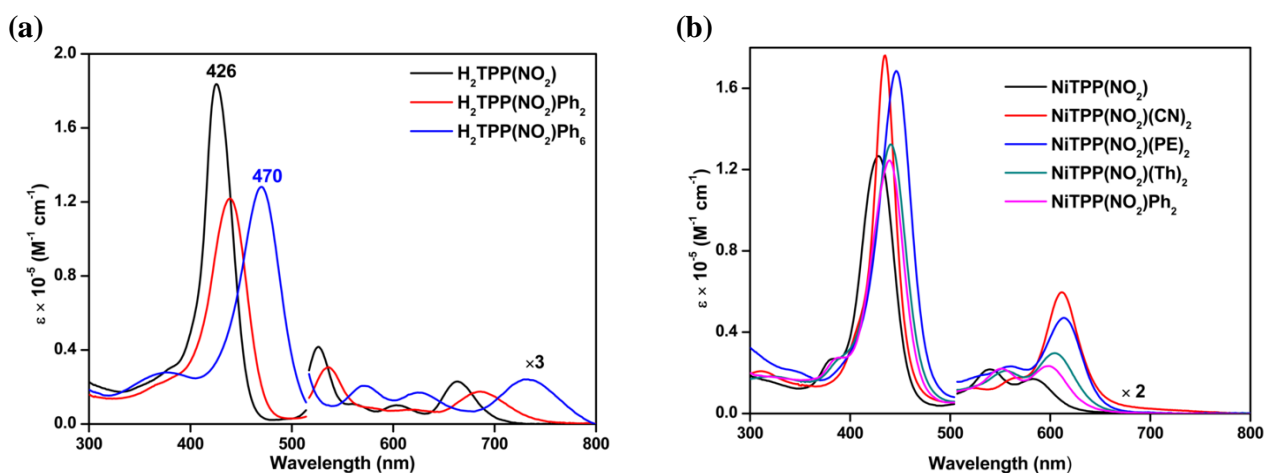
Figure 3. Electronic absorption spectra of (a) $H_2TPP(NO_2)Ph_n$ (n = 0, 2 and 6) and (b) $NiTPP(NO_2)X_2$ (X = H, CN, PE, Th and Ph) in CH_2Cl_2 at 298 K. The porphyrin concentration was maintained between 7 - 10 μM.

The observed red shift of $Q_x(0,0)$ band is in accordance with increment in the number of substituents ($H_2TPP(NO_2) < H_2TPP(NO_2)X_2 < H_2TPP(NO_2)X_6$) and the extent of nonplanrity of the porphyrin π-system as evidenced from the crystal structures [10] and DFT calculations. Further, among the same series ($H_2TPP(NO_2)X_2$ or $H_2TPP(NO_2)X_6$), the electron withdrawing and/or conjugatively resonating substituents exhibited large bathochromic shift. Further, mixed substituted $H_2TPP(NO_2)(PE)_6$ showed a dramatic red-shift in the B band (68 nm) and $Q_{x(0,0)}$ (87 nm) relative to $H_2TPP(NO_2)$. The spectral features of $H_2TPP(NO_2)X_6$ with mixed substituent pattern are similar to those of β-octabromo [25] or β-octaphenyl-TPPs [26]. The red-shift in the highly substituted porphyrins has been ascribed to the nonplanarity of the porphyrin ring in combination with the inductive or conjugative interaction of the substituents that are in direct conjugation with the π-system.

Electronic absorption spectra of representative $CuTPP(NO_2)X_2$ (X = H, CN) are shown in figure 4a. The introduction of two more electron withdrawing groups on the other opposite pyrrole positions of $CuTPP(NO_2)$ showed bathochromic shift in their spectral features with considerable
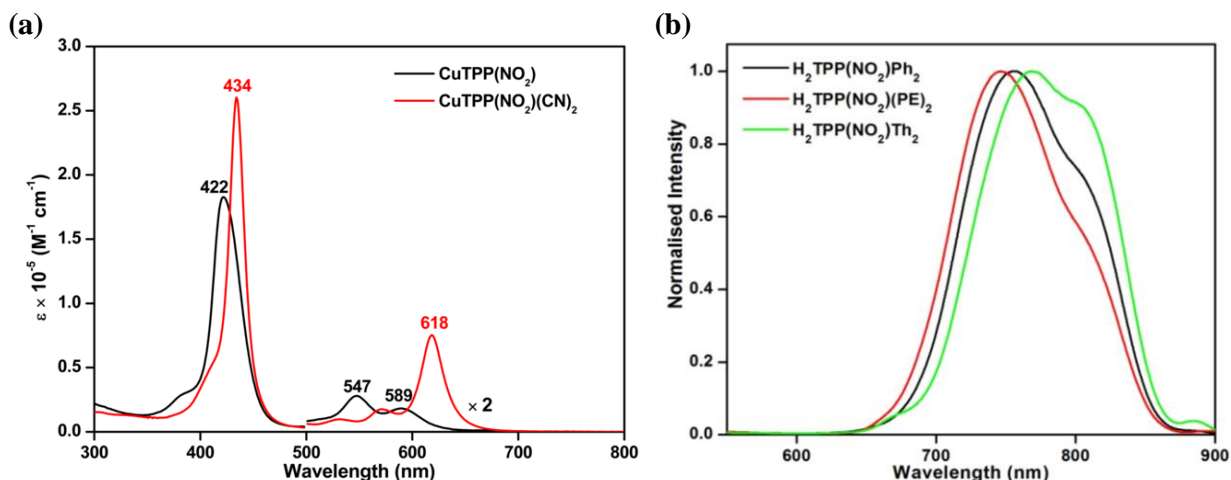
Figure 4. (a) Overlayed optical absorption spectra of $CuTPP(NO_2)$ (8.87 μM) and $CuTPP(NO_2)(CN)_2$ (5.18 μM) in CH_2Cl_2 at 298 K. (b) Fluorescence spectra of $H_2TPP(NO_2)X_2$ (X = Ph, PE, Th) in CH_2Cl_2 at 298 K.

increment in molar absorptivity (ε). Generally, metal complexes, $MTPP(NO_2)X_2$ exhibited a B band and two Q bands with the extent of red-shift of the B band being about 7 - 20 nm and 10 - 30 nm in $Q_x(0,0)$ transitions relative to their corresponding $MTPP(NO_2)$. $MTPP(NO_2)(CN)_2$ complexes showed considerable gain in the intensity of the longest wavelength, $Q_x(0,0)$ band relative to the $Q_x(1,0)$ band (Figure 4a) and this is possibly due to stabilization of a_{1u} relative to

a_{2u} of MTPP(NO$_2$)(CN)$_2$ and thereby increasing the transition probability of a_{2u} to $e_g(\pi^*)$ relative to a_{1u} to $e_g (\pi^*)$ [27]. MTPP(NO$_2$)X$_6$ showed dramatic red-shift of 30 - 70 nm in the Soret band and 35 - 100 nm in the $Q_x(0,0)$ band as compared MTPP(NO$_2$). As expected (Table 1), the bands are more blue-shifted with the increase in electronegativity of the metal ion [28]. Generally, MTPP(NO$_2$)(Ph)$_n$ derivatives show blue-shifted absorption spectral features relative to MTPP(NO$_2$)(PE)$_n$ or MTPP(NO$_2$)(CN)$_n$ derivatives. This is possibly due to the variable steric crowding and the electronic nature of the substituent that induces conformational differences between the macrocycles as well as the substituent effects. A pronounced red-shift in the

Table 1. Optical absorption spectral data of mixed substituted porphyrins

Porphyrin	B band(s), nm	Q bands, nm
H$_2$TPP(NO$_2$)	426(5.34)	526(4.21), 604(3.62), 664(3.95)
H$_2$TPP(NO$_2$)Br$_2$	436(5.23)	536(4.08), 623(3.43), 683(3.91)
H$_2$TPP(NO$_2$)Ph$_2$	439(5.09)	536(4.01), 686(3.80)
H$_2$TPP(NO$_2$)(PE)$_2$	444(5.38)	540(4.25), 583(3.99), 687(3.93)
H$_2$TPP(NO$_2$)Th$_2$	440(5.24)	540(4.19), 695(4.01)
H$_2$TPP(NO$_2$)(CN)$_2$	440(5.47)	541(4.14), 585(4.00), 645(3.79), 702(4.30)
H$_2$TPP(NO$_2$)Br$_6$	371(4.39), 468(5.11)	628(3.98), 739(3.80)
H$_2$TPP(NO$_2$) Ph$_6$	377(4.44), 470(5.11)	571(3.83), 624(3.75), 729(3.90)
H$_2$TPP(NO$_2$)(PE)$_6$	494(5.22)	586(4.29), 666(sh), 751(3.43)
H$_2$TPP(NO$_2$)Th$_6$	325(4.65) , 481(4.90)	589(3.61), 644(3.75), 754(3.40)

Values in parentheses refer to log ε (ε in Mol^{-1} cm^{-1}).

absorption spectral features of the mixed substituted cyano, phenylethynyl and bromoporphyrins is due to push-pull, extended conjugation and/or nonplanar distortion of the porphyrin ring. The red-shift exhibited by nonplanar porphyrins is also supported by theoretical studies [22,23].

The synthesized free base and Zn(II) complexes of mixed substituted porphyrins were characterized by fluorescence spectroscopy to elucidate the role of substitution and the effect of nonplanarity. The steady state emission spectra of H$_2$TPP(NO$_2$)X$_2$ (X = Ph, PE and Th) in CH$_2$Cl$_2$ is shown in Figure 4b. Table A6 in Appendix 1 lists emission data of MTPP(NO$_2$)X$_n$ in CH$_2$Cl$_2$ at 298 K. H$_2$TPP(NO$_2$)X$_2$ (X = CN, Ph, PE and Th) exhibited red-shifted emission (75 -

110 nm) than that of H_2TPP in CH_2Cl_2. Notably, highly red shifted emission bands ($\Delta\lambda_{max} = 160$ - 170 nm) with feeble fluorescence intensity were observed for $H_2TPP(NO_2)X_6$ (X = PE and Th) in comparison to H_2TPP in CH_2Cl_2. The representative emission spectra of $MTPP(NO_2)X_n$ (M = 2H and Zn(II); n = 0, 2 and 6, X = Th, Ph, CN and PE) were shown in Figures A7, A8 and A9 in Appendix 1. The free-base porphyrins exhibited an interesting trend in the red-shift of their corresponding emission bands and aligns in the following order: $H_2TPP < H_2TPP(NO_2)(CN)_2 < H_2TPP(NO_2)(PE)_2 < H_2TPP(NO_2)Ph_2 < H_2TPP(NO_2)Th_2 < H_2TPP(NO_2)(PE)_6$. The increasing order of red-shift and the decrement in the quantum yields (Table A6 in Appendix 1) are in accordance with the increasing order of nonplanarity of the porphyrin macrocycle as evidenced from X-ray crystallography and DFT calculations. The same trend was also observed for Zn(II) complexes as expected. Notably, $H_2TPP(NO_2)X_6$ (X = Ph, Th and Br) failed to show emission spectrum due to enhanced nonplanarity which reduces the singlet excited state lifetime in comparison to planar porphyrins as seen in $H_2TPP(Et)_8$ and $H_2TPP(Ph)_8$ [29]. Further, the quenching of emission in $H_2TPP(NO_2)Br_2$ and $H_2TPP(NO_2)Br_6$ is ascribed to the combination of nonplanarity and heavy atom effect of bromo groups that are in direct conjugation with the porphyrin π-system. Similar behavior was reported for β-brominated porphyrins, for example, $MTPPBr_4$ exhibited weak red-shifted emission while $MTPPBr_8$ failed to show singlet emission [25].

2.3.5 ^{1}H NMR Studies

$H_2TPP(NO_2)$ exhibits characteristic chemical shifts arising from the β-pyrrole (9.10 - 8.71 ppm) and *meso*-phenyl (8.29 - 7.70 ppm) proton resonances. The ^{1}H NMR spectra of free base mixed substituted porphyrins ($H_2TPP(NO_2)X_n$) (X = Br, Ph, PE, Th and CN; n = 0, 2 and 6) exhibit resonances arising from *meso*-phenyls, β-pyrrole proton(s), β-substituents (Ph or Th or PE) and imino hydrogens (Figures 5, 6 and A10 to A27 in Appendix 1). The chemical shifts of the *meso*-phenyl protons of $H_2TPP(NO_2)X_n$ are comparable to those observed for the corresponding $H_2TPP(NO_2)$. The β-pyrrole resonances of $H_2TPP(NO_2)X_2$ (X = Br, Ph, Th and PE) are marginally upfield shifted (~ 0.1 - 0.2 ppm) than that of $H_2TPP(NO_2)$ whereas $H_2TPP(NO_2)(CN)_2$ exhibited 0.25 ppm downfield shift due to strong electron withdrawing nature of cyano groups. The β-pyrrole proton of $H_2TPP(NO_2)X_6$ (X = Br, Ph, PE and Th) is 0.47 - 0.80 ppm upfield shifted than $H_2TPP(NO_2)$. The *meso*-phenyl protons of $H_2TPP(NO_2)X_6$ (X = Br, PE and Th) is marginally shifted in comparison to $H_2TPP(NO_2)$ whereas $H_2TPP(NO_2)Ph_6$ is 0.25 -

Figure 5. ^{1}H NMR spectrum of $H_2TPP(NO_2)Ph_2$ in $CDCl_3$.

Figure 6. ^{1}H NMR spectrum of $H_2TPP(NO_2)(PE)_6$ in $CDCl_3$

0.41 ppm upfield shifted possibly due to the ring current effect of β-pyrrole phenyl protons. $H_2TPP(NO_2)Ph_6$ exhibited characteristic upfield shifted β-phenyl protons in the range of 6.90 - 6.47 ppm which is attributed to the ring current effect of β-pyrrole phenyl protons whereas β-phenylethynyl protons resonate between 7.18 - 7.36 ppm indicating phenyl protons are distant from the ring current. The core imino protons, β-pyrrole protons and β-thienyl C-3 protons of H_2TPPTh_n (n = 2 and 6) resonates at the downfield region is possibly due to the inductive effect of 2-thienyl groups which leads to decrement in the ring current of the porphyrin π-system [21].
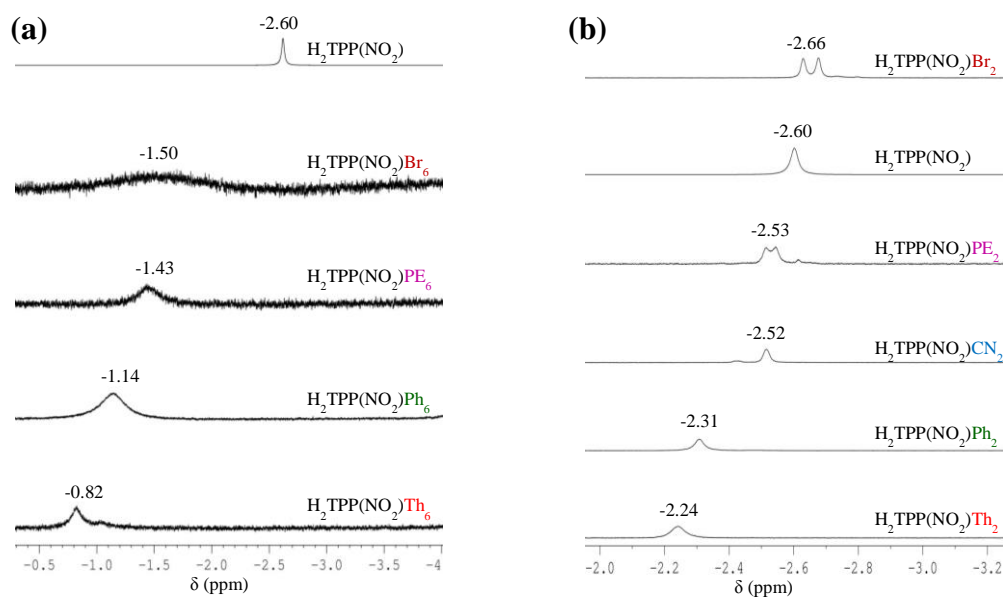
Figure 7. The representative ^1H NMR spectra of imino proton region of (a) $H_2TPP(NO_2)X_6$ (X = Br, PE, Ph and Th) and (b) $H_2TPP(NO_2)X_2$ (X = Br, PE, Ph, Th and CN) in CDCl$_3$ at 298 K.

Figure 7 shows the ^1H NMR spectra of imino proton region of $H_2TPP(NO_2)X_6$ and $H_2TPP(NO_2)X_2$ in CDCl$_3$ at 298 K. The core imino-protons of $H_2TPP(NO_2)Br_6$ (-1.5 ppm), $H_2TPP(NO_2)(PE)_6$ (-1.43 ppm), $H_2TPP(NO_2)Ph_6$ (-1.14 ppm) and $H_2TPP(NO_2)(Th)_6$ (-0.82 ppm) are downfield-shifted relative to $H_2TPP(NO_2)$ (-2.60 ppm) as shown in Figure 7a. The imino proton resonances of $H_2TPP(NO_2)X_2$ series, $H_2TPP(NO_2)(PE)_2$ (-2.53 ppm), $H_2TPP(NO_2)(CN)_2$ (-2.52 ppm), $H_2TPP(NO_2)Ph_2$ (-2.31 ppm) and $H_2TPP(NO_2)(Th)_2$ (-2.24 ppm) are downfield shifted than $H_2TPP(NO_2)$ whereas $H_2TPP(NO_2)Br_2$ (-2.65 ppm) is slightly upfield shifted (Figure 7b). Further, the downfield shift of the resonances is due to substituent effects and/or the nonplanar conformation as observed in the X-ray crystal structures and optimized geometries. Nonplanarity of the macrocycle causes the broad features of the imino-protons to resonate at

downfield region relative to that in planar porphyrins (Figure 7a) [30]. The reason for the largest downfield shift of NH protons of $H_2TPP(NO_2)(Th)_6$ is due to enhanced nonplanarity and inductive effect induced by thienyl groups which leads to decrement in the ring current of the macrocycle [21].

The ^1H NMR spectra of $MTPP(NO_2)X_n$ (M = Zn(II) and Ni(II); n = 2 and 6) complexes are devoid of imino-protons revealing that metal ion got inserted into the porphyrin ring. The β protons resonances for $NiTPP(NO_2)X_n$ are marginally upfield shifted (0.03 - 0.11 ppm) whereas in case of $ZnTPP(NO_2)X_n$ are marginally downfield shifted (0.02 - 0.26 ppm) in comparison to their corresponding $H_2TPP(NO_2)X_n$ derivatives. The *meso*-phenyl protons resonances of $MTPP(NO_2)X_n$ are marginally upfielded (0.05 - 0.43 ppm) corresponding to those of free base derivatives. The integrated intensities of the proton resonances of these mixed substituted porphyrins are consistent with the proposed structures.

2.3.6 Protonation and Deprotonation Studies

To examine the effect of mixed substitution on nonplanarity, we have carried out protonation and deprotonation studies in toluene using trifluoroacetic acid (TFA) and tetrabutylammonium hydroxide (TBAOH), respectively. Figure 8 shows the UV-Visible spectral changes of $H_2TPP(NO_2)Br_6$ while increasing the concentration of TFA (0.33 - 6.29 $\times$ 10^{-5} M) and TBAOH (0.33 - 6.62 $\times$ 10^{-6} M), respectively. Table 2 lists the protonation and deprotonation constants of various free base mixed substituted porphyrins. Figure 8a shows the concomitant decrement in absorbance of $H_2TPP(NO_2)Br_6$ at 468 nm and rising of a new band at 494 nm while increasing the concentration of TFA. As protonation proceeds, the multiple Q bands are disappearing and a new single broad band grows at 753 nm accompanied with the red-shift of 16 nm in $Q_x(0,0)$ band. In all cases, we could obtain diprotonated porphyrin species which is further confirmed by Hill plot having the slope value of ~ 2 as shown in Figures 8a inset, A28 and Table 2. All diprotonated species of mixed substituted porphyrins are stable and showing aromatic nature as evidenced by the UV-Visible spectral features. $H_2TPP(NO_2)X_6$ (X = Br, Ph and Th) exhibits ~ 6 - 288 fold higher protonation constants (β_2) in comparison to H_2TPPX_8 (X = Br, Cl) in toluene which is ascribed to the combined effect of mixed substitution and nonplanarity. The observed $log\beta_2$ values of H_2TPPX_8 (X = Br, Cl) in toluene are comparable to those observed in CH_2Cl_2 [31].

$H_2TPP(NO_2)(PE)_6$ has shown ~ 5.52 - 18.6 $\times$ 10^2 fold lower β_2 value which is ascribed to electron withdrawing nature of the phenylethynyl groups and less nonplanar conformation as
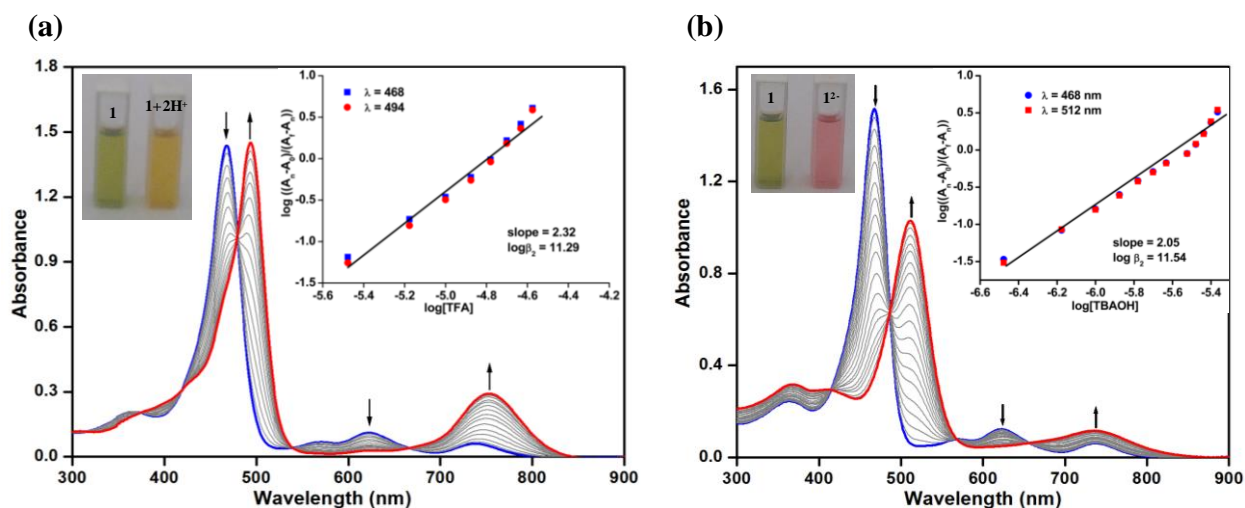
Figure 8. UV-Visible spectral titration of $H_2TPP(NO_2)Br_6$ (9×10^{-6} M) with (a) TFA and (b) TBAOH in toluene, insets show the corresponding Hill plots.

Table 2. Protonation and deprotonation constants of free base mixed substituted porphyrins in toluene at 298K

Porphyrin	TFA			TBAOH		
	$log\beta_2$	slope	r^2	$log\beta_2$	slope	r^2
$H_2TPP(NO_2)Br_6$	11.29	2.32	0.93	11.54	2.05	0.94
$H_2TPP(NO_2)Ph_6$	11.74	1.99	0.88	-	-	-
$H_2TPP(NO_2)Th_6$	11.21	2.12	0.84	7.91	1.65	0.80
$H_2TPP(NO_2)PE_6$	8.47	2.01	0.85	11.34	2.36	0.97
H_2TPPBr_8	10.53	2.10	0.97	10.40	2.00	0.91
H_2TPPCl_8	9.21	2.01	0.99	10.21	1.90	0.96
$H_2TPP(NO_2)Br_2$	7.92	2.50	0.98			
$H_2TPP(NO_2)Ph_2$	9.54	1.91	0.98			
$H_2TPP(NO_2)Th_2$	8.76	1.95	0.97			
$H_2TPP(NO_2)PE_2$	8.65	2.64	0.99			
$H_2TPP(NO_2)CN_2$	3.69	2.18	0.93			

compared to $H_2TPP(NO_2)X_6$ (X = Br, Ph and Th). $H_2TPP(NO_2)(CN)_2$ exhibited much lower logβ_2 value (3.69) than that of $H_2TPP(NO_2)X_2$ (X = Br, Ph, PE and Th) which is attributed to the combined effect of quasi-planar structure ($\Delta C_\beta = \pm0.5$ Å and over all mean plane deviation of porphyrin core, $\Delta24 = 0.234$ Å) and strong electron withdrawing nature of the cyano and nitro substituents. $H_2TPP(NO_2)X_2$ (X = Br, Ph, PE and Th) were shown lower logβ_2 values (7.9 - 9.54) in comparison to H_2TPPR_4 (R = Me, Ph, Th and Br) with logβ_2 values (9.03 - 9.96) [21h] possibly due to the strong electron accepting nature of nitro group. Figure 8b shows the concomitant decrement in the absorbance of $H_2TPP(NO_2)Br_6$ at 468 nm while increasing the concentration of TBAOH, and a new band rises at 512 nm. As deprotonation proceeds the multiple Q bands of the neutral compound disappear, and a new band rises at 736 nm. The inset shows Hill plot with the slope value of ~ 2 and the logβ_2 value of 11.54 which reveals the acidic nature of the NH protons due to electron withdrawing nature of NO_2 and Br substituents. Notably, $H_2TPP(NO_2)(PE)_6$ has shown close logβ_2 value to $H_2TPP(NO_2)Br_6$ reflecting electron accepting nature of the substituents (nitro and phenylethynyl groups) and induced nonplanarity by mixed substitution. Further, $H_2TPP(NO_2)Th_6$ shows lower deprotonation constant as compared to $H_2TPP(NO_2)(PE)_6$ and $H_2TPP(NO_2)Br_6$ which is interpreted in terms of conjugative effect of 2-thienyl groups [21]. Under similar conditions, $H_2TPP(NO_2)Ph_6$ was showing incomplete deprotonation with split Soret bands (Figure A29c in Appendix 1) even at higher concentration of the base. This is possibly due to the electron rich nature of the porphyrin core which prevents the formation of dianionic species. Moreover, at very high concentrations of TBAOH, the reactant is in equilibrium with the anionic species and doesn't move forward to complete. The $H_2TPP(NO_2)X_2$ (X = Br, Ph, PE, Th and CN) doesn't show any spectral changes upon addition of very high concentration of TBAOH (5.97×10^{-4} M) which indicates the moderate nonplanar conformation ($\Delta C_\beta = \pm0.67$ - 0.73 Å) of the porphyrin π-system as compared to $H_2TPP(NO_2)X_6$ ($\Delta C_\beta = \pm1.01$ - 1.24 Å).

2.3.7 Electrochemistry

The redox potentials of porphyrin π-system are influenced by the nonplanar conformation, nature of the substituents and the core metal ions. To determine the influence of macrocyclic nonplanarity and the combined effects of electron donor and acceptor groups at the β-pyrrole positions, we have examined the electrochemical redox properties of these mixed susbtituted

porphyrins by cyclic voltammetric studies. Under similar conditions, the corresponding MTPP(NO$_2$) and MTPP [11] derivatives were also examined, and the electrochemical redox data (vs Ag/AgCl) is listed in Table 3.

The influence of different β-substituents on redox potentials for CuTPP(NO$_2$)X$_2$ and CuTPP(NO$_2$)X$_6$ are shown in Figure 9. Table A7 in Appendic 1 lists the electrochemical redox data (vs Ag/AgCl) of various metal complexes in CH$_2$Cl$_2$ at 298 K. The mixed substituted porphyrins exhibited two successive one-electron electrochemical oxidations and reductions whereas Co(II) complexes have shown first metal centered redox behavior followed by π-system. Generally, the first oxidation of Co(II) porphyrins is metal-centered process, and is well documented in literature [32]. Further, we have carried out the oxidation of Co(II) porphyrins to Co(III) porphyrins by adding aliquots of *tert*-butyl hydroperoxide (TBHP) in CH$_2$Cl$_2$ as chemical oxidant which is reflected in the UV-Visible spectral changes as shown in the Appendix 1 (Figure A30 and Table S8 in Appendix 1).

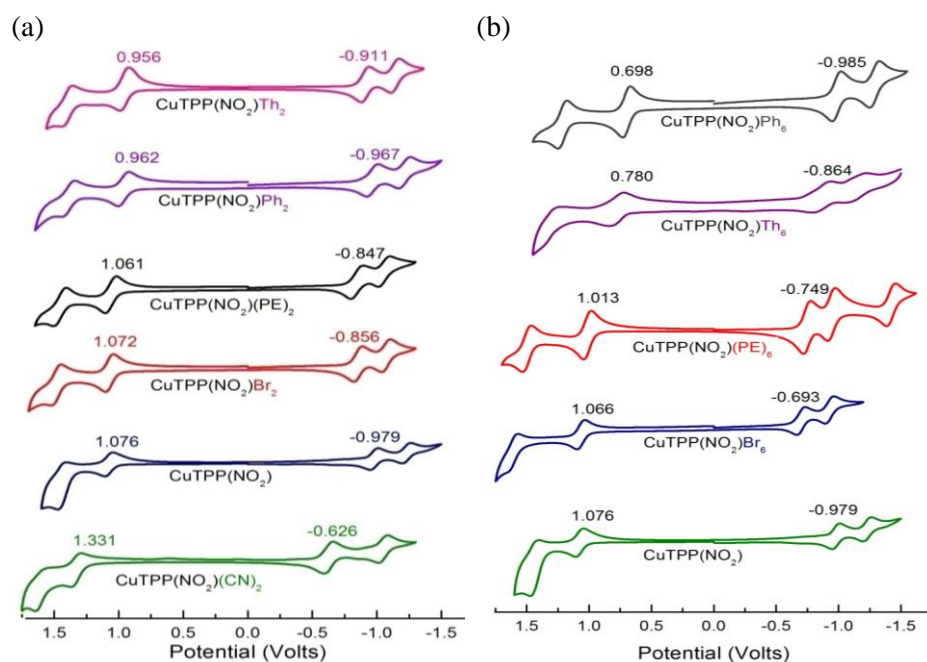**Figure 9.** Cyclic voltammograms of (a) CuTPP(NO$_2$)X$_2$ (~ 1 mM) and (b) CuTPP(NO$_2$)X$_6$ (~ 1 mM) in CH$_2$Cl$_2$ containing 0.1 M TBAPF$_6$ using Ag/AgCl as reference electrode with a scan rate of 0.10 V/s at 298 K

The effect of mixed β-substitution (tri and hepta) as well as the effect of core metal ion on redox potentials of MTPP(NO$_2$)X$_n$ (n = 0, 2 and 6; X = Br, CN, PE, Ph and Th; M = 2H, Co(II), Ni(II), Cu(II) and Zn(II)) are shown in Figures A31 - A34 in Appendix 1.

The first ring oxidation potentials for MTPP(NO$_2$)X$_2$ (X = Br, Ph, PE, Th and CN and M = 2H, Co(II), Ni(II), Cu(II) and Zn(II)) span a range from 0.85 to 1.33 V whereas reduction potential varies from -0.63 to -1.07 V (Tables 3 and S7 in Appendix 1). The first ring redox potentials of MTPP(NO$_2$)(CN)$_2$ have shown 200 - 350 mV anodic shift in comparison to MTPP(NO$_2$)Ph$_2$ which is attributed to the strong electron withdrawing nature of cyano substituents. The metal centered reduction potential of CoTPP(NO$_2$)(CN)$_2$ is 470 mV anodically shifted as compared to CoTPP due to strong electron withdrawing nature of nitro and cyano groups. The metal centered redox potentials are altered according to the electronic nature of the substituents rather than the influence of nonplanarity. Notably, tri-mixed substituted porphyrins have shown the following trend in their first oxidation potentials: MTPP(NO$_2$)Ph$_2$ $\leq$ MTPP(NO$_2$)Th$_2$ < MTPP(NO$_2$) < MTPP(NO$_2$)(PE)$_2$ < MTPP(NO$_2$)Br$_2$ < MTPP(NO$_2$)(CN)$_2$. This trend is in accordance with the electronic nature of the substituents. The cathodic shift in the oxidation potentials of MTPP(NO$_2$)Ph$_2$ relative to MTPP(NO$_2$) is explained in terms of electron donating nature of phenyl groups. For the Hammett equation $E_{1/2} = 2\sigma\rho$ for MTPP(NO$_2$)X$_2$, the plot of the first ring oxidation and reduction *vs*. the Hammett parameter (σ_p) of the substituents (X) [33] in MTPP(NO$_2$)X$_2$ was examined to delineate the role of X on the redox potentials and they show more linear trend in reduction and oxidation (Figure A36 and Table 4). The reaction constant (ρ) for the oxidation of MTPP(NO$_2$)X$_2$ is in the range 0.12 to 0.25 V whereas for the reduction it ranges from 0.12 to 0.19 V. The effects of tri-substitution in CuTPP(NO$_2$)X$_2$ on redox potentials and HOMO-LUMO gap is shown in the Figure A35 in Appendix 1. Almost same trend was observed for H$_2$TPP(NO$_2$)X$_2$ and other metal complexes (Table 4). In MTPP(NO$_2$)X$_2$ series, the first ring redox potentials varied according to the electronic nature of the substituents with marginal modulation in HOMO-LUMO gap (~ 0.2 V as compared to MTPP(NO$_2$)) which is in accordance with observed moderate nonplanar conformation of MTPP(NO$_2$)X$_2$ series (*vide supra*).

Further, we have carried out the electrochemical studies of MTPP(NO$_2$)X$_6$ in order to examine the effect of number of substituents and nonplanarity (Figures A32 - A34 in Appendix 1). The first ring oxidation potentials of these porphyrins ranges from 0.68 to 1.31 V whereas reduction

potential varies from -0.69 to -1.08 V which shows the broader range in comparison to $MTPP(NO_2)X_2$. The metal centered reduction potentials of $CoTPP(NO_2)X_6$ is 0.2 - 0.6 V anodically shifted than CoTPP whereas oxidation potentials are less shifted (0.04 - 0.2 V). This indicates that the electron withdrawing groups influence significantly the metal centered reduction rather than oxidation. For the Hammett equation $E_{1/2} = 6\sigma\rho$ for $MTPP(NO_2)X_6$, the Hammett plots were constructed to delineate the role of X on the potentials and they show linear trend in reduction whereas more scattered points in oxidation were observed with poor r^2 values (Figure A36 and Table 4). The scattered points of oxidation in the Hammet plot indicates the nonplanar confirmation of macrocycle as evidenced from DFT calculations. This is further supported by downfield resonances of NH signals of $H_2TPP(NO_2)X_6$ in ^1H NMR spectroscopy. Figure 10 shows the cyclic voltammograms of $CuTPP(NO_2)X_n$ (X = Ph or Th; n = 0, 2, 6) bearing β-pyrrole phenyl or thienyl substituents. The oxidation potentials of $CuTPP(NO_2)Ph_6$ is ~ 0.38 V cathodically shifted in comparison to $CuTPP(NO_2)$ whereas reduction is almost unaltered, indicating that each phenyl groups shifts 60 mV cathodic (Figure 8) due to the electron donating nature of Ph groups and increased nonplanarity. Notably, $CuTPP(NO_2)Th_6$ exhibited 0.3 V cathodic shift in oxidation relative to $CuTPP(NO_2)$ whereas 0.12 V anodic shift in reduction was observed. The observed cathodic shift in oxidation is ascribed to the combined effect of electron releasing conjugative nature of 2-thienyl groups and highly nonplanar conformation of the macrocycle whereas anodic shift in reduction is due to electron withdrawing inductive effect of 2-thienyl groups [21].

Notably, the first oxidation potentials of $MTPP(NO_2)X_6$ (X = Ph and Th) are more cathodically shifted (0.15 - 0.25 V) while reduction potentials are marginally cathodic (0.03 - 0.06 V) relative to their corresponding $MTPP(NO_2)X_2$ derivatives due to nonplanar conformation of the macrocycle which destabilizes the HOMO. The ρ (reactivity constant) for the oxidation of $MTPP(NO_2)X_6$ is in the range of 0.15 to 0.26 V whereas for the reduction it ranges from 0.16 to 0.21 V. The higher ρ values for the oxidation of $MTPP(NO_2)X_6$ as compared to $MTPP(NO_2)X_2$ systems indicate the ease of oxidations due to enhanced nonplanarity of the macrocycle. β-Substituted TPP series, viz. $MTPP(NO_2)X_2$, $MTPP(NO_2)X_6$, $MTPPX_n$ (n = 1, 4) exhibited ρ values higher than that of reported for the β-octabromo/chloro MT(4-X-phenyl)P ($\rho = 0.03 - 0.08$ V) [34] and MT(4-X-phenyl)P series ($\rho = 0.065$ V) [35]. This is anticipated since the substitution at the β-pyrrole position is in direct conjugation with the porphyrin π-system so that higher ρ

Table 3. Electrochemical redox potentials (in V vs Ag/AgCl) of mixed substituted porphyrins in CH_2Cl_2 containing 0.1 M $TBAPF_6$ with a scan rate of 0.1 V/s at 298 K.

Porphyrin	Oxidation (mV)		Reduction (mV)		ΔE (mV)
	I	II	I	II	
H_2TPP	1000	1335	-1230	-1540	2230
$H_2TPP(NO_2)$	1100	1286	-874	-1086	1974
$H_2TPP(NO_2)Br_2$	1118	1214	-754	-824	1872
$H_2TPP(NO_2)Ph_2$	1009	1130	-849	-1028	1858
$H_2TPP(NO_2)(PE)_2$	1123	1233	-752	-827	1875
$H_2TPP(NO_2)Th_2$	1007	1132	-800	-925	1807
$H_2TPP(NO_2)(CN)_2$	1294	1462	-519	-827	1813
$H_2TPP(NO_2)Br_6$	1045[i]	1288[i]	-642[i]	-973[i]	1687
$H_2TPP(NO_2)Ph_6$	804[i]	1091[i]	-921[i]	-1354[i]	1725
$H_2TPP(NO_2)(PE)_6$	1098[i]	1185[i]	-659	-732	1757
$H_2TPP(NO_2)Th_6$	806[i]	1033	-805	-1345	1611

[i]refers to irreversible peak potential
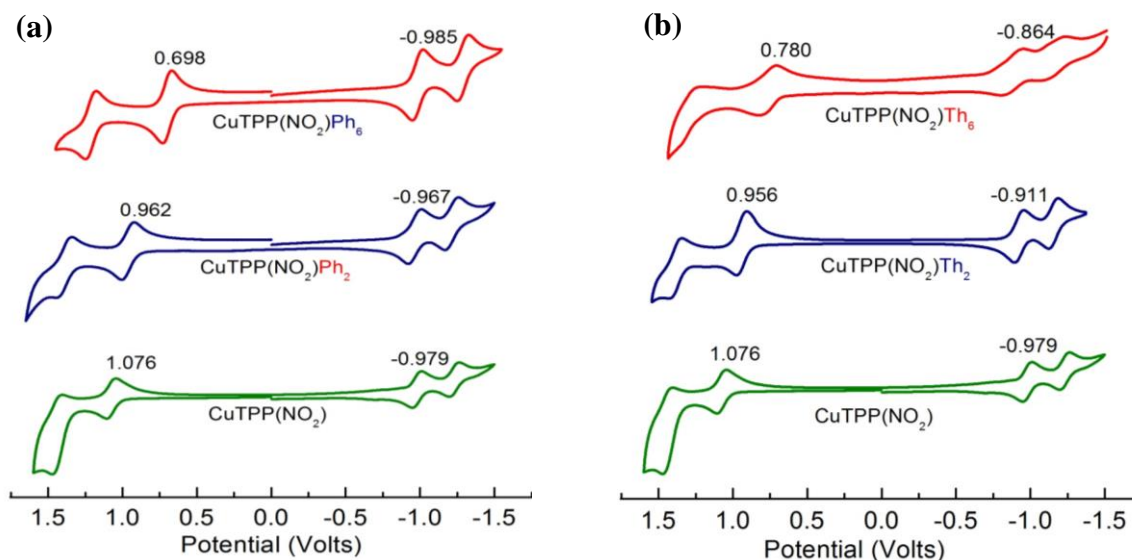
Figure 10. Cyclic Voltammograms of (a) $CuTPP(NO_2)Ph_n$ and (b) $CuTPP(NO_2)Th_n$ (n = 0, 2 and 6) in CH_2Cl_2 containing 0.1 M $TBAPF_6$ using Ag/AgCl as reference electrode with a scan rate of 0.1 V/s at 298 K. The porphyrin concentration was maintained ~ 1mM.
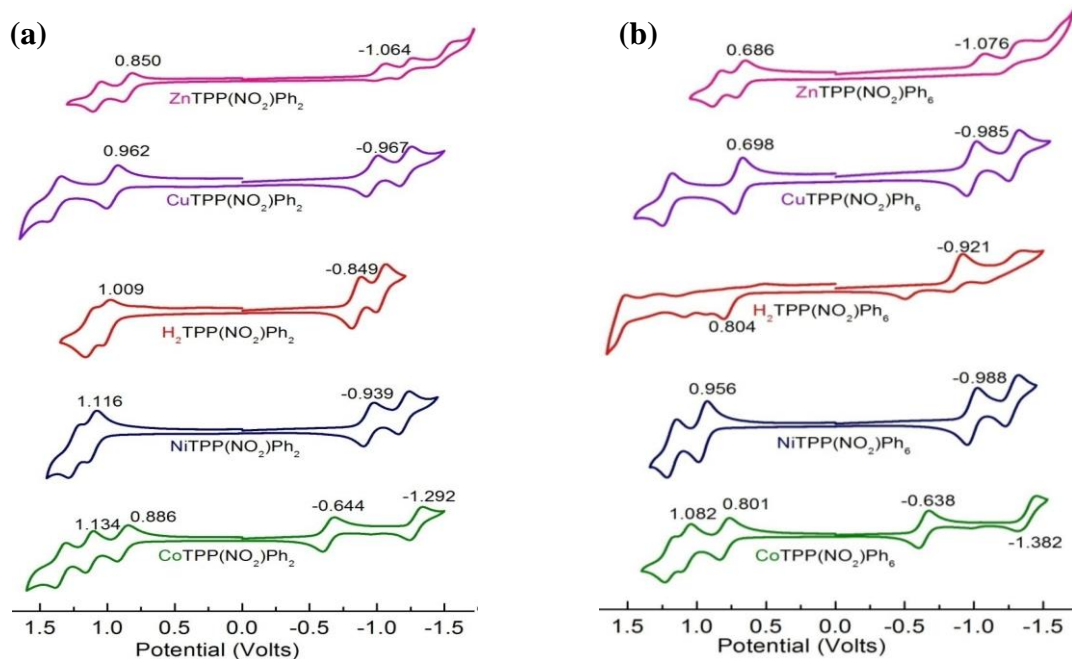
Figure 11. Cyclic Voltammograms of (a) $MTPP(NO_2)Ph_2$ and (b) $MTPP(NO_2)Ph_6$ (M = 2H, Co(II), Ni(II), Cu(II), Zn(II)) in CH_2Cl_2 containing 0.1 M $TBAPF_6$ using Ag/AgCl as reference electrode at 298 K.

Table 4. Summary of Hammett plots with reaction constants (ρ) and correlation coefficients (r^2) of first ring redox potentials (vs Ag/AgCl) for various mixed substituted porphyrins[a]

Porphyrin	First oxidation		First reduction	
	ρ (V)	r^2	ρ (V)	r^2
$H_2TPP(NO_2)X_2$	0.193	0.86	0.249	0.98
$CuTPP(NO_2)X_2$	0.251	0.86	0.252	0.98
$NiTPP(NO_2)X_2$	0.121	0.77	0.154	0.87
$ZnTPP(NO_2)X_2$	0.146	0.92	0.261	0.99
$H_2TPP(NO_2)X_6$	0.117	0.23	0.194	0.95
$CuTPP(NO_2)X_6$	0.154	0.31	0.206	0.97
$NiTPP(NO_2)X_6$	0.187	0.62	0.232	0.97
$ZnTPP(NO_2)X_6$	0.117	0.42	0.161	0.88

[a]$MTPP(NO_2)X_n$ where X = Br, CN, Ph, PE and Th.

values were observed. The effect of core metal ion on the redox potentials of the representative porphyrins $MTPP(NO_2)Ph_n$ (n = 2 and 6; M = Co(II), Ni(II), Cu(II) and Zn(II)) is shown in Figure 11. The first ring oxidation potentials of these porphyrins have shown the following trend: Zn(II) < Cu(II) < H_2 < Ni(II) < Co(II) for both tri- and hepta-substituted porphyrins according to their difference in their electronegativity. In $MTPP(NO_2)X_6$ series, the first ring redox potentials varied significantly according to the electronic nature of the substituents and enhanced nonplanarity upon substitution which results the dramatic reduction in HOMO-LUMO gap (0.54-to-0.66 V) as referenced from MTPP (Figure 12). By means of unsymmetrical substitution, we are able to tune the redox potentials with dramatic decrement in the HOMO-LUMO gap. The fairly broader range of σ values for the first ring redox potentials of mixed substituted porphyrins is possibly due to the effect of the core metal ion and the nature of the mixed substituents at the β-pyrrole positions. As reported earlier, the oxidation potentials are largely influenced by the substituent effect and nonplanarity of the porphyrin macrocycle while the reduction potentials are independent of structural change [36]. Almost planar structure of H_2TPPBr_2 [10] is anticipated to show variable degrees of nonplanarity with an increase in size or shape of the substituent X in $MTPP(NO_2)X_6$ derivatives.
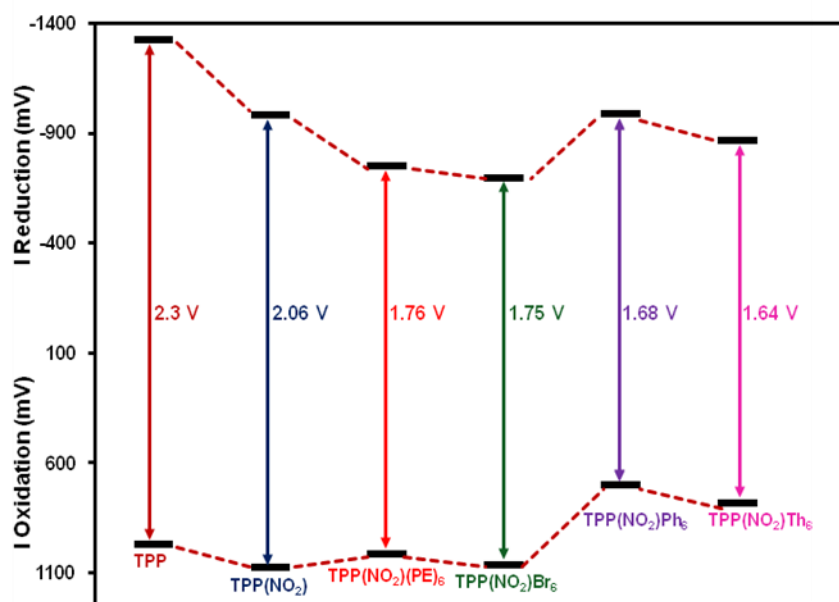
Figure 12. The HOMO-LUMO variation of $CuTPP(NO_2)X_6$ where X = PE, Br, Ph and Th in comparison to $CuTPP(NO_2)$ and CuTPP.

The crystal structure of H_2TPPBr_6 showed considerable nonplanar conformation of the porphyrin ring [10]. The ease of oxidation in $MTPP(NO_2)X_6$ relative to the corresponding $MTPP(NO_2)X_2$ derivatives is ascribed to the electronic effects of the substituents and nonplanar distortion of the macrocycle; however, the reduction potentials are predominantly dependent on the nature of the substituents.

The electrochemical redox potentials and UV-Visible spectral data of these unsymmetrically substituted free-base porphyrins were compared with the literature having symmetrical β-pyrrole substituents, H_2TPPX_4 (X = Br, Ph, Th and CN) and H_2TPPX_8 (X = Br, PE and Ph) derivatives

Table 5. Comparison of first ring redox data ($\Delta E_{1/2}$) with longest wavelength band energy $Q_x(0,0)$ of various porphyrins in CH_2Cl_2 at 298 K.

Porphyrin	B (nm)	$Q_x(0,0)$ (nm)	$Q_x(0,0)$ (eV)	[b]$\Delta E_{1/2}$ (V)	ref
$TPP(NO_2)(PE)_2$	444	687	1.80	1.87	a
$TPP(NO_2)Ph_2$	439	686	1.80	1.85	a
$TPP(NO_2)Br_2$	436	683	1.82	1.87	a
$TPP(NO_2)Th_2$	440	695	1.78	1.80	a
$TPP(NO_2)(CN)_2$	440	702	1.77	1.81	a
$TPP(PE)_4$	452	690	1.80	1.90	a
$TPPPh_4$	434	677	1.83	2.02	39a
$TPPBr_4$	436	685	1.81	1.84	40a
$TPPTh_4$	445	701	1.77	1.94	24b
$TPP(CN)_4$	449	729	1.70	1.66	9b
$TPP(NO_2)(PE)_6$	494	751	1.65	1.75	a
$TPP(NO_2)Ph_6$	470	729	1.70	1.72	a
$TPP(NO_2)Br_6$	468	739	1.67	1.68	a
$TPP(NO_2)Th_6$	481	754	1.64	1.61	a
$TPP(PE)_8$	506	761	1.63	1.71	39b
$TPPPh_8$	468	724	1.71	1.84	40b
$TPPBr_8$	469	743	1.67	1.64	28a
TPP	414	646	1.92	2.23	16f

[a]refers this work, [b]$\Delta E_{1/2} = I$ oxidation - I reduction

as shown in Table 5. The $\Delta E_{1/2}$ from the redox potentials correlates fairly well with the HOMO-LUMO gap calculated from the longest wavelength band in the optical absorption spectra of these mixed substituted porphyrins. $Q_x(0,0)$ and $\Delta E_{1/2}$ of mixed tri- and hepta-substituted porphyrins are of comparable energy relative to β-tetra and octasubstituted porphyrins (H_2TPPX_n, n = 4 and 8) as indicated in Table 5. These results clearly indicate that the tri- and hepta mixed substitution can compensate the effect of homo tetra- and octa substituted porphyrins.

2.4 CONCLUSIONS

Two new families of novel mixed substituted porphyrins and their complexes have been synthesized and characterized. The crystal structures analyses and DFT fully optimized geometries of $MTPP(NO_2)X_2$ and $MTPP(NO_2)X_6$ revealed moderate and highly nonplanar saddle shape conformations, respectively. These unsymmetrically substituted porphyrins exhibited dramatic red-shift in their B and $Q_x(0,0)$ bands as compared to $MTPP(NO_2)$ and MTPP. The dramatic downfield shift of NH proton resonances and the higher protonation/deprotonation constants of $H_2TPP(NO_2)X_6$ readily reflects the electronic effects of the mixed substituents (X) and nonplanarity of the macrocycle as compared to $H_2TPP(NO_2)X_2$. The fairly broader range of first ring redox potentials (0.68 to 1.31 V for oxidation and -0.64 to -1.10 V for reduction) and σ values of $MTPP(NO_2)X_6$ clearly indicate the redox tunablity achieved by means of unsymmetrical substitution. Further, the HOMO-LUMO gap considerably decreases as we increase the number of β-substituents from 3 to 7 i.e., $MTPP(NO_2)X_2$ to $MTPP(NO_2)X_6$. The remarkable red-shift in electronic spectral features, downfield shift of NH protons, the variation in protonation and deprotonation constants, the significant shift in redox potentials of these porphyrins are interpreted in terms of both an inductive and resonance interactions of susbtituents on porphyrin π-system as well as nonplanarity of the macrocycle. The $\Delta E_{1/2}$ obtained from the redox potentials as well as from spectral data ($Q_x(0,0)$ band) suggests that the unsymmetrical tri- and hepta-substitution can compensate the effect of homo tetra- and octa-substitution of porphyrins (H_2TPPX_n, n = 4 and 8). By means of β-pyrrole mixed substitution on the porphyrin macrocycle, we were able to achieve the remarkable bathochromic shift in electronic spectral bands, varying degrees of nonplanarity, higher reactivity constants (ρ values) and tunable electrochemical redox properties with dramatic reduction in HOMO-LUMO gap.

Currently we are utilizing these mixed substituted porphyrins for nonlinear optical studies, catalytic and sensor applications and will report on these studies in near future.

Appendix Information.

Figures of optical absorption and emission spectra, ^{1}H NMR spectra, UV-Visible titrations for protonation and deprotonation, cyclic votammetric studies and XRD data of novel mixed substituted porphyrins are available in Appendix 1.

2.5 REFERENCES

1.   Kaim, W.; Schwederski, B.,"Bioinorganic Chemistry: Inorganic Elements in the Chemistry of Life: An Introduction and Guide", John Wiley & Sons, **1987.**

2   Senge, M. O., "Highly substituted porphyrins", pp. 239-347. In Kadish, K. M.; Smith, K. M.; Guilard R., Eds., The porphyrin hand book, Vol. 1, Academic Press, San Diego, **2000**.

3   Retsek, J. L., Medforth, C. J.; Nurco, D. J.; Gentemann, S.; Chirvony, V. S.; Smith, K. M.; Holten D. "Conformational and electronic effects of phenyl-ring fluorination on the photophysical properties of nonplanar dodecaarylporphyrins", *J. Phys. Chem. B* **2001,** *105*, 6396-6411.

4.   Hombrecher, H. K.; Gherdan, V. M.; Ohm, S; Cavaleiro, J. A. S.; Neves, M. G. P. M.   S.; Condesso, M. F., "Synthesis and electrochemical investigation of *β*-alkyloxy substituted *meso*- tetraphenylporphyrins", *Tetrahedron* **1993**, *49*, 8569-8578.

5.   Shea, K. M., Jaquinod, L; Smith, K. M., "Dihydroporphyrin Synthesis: New Methodology", *J. Org. Chem*. **1998**, *63*, 7013-7021.

6.   Bartoli, J. F.; Mansuy, O.; Le, B.-O.; Ozette, K. L. B.; Palacio, M.; Mansuy, D., "New manganese *β*-polynitroporphyrins as particularly efficient catalysts for biomimetic hydroxylation of aromatic compounds with H_2O_2", *J. Chem. Soc., Chem. Commun.* **2000**, 827-828.

7.   Chirvony, V. S.; van Hoek, A.; Schaafsma, T. J.; Pershukevich, P. P.; Filatov, I. V.; Avilov, I. V.; Shishporenok, S. I.; Terekhov, S. N.; Malinovskii, V. L., "On the Nature of

the Fluorescent State in *β*-Nitrotetraarylporphyrin", *J. Phys. Chem. B* **1998**, *102*, 9714-9724.

8. Sen, A.; Krishnan, V., "Synthesis, spectral and electrochemical properties of donor/acceptor substituted fluoroarylporphyrins", *Tetrahedron Lett.* **1996**, *37*, 5421-5424.

9. Duval, H.; Bulach, V.; Fischer, J.; Weiss, R., "Four-coordinate, low-spin (S = 0) and six-coordinate, high-spin (S = 1) nickel(II) complexes of tetraphenylporphyrins with β-pyrrole electron-withdrawing substituents: Porphyrin-core expansion and conformation", *Inorg. Chem.* **1999**, *38*, 5495-5501.

10. Jaquinod, L.; Khoury, R. G.; Shea K. M.; Smith, K. M., "Regioselective syntheses and structural characterizations of 2,3-dibromo and 2,3,7,8,12,13-hexabromo-5,10,15,20-tetraphenylporphyrins", *Tetrahedron* **1999**, *5*, 13151-13158.

11. Bhyrappa, P.; Sankar, M.; Varghese, B., "Mixed substituted porphyrins: Structural and electrochemical redox properties", *Inorg. Chem*. **2006**, *45*, 4136-4149.

12. Chaudhri, N. ; Sankar, M., "Colorometric naked-eye detection of CN^-, F^-, CH_3COO^- and $H_2PO_4^-$ ions by highly nonplanar electron deficient perhaloporphyrins" , *RSC Adv.* **2015**, *5*, 3269-3275.

13. Sheldrick, G. M. ; SIR97 and SHELX97, "Programs for Crystal Structure Refinement", University of Göttingen, Göttingen (Germany), **1997.**

14. Hill, A. V. , "The possible effects of the aggregation of the molecules of haemoglobin on its dissociation curves", *J. Physiol. London*. **1910**, *40*, IV-VII.

15. Scheidt, W. R.; Lee, Y. J., "Recent advances in the stereochemistry of metallotetrapyrroles", *Struct. Bonding (Berlin)* **1987**, *64*, 1-70.

16. Scheidt, W. R., In "The Porphyrin Handbook"*,* Kadish, K. M., Smith, K. M., Guilard, R., Eds.; Academic Press, New York, **2000**; Vol. 3, 49-112.

17. Duval, H.; Bulach, V.; Fischer, J.; Weiss, R., " Four-coordinate, low-spin (S = 0) and six-coordinate, high-spin (S = 1) nickel(II) complexes of tetraphenylporphyrins with β-

pyrrole electron-withdrawing substituents: Porphyrin-core expansion and conformation", *Inorg. Chem.* **1999**, *38*, 5495-5501.

18.   Bhyrappa, P.; Arunkumar, C.; Varghese, B., "Influence of Mixed Substituents on the Macrocyclic Ring Distortions of Free Base Porphyrins and Their Metal Complexes", *Inorg. Chem.* **2009**, *48*, 3954-3965.

19.   Alemayehu, A. B.; Hansen, L. K.; Ghosh, A., "Nonplanar, Noninnocent, and Chiral: A Strongly Saddled Metallocorrole", *Inorg. Chem.* **2010**, *49*, 7608-7610.

20.   Terazono, Y.; Patrick, B. O.; Dolphin, D., "Synthesis, crystal structures, and redox potentials of 2,3,12,13-tetrasubstituted 5,10,15,20-tetraphenylporphyrin zinc(II) complexes", *Inorg. Chem.* **2002**, *41*, 6703-6710.

21.   Bhyrappa, P.; Velkannan, V., "*β*-Tetrakis(2-thienyl)-meso-tetraphenylporphyrins: Synthesis, structural and electrochemical redox properties", *Inorg. Chim. Acta* **2012**, *387*, 64-73.

22.   Parusal, A. B. J.; Wondimagegn, T.; Ghosh, A., "Do nonplanar porphyrins have red-shifted electronic spectra? A DFT/SCI study and reinvestigation of a recent proposal", *J. Am. Chem. Soc.* **2000**, *122*, 6371-6374.

23.   DiMangno, S. G.; Wertsching, A. K.; Ross, C. R. II., "Electronic consequences of nonplanar core conformations in electron-deficient porphyrins: The structure and spectroscopic properties of [5,10,15,20-Tetrakis(heptafluoropropyl)-porphinato] cobalt(II)", *J. Am. Chem. Soc.* **1995**, *117*, 8279-8280.

24.   Meot-Ner, M.; Adler, A. D., "Substituent effects in noncoplanar π systems. *ms*-porphins ", *J. Am. Chem. Soc.* **1975**, *97*, 5107-5111.

25.   Bhyrappa, P.; Krishnan, V., "Octabromotetraphenylporphyrins and its metal derivatives. Electronic structure and electrochemical properties", *Inorg. Chem.* **1991**, *30*, 239-245.

26.   Fukuzumi, S.; Kojima, T., "Photofunctional nanomaterials composed of multiporphyrins and carbon-based π-electron acceptors", *J. Mater. Chem.* **2008**, *18*, 1427-1439.

27. Haddad, R. E.; Gazeau, S.; Pecaut, J.; Marchon, J.-C.; Medforth, C.J.; Shelnutt, J. A., "Origin of the red-shift of the optical absorption bands of nonplanar tetraalkylporphyrins", *J. Am. Chem. Soc.* **2005**, *125*, 1253-1268.

28 Shelnutt, J. A.; Ortiz, V., "Substituent effects on the electronic structure of metalloporphyrins: A quantitative analysis in terms of four-orbital-model parameters", *J. Phys. Chem.* **1985**, *89*, 4733-4739.

29. Retsek, J. L.; Medforth, C. J.; Nurco, D. J.; Gentemann, S.; Chirvony, V. S.; Smith, K. M.; Holten, D., "Conformational and electronic effects of phenyl-ring fluorination on the photophysical properties of nonplanar dodecaarylporphyrins", *J. Phys. Chem. B* **2001**, *105*, 6396-6411.

30. Medforth, C. J.; Smith, K. M., "The synthesis and solution conformation of dodecaphenylporphyrin", *Tetrahedron Lett*. **1990**, *31*, 5583-5586.

31 Fang, Y.; Bhyrappa, P.; Ou, Z.; Kadish, K. M., "Planar and nonplanar free base tetraarylporphyrins : *β*-pyrrole substituents and geometric effects on electrochemistry, spectroelectrochemistry, and protonation/deprotonation in nonaqueous media", *Chem. Eur. J*. **2014**, *20*, 524-532.

32 Kadish, K. M.; Royal, G.; Van Caemelbecke, E.; Gueletti, L., "The Porphyrin Handbook", Vol. 9, Eds. Kadish, K. M.; Smith, K. M.; Guilard, R. Academic Press, San Diego, **2000**, 1-219

33 Hansch, C.; Leo, A.; Taft, R. W., "A survey of Hammett substituent constants and resonance and field parameters", *Chem. Rev*. **1991**, *91***,** 165-195.

34 Ghosh, A.; Halvorsen, I.; Nilsen, H. J.; Steene, E.; Wondimagegn,T.; Lie, R.; Van Caemelbecke, E.; Guo, N.; Ou, Z.; Kadish, K. M., "Electrochemistry of nickel and copper β-octahalageno-*meso*-tetraaryl-porphyrins. Evidence for important role played by saddling-induced metal(d_{x2-y2})-porphyrin("a_{2u}") orbital interactions" , *J. Phys. Chem. B* **2001**, *105*, 8120-8124.

35 Kadish, K. M.; Morrison, M. M., "Solvent and substituent effects on the redox reactions of *para*-substituted tetraphenylporphyrin", *J. Am. Chem. Soc.* **1976**, *98*, 3326-3328.

36   D'Souza, F.; Zandler, M.; Tagliatesta, P.; Ou, Z.; Shao, J.; Van Caemelbecke, E.; Kadish, K. M., "Electronic, spectral, and electrochemical properties of $(TPPBr_x)Zn$ where $TPPBr_x$ is the dianion of β-brominated-pyrrole tetraphenylporphyrin and x varies from 0 to 8", *Inorg. Chem.* **1998**, *37*, 4567-4572.

CHAPTER 3

Ratiometric Colorimetric "Naked Eye" Selective Detection of CN⁻ Ions by Electron Deficient Ni(II) Porphyrins and Their Reversibility Studies
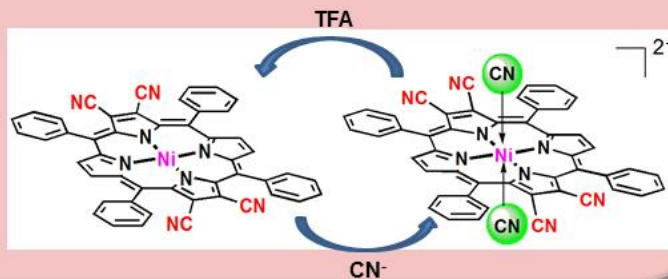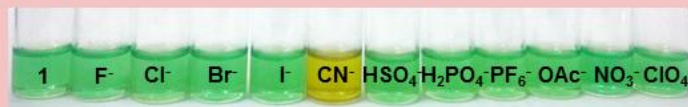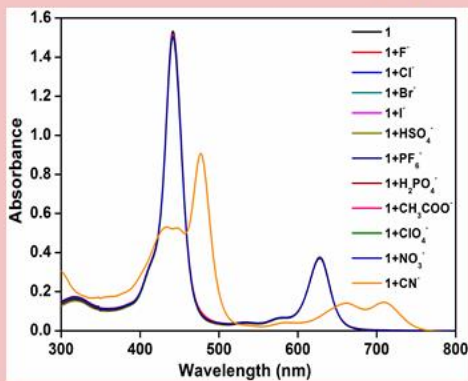
CHAPTER 3

RATIOMETRIC COLORIMETRIC "NAKED EYE" SELECTIVE DETECTION OF CN⁻ IONS BY ELECTRON DEFICIENT NI(II) PORPHYRINS AND THEIR REVERSIBILITY STUDIES

3.1 INTRODUCTION

The design of anion receptors with high selectivity has been the subject of intensive research due to their potential applications in environmental, clinical, chemical and biological sectors [1-4].Cyanide is one among the toxic anions; even as little as 0.5 - 3.5 mg cyanide per kg of body weight is lethal to humans where it binds with cytochrome c inside the cells and interferes the mitochondrial electron transport chain, thus inhibiting cellular respiration causing hypoxia [5]. Cyanide ions could be absorbed through the lungs, skin, and gastrointestinal tract leading to vomiting, convulsion, loss of consciousness, and eventual death [6]. Despite their toxicity, their outstanding applications in various industrial processes [7] including electroplating, metallurgy, heap leaching of gold ore, polymer synthesis, steel manufacturing and as raw materials for synthetic fibers, resins and herbicides are inevitable,which raises the risk for accidental or intentional release of cyanide ions into environment as a toxic contaminant [6].

All the above aspects demand an efficient sensing system to monitor cyanide concentration from contaminant sources. A variety of instrumental techniques have been developed for the determination of cyanide, including ion chromatography, voltammetry, amperometry, fluorometry, ion selective electrode and potentiometry. But the primary disadvantage of these techniques is the use of time-consuming procedures and sophisticated instrumentation. Now-a-days, the most attractive approach focuses on highly selective colorimetric cyanide ion sensors, which allows "naked eye" detection of CN⁻ ions by means of colour change [8]. Various approaches to the novel colorimetric chemosensors for anions are displacement assay, chemodosimetric method, nucleophilic addition to carbonyl group or activated carbon-carbon double bond, host-guest interactions through hydrogen bonding, anion induced deprotonation etc [1-4]. However, they do suffer with one or more limitations such as poor selectivity especially in the

presence of fluoride or acetate ions. Most of the chemodosimeters are irreversible, others require specific conditions, such as high temperature or basic media, only works in an organic media, complicated multi-step synthesis [9]. All these drawbacks challenge us to fabricate a unique reversible, specific, colorimetric optical probe capable of 'naked eye' detection' of CN^- ions with extremely low detection limits.
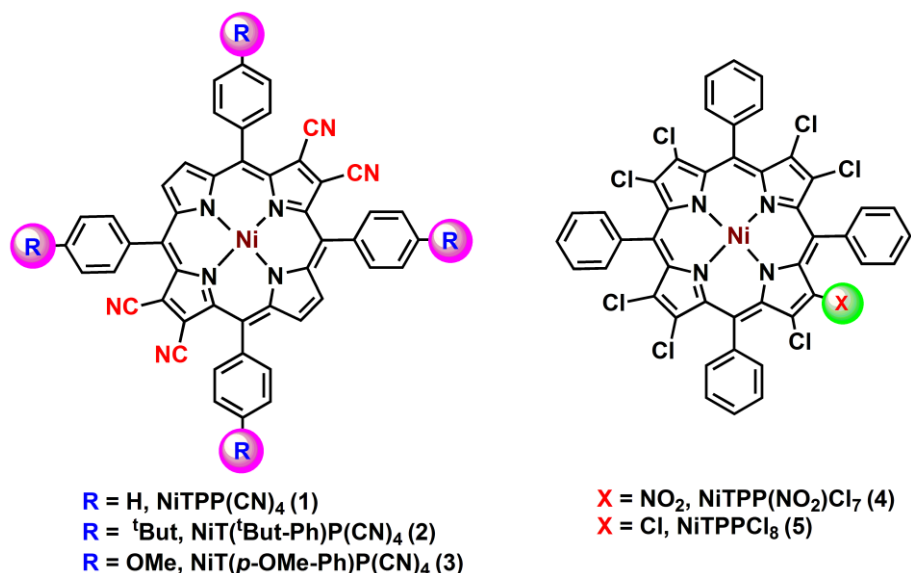

R = H, NiTPP(CN)$_4$ (1)
R = ^{t}But, NiT(^{t}But-Ph)P(CN)$_4$ (2)
R = OMe, NiT(p-OMe-Ph)P(CN)$_4$ (3)

X = NO$_2$, NiTPP(NO$_2$)Cl$_7$ (4)
X = Cl, NiTPPCl$_8$ (5)

Chart 1. Molecular structures of β-substituted Ni(II) porphyrins **1-5**.

Porphyrin-based receptors for anions have been constructed through the derivatization of *meso*-positions [10] having appropriate binding pockets whereas only a few reports on β-functionalized porphyrins [11] due to their synthetic difficulties. Metalloporphyrins have been utilized for the detection of CN^- ions due to intrinsic affinity of cyanide for many metals such as zinc, rhodium, and copper coordinated to porphyrins as described in chapter 1. Recently, cyanide sensing through chemodosimetric method by a new calix[4]pyrrole derivative, Pd-calixphyrin, cobalt corrins, and subphthalocyanine dye have been reported in the literature as discussed in earlier chapter. In general, square planar Ni(II) porphyrins exhibited very weak axial ligation and extremely low binding constants (β_2 = 0.3 - 38 M^{-2}) with nitrogenous bases [12,13]. Herein, we are reporting an easy, rapid, reusable, selective and sensitive 'naked eye' colorimetric cyanide ion sensing by highly electron deficient planar and nonplanar β-substituted Ni(II) porphyrins (**1-5**, Chart 1) with extremely high binding constants (β_2 = 10^{16} - 10^8 M^{-2}) through coordinative interactions for the first time in porphyrin chemistry.

3.2 EXPERIMENTAL SECTION

3.2.1 Materials

Pyrrole, benzaldehyde, $Ni(OAc)_2 \cdot 4H_2O$, TFA, pyridine and Na_2SO_4 were purchased from HiMedia, India and used as received. 4-Anisaldehyde was purchased from SDFCL and *p*-^{t}Bu-benzaldehyde and copper(I) cyanide were purchased from Alfa Aesar and used as received. The tetrabutylammonium salts (TBAX, X = CN^-, F^-, Cl^-, Br^-, I^-, HSO_4^-, OAc^-, $H_2PO_4^-$, ClO_4^-, PF_6^- and NO_3^-) were purchased from Alfa Aesar and used as received. Dry CH_2Cl_2 for CV studies was distilled thrice from CaH_2 and the toluene (for UV-Visible spectral studies) was dried and distilled from sodium-benzophenone mixture.

3.2.2 Instrumentation and methods

MALDI-TOF-MS spectra were measured using a BrukerUltrafleXtreme-TN MALDI-TOF/TOF spectrometer using HABA as a matrix. The X-ray quality single crystals of **1**(Pyridine)$_2$ and **3** were obtained by direct diffusion of hexane into $CHCl_3$/pyridine and pure $CHCl_3$ solutions of **1** and **3**, respectively. The single crystals of **4-5** were obtained by direct diffusion of hexane into saturated toluene solution of **4** and **5**. X-ray quality single crystals of **3•CN$^-$** was obtained by direct diffusion of *n*-hexane into the $CHCl_3$ solution of **3** containing small amount of TBACN. Single-crystal XRD data of **1**, **3-5** and **3•CN$^-$** were collected on a Bruker Apex-II CCD diffractometer equipped with a liquid cryostat. The data collection was done at 293 K as explained in chapter 2. The structures were solved by direct methods by using SIR97 and SHELX-97 [14]. In case of **1**(Py)$_2$ and **3**, SQUEEZE procedure [15] was implemented in order to correct electron density contribution from disordered solvent molecules. The crystallographic data of these Ni(II) porphyrins are summarized in Table A2 in Appendix 2. CCDC-1043611 (**1**(pyridine)$_2$), 1043609 (**3**), 1043615 (**4**), 1044025 (**5**) and 1043610 (**1•CN$^-$**) contain the crystallographic supplementary data. Elemental analysis, CV studies and DFT calculations were carried out as described in chapter 1.

For UV-Vis titrations, the concentrations of **1-5** were kept in the range of 9 - 13 μM throughout the experiments whereas the stock solution of anions was maintained in between 4 to 8 mM as per their need. The temperature inside the cell was 298±0.2 K. The

association constants (β_2) and stoichiometry for anion binding were calculated using Hill equation [16]. The limit of detection (LOD) values has been calculated by using the intercept of plotted graph between (A_{min}-A)/(A_{min}-A_{max}) and log[A⁻] [17]. For the practical utility of these sensors, the test strips were prepared by cutting the Whatman filter paper (grade 1) and dipped in 1 mM toluene solution of **1-5** for few seconds and dried. These test strips were dipped in different anion solutions for 1-2 seconds.The colour change from green to yellow (**1-3**) and brown to green (**4-5**) were observed only with cyanide ions. The similar results were observed when these test strips were exposed to neutral aqueous solution of tested anions.

3.2.3 General procedure for the Synthesis of Nickel(II) complexes of *β*-tetracyano-*meso*-tetraphenylporphyrins (1-3):

NiTPPBr$_4$ (0.5 g, 0.507mmol) and copper(I)cyanide (1.816 g, 20.27mmol) were taken in 250 mL two neck RB. To this, 50 mL of pyridine was added and heated at 90ºC for 24 hours under argon atmosphere. At the end of this period, the reaction mixture was cooled and filtered through G-4 sintered crucible to remove excess copper cyanide. Solvent was removed under vacuum and then the crude product was loaded on silica column and purified using CHCl$_3$ as eluent. The similar procedure was employed for the preparation of **2-3**. The yield was found to be ~ 40% in all cases (**1-3**).

NiTPP(CN)$_4$ (1): UV/Vis (CH$_2$Cl$_2$): λ_{max} (nm) (logε)440 (5.10), 630(4.50). ^{1}H NMR in CDCl$_3$: δ (ppm) 8.77 (s, 4H, *β*-pyrrole-H), 7.89-7.83 (m, 12H, *meso-o-* and *m*-phenyl-H), 7.75-7.71 (m, 8H, *meso-m-* and *p*-phenyl-H). ESI-MS (m/z): found 771.9 [M+H]⁺, calcd. 771.2.Anal. Calcd for C$_{48}$H$_{24}$N$_8$Ni: C, 74.73; H, 3.14; N, 14.53%. Found: C, 74.52; H, 3.39;N, 14.65%.

NiT(*p*-^{t}But-Ph)P(CN)$_4$ (2): UV/Vis (CH$_2$Cl$_2$): λ_{max} (nm) (logε)445 (5.13), 632(4.47).^{1}H NMR in CDCl$_3$: δ (ppm) 8.81 (s, 4H, *β*-pyrrole-H), 7.77-7.70 (m, 16H, *meso-o-* and *m*-phenyl-H), 1.54 (s, 36H, CH$_3$ of ^{t}But). ESI-MS (m/z): found 1020.7 [M+H•Na]⁺, calcd. 1020.0.Anal. Calcd for C$_{64}$H$_{56}$N$_8$Ni: C, 77.19; H, 5.67; N, 11.25%. Found: C, 77.31; H, 5.50;N, 11.43%.

NiT(*p*-OMe-Ph)P(CN)₄(3):UV/Vis (CH₂Cl₂): λ_{max} (nm) (logε)450 (5.07), 636(4.54). ^{1}H NMR in CDCl₃: δ (ppm) 8.74 (s, 4H, *β*-pyrrole-H), 7.75 (d, 8H, *J* = 8.5 Hz,*meso-o*-phenyl-H), 7.24 (d, 8H, *J* = 8.5 Hz,*meso-m*-phenyl-H), 4.04 (s, 12H*, OCH₃ meso-m*-phenyl-H). MALDI-TOF-MS (m/z): found 892.6 [M+H]$^+$, calcd. 892.6.Anal. Calcd for C₅₂H₃₂N₈O₄Ni•0.5H₂O: C, 69.35; H, 3.69; N, 12.44%. Found: C, 69.40; H, 3.78;N, 12.55%.

3.3 RESULTS AND DISCUSSION

3.3.1 Synthesis and characterization

Ni(II) *β*-tetracyano-*meso*-tetraphenylporphyrins (**1**-**3**) were prepared by nucleophilic substitution at *β*-pyrrole positions of the tetrabromoporphyrins using modified literature
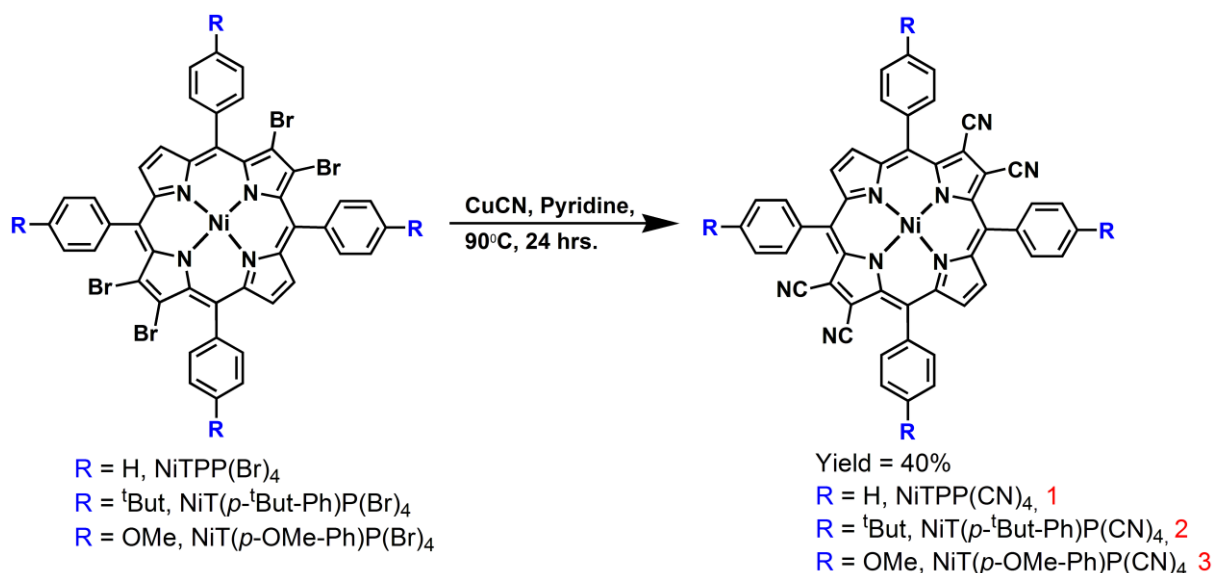
Scheme 1. Synthetic route for the preparation of **1**-**3***via* nucleophilic substitution at *β*-pyrrole positions.
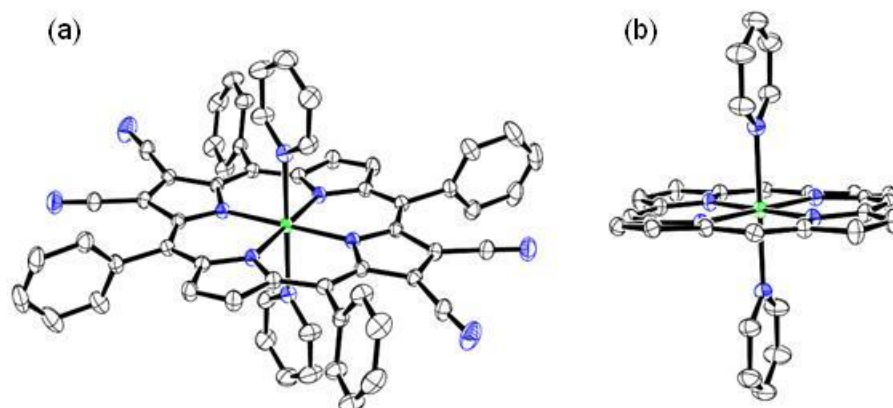
Figure 1 The ORTEP diagrams showing (a) top and (b) side views of **1** with axial coordination of pyridine molecules. In side view, the *β*-substituents and *meso*-phenyl groups are not shown for clarity.

methods [18] as shown in Scheme 1 and Ni(II) perhaloporphyrins (**4-5)** were synthesized by direct substitution at *β*-pyrrole position of macrocyclic ring according to reported procedure [19] as shown in Scheme 1 in appendix 2. These porphyrins were characterized by various spectroscopic techniques, elemental and single crystal XRD analyses. Figure 1 represents the side and top views of $NiTPP(CN)_4(Py)_2$ complex.

The representative absorption spectra of **1** and **3-5** were shown in CH_2Cl_2 at 298 K as shown in Figure 2. Table A1 in the Appendix 2 lists the electronic absorption spectral data of **1-5** in CH_2Cl_2. **3** exhibited 10 nm red shift in the Soret band as compared to **1** which is attributed to the electron donating effect of methoxy substituents. **1-3** exhibited considerable gain in the intensity of the longest wavelength $Q_x(0,0)$ band relative to the $Q_x(1,0)$ band due to extensive stabilization of a_{1u} relative to a_{2u} by means of *β*-cyano substitution which leads to increased transition probability of a_{2u} to $e_g(\pi^*)$ relative to a_{1u} to $e_g(\pi^*)$ [18]. **4** has shown red-shifted optical absorption spectra ($\Delta\lambda$ = 9-13 nm) ascompared to **5** due to electron withdrawing nature of nitro group and increased nonplanarity induced by mixed substitution. ^{1}H NMR spectra exhibited resonances arising from *β*-pyrrole, *meso*-phenyl, imino protons and *β*-substituents. The integrated intensities are consistence with the proposed structures. Figure 3 shows the ^{1}H NMR spectrum of **1** in $CDCl_3$ at 298 K. In ^{1}H NMR spectra of **1-3**, the *β*-pyrrole protons exhibited a singlet at

80

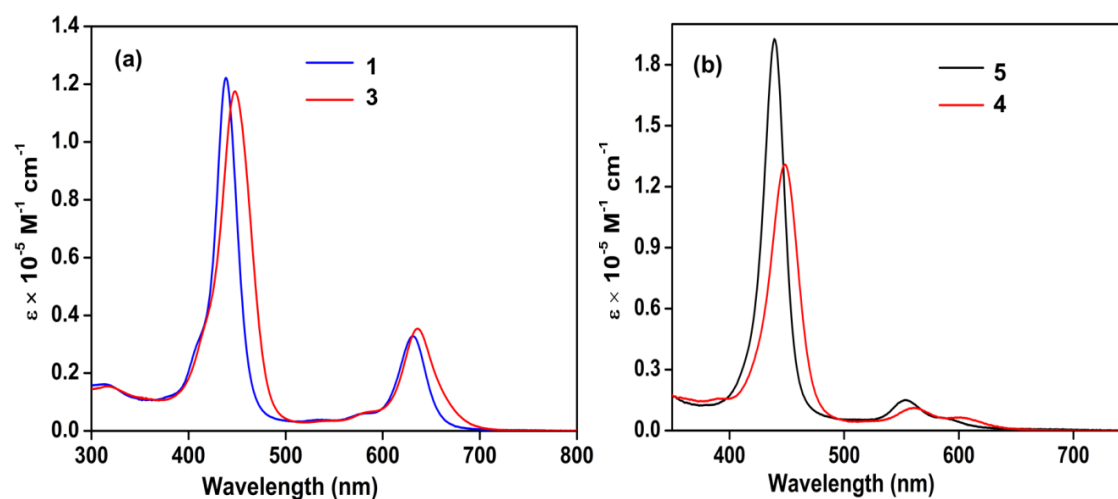8.74 - 8.81 ppm indicating the antipodal positions of *β*-cyano groups (Figures A2-A3, Appendix 2).

Figure 2. UV-Vis absorption spectra of (a) **1** and **3** as well as (b) **4-5** in CH_2Cl_2 at 298 K.
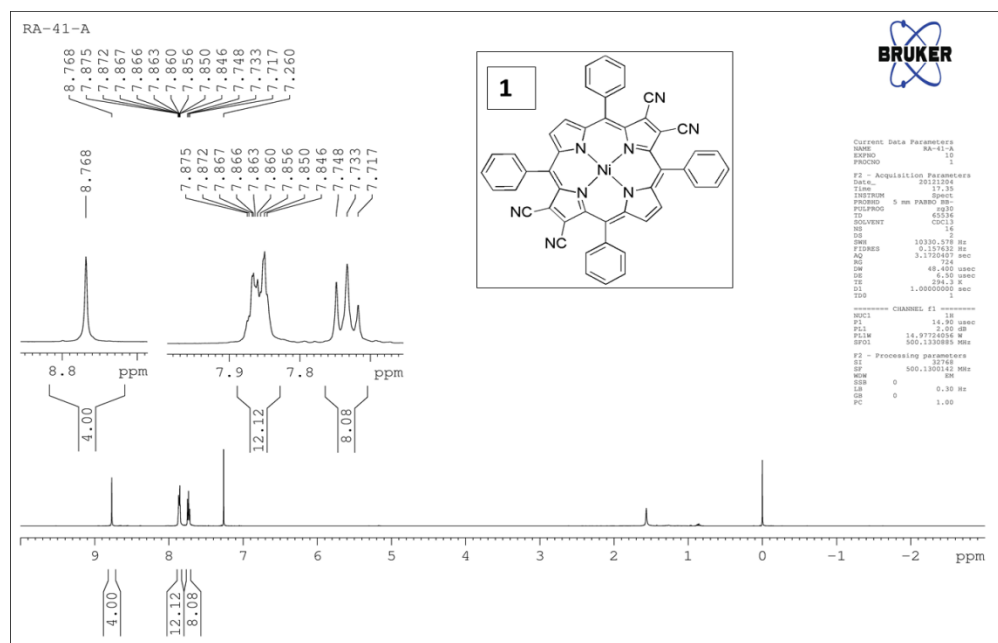

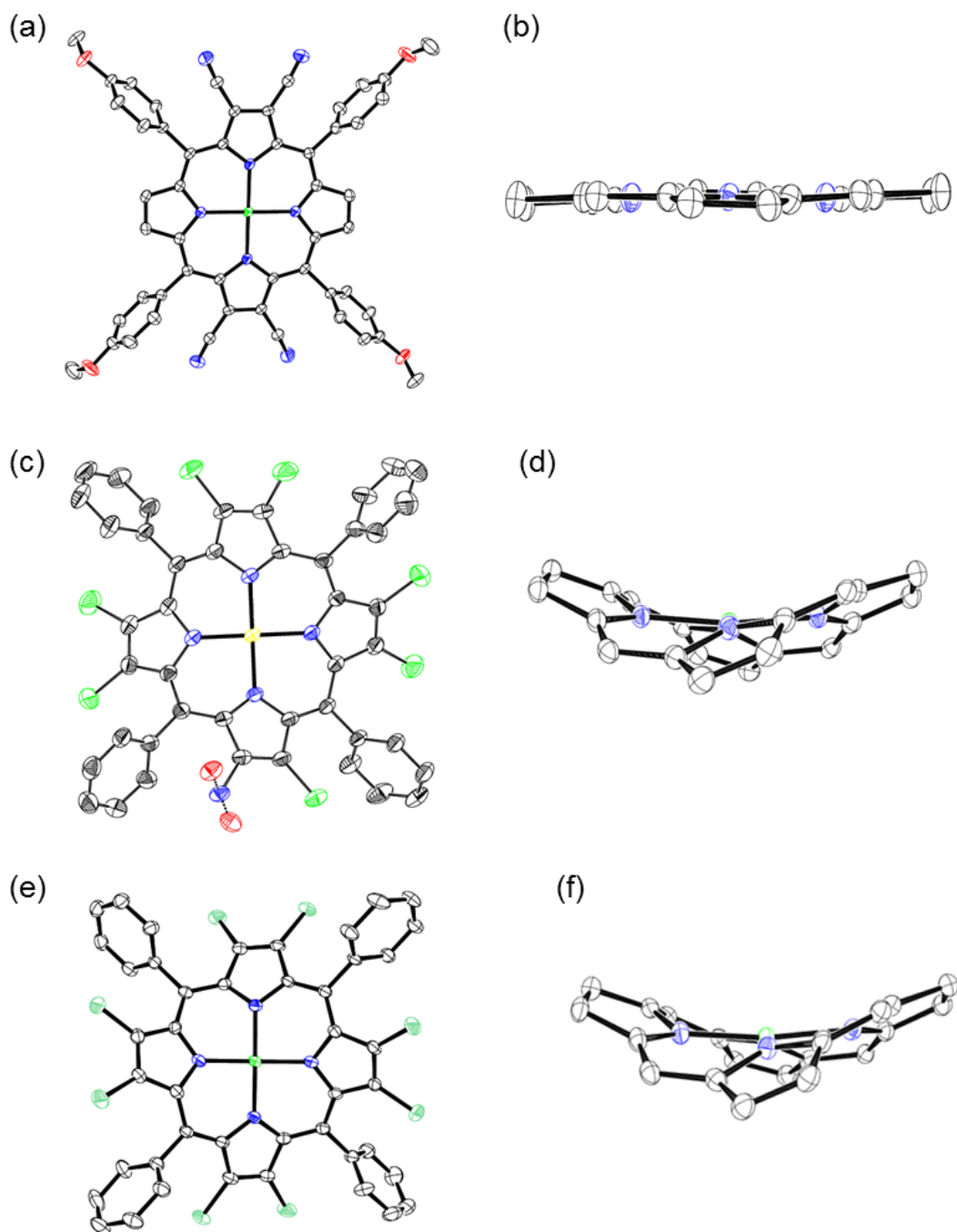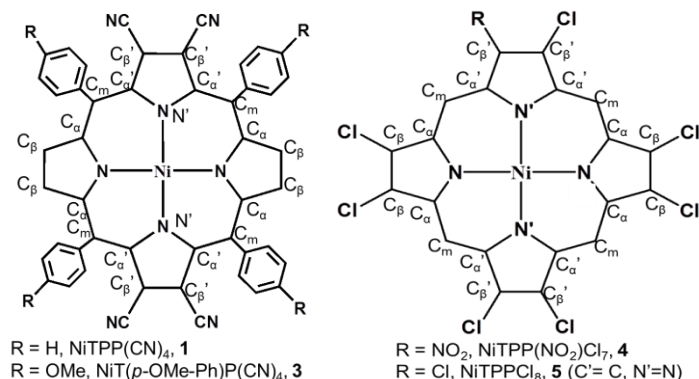**Figure 3.** ^{1}H NMR spectrum of **1** in $CDCl_3$ at 298 K.

Figure 4. ORTEP diagrams showing top and side views of **3** (a-b), **4** (c-d) and 5(e-f), respectively.Hydrogens are not shown for clarity, and in side views, the *β*-substituents and *meso*-phenyl groups are not shown for clarity.

Table 1.Crystal structure data of **1**(Py)$_2$(NiTPP(CN)$_4$)(Py)$_2$), **3** (NiT(*p*-OMe-Ph)P(CN)$_4$), **4** (NiTPP(NO$_2$)Cl$_7$), **5** (NiTPPCl$_8$) and **3•CN⁻**(NiT(*p*-OMe-Ph)P(CN)$_4$(CN⁻).

	1(Py)$_2$	**3**	**4**	**5**	**3•CN⁻**
Empirical Formula	C$_{58}$H$_{34}$N$_{10}$Ni	C$_{52}$H$_{32}$N$_8$NiO$_4$	C$_{44}$H$_{20}$Cl$_7$N$_6$NiO$_{0.5}$	C$_{44}$H$_{20}$Cl$_8$N$_4$Ni	C$_{69}$H$_{68}$N$_{10}$NiO$_4$
Formula wt.	929.66	891.56	947.52	946.95	1160.04
Crystal system	Triclinic	Monoclinic	Monoclinic	Monoclinic	Triclinic
Space group	P -1	C 2/c	P 21/c	P 21/c	P -1
a (Å)	9.340(5)	20.844(5)	14.4707(9)	14.5050(10)	14.154(5)
b (Å)	11.856(5)	10.732(5)	27.1087(15)	27.0592(17)	15.514(5)
c (Å)	13.471(5)	23.220(5)	10.8020(6)	10.7278(7)	16.154(5)
α (º)	87.223(5)	90.000(5)	90.00	90.00	61.669(5)
β (º)	70.308(5)	114.682(5)	110.527(2)	111.70	78.484(5)
γ (º)	68.356(5)	90.000(5)	90.00	90.00	86.358(5)
Volume (Å^3)	1300.5(10)	4720(3)	3968.4(4)	3912.1(4)	3057.4(17)
Z	1	4	4	4	2
ρ_{calc} (g/cm^3)	1.187	1.415	1.586	1.608	1.260
λ (Å)	0.71073	0.71073	0.71073	0.71073	0.71073
T (˚C)	293 K	293 K	293 K	296 K	293 K
No. of total reflns.	6639	3699	9684	34311	25054
No. of indepnt. reflns.	6639	3699	9684	5467	4230
R	0.0418	0.0642	0.0534	0.0421	0.0437
R$_w$	0.1178	0.1952	0.1498	0.0910	0.1058
GOOF	1.024	1.074	1.046	0.896	1.043
CCDC No	1043611	1043609	1043615	1044025	1043610

The X-ray quality single crystals of **1**(Pyridine)$_2$ and **3** were obtained by direct diffusion of hexane into CHCl$_3$/pyridine and pure CHCl$_3$ solutions of **1** and **3**, respectively. The single crystals of **4**-**5** were obtained by direct diffusion of hexane into saturated toluene solution of **4** and **5.** The crystallographic data of these porphyrins are listed in Table 1. ORTEP top and side

Table 2. Selected average bond lengths and bond angles of **1**(Py)$_2$(NiTPP(CN)$_4$)(Py)$_2$, **3** (NiT(*p*-OMe-Ph)P(CN)$_4$, **4** (NiTPP(NO$_2$)Cl$_7$, **5** (NiTPPCl$_8$) and **3•CN⁻** (NiT(*p*-OMe-Ph)P(CN)$_4$(CN⁻).

R = H, NiTPP(CN)$_4$, **1**
R = OMe, NiT(*p*-OMe-Ph)P(CN)$_4$, **3**

R = NO$_2$, NiTPP(NO$_2$)Cl$_7$, **4**
R = Cl, NiTPPCl$_8$, **5** (C'= C, N'=N)

	1(Py)$_2$	**3**	**4**	**5**	**3.CN⁻**
Bond Lengths (A°)					
Ni -N	2.035(16)	1.949(3)	1.906(2)	1.907(3)	2.039(4)
Ni -N'	2.074(16)	1.971(3)	1.912(2)	-	2.062(4)
N -C$_\alpha$	1.370(2)	1.381(5)	1.382(4)	1.383(5)	1.373(6)
N'-C$_\alpha$'	1.373(2)	1.390(5)	1.376(4)	-	1.374(6)
C$_\alpha$-C$_\beta$	1.452(2)	1.430(6)	1.447(4)	1.445(6)	1.439(7)
C$_\alpha$'-C$_\beta$'	1.450(2)	1.429(5)	1.447(4)	-	1.434(7)
C$_\beta$- C$_\beta$	1.337(3)	1.323(6)	1.347(8)	1.354(5)	1.328(7)
C$_\beta$'-C$_\beta$'	1.378(2)	1.362(5)	1.346(5)	-	1.366(7)
C$_\alpha$-C$_m$	1.398(2)	1.384(5)	1.393(4)	1.393(6)	1.383(7)
C$_\alpha$'-C$_m$	1.409(3)	1.387(6)	1.395(4)	-	1.409(7)
ΔC$_\beta$[a]	**0.0721**	**0.059**	**0.871**	**0.898**	**0.184**
Δ24[b]	**0.0604**	**0.0473**	**0.525**	**0.535**	**0.113**
ΔNi	**0.000**	**0.000**	**0.004**	**0.001**	**0.309**
Bond Angles (º)					
N- Ni-N	180(0)	180.0(1)	172.3(10)	171.4(13)	160.9(15)
N'- Ni -N'	180(0)	180.0(1)	171.5(10)	-	164.8(15)
Ni -N-C$_\alpha$	126.7(12)	128.1(2)	125.6(11)	125.5(3)	126.5(4)
Ni -N'-C$_\alpha$'	125.8(12)	127.3(2)	125.4(10)	-	125.7(4)
N- C$_\alpha$-C$_m$	126.6(15)	126.4(3)	123.9(4)	123.8(6)	126.5(7)
N'-C$_\alpha$'-C$_m$	125.6(16)	125.8(3)	124.1(4)	-	125.3(6)
N-C$_\alpha$-C$_\beta$	109.4(15)	110.8(3)	108.4(3)	108.4(4)	109.3(5)
N'-C$_\alpha$'-C$_\beta$'	109.0(15)	110.0(3)	108.3(3)	-	109.2(5)
C$_\beta$-C$_\alpha$-C$_m$	123.9(16)	122.8(4)	127.0(3)	127.0(4)	124.2(6)
C$_\beta$'-C$_\alpha$'-C$_m$	125.4(16)	124.2(4)	126.8(3)	-	125.5(7)
C$_\alpha$-C$_\beta$-C$_\beta$	107.3(2)	107.3(4)	107.6(3)	107.5(4)	107.6(5)
C$_\alpha$'-C$_\beta$'- C$_\beta$'	106.9(15)	107.2(3)	107.5(3)	-	107.2(5)
C$_\alpha$-N-C$_\alpha$	106.6(13)	103.8(3)	107.1(2)	107.3(4)	106.3(4)
C$_\alpha$'- N'- C$_\alpha$'	108.1(14)	105.3(3)	107.6(2)	-	107.2(4)
C$_\alpha$-C$_m$-C$_\alpha$	124.9(16)	122.3(4)	120.0(3)	120.1(4)	124.5(5)

[a]ΔC$_\beta$ refers mean plane deviation of *β*-carbon atoms, [b]Δ24 refers mean plane deviation of 24 core atoms

views of these porphyrins are shown in Figures 1 and 4. The selected bond lengths and bond angles are given in Table 2. Notably, **1** and **3** have shown planar conformation of porphyrin macrocyle (ΔC_β = 0.06 - 0.07 Å and $\Delta 24$ = 0.05 - 0.06 Å) whereas **4-5** exhibited nonplanar conformations with the displacements of β-pyrrole carbons, ΔC_β = ± 0.9 Å and the 24 atoms core, $\Delta 24$ = ± 0.53 Å, which is attributed to the steric hindrance between β-substituents and *meso*-phenyl groups [21]. **1** and **3** exhibited longer C_β'-C_β' bond distance (1.37 Å) for β-pyrrole carbons having CN substituents as compared to antipodal β-pyrrole carbons bearing no substitution (C_β-C_β = 1.32 Å) which is further supported by increment in C_β'-C_α'-C_m angle (125º) with concomitant decrement in N'-C_α'-C_m (125.7º). Similarly, **4** and **5** exhibited longer C_β-C_β distance (1.35 Å) with increment in C_β-C_α-C_m angle (~127º) with concomitant decrement in N-C_α-C_m (~124º), indicating severe steric repulsion between β-substituents which leads to nonplanar conformation of porphyrin macrocycle as compared planar porphyrins [21].The N-Ni-N bond angles are exactly 180º for planar porphyrins (**1** and **3**) whereas these angles are deviated (171-172º) for porphyrins, **4** and **5** due to nonplanar conformation. The observed UV-Vis and ^{1}H NMR spectroscopic data of these Ni(II) porphyrins is in accordance with obtained single crystal X-ray structures.
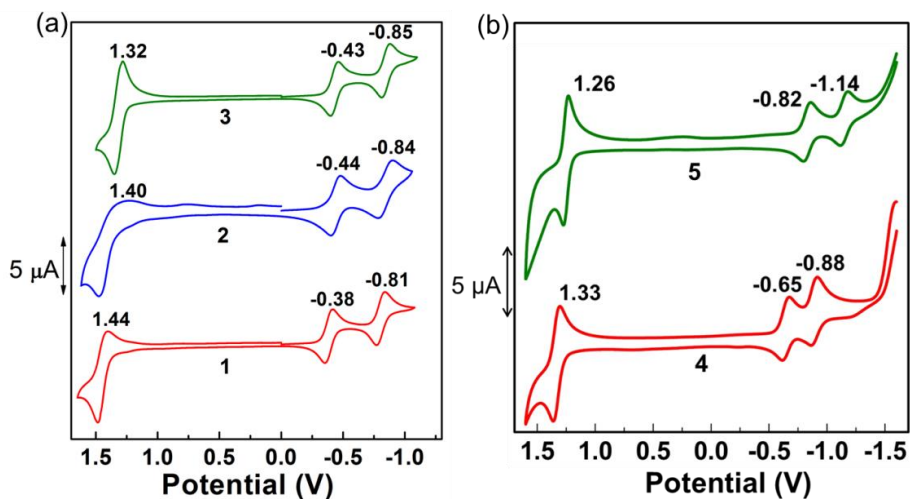
Figure 5 Cyclic Voltammograms of **1**-**3** (a) and **4**-**5** (b) in CH_2Cl_2 containing 0.1 M TBAPF$_6$ as the supporting electrolyte using Ag/AgCl as reference electrode.

To examine the effect of *β*-susbtituents and nonplanarity of the macrocyle on electrochemical redox potentials, we have carried out cyclic voltammetric studies. Cyclic voltammograms of **1**-**5** in CH_2Cl_2 containing 0.1 M $TBAPF_6$ as supporting electrolyte are shown in Figure 5. The redox data (*vs* Ag/AgCl) is listed in Table A2 in Appendix 3. **1**-**5** exhibited one two-electron reversible electrochemical oxidation and two successive one-electron reductions. The first oxidation potentials of **1**-**3** exhibit 300-480 mV anodic shift in comparison to NiTPP suggesting that each of the *β*-cyano group shifts ~130 mV anodically which is due to the strong electron-withdrawing nature of the *β*-cyano substituents [21]. Further, the anodic shift in first oxidation of **4** and **5** as compared to NiTPP is ascribed to the combined effect of electron-withdrawing nature of nitro and chloro substituents as well as the highly nonplanar conformation of macrocycle. The cathodic shift (80-150 mV) in first ring oxidation potentials of **2**-**3** in comparison to **1** is ascribed to electron donating ᵗbutyl and methoxy substituents present at the *meso*-phenyl rings of **2** and **3**, respectively. The observed redox potentials indicate the highly electron deficient nature of porphyrin π-system [18,21].

3.3.2 Cyanide ion sensing

The anion recognition properties of all synthesized porphyrins (**1**-**5**) were studied in toluene with various anions, using UV-Visible spectroscopy with the addition of the aliquot anion in the form of TBA salts. Importantly, an additional remarkable feature of these sensors **1**-**5** was pinpointed, as their ability to specifically recognize cyanide in an admixture of anions. **1**-**5** have shown red-shifted UV-Visible spectra with colorimetric 'naked eye' detection of cyanide ions (green to yellow for **1**-**3** and reddish brown to green for **4**-**5**) whereas no observable shift was found with other tested anions as shown in Figs.6 and A3 in Appendix 3. **1**-**5** were titrated with CN^- ions in toluene at 298 K and monitored by UV-Vis absorption spectroscopy. The broad Soret of **1**-**5** upon addition of CN^- ions is due to charge-transfer transitions [23]. The metal *d*-orbital energies in metalloporphyrins can be perturbed by the presence of axial ligands. Herein, the electron deficient porphyrin π-system makes Ni(II) metal centre to bind with highly basic cyanide (pK_a = 9.3) ions. UV-Vis titration of **1** with cyanide ions is shown in Figure 7. Both the Soret (35 nm) and Q bands (77 nm) are shifted to longer wavelengths upon increasing the
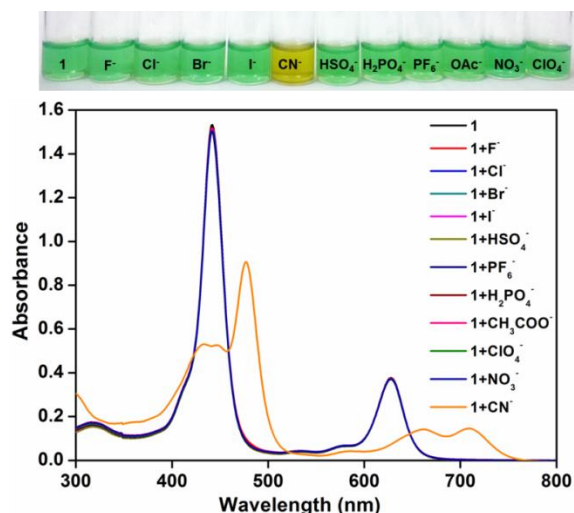
Figure 6 (Top) Colorimetric response of **1** with tested anions in toluene; (b) UV-Vis spectra of **1** $(3.33 \times 10^{-6}$ M) upon addition of excess TBA salts of tested anions in toluene at 298K.

concentration of TABCN indicating the axial coordination of CN$^-$ ions to **1**. For **1**, well-anchored isosbestic points were observed at 457, 526 and 647 nm during the course of the cyanide binding experiment. Stoichiometry for **1** was established using Job's plot (Figure 7 inset) which has a maxima at a cyanide molar ratio of ~ 0.65 indicating that **1** is capable of binding with 2 equivalents of CN$^-$ ions to form **1•**2CN$^-$ adduct. Similar UV-Vis spectral profiles were observed for **2-5** with CN$^-$ ions as shown in Figure A7 in Appendix 2. Stoichiometry for **2-3** was calculated using Job's plot (Figure A4 in Appendix 2). The binding constants for **1-5** with cyanide ions were calculated using Hill equation [16] and the corresponding binding parameters are presented in Table 3. The stoichiometry for **4** and **5** was confirmed by Hill plot as shown in insets of Figure A4 in Appendix 2. The Hill plot shows a straight line between $\log[CN^-]$ and $\log(A_i-A_0/A_f-A_i)$ having slope value 2, which indicates 1:2 (porphyrin-to-cyanide) stoichiometry. The magnitude of Hill coefficient (n) for **1**-**3** clearly reflects the extent of cooperativity between supramolecular binding events [3,24].
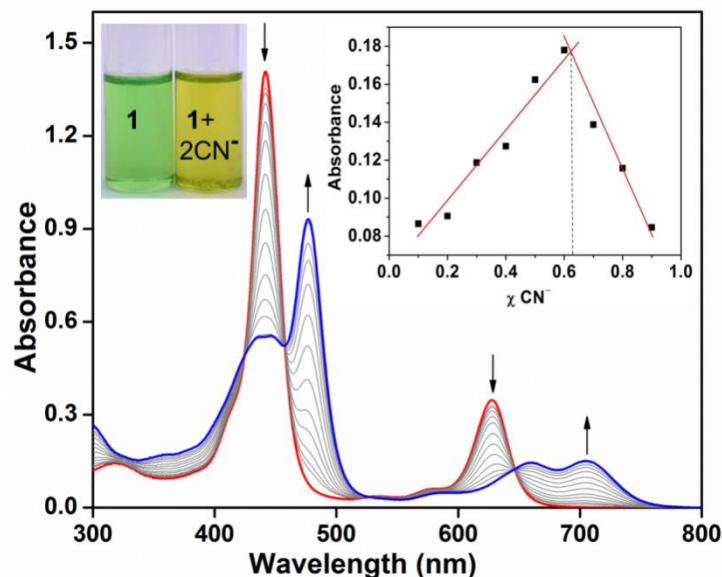
Figure 7. UV-visible spectral titrations of **1** (9.35 µM) upon addition of aliquots of TBACN (0-0.03M) in toluene, inset shows corresponding Job's plot.

Ni(II) cyanoporphyrins (**1-3)** exhibited very high binding constants, β_2 (10^{16} - 10^{12} M^{-2}) owing to their high electron deficient nature as compared to nonplanar perhaloporphyrins, **4** and **5** (10^9 – 10^8 M^{-2}) as indicated by their reduction potentials (Table A2 in Appendix 2). The trend along the series of porphyrins tracks the β_2 values (**1** > **2** > **3** >**4** > **5**), with the more electron deficient porphyrins displaying larger Hill Coefficients (Table 1). The detection limits (LOD) for CN⁻ ions were calculated in presence of **1-5** in toluene (Table 3) [17]. These porphyrins are able to detect as low as ~ 0.11 ppm solution of cyanide ions. Hence these sensors **1**-**5** were very selective and sensitive for cyanide ions.

Table 3. Binding constant data[a] of Ni(II) porphyrins and their CN⁻ ion detection limits in toluene at 298 K.

Porphyrin	β_2	r^2	n	LOD (ppm)	m
1	3.86×10^{16}	0.87	3.33	0.108	2
2	1.95×10^{16}	0.92	3.33	0.108	2
3	6.70×10^{12}	0.90	2.68	0.104	2
4	1.21×10^{9}	0.99	2	0.062	2
5	7.79×10^{8}	0.97	2	0.103	2

[a]Within the error of ±0.04; n = Hill coefficient; LOD = Limit of detection; m = Stichiometry

Interestingly, the most commonly interfering anions especially basic anions such as fluoride, acetate and dihydrogenphosphate didn't show any response with these sensors. The competition experiments were performed to ascertain the selectivity of synthesized porphyrins using two equivalents of cyanide ions and 10 equivalents of interfering anions in toluene. The representative bar graph observed for **1** is shown in Figure 8, which
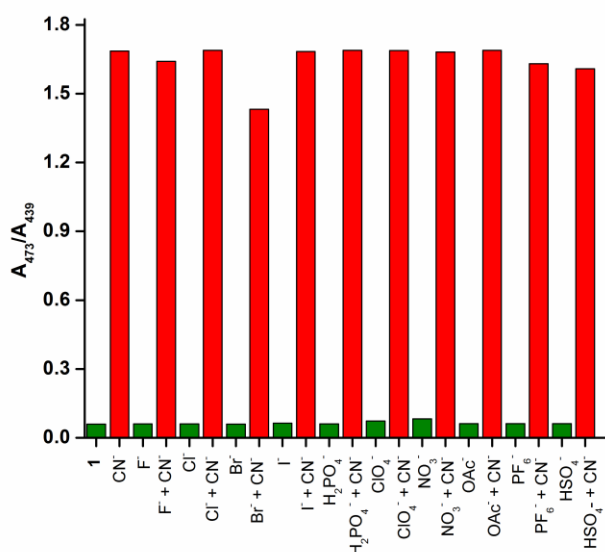
Figure. 8 Ratiometric absorbance changes (A_{473}/A_{439}) of **1** (1.01×10^{-5} M) on addition of 2 equiv. of CN^- and 10 equiv of other anions. Green bars indicate the blank and in presence of other interfering anions, and red bars indicate the addition of CN^- to the interfering anions.

Table 4. Electrochemical first ring redox potentials (in mV *vs* Ag/AgCl) upon addition of CN^- ions to **1-5** in CH_2Cl_2 containing 0.1 M TBAPF$_6$ with a scan rate of 0.1 V/s.

Porphyrin	Porphyrin (without CN⁻)		Porphyrin•2CN⁻	
	1ˢᵗ Ox	1ˢᵗ Red	1ˢᵗ Ox	1ˢᵗ Red
1	1480	-392	1132	-552
2	1400	-416	1135	-675
3	1332	-420	1000	-612
4	1340	-630	820	-860
5	1280	-810	783	-1102

89

clearly demonstrate the tolerance of **1** towards these potentially interfering anions and thus can be used quantitatively and selectively to detect cyanide ions. The similar results were observed for **2**-**5** as shown in Figure A5 in the Appendix 2.

Notably, the plots of the absorbance changes (ΔA) *vs* [CN⁻] show sigmoidal curves, which indicate that cyanide ions bind to **1-3** in a cooperative manner as shown in Figure 9a. Nevertheless, in order to get further insight into the binding ability of these sensors **1-5** with CN⁻ ions, we have carried out differential pulse voltammetric (DPV) studies of **1-5** with addition of cyanide ions (Figs. 9b and A6 in Appendix 2).

The addition of cyanide ions to **1** results a cathodic shift of 250 mV in first oxidation and 160 mV in first reduction which is expected upon going from neutral porphyrin to dinegatively charged porphyrin adduct (**1**•2CN⁻). This shift in potential is further in
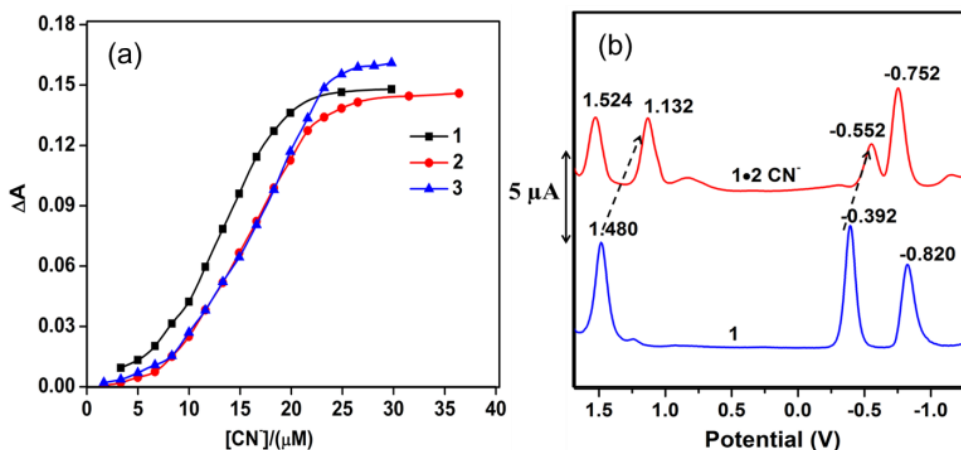
Figure 9 (a) sigmoidal curve for **1-3**, [CN⁻] *vs* ΔA indicating positive cooperative behavior. (b) DPV (in V *vs*. Ag/ AgCl) traces recorded for **1** (blue) and **1**•2CN⁻(red) in CH_2Cl_2 containing 0.1 M $TBAPF_6$ as the supporting electrolyte with a scan rate of 0.1 V/s at 298 K.

Consistent with rising of HOMO (from DFT studies). Table 4 represents the electrochemical first ring redox data of **1-5** in presence and absence of CN⁻ ions.

3.3.3 Reversibility studies

To acknowledge the range of applicability,the reversibility and reusability of the sensors **1-5** are the key events that have to be determined [25]. **1** was treated with 2 equivalents of

cyanide ions in toluene forming **1•2CN⁻** as visualized by colorimetric change from green to yellow accompanied by UV-visible spectral changes as shown in Figure 10. Switching off the cyanide ion binding was carried out using TFA. As shown in the Figure 10, the addition of aliquots of 1 mM solution of TFA in toluene to the solution containing **1•2CN⁻** adduct immediately restored to **1** with colorimetric change from yellow to green.
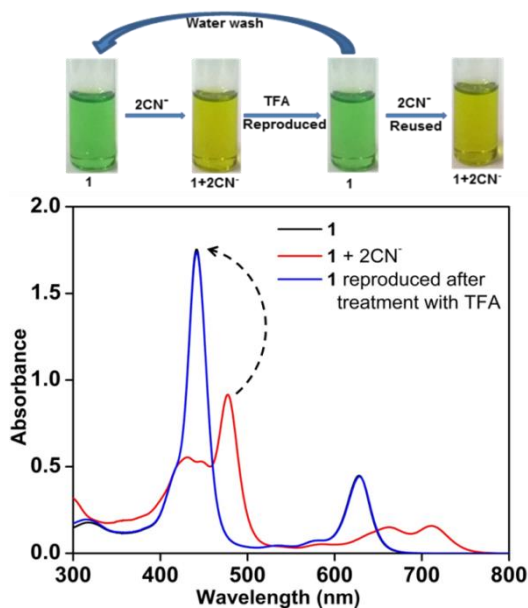
Figure 10. Colorimetric response of **1** for reversibility and reusability test with CN⁻ ions (top) and their corresponding UV-Visible spectral changes in toluene at 298 K (bottom).

To confirm the reusability, the resulting mixture was washed with water and dried over anhydrous Na₂SO₄. The recovered **1** was treated with 2 equivalents of CN⁻ ions, which showed similar spectral features as that of fresh solution of **1** with cyanide ions. The similar results were observed for **2**-**5** indicating their recoverability and reusability (Figure A7 in Appendix 2). For the practical application of **1**-**5**, test kits were prepared by immersing Whatman filter papers in toluene solution of **1**-**5** (1 mM) and then dried in air. These test kits coated with **1** were exposed to different anion solutions (1 mM) in toluene for 1 - 2 seconds, the colour change from green to yellow was observed only with CN⁻ ion in toluene (Figure 11a), whereas there was no colour change observed for other anions. Notably, the similar results were observed when these test kits were exposed to neutral aqueous solutions of various anions (Figure 11b). Test strips prepared for **2**-**5**

exhibited similar colorimetric changes with cyanide ions in toluene and aqueous solutions as shown in the Figures A8 and A9 in the Appendix 2.
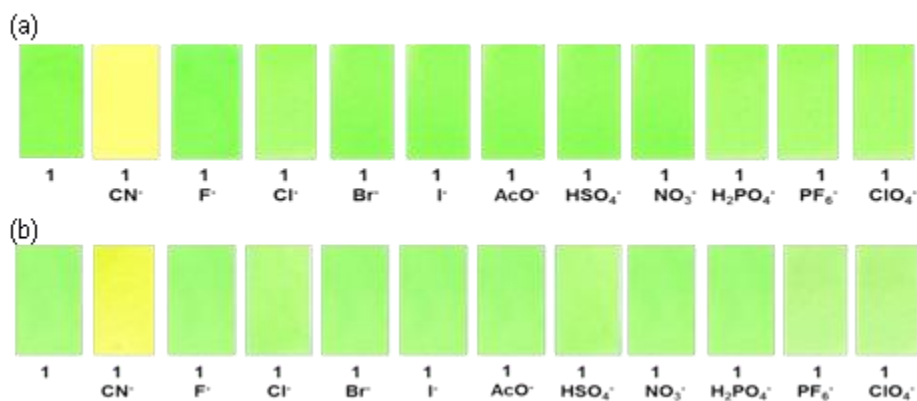
Figure 11 Photographs of test kits with **1** (1 mM) for detecting the cyanide ion in (a) toluene solution (b) neutral aqueous solution with other anions.

3.3.4 DFT calculations

The ground state geometry optimization of **1** and **4** in gas phase was carried out by DFT calculations using B3LYP functional with LANL2DZ basis set. Figures 12 and A8 in Appendix 2 represent the fully optimized geometries of **1**•2CN⁻ and **4**•2CN⁻ which exhibit planar and severe nonplanar conformations, respectively. The pictorial views of frontier molecular orbitals (FMOs) of **1**, **4**, **1**•2CN⁻ and **4**•2CN⁻ were shown in Figures 13,14 and A11-A12 in the Appendix 2.
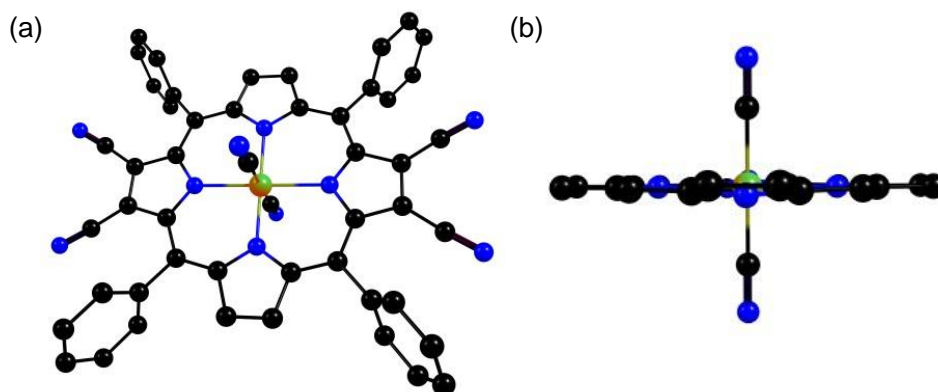
Figure 12. B3LYP/LANL2DZ-Optimized geometry showing (a) top as well as (b) side views of NiTPP(CN)₄•2CN⁻; hydrogens are omitted for clarity. In side view, the *β*-Cyano and *meso*-phenyl groups are not shown for clarity.
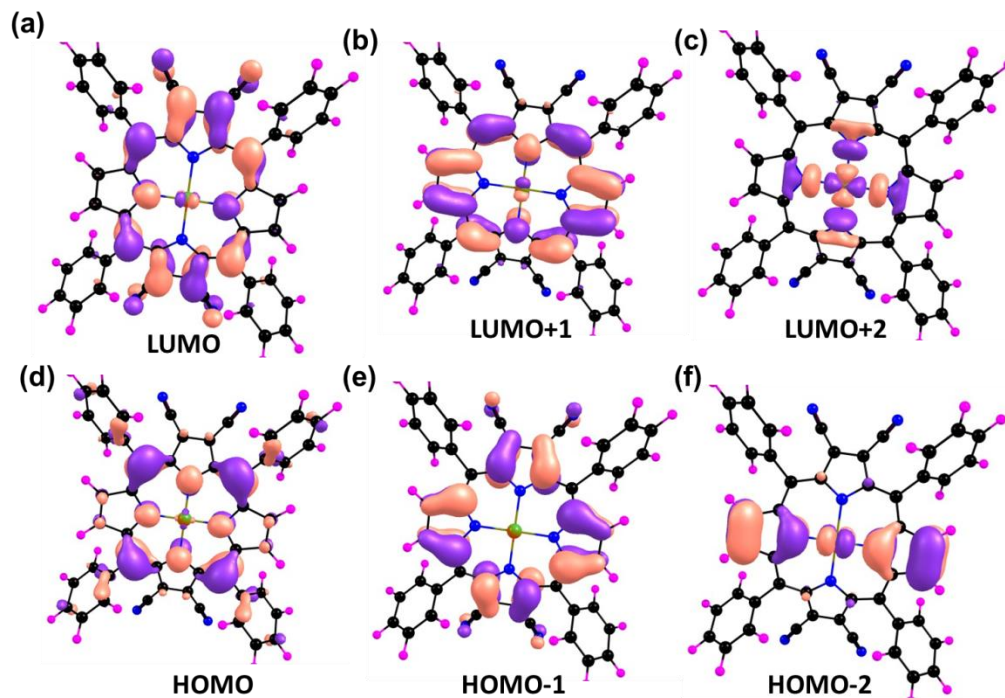
Figure 13. Pictorial representation of frontier molecular orbitals of NiTPP(CN)$_4$ (**1**) obtained by DFT calculations using B3LYP as density functional with LANL2DZ basis sets in gas phase.
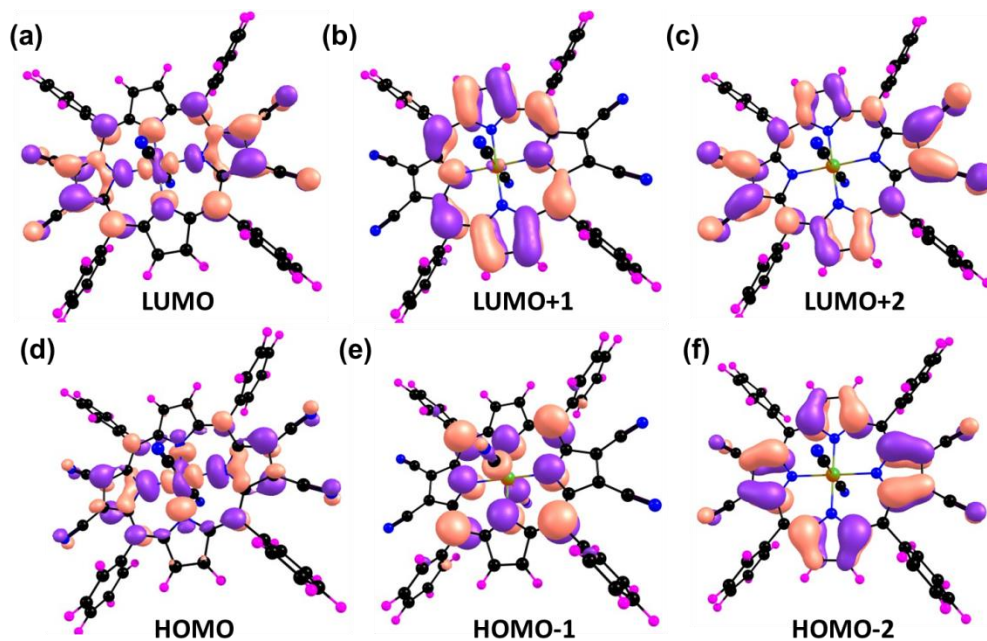
Figure 14. Pictorial representation of frontier molecular orbitals of NiTPP(CN)$_4$•2CN$^-$ (**1**•2CN$^-$) obtained by DFT calculations using B3LYP as density functional with LANL2DZ basis sets in gas phase.

The HOMO and HOMO-1 are found to be a_{1u} and a_{2u}, respectively as expected for **1** containing β-cyano substituents whereas switching was observed for **1**•2CN⁻. This indicates perturbation of FMOs upon axial ligation by cyanide ions. The "a_{2u}-type" singly occupied b_2 and SUMO b_1 for saddle shaped **4** are in accordance with the reported literature [26]. The switching of these orbitals occur upon cyanide binding. UV-Vis spectra obtained for **1**, **4**, **1**•2CN⁻ and **4**•2CN⁻ using TD-DFT calculations are in accordance with experimental UV-Vis spectra (Figures A18-19 in the Appendix A2). The observed broad features of Soret band of **1**-**5**•2CN⁻ is possibly due to ligand to metal charge transfer [19] as reflected in FMO diagrams (Figures 15 and A13 in the Appendix 2).
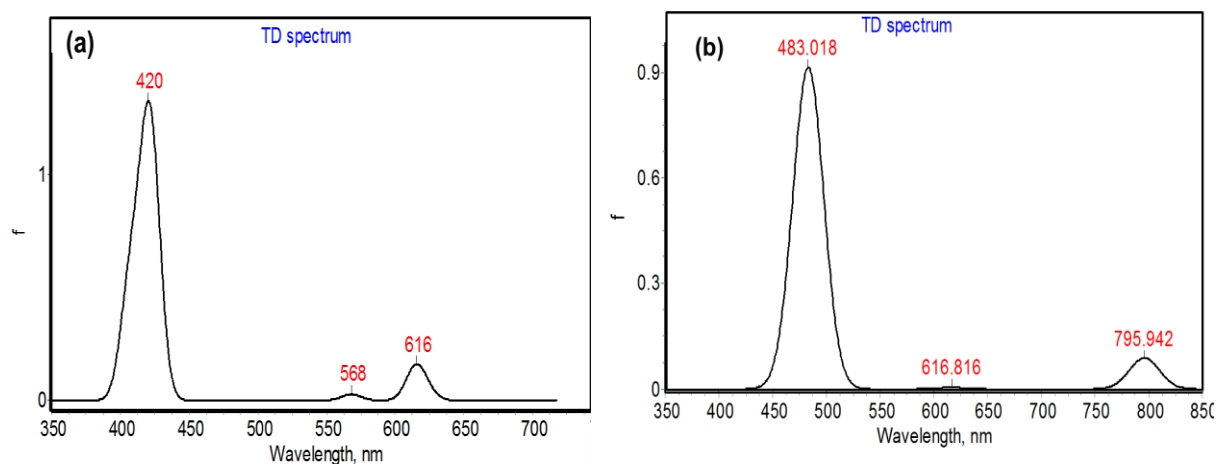
Figure 15. Theoretical UV-Visible spectra of (a) **1** and (b) **1**•2CN⁻ obtained by TD-DFT calculations in gas phase.

1-**5** remained EPR inactive in presence of excess cyanide ions which indicate the axial ligation of CN⁻ ions to Ni(II) metal centre. This is further evidenced by single crystal X-ray structure of **3** with axial coordination of CN⁻ ion and charge balanced by TBA cation which is present in the crystal lattice (Figures A14 in the Appendix 2). CN⁻ strongly coordinates to Ni(II) metal centre with a distance 1.970(5) Å. Further, Ni(II) ion is 0.309 Å deviated from the porphyrin mean plane in order to bind with cyanide ion effectively. The longer Ni(II)–N_{core} distance in **1**(Py)$_2$ and **3**•CN⁻ as compared to **3**-**5** is due to axial coordination of pyridine and cyanide ion, respectively which leads porphyrin core expansion. To the best of our knowledge, single crystal X-ray structure of five coordinate
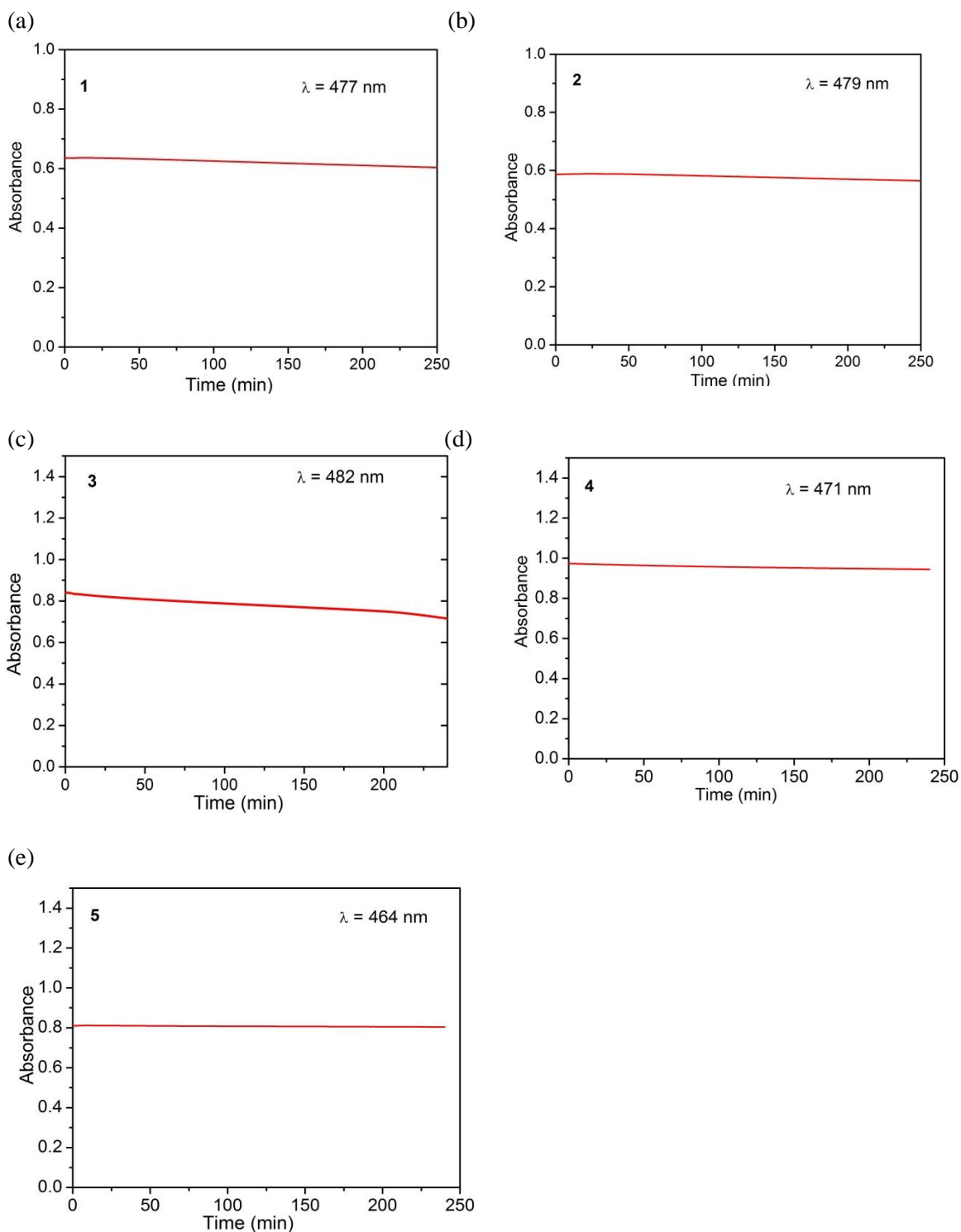
Figure 16. The time-dependent absorption changes of **1-5** after addition cyanide ions for 4 hours in toluene at 298 K.

Ni(II) porphyrin complex is not known in the literature. However, electronic absorption spectral studies revealed stable six coordinate Ni(II) porphyrin complexes in solution

which is confirmed by time-dependent absorption spectral profiles **1-5** in presence of cyanide ions as shown in Figure 16. Further, the six coordinate complex of **1** in presence of cyanide ions (**1**•2CN⁻) was confirmed by MALDI-TOF mass spectrometry analysis (Figure A15 in the Appendix 2). Also, we have recorded the UV-Vis spectra for some Ni(II) porphyrins (NiTPP, NiOPP, NiDPP, NiT(2,6-DCP)P and NiT(*p*-ᵗBut-Ph)PBr₄) with CN⁻ ions and found no spectral changes (Figure A16 in the Appendix 2) observed even with excess of CN⁻ ions which clearly suggests that highly electron deficient Ni(II)-porphyrin metal centre is necessary for CN⁻ ion recognition. Further, it is revealed that the reduction potential positive than -0.8 V makes them a suitable candidate for CN⁻ ion detection (Figures A17 and Table A3 in the Appendix 2).

X=CN, Y=Z=H, R=H, **1**
X=CN, Y=Z=H, R=ᵗBut, **2**
X=CN, Y=Z=H, R=OCH₃, **3**
X=Y=Cl, Z=NO₂, R=H, **4**
X=Y=Z=Cl, R=H, **5**
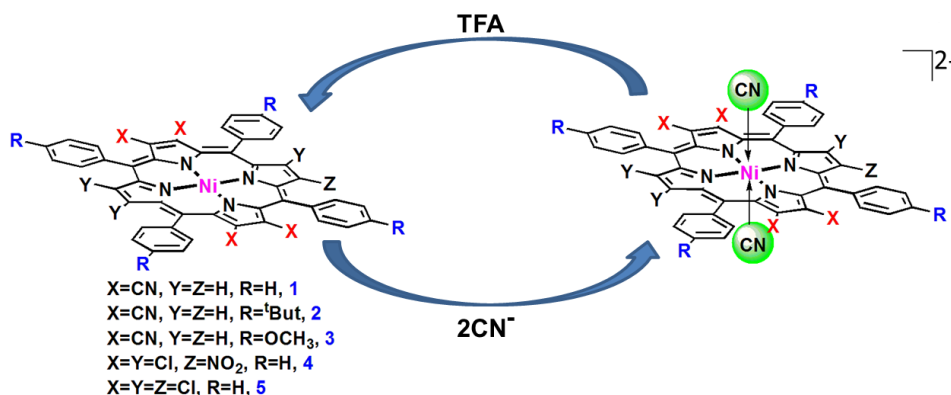
Scheme 2. Schematic representation of CN⁻ ions binding to **1**-**5** and their reversibility in presence of trifluroacetic acid (TFA) followed by reusability after water wash.

Based on our experimental and theoretical studies, we are representing the plausible mechanism of cyanide ion recognition and their reversibility with TFA of **1**-**5** in Scheme 2.

3.4 CONCLUSIONS

In summary, we have demonstrated that **1-5** displays a specific, colorimetric and ratiometric response to cyanide ions over the other coexisting anions in toluene. Highly electron deficient planar porphyrins, **1-3** exhibit very high binding constants β_2 (~ 10^{16} - 10^{12} M^{-2}) and bind with 2 equivalent of cyanide ions in a highly cooperative fashion as compared to nonplanar porphyrins **4** and **5**. Cyanide binding also perturbs the redox chemistry and each of the Ni(II) porphyrin•2CN⁻ adduct is much more easily oxidized

than the parent porphyrin. These porphyrins are being able to detect (LOD) < 0.11 ppm of cyanide ions. The reversibility studies revealed that the sensors **1-5** can be recoverable and reusable for cyanide detection without losing their sensing ability.

3.5 References

References

1   Steed, J. W.; Atwood, J. L. In *Supramolecular Chemistry*, Wiley, New York, **2000**; pp. 198.

2   Bianchi, A.; Bowman-James, K.; Garcia-Espana E., In *Supramolecular Chemistry of Anions, Ed.*, Wiley-VCH, New York, 1997.

3   Pistner, A. J.; Lutterman, D. A.; Ghidiu, M. J.; Ma, Y.-Z.; Rosenthal, J., "Synthesis, electrochemistry and photophysics of a pamily of phlorin macrocycles that display Cooperative Fluoride Binding" *J. Am. Chem. Soc.* **2013**, *135*, 6601-6607.

4   D'Souza, F.; Subbaiyan, N. K.; Xie, Y.; Hill, J. P.; Ariga, K.; Ohkubo, K.; Fukuzumi, S., "Anion-Complexation-Induced Stabilization of Charge Separation" *J. Am. Chem. Soc.* **2009**, *131*, 16138-16146.

5   Kulig, K.W.; *Cyanide Toxicity*, U.S. Department of Health and Human Services, Atlanta, GA, **1991**.

6   Koenig, R., "Wildlife deaths are grim wake-up call in eastern Europe" *Science* 2000, *287*, 1737-1738.

7   Miller, G.C.; Pritsos, C. A. *Cyanide: Soc. Ind. Econ. Aspects, Proc. Symp. Annu. Meet TMS,* **2001**, pp. 73

8   Goswami, S.; Manna, A.; Paul, S.; Das, S. K.; Aich, K.; Nandi, P. K., : Resonance – assisted hydrogen bonding induced nucleophilic addition to hamper ESIPT: ratiometric detection of cyanide in aqueous media" *Chem. Commun*. **2013**, *49*, 2912-2914 and references therein.

9   Kang, J.; Song, E. J.; Kim, H.; Kim, Y.-H.; Kim, Y.; Kim, S.-J.; Kim, C., " Specific naked eye sensing of cyanide by chromogenic host: studies on the effect of solvents" *Tetrahedron Lett*. **2013**, *54*, 1015-1019.

10   Gilday, L. C.; White, N. G.; Beer, P. D., " Halogen- and hydrogen-bonding triazole-functionalized porphyrin based receptors for anion recognition" *Dalton Trans*. **2013**, *42*, 15766-15773

11   Starnes, S. D.; Arungundram, S.; Saunders, C. H., " Anion sensors based on *β-β'*-disubstituted porphyrins" *Tetrahedron Lett*. **2002**, *43*, 7785-7788.

12   Song,Y.; Haddad, R. E.; Jia, S.-L.;Hok, S.; Olmstead, M. M.; Nurco, D. J.; Sehore, N. E.; Zhang, J.; Ma, J.-G.;Smith, K. M.;Gazeau, S.; Pecaud, J.; Marchon, J.-C.;Medforth,C. J.; Shelnutt, J. A., " Energetics and structural consequences of axial axial ligand coordination in nonplanar nickel porphyrins" *J. Am. Chem. Soc.* **2005**, *127*, 1179-1192.

13   Sankar, M.; Arunkumar, C.; Bhyrappa, P., "Unusual solvent dependent electronic absorption properties of Cu(II) and Ni(II) perhaloporphyrins" *J. Porphyrins Pthalocyanines* **2004**, *8*, 1343-1355.

14   Sheldrick, G. M.; SIR97 and SHELX97, *Programs for Crystal Structure Refinement*, University of Göttingen, Göttingen, Germany, 1997.

15   Spek, A. L.; *PLATON*, *A Multipurpose Crystallographic Tool*, Utrecht University, Utrecht, The Netherlands, 2001.

16   Hill, A. V. *J. Physiol. London*.1910, *40*, IV.

17   Caballero, A.; Martinez, R.; Lloveras, V.; Ratera, I.; Vidal-Gancedo, J.; Wurst, K.; Tarraga, A.; Molina , P.; Veciana, J., " Highly selective chromogenic and redox or fluorescent sensors of Hg^{2+} in aqueous environment based on 1,4-disubstituted azines" *J. Am. Chem. Soc.* **2005**, *127*, 15666-15667.

18   Callot, H. J. *Bull. Chim. Soc. Fr*. 1974, 1492-96.

19   Donohoe, R. J.; Atamian, M.; Bocian, D. F., "Characterization of singly reduced iron (II) porphyrins" *J. Am. Chem. Soc.***1987**, *109*, 5593-5599.

20   Senge, M. O.; In *The Porphyrin Handbook,* Vol. 1 (Eds. K. M. Kadish, K.M. Smith, R. Guilard) *Academic Press*, *New York*, 2000, pp 239.

21   Giraudeau, A.; Callot, H. J.; Gross, M., " Effect of electron withdrawing substituents on the electrochemical oxidation of porphyrins" *Inorg. Chem.* **1979**, *18*, 201-206.

23   Priyadarshy, S.; Therien M. J.; Beratan, D. N., "Acetylenyl-linked, porphyrin-bridged, donor-acceptor molecules: A theoretical analysis of the molecular first hyperpolarizability in highly conjugated push-pull chromophore structures", *J. Am. Chem. Soc.* **1996**, *118*, 1504-1510.

24   Takeuchi, M.; Shioya, T.; Swager, T. M.; *Angew. Chem. Int. Ed.,* "Allosteric fluoride anion recognition by a doubly strapped porphyrin" **2001**, *40*, 3372-3376.

25   Farinha, A. S. F.; Calvete, M. J. F.; Paz, F. A. A.; Tome, A. C.; Cavaleiro, J. A. S.; Sessler, J. L.; Tome, J. P. C., "Octatosylaminophthalocyanine : A reusable chromogenic anion chemosensors" *Sens. Actuators, B.* **2014**, *201*, 387-394.

26   Ghosh, A.; Helvorsen, I.;Nilsen, H. J.; Steene, E.; Wondimagegn, T.; Lie, R.; Caemelbecke, E. V.; Guo, N.; Ou, Z.; Kadish, K. M., " Electrochemistry of Nickel and copper *β*-octahalogeno-*meso*-tetraaryporphyrins. Evidence for important role played by saddling-induced metal ($d_x{}^2{}_{-y}{}^2$) porphyrin ("a_{2u}") orbital interactions" *J. Phy. Chem. B.* **2001**, *105,* 8120-8124.

CHAPTER 4

Synthesis, Spectroscopic, Electrochemical Redox, Solvatochromism and Anion Binding Properties of β-Tetra- and -Octaphenylethynyl Substituted Meso-Tetraphenylporphyrins
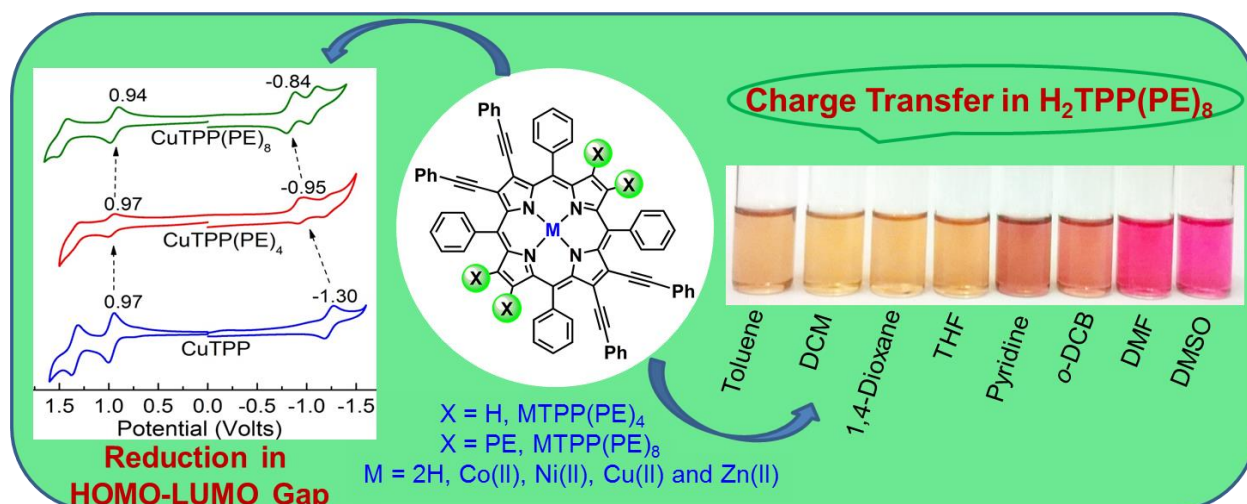
CHAPTER 4

SYNTHESIS, SPECTROSCOPIC, ELECTROCHEMICAL REDOX, SOLVATOCHROMISM AND ANION BINDING PROPERTIES OF *β*-TETRA- AND -OCTAPHENYLETHYNYL SUBSTITUTED *MESO*-TETRAPHENYLPORPHYRINS

4.1 INTRODUCTION

Substituted porphyrins have unique electronic and optical properties that empower their use as model compounds of biological importance and potential material applications [1,2]. The structural, spectral and electrochemical redox properties of porphyrins can be tuned by peripheral functionalization of porphyrin ring [3,4]. Particularly, the *β*-functionalization of *meso*-tetraphenylporphyrins exerts much larger steric and electronic effects on the porphyrin π-system as discussed in chapter.

X = H, MTPP(PE)$_4$
X = PE, MTPP(PE)$_8$
M = 2H, Co(II), Cu(II), Ni(II), and Zn(II)
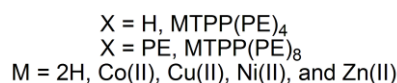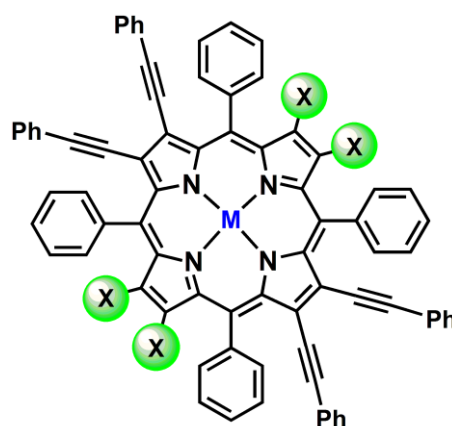
Chart 1. Chemical structures of *β*-phenylethynyl substituted porphyrins.

Notably, *meso*-phenylethynyl appended 'push-pull porphyrins' have attracted attention as potential NLO materials [5,6] and sensitizers in porphyrin-sensitized solar cells (PSSC) [7]. The substitution of *β*-phenylethynyl groups at the porphyrin periphery induces interesting changes in optical absorption and electrochemical redox properties [8-10]. In general, *β*-ethynyl linker minimizes the steric interaction between the *meso*-aryl and *β*-phenyl groups [8-10]. These planar porphyrins are potential precursors for photochemical or thermal Bergman cyclization reactions [8]. The distinctive

physicochemical properties and potential applications of *β*-phenylethynyl substituted porphyrins [8-10] prompted us to synthesize and explore the unique properties of *β*-tetra- and -octaphenylethynyl substituted porphyrins and their metal complexes.

Herein, we report the facile synthesis, photophysical, electrochemical redox, solvatochromism and anion binding properties of two series of *β*-phenylethynyl substituted porphyrins viz. 2,3,12,13-*tetrakis*(phenylethynyl)-5,10,15,20-tetraphenylporphyrin (H$_2$TPP(PE)$_4$), 2,3,7,8,12,13,17,18-*octakis*(phenylethynyl)-5,10,15,20-tetraphenylporphyrin (H$_2$TPP(PE)$_8$), and their metal (Co(II), Ni(II), Cu(II), Zn(II)) complexes (Chart 1). These porphyrins were characterized by UV-Visible, fluorescence, ^{1}H NMR and mass spectroscopic techniques. To the best of our knowledge, photophysical, electrochemical redox, solvatochromism, and anion binding properties of *β*-tetra- and -octaphenylethynyl appended *meso*-tetraphenyl-porphyrins have not been studied so far.

4.2 EXPERIMENTAL SECTION

4.2.1 Chemicals and materials

All the reagents employed in the present work were purchased from Sigma Aldrich and used as received without further purification. All solvents employed in the present work were of analytical grade and distilled or dried before use. The tetrabutylammonium salts (TBAX, X = CN$^-$, F$^-$, Cl$^-$, Br$^-$, I$^-$, HSO$_4^-$, OAc$^-$, H$_2$PO$_4^-$, ClO$_4^-$, PF$_6^-$ and NO$_3^-$) used for sensing applications were purchased from Alfa Aesar and used as received.

4.2.2 Instrumentation and methods

Fluorescence life time measurements in ns time domain were recorded in CH$_2$Cl$_2$ using Horiba Jobin Yvon "fluorocube fluorescence life time system" equipped with NanoLED (635 nm) source. The binding constants were calculated using Hill equation as described in chapter 3.

4.2.3 General procedure for the synthesis of *β*- tetra- or octaphenylethynyl substituted *meso*-tetraphenylporphyrins

H$_2$TPPBr$_4$ [11] or H$_2$TPPBr$_8$ [12] (0.108 mmol) and Pd(PPh$_3$)$_4$ (20 mol%) were dissolved in 50 mL of distilled 1,4-dioxane and purged with Ar gas for 15 minutes. To

this, tributyl(phenylethynyl)stannane (10 equiv. for H_2TPPBr_4 and 20 equiv. for H_2TPPBr_8) in 10 mL of degassed dioxane was added and heated to 80 °C for 1 hour under Ar atmosphere. After completion of the reaction, the solvent was removed by vacuum distillation. The crude porphyrin was redissolved in $CHCl_3$ (20 mL) and purified on silica column using $CHCl_3$/hexane mixture (7:3, v/v) to 100% $CHCl_3$ as eluent. The desired products were recrystallized from $CHCl_3$/CH_3OH mixture (1:3, v/v). Yields were found to be 68% and 70% for β-tetra- and octa-phenylethynyl substituted porphyrins, respectively.

2,3,12,13-tetra(phenylethynyl)-5,10,15,20-tetraphenyl porphyrin, ($H_2TPP(PE)_4$)

Yield = 68%; UV/Vis.(CH_2Cl_2):λ_{max}(nm) (logε) 453 (5.43), 544 (4.32), 590 (4.45), 632 (4.11); ^{1}H NMR (400 MHz, CDCl$_3$) δ (ppm) 8.71 (s, 4H, β-pyrrole-H) , 8.25 (d, 8H, J = 6.5 Hz, *meso-o*-phenyl-H), 7.80-7.69 (m, 12H, *meso-m*- and *p*-phenyl-H), 7.36-7.33 (m, 8H, β-pyrrole-*o*-PE-H),7.29-7.26 (m, 12H, β-pyrrole-*m- and p*-PE-H), -2.55 (s, 2H, imino-H). MALDI-TOF-MS (m/z): found 1016.44 [M+H]$^+$, calcd. 1016.24. Anal. calcd. for $C_{76}H_{46}N_4$: C, 89.91; H, 4.57; N, 5.52. Found: C, 89.73; H, 4.64; N, 5.61.

2,3,7,8,12,13,17,18-octa(phenylethynyl)-5,10,15,20-tetraphenylporphyrin ($H_2TPP(PE)_8$)

Yield = 70%; UV/Vis.(CH_2Cl_2): λ_{max}(nm) (logε) 507 (5.48), 590 (4.45), 633 (4.11), 692 (3.76); ^{1}H NMR (500 MHz, CDCl$_3$) δ (ppm): 8.42 (d, 8H, J = 7.5 Hz, *meso-o*-phenyl-H), 7.77 (t, 8H, J = 7.5 Hz, *meso-m*-phenyl-H), 7.65 (t, 4H, J = 7.5 Hz, *meso-p*-phenyl-H), 7.29 (d, 16H, J = 7.3 Hz, β-pyrrole-*o*-PE-H), 7.26-7.20 (m, 24H, β-pyrrole-H, *m*- and *p*-PE-H), -1.34 (s, 2H, imino-H). MALDI-TOF-MS (m/z): found 1417.15 [M+H]$^+$, calcd. 1417.72. Anal. calcd. for $C_{108}H_{62}N_4$: C, 91.63; H, 4.41; N, 3.96. Found: C, 91.55; H, 4.60; N, 3.72.

Synthesis of Co(II), Ni(II), Cu(II) and Zn(II) complexes

Corresponding free base porphyrins viz. ($H_2TPP(PE)_4$ or $H_2TPP(PE)_8$ (0.02 mmol) was dissolved in 15 mL of $CHCl_3$. To this, 10 equiv. of $M(OAc)_2 \bullet nH_2O$ (M = Co(II), Cu(II) and Zn(II)) in 2 mL of methanol was added and refluxed on water bath for 50 minutes. The solvent was then evaporated to dryness and redissolved in minimum amount of $CHCl_3$ and washed with water (2×15 mL). The crude product was purified

by column chromatography on silica column using $CHCl_3$ as eluent. Yields were found to be 85-90%. Further, Ni(II) complexes were prepared by refluxing free base porphyrins and $Ni(OAc)_2 \cdot 4H_2O$ (10 equiv.) in DMF for 2 hours under Ar atmosphere followed by the precipitation with water. The crude product was purified on silica column using $CHCl_3$ as eluent. The yield was found to almost quantitative.

NiTPP(PE)$_4$: Yield = 90%; UV/Vis. (CH_2Cl_2): λ_{max}(nm) (logε) 457 (5.20), 625 (4.42); ^{1}H NMR (400 MHz, $CDCl_3$) δ (ppm) 8.57 (s,4H**,** *β*-pyrrole-H), 8.00-7.98(m, 8H, *meso-o-* phenyl-H), 7.66-7.61(m, 12H, *meso-m* and *p*-phenyl-H), 7.27-7.26 (m, 20H, *β*-pyrrole-*o, m* and *p*-PE-H); MALDI-TOF-MS (m/z): found 1072.85 [M+H]$^+$, calcd. 1072.91. Anal. calcd. for $C_{76}H_{44}N_4Ni \cdot 0.5H_2O$: C, 84.45; H, 4.20; N, 5.18. Found: C, 84.31; H, 4.11; N, 5.34.

ZnTPP(PE)$_4$: Yield = 89%; UV/Vis. (CH_2Cl_2): λ_{max}(nm) (logε) 457 (5.50), 579 (4.35), 627 (4.68); ^{1}H NMR (400 MHz, $CDCl_3$) δ (ppm) 8.69 (s, 4H**,** *β*-pyrrole-H), 8.20-8.15 (m, 8H, *meso-o*-phenyl-H), 7.73-7.67 (m, 12H, *meso-m* and *p*-phenyl-H), 7.40-7.36 (m, 8H, *β*-pyrrole-*o*-PE-H),7.30-7.26 (m, 12H, *β*-pyrrole-*m*- and *p*-PE-H); MALDI-TOF-MS (m/z): found 1078.74 [M]$^+$, calcd. 1078.60. Anal. calcd. for $C_{76}H_{44}N_4Zn$: C, 84.63; H, 4.11; N, 5.19. Found: C, 84.70; H, 4.18; N, 5.04.

CoTPP(PE)$_4$: Yield = 92%; UV/Vis. (CH_2Cl_2): λ_{max}(nm) (logε) 452 (5.39), 589 (4.35), 622 (4.44); MALDI-TOF-MS (m/z): found 1073.03 [M+H]$^+$, calcd. 1073.15. Anal. calcd. for $C_{76}H_{44}N_4Co$: C, 84.14; H, 4.14; N, 5.23. Found: C, 84.15; H, 4.18; N, 5.19.

CuTPP(PE)$_4$: Yield = 90%; UV/Vis. (CH_2Cl_2): λ_{max}(nm) (logε) 453 (5.36), 574 (4.21), 625 (4.57); MALDI-TOF-MS (m/z): found 1076.86 [M]$^+$, calcd. 1076.76. Anal. calcd for $C_{76}H_{44}N_4Cu$: C, 84.78; H, 4.12; N, 5.20. Found: C, 84.61; H, 4.19; N, 5.25.

NiTPP(PE)$_8$: Yield = 88%; UV/Vis. (CH_2Cl_2): λ_{max}(nm) (logε) 497 (5.54), 604 (4.63), 651 (4.47); ^{1}H NMR (400 MHz, $CDCl_3$) δ (ppm) 8.23 (d, 8H**,** J = 8 Hz, *meso-o*-phenyl-H), 7.71 (t, 8H, J = 8 Hz, *meso-m*-phenyl-H), 7.61 (t, 4H, *meso-p*-phenyl-H), 7.30-7.22 (m, 40H, *β*-pyrrole-*o, m*- and *p*-PE-H); MALDI-TOF-MS (m/z): found 1473.21 [M+H]$^+$, calcd. 1473.39.

ZnTPP(PE)$_8$: Yield = 87%; UV/Vis. (CH$_2$Cl$_2$): λ_{max}(nm) (logε) 505 (5.47), 619 (4.51); ^{1}H NMR (400 MHz, CDCl$_3$) δ (ppm) 8.34 (d, 8H, J = 8 Hz, *meso-o*-phenyl-H), 7.72 (t, 8H, J = 8 Hz, *meso-m*-phenyl-H), 7.60 (t, 4H, J = 4 Hz, *meso-p*-phenyl-H), 7.36-7.31 (m, 16H, *β*-pyrrole-*o*-PE-H), 7.27-7.20 (m, 24H, *β*-pyrrole-*m*-and *p*-PE-H); MALDI-TOF-MS (m/z): found 1479.05 [M+H]$^+$, calcd. 1479.08.

CoTPP(PE)$_8$: Yield = 91%; UV/Vis. (CH$_2$Cl$_2$): λ_{max}(nm) (logε) 496 (5.58), 604 (4.65), 647 (4.47); MALDI-TOF-MS (m/z): found 1473.18 [M+H]$^+$, calcd. 1473.63. Anal. calcd. for C$_{108}$H$_{60}$N$_4$Co: C, 88.09; H, 4.11; N, 3.80. Found: C, 87.96; H, 4.04; N, 3.97.

CuTPP(PE)$_8$: Yield = 94%; UV/Vis.(CH$_2$Cl$_2$): λ_{max}(nm) (logε) 505 (5.50), 618 (4.70), 661 (4.20); MALDI-TOF-MS (m/z): found 1478.06 [M+H]$^+$, calcd. 1478.24

4.3 Result and Discussion

4.3.1 Synthesis and characterisation

The precursors, *β*-bromoporphyrins viz. H$_2$TPPBr$_4$ and H$_2$TPPBr$_8$ were synthesized using reported procedures [11,12]. H$_2$TPP(PE)$_4$ and H$_2$TPP(PE)$_8$ were synthesized in 68-70% yield by Stille coupling of H$_2$TPPBr$_4$ or H$_2$TPPBr$_8$ with tributyl(phenylethynyl)stannane in refluxing 1,4-dioxane for 1 hour under argon atmosphere as shown in scheme 1. Notably, we could obtain desired products in lesser time scale (1 hour) as compared to reported literature [8,10]. Further, Co(II), Cu(II) and Zn(II) complexes were prepared by refluxing 10 equiv. of M(OAc)$_2$•nH$_2$O in CHCl$_3$/MeOH mixture whereas Ni metallation was carried out by refluxing in DMF with 10 equivalents of Ni(OAc)$_2$•4H$_2$O. ^{1}H NMR and mass spectra of synthesized porphyrins were shown in Figures A1-A13 in the Appendix 3). It is known from the literature that MTPP(PE)$_8$ (M = 2H and Zn(II)) [8] and MT(*p*-^{t}Bu-Ph)P(PE)$_4$ (M = Co(II), Cu(II) and Zn(II)) [10] exhibited planar conformation (Figures A14-15 and Table A1 in the Appendix 3) whereas NiTPP(PE)$_8$ showed moderately nonplanar conformation due to smaller size of Ni(II) ions and effective bonding of Ni(II) ion with porphyrin nitrogens [8]. The optical absorption spectra of H$_2$TPP(PE)$_4$, H$_2$TPP(PE)$_8$ and their metal complexes were recorded in CH$_2$Cl$_2$ at 298 K.

Representative absorption spectra of $H_2TPP(PE)_4$ and $H_2TPP(PE)_8$ are shown in Figure 1.

Table 1 lists the absorption spectral data of these porphyrins in CH_2Cl_2 at 298 K. Free base porphyrins exhibited a characteristic Soret band (B band) and three Q bands whereas metal

X = H, H_2TPPBr_4
X = Br, H_2TPPBr_8

X = H, $H_2TPP(PE)_4$, Yield = 68%
X = PE, $H_2TPP(PE)_8$, Yield = 70%

Scheme 1. Synthetic route to *β*-phenylethynyl substituted porphyrins

(a)

(b)
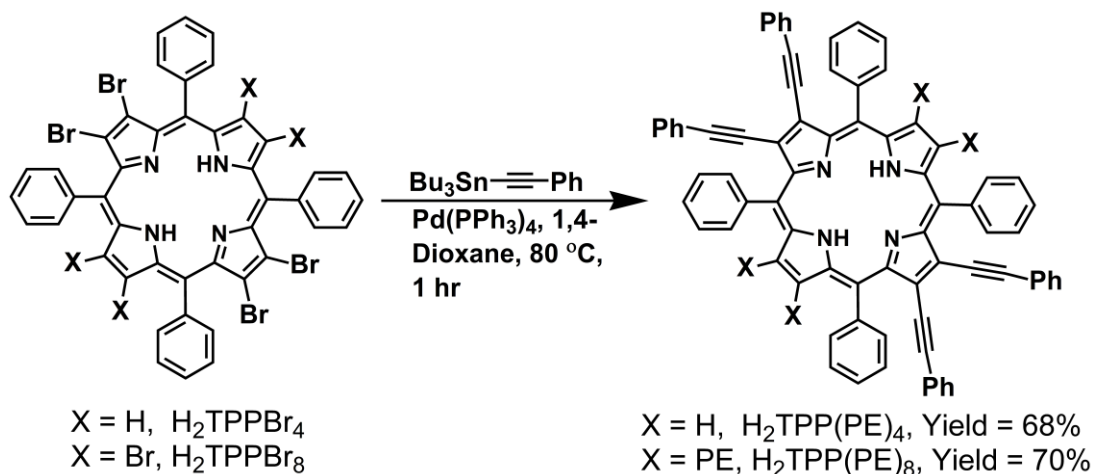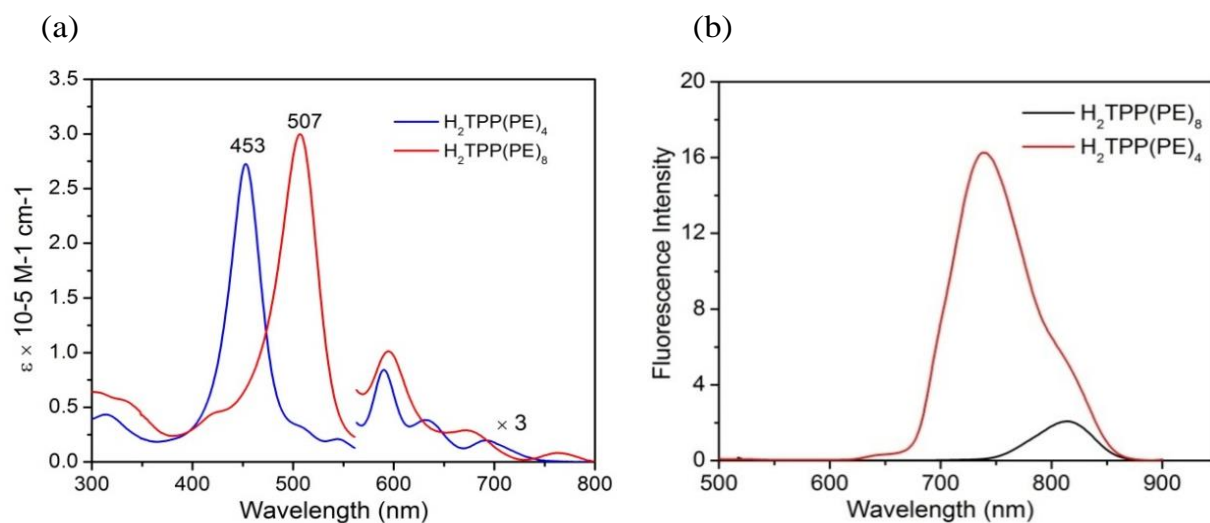
Figure 1. (a) UV-Visible absorption spectra of $H_2TPP(PE)_4$ and $H_2TPP(PE)_8$; (b) Fluorescence spectra of $H_2TPP(PE)_4$ and $H_2TPP(PE)_8$ in CH_2Cl_2 at 298 K.

derivatives exhibited a Soret and two Q bands. $H_2TPP(PE)_4$ exhibited red shift in B ($\Delta\lambda_{max}$ = 36 nm) and $Q_x(0,0)$ ($\Delta\lambda_{max}$ = 45 nm) bands whereas $H_2TPP(PE)_8$ exhibited larger red shift in Soret band ($\Delta\lambda_{max}$ = 92 nm) and $Q_x(0,0)$ band ($\Delta\lambda_{max}$ = 117 nm) as compared to H_2TPP suggesting that each of the PE group shifts ~9-11 nm. The observed remarkable red shift both in Soret and Q bands was interpreted in terms of

extended conjugation by PE groups with porphyrin π-system as well as electron withdrawing nature of PE susbtituents [8,9]. The B and Q bands of these porphyrins exhibited an interesting trend in red-shift: $H_2TPP < H_2TPP(PE)_4 < H_2TPP(PE)_8$. The metal complexes exhibited blue-shift in both B and Q bands due to stabilisation of HOMOs as expected.

Table 1. Optical absorption spectral data of synthesised porphyrins in CH_2Cl_2 at 298 K. Values in the parenthesis represent $\log\varepsilon$ values.

Porphyrin	B band, nm	Q band(s), nm
$H_2TPP(PE)_4$	453(5.43)	590(4.45), 633(4.11), 692(3.76)
$H_2TPP(PE)_8$	507(5.48)	594(4.53), 672(3.99), 764(3.44)
$CoTPP(PE)_4$	452(5.39)	589(4.35), 622(4.44)
$CoTPP(PE)_8$	496(5.58)	604(4.65), 647(4.47)
$NiTPP(PE)_4$	457(5.20)	625(4.42)
$NiTPP(PE)_8$	497(5.54)	604(4.63), 651(4.47)
$CuTPP(PE)_4$	453(5.36)	574(4.21), 625(4.57)
$CuTPP(PE)_8$	505(5.50)	618(4.70), 661(4.20)
$ZnTPP(PE)_4$	457(5.50)	579(4.35), 627(4.68)
$ZnTPP(PE)_8$	505(5.47)	619(4.51)

The synthesized free base and Zn(II) porphyrins were characterized by fluorescence spectroscopy to elucidate the effect of polyphenylethynyl substituents on porphyrin π-system. Figure 1(b) represents the steady state emission spectra of $H_2TPP(PE)_4$ and $H_2TPP(PE)_8$.

The representative emission spectra of $ZnTPP(PE)_n$ (n = 4, 8) are shown in Figure A16 in Appendix 3. Significant red shifted emission ($\Delta\lambda_{max}$ = 76-90 nm) was observed for $MTPP(PE)_8$ as compared to $MTPP(PE)_4$. However, weak fluorescence intensities and decreased quantum yields were observed for $MTPP(PE)_8$ (M = 2H and Zn(II)) as

Figure 2. ^{1}H NMR spectrum of H$_2$TPP(PE)$_4$ in CDCl$_3$ at 298 K

Figure 3. ^{1}H NMR spectrum of ZnTPP(PE)$_4$ in CDCl$_3$ at 298 K.

108

compared to MTPP(PE)$_4$ or MTPP (*vide infra*). ^{1}H NMR spectrum of H$_2$TPP(PE)$_4$ exhibits characteristic resonances arising from *β*-pyrrole protons, *meso*-phenyl, *β*-phenylethynyl (PE) and imino hydrogens (NH) while H$_2$TPP(PE)$_8$ is devoid of *β*-protons. The *ortho* protons of *meso*-phenyl of H$_2$TPP(PE)$_8$ are marginally ($\Delta\delta = 0.17$ ppm) downfield shifted while *meta-* and *para*-protons of *meso*-phenyl and *β*-phenyl-ethynyl protons are marginally ($\Delta\delta = 0.03$-0.06 ppm) upfield shifted as compared to H$_2$TPP(PE)$_4$. Notably, the core imino protons of H$_2$TPP(PE)$_8$ (-1.34 ppm) are downfield shifted as compared to which are interpreted in terms of the electron withdrawing and conjugative effect of PE groups [9,10]. ^{1}H NMR spectra of MTPP(PE)$_4$ (M = Ni(II) and Zn(II)) complexes are devoid of imino protons, indicating that metal got inserted into the porphyrin ring. The *meso*-phenyl proton resonances of MTPP(PE)$_4$ (M = Ni(II) and Zn(II)) are 0.05-0.06 ppm upfield shifted as compared to corresponding free base porphyrins. The integrated intensities of proton resonances of these *β*-phenylethynyl substituted porphyrins are in consistent with the proposed structures (Figures 3,4 and A1-A4, Appendix 3).

4.3.2 Electrochemical Redox Properties
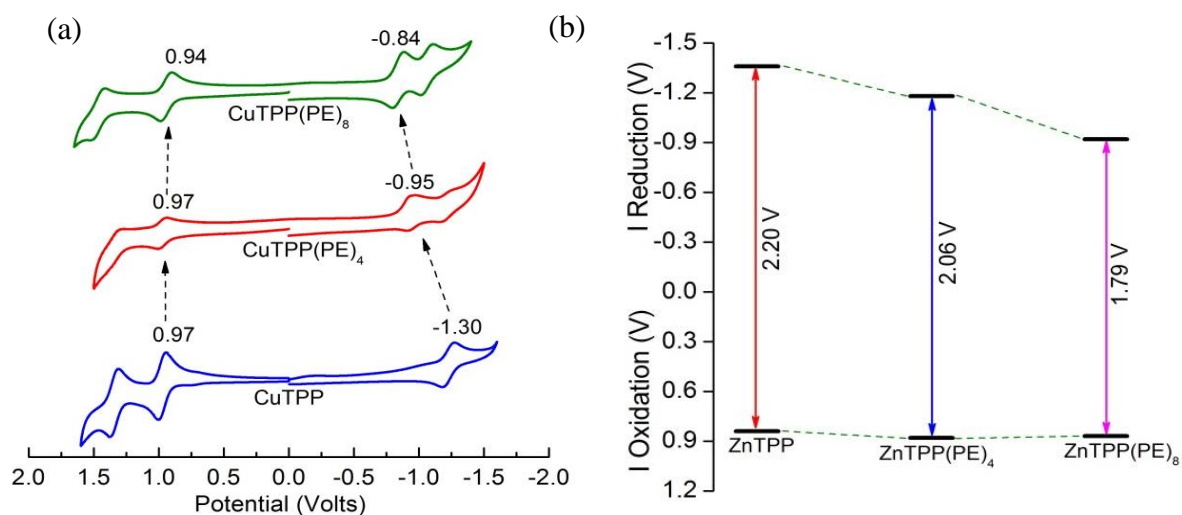
Figure 4. (a) Cyclic Voltammograms of CuTPP(PE)$_n$ (n = 0, 4 and 8) in CH$_2$Cl$_2$ containing 0.1 M TBAPF$_6$ using Ag/AgCl as reference electrode with a scan rate of 0.1 V/s at 298 K, **(b)** Variation of LUMO levels of ZnTPP(PE)$_4$ and ZnTPP(PE)$_8$ in reference to ZnTPP.

To examine the influence of phenylethynyl (PE) substituents on porphyrin π-system, the electrochemical redox behaviour of these porphyrins was studied by cyclic voltammetry in CH_2Cl_2 at 298 K. Under similar conditions, the corresponding MTPP derivatives were also examined and the electrochemical redox data (*vs* Ag/AgCl) is listed in Table 2. The cyclic voltammograms of $CuTPP(PE)_n$ (n = 0, 4 and 8) complexes are shown in Figure 4. These porphyrins exhibited two successive

Table 2. Electrochemical redox data of synthesized porphyrins (in V *vs* Ag/AgCl) in CH_2Cl_2 containing 0.1 M TBAPF$_6$ with a scan rate of 0.1 V/s at 298 K.

Porphyrin	Oxidation (V)		Reduction (V)		ΔE (V)
	I	II	I	II	
H_2TPP	1.00	1.34	-1.23	-1.54	2.23
$H_2TPP(PE)_4$	1.03	1.21[a]	-0.88	-0.98[a]	1.91
$H_2TPP(PE)_8$	0.99	1.12	-0.79	-1.06	1.78
$NiTPP$	1.02	1.32	-1.28	-1.72	2.30
$NiTPP(PE)_4$	1.07	1.25	-0.96	-1.21	2.03
$NiTPP(PE)_8$	1.14	1.25	-0.80	-1.07	1.94
$CuTPP$	0.97	1.35	-1.30	-1.71[a]	2.30
$CuTPP(PE)_4$	0.97	1.34	-0.95	-1.22	1.92
$CuTPP(PE)_8$	0.94	1.46	-0.84	-1.06	1.78
$ZnTPP$	0.84	1.14	-1.36	-1.77	2.20
$ZnTPP(PE)_4$	0.88	1.09	-1.18	-1.36[a]	2.06
$ZnTPP(PE)_8$	0.87	1.10	-0.92	-1.35[a]	1.79

[a]data obtained from DPV

reversible one-electron oxidations and one-electron reductions (Figure A17, Appendix 3). However, the first oxidation and first reduction of Co(II) complexes is a metal centered process which is well documented in literature. Analysis of electrochemical redox data of $MTPP(PE)_n$ (n = 0, 4, and 8; M = 2H, Ni(II), Cu(II), Zn(II)) revealed

marginal changes in first ring oxidation (10 - 100 mV) and a drastic anodic shift (450-500 mV) in first ring reduction potential with increase in number of phenylethynyl groups (Figures 4 and A17, Appendix 3). The anodic shift in first ring reduction potentials were interpreted in terms of electron withdrawing and conjugative effects of PE substituents. Similarly, for $CoTPP(PE)_n$ (n = 4, 8) complexes, the $Co^{II/III}$ oxidation potentials marginally shifted (anodic shift) by ~0.06 V while the $Co^{II/I}$ reduction is shifted anodically by 0.23-0.49 V as compared to CoTPP (Table A2, appendix 3). The first reduction potential of these porphyrins followed the trend 2H > Ni(II) > Cu(II) > Zn(II) according to the difference in their electronegativity. As we increase the number of phenylethynyl groups, the HOMO-LUMO gap of $MTPP(PE)_n$ decreases (0.38 - 0.55 V) as compared to MTPP as shown in Figures 4b and A18, Appendix 3 due to extensive stabilization of LUMO. The electrochemical redox data of these porphyrins clearly indicate the electron deficient nature porphyrin π-system [9].

4.3.3 Photophysical Studies

In order to understand the effect of polyphenylethynyl substitution, we have carried out quantum yield and life time measurements. Table 3 lists emission spectral data and the comparative values of quantum yields, Stokes shifts, radiative (k_r) and non-radiative (k_{nr}) rate constants of synthesized porphyrins. $MTPP(PE)_n$ (M = 2H, Zn(II); n = 4, 8) exhibit planar confirmation as evidenced from their deviation of β-pyrrole carbons from the porphyrin mean plane, ΔC_β (0.040-0.094 Å) and deviation of 24 core atoms from porphyrin mean plane, $\Delta 24$ values (0.032-0.068 Å) (Table A1, Appendix 3) [8,10]. $MTPP(PE)_4$ and $MTPP(PE)_8$ exhibited decreased fluorescence quantum yields and shorter lifetimes than MTPP which is attributed to intramolecular charge transfer (ICT) from porphyrin core to acceptor PE moieties [9,13,14]. The observed radiative rate constants (k_r) of $MTPP(PE)_n$ are nearly 2-8 times lower than H_2TPP whereas nonradiative rate constants (k_{nr}) are 2-7 fold higher than H_2TPP. In X-ray structures, the phenylethynyl groups are almost perpendicular to porphyrin mean plane which indicates some extent of intramolecular charge transfer must be involved in ground and singlet excited state resulting into

reduced k_r and enhanced k_{nr}, poor quantum yields, large Stokes shifts and shortened lifetime values as compared to that of MTPP (Table 3). The photophysical data clearly

support the possibility of intramolecular charge transfer (ICT) from porphyrin core to phenylethynyl moieties [9,13,14].

Table 3. Photophysical data of MTPP(PE)$_n$ (M = 2H and Zn; n = 0, 4, 8) in CH$_2$Cl$_2$.

Porphyrin	$\lambda_{em, nm}$	Stokes shift (cm^{-1})	Φ_f	τ (ns)	k_r (s^{-1})	k_{nr} (s^{-1})	k (s^{-1})
H$_2$TPP	654,718	165	0.11	9.15	1.2×10^7	9.7×10^7	1.09×10^8
H$_2$TPP(PE)$_4$	739	919	9.6×10^{-3}	1.57	6.1×10^6	6.3×10^8	6.37×10^8
H$_2$TPP(PE)$_8$	814 (w)	804	5.2×10^{-3}	1.44	3.6×10^6	6.9×10^8	6.95×10^8
ZnTPP	598,644	372	3.0×10^{-2}	1.59	1.9×10^7	6.4×10^8	6.62×10^8
ZnTPP(PE)$_4$	644	421	1.9×10^{-2}	0.55	3.4×10^7	1.8×10^9	1.81×10^9
ZnTPP(PE)$_8$	736 (w)	2568	2.3×10^{-3}	0.97	2.4×10^6	1.0×10^9	1.02×10^9

W = Weak emission intensity

4.3.4 Solvatochromism Studies

The Soret band of H$_2$TPP(PE)$_8$ in various solvents lies between 506 and 524 nm and is seen to have red-shift with increasing solvent polarity. This positive solvatochromism [15,16] is ascribed to the possibility of charge transfer between the electron rich porphyrin core and the electron deficient peripheral PE groups. Notably, the *β*-phenylethynyl substituted porphyrins have been shown to exhibit charge transfer characteristics [5,6,10]. The photophysical properties of these porphyrins are unusual in that they evince considerable charge-transfer character mixed into the porphyrin B- and Q-type transitions [5,6,10,14] due to π-delocalisation of *β*- substituent with In order to gain further insight into the photophysical processes in these compounds, we recorded the absorption and emission spectra of MTPP(PE)$_n$ (M = 2H, Zn(II); n = 0, 4 and 8) in different solvents and the results are summarized in Table 4 and A3 in the Appendix 3.
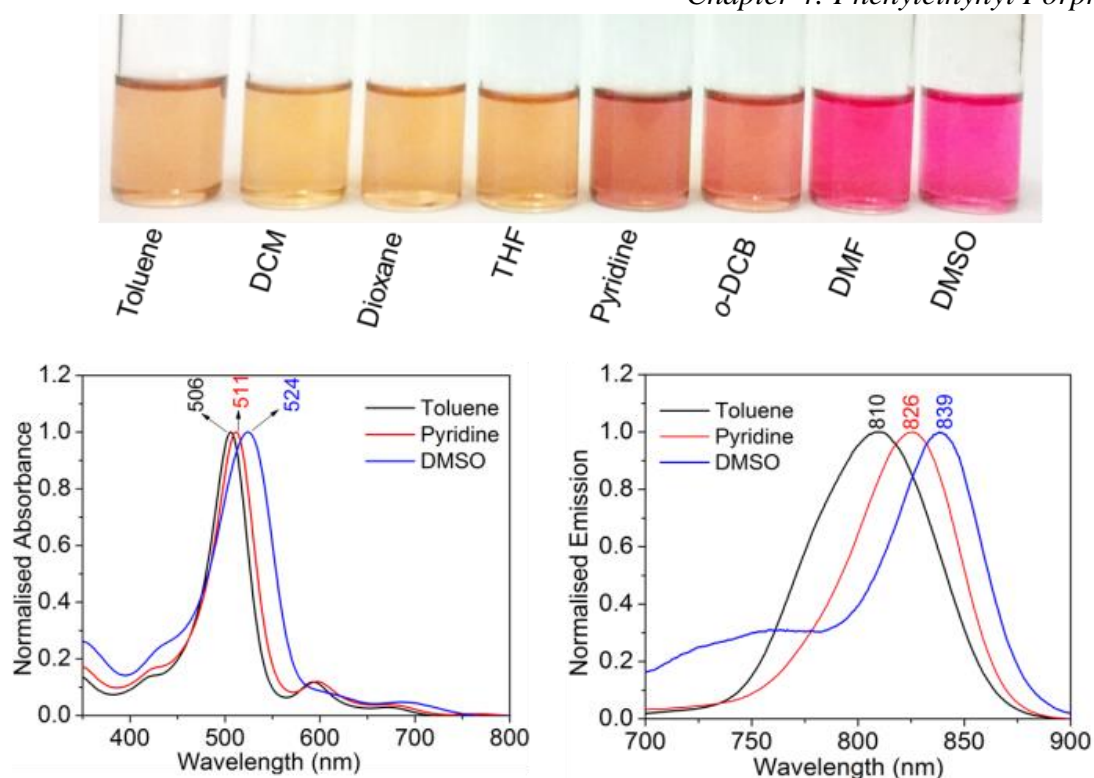
Figure 5. (top) Colorimetric response of $H_2TPP(PE)_8$ in different solvents; (bottom) UV Visible and fluorescence spectra of $H_2TPP(PE)_8$ in different solvents at 298 K.

porphyrin π-system. This is further supported by the increased bandwidth of the Soret band (B band) of $H_2TPP(PE)_8$ (FWHM = 49 nm) and $ZnTPP(PE)_8$ (FWHM = 36 nm) as compared to H_2TPP (FWHM = 14 nm) and $ZnTPP$ (FWHM = 11 nm) [16]. Furthermore, the possibility of deprotonation by various solvents listed in Table 4 is ignored as the UV-Vis spectral profiles of deprotonated $H_2TPP(PE)_8$ is completely different as that of solvent dependent profiles (Figure A19, Appendix 3). The absorption spectra of $H_2TPP(PE)_4$ are nearly independent of solvent polarity and shows no appreciable colour change in different solvents (Figure A20, Appendix 3) with marginal shift (2-7 nm) which indicates weak intramolecular interaction between donor and acceptor groups in the ground state. Notably, $ZnTPP(PE)_4$ and $ZnTPP(PE)_8$ exhibit 13-18 nm shift in their Soret band while increasing solvent polarity from toluene to DMSO.

However, there is no regular trend observed with solvent polarities in Zn(II) complexes which is due to combined solvatochromism arising from axial ligation of coordinating solvents and intramolecular interaction between donor (porphyrin core) and acceptor (PE) groups in the ground state (Figure A21, Appendix 3) [16].

Table 4. Electronic spectral data of $H_2TPP(PE)_8$ in different solvents at 298 K.

Solvent	B band, nm	Q band(s), nm	λ_{em}, nm
Toluene	506(5.52)	593(4.59), 673(3.97), 759(2.61)	810
DCM	507(5.41)	595(4.48), 672(3.96), 762(3.44)	814
Dioxane	506(5.64)	594(4.68), 672(4.17), 763(3.43)	820
THF	504(5.43)	593(4.48), 669(3.96), 760(3.10)	823
Pyridine	511(5.45)	597(4.53), 674(4.03), 765(3.22)	826
o-DCB	510(5.47)	595(4.57), 673(4.01), 760(3.32)	809
DMF	521(5.30)	605(4.15), 678(3.96)	765
DMSO	524(5.20)	691(3.87)	839

In pyridine, a highly red-shifted absorption spectrum was observed for Zn(II) complexes which is probably due to the strong axial coordination of pyridine to the zinc metal centre [17,18,19]. A distinctive bathochromic shift (20-30 nm) in emission band was also observed (Figures 5b and A21, Appendix 3) for free bases and Zn(II) complexes as we move from less polar solvent (toluene) to more polar solvent (DMSO) along with successive decrease in fluorescence intensity. $H_2TPP(PE)_4$ exhibits broad structureless weak emission in high polar solvents like DMF and DMSO. These results suggests an internal charge transfer which results from stabilization of polar excited state by polar solvents and is well documented with donor-acceptor fluorophores [15,6,20]. $H_2TPP(PE)_8$ exhibited blue shifted emission (negative solvetochromism) in DMF. This is possibly due to less stable and less polar excited state than the ground state which is further supported by the lower life time (0.66 ns) as compared to other solvents such as CH_2Cl_2, toluene, THF and dioxane (life time 1.3 to 1.6 ns) (Table A4, appendix) [15]. We observed almost linear fit between Stokes shift of $H_2TPP(PE)_8$ in different solvents and dielectric constant which

indicates enhanced charge transfer in polar solvents (Figure A22, Appendix 3). The solvent induced changes were examined according to the Lippert–Mataga method [21]. According to this method, the plot between the observed Stokes shift (v_{st}) and solvent orientation polarizability (Δf) must be linear for simple solvent-solute interactions whereas nonlinear fit will be observed in case of solvent-solute interactions associated with charge transfer (CT) and hydrogen bonding interactions [21]. In case of $H_2TPP(PE)_8$, we observed nonlinear fit indicating charge transfer interactions. While $ZnTPP(PE)_8$ exhibited more scattered points due to the combined effect of charge transfer and axial ligation (Figure A22, Appendix 3) [17,18].

4.3.5 Anion Binding Studies

A wide variety of porphyrinoids as explained in chapter 2 and organic sensors [22,23] were utilised for colorimetric detection of toxic anions. A qualitative assessment of colorimetric responses of $MTPP(PE)_n$ (M = 2H, Zn and n = 4, 8) to various anions have also been carried out in CH_2Cl_2 at 298 K with various anions in the form of TBA salts. $H_2TPP(PE)_8$ selectively detects F^- and CN^- ions which are reflected by red-shifted UV-Visible spectra with colorimetric 'naked eye' detection of F^- and CN^- ions (reddish brown to dark pink) whereas no observable shift was found with other tested anions as shown in Figure 6. These anions are detected *via* anion induced deprotonation mechanism as the UV-Visible spectral profiles obtained for $H_2TPP(PE)_8$ with F^- and CN^- resemble the optical absorption spectrum obtained by the addition of TBAOH (Figure A19, Appendix 3). Further, we have recorded the ^{1}H NMR of $H_2TPP(PE)_8$ in presence of CN^- and F^- ions in $CDCl_3$ at 298 K. The disappearance of NH signal confirms the anion induced deprotonation mechanism as shown in Figure A23a in the Appendix 3. The dianionic species formed after deprotonation have stronger hydrogen bonding with protonated anion (HCN or HF) which leads to large spectral shift [24,25]. While using TBAOH, the formed dianionic species and water are in equilibrium with reactant ($H_2TPP(PE)_8$) possibly due to weaker hydrogen

(a)　　　　　　　　　　　　　　　　　　　(b)
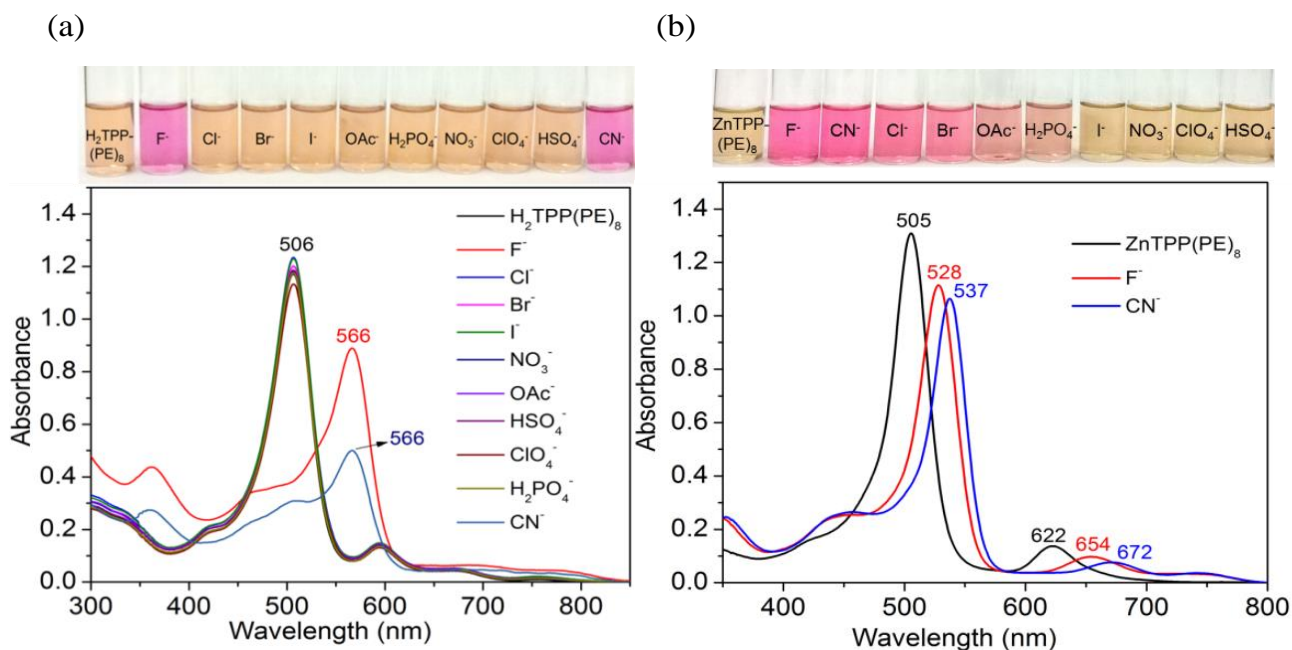
Figure 6. (a) Colorimetric response of $H_2TPP(PE)_8$ with tested anions (Top); UV-Vis spectra of $H_2TPP(PE)_8$ upon addition of excess of TBA salts of tested anions (bottom). (b) Colorimetric response of $ZnTPP(PE)_8$ with tested anions (Top); UV-Vis spectra of $ZnTPP(PE)_8$ upon addition of F^- and CN^- ions in the form of TBA salts (bottom) in CH_2Cl_2 at 298 K.

bonding interactions (Figure A23b, Appendix 3). Interestingly, $H_2TPP(PE)_4$ doesn't show any UV-Vis spectral change and colorimetric response even towards highly basic anions like F^- and CN^- (Figure A24, Appendix 3). Notably, $ZnTPP(PE)_8$ is able to detect F^-, Cl^-, Br^-, CN^-, CH_3COO^- and $H_2PO_4^-$ ions which have shown considerable red-shifts in Soret ($\Delta\lambda_{max} = 19\text{-}32$ nm) and Q bands ($\Delta\lambda_{max} = 30\text{-}50$ nm) in CH_2Cl_2. Figure 6b represent the colorimetric 'naked eye' detection of these anions by $ZnTPP(PE)_8$. Table 5 and A5 list the UV-Vis spectral data of $ZnTPP(PE)_8$, $H_2TPP(PE)_8$ and $ZnTPP(PE)_4$ in presence of different anions in CH_2Cl_2 at 298 K. The shift in B and Q bands are in accordance with the basicities of anions (pK_a) except Cl^- ion due to effective CT from chloride ion to porphyrin than F^- ion. No observable UV-Vis shifts and detectable colour changes are observed with I^-, NO_3^-, ClO_4^- and HSO_4^- ions.

Table 5. Optical absorption data of ZnTPP(PE)$_8$ (**1**) in presence of different anions in CH$_2$Cl$_2$ at 298 K.

Porphyrin	B band, nm	Q band(s), nm	ΔB, nm	ΔQ, nm
1	505(5.52)	622(4.54)	-	-
1+CN$^-$	537(5.43)	672(4.38)	32	50
1+F$^-$	528(5.44)	654(4.32)	23	32
1+Cl$^-$	535(5.41)	665(4.29)	30	43
1+Br$^-$	505(5.39), 533(sh)	622(4.0), 648(sh)	0	0
1+OAc$^-$	528(5.42)	652(4.37)	23	30
1+H$_2$PO$_4^-$	524(5.37)	646(4.34)	19	24

ΔB = Shift in B band w.r.t ZnTPP(PE)$_8$ (**1**) ; ΔQ = Shift in Q band w.r.t ZnTPP(PE)$_8$

4.3.6 Axial ligation Studies

UV-Vis titrations were carried for ZnTPP(PE)$_n$ with basic anions in order to measure binding constants and stoichiometry of complexation [17,18]. Figure 7 represent the UV-Vis spectral titrations of ZnTPP(PE)$_8$ and ZnTPP(PE)$_4$ with CN$^-$ ions in toluene at 298 K. Both the Soret ($\Delta\lambda_{max} = 32$ nm) and Q bands ($\Delta\lambda_{max} = 50$ nm) are red shifted upon increasing the concentration of TBACN indicating the axial coordination of CN$^-$ ions to ZnTPP(PE)$_8$ with well-anchored isosbestic points at 462, 521, 554 and 645 nm during the course of CN$^-$ ion binding experiment.

Similar, UV-Vis spectral profiles were observed for ZnTPP(PE)$_8$ with F$^-$, Cl$^-$, CH$_3$COO$^-$ and H$_2$PO$_4^-$ ions. Figure A25 in Appendix 3 represent the UV-Vis titration of ZnTPP(PE)$_8$ with Cl$^-$, and CH$_3$COO$^-$ ions in toluene at 298 K. The binding constants were calculated using Hill equation [25] and the corresponding binding data are presented in Table 6. The binding constants are increasing as the basicity of anion increases except for Cl$^-$ and F$^-$ ions. The higher binding constant was observed for Cl$^-$ ions as compared to F$^-$ ions with ZnTPP(PE)$_8$ is possibly due to effective charge transfer from Cl$^-$ ion to Zn metal center. It is known from the literature that Cl$^-$ binds effectively with Zn(II) porphyrins as compared to Br$^-$ and I$^-$ anions according to their basicity [17,19]. The stoichiometry of complexation was confirmed by Hill plot (Figure 8 inset and Table 6). The Hill plot shows a straight line between log[CN$^-$] and
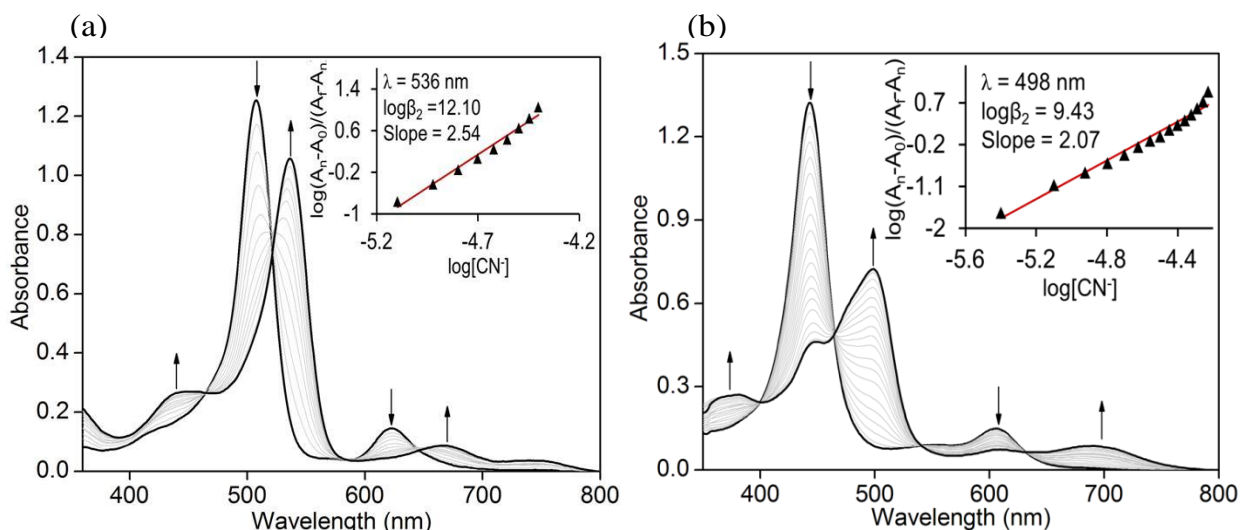
Figure 7. UV-Vis titration of (a) $ZnTPP(PE)_8$ (4 μM) and (b) $ZnTPP(PE)_4$ while increasing the concentration of cyanide ions (6 - 47.5 μM) in toluene at 298 K. Inset shows the corresponding Hill plot.

Table 6. Binding constant data of $ZnTPP(PE)_n$ with anions in toluene at 298K and n represents the stoichiometry of complexation.

Porphyrin	Anion	$\beta_2 (M^{-2})$	$\log \beta_2$	n
$ZnTPP(PE)_8$	CN^-	1.26×10^{12}	12.10	2.5
	Cl^-	8.71×10^{11}	11.94	2.3
	CH_3COO^-	2.09×10^{9}	9.32	1.7
	$H_2PO_4^-$	3.98×10^{7}	7.60	1.8
	F^-	8.13×10^{6}	6.91	1.7
$ZnTPP(PE)_4$	CN^-	2.69×10^{9}	9.43	2.1

$\log(A_i-A_0/A_f-A_i)$ having slope value ~2, which indicates 1:2 (porphyrin-to-cyanide) stoichiometry. These results clearly reveal enhanced Lewis acidic nature of Zn(II) center due to electron withdrawing nature of polyphenyethynyl groups. To the best of our knowledge, this is first report on Zn(II) porphyrins [17-19] showing very high binding constants (10^{12} – 10^{7} M^{-2}) with anions as compared to ZnTPP [17].

4.4 CONCLUSIONS

Phenylethynyl-substituted porphyrins were synthesized by Stille coupling reaction in shorter timescale as compared to literature methods. $H_2TPP(PE)_8$ exhibited red shift of

92 nm in Soret and 117 nm in longest wavelength, $Q_x(0,0)$ bands as compared to H_2TPP. $MTPP(PE)_n$ exhibited only marginal shift in first oxidation potentials (10 - 100 mV) whereas profound anodic shifts were found in the first ring reduction potentials ($\Delta E_{red} = 450 - 500$ mV), which are interpreted in terms of electron withdrawing and conjugative effect of phenylethynyl substituents. Hence, we could observe substantial decrement in the HOMO-LUMO gap. The free base and Zn(II) porphyrins exhibited lower fluorescence quantum yields and lifetime values as compared to MTPPs. $MTPP(PE)_8$ display a strong solvatochromism which is reflected by a large red-shift in their absorption and emission maxima while increasing the solvent polarity. These porphyrins exhibited lower radiative rate constants (k_r) and enhanced nonradiative rate constants (k_{nr}) as compared to MTPP. The decrement in fluorescence lifetime values, quantum yields, radiative rate constants (k_r) and profound solvatochromism with enhanced nonradiative rate constants (k_{nr}) have been interpreted in terms of intramolecular charge transfer (ICT) from porphyrin core to phenyethynyl moieties. Further, $ZnTPP(PE)_8$ was utilized for the colorimetric "naked-eye" detection of CN^-, F^-, Cl^-, Br^-, $H_2PO_4^-$ and CH_3COO^- ions through axial coordination of anion to Zn(II) metal centre. The enhanced Lewis acidity of $ZnTPP(PE)_8$ is further proved by axial ligation studies. Moreover, $ZnTPP(PE)_8$ exhibited extremely very high binding constants (10^{12} - 10^7 M^{-2}) with anions as compared to ZnTPP.

4.5 REFERENCES

1.   D'Souza, F.; Ito, O., "Photoinduced electron transfer in supramolecular systems of fullerenes functionalized with ligands capable of binding to zinc porphyrins and zinc phthalocyanines", *Coord. Chem. Rev*. **2005**, *249*, 1410-1422.

2.   Drain, C. M.; Varotto, A.; Radivojevic, I., "Self-organized porphyrinic materials", *Chem. Rev.* **2009**, *109*, 1630-1658.

3.   Giraudeau, A.; Callot, H. J.; Jordan, J.; Ezhar, I.; Gross, M., "Substituent effects in the electroreduction of porphyrins and metalloporphyrins", *J. Am. Chem. Soc.* **1979***, 101*, 3857-3862.

4.   Medforth, C. J.; Senge, M. O.; Smith, K. M.; Sparks L. D.; Shelnut, J. A., "Nonplanar distortion modes for highly substituted porphyrins", *J. Am. Chem. Soc.* **1992**, *114*, 9859−9869.

5. Priyadarshy, S.; Therien M. J.; Beratan, D. N., "Acetylenyl-linked, porphyrin-bridged, donor-acceptor molecules: A theoretical analysis of the molecular first hyperpolarizability in highly conjugated push-pull chromophore structures", *J. Am. Chem. Soc.* **1996**, *118*, 1504-1510.

6. LeCours, S. M.; Guan, H. W.; DiMagno, S. G.; Wang C. H.; Therien, M. J., "Push-Pull arylethynyl porphyrins: New chromophores that exhibit large molecular first-order hyperpolarizabilities", *J. Am. Chem. Soc*. **1996**, *118*, 1497-1503.

7. Reddy, N. M.; Pan, T.Y.; Rajan, Y. C.; Guo, B. C.; Lan, C. M.; Diau, E. W. G.; Yeh, C. Y., "Porphyrin sensitizers with π-extended pull units for dye-sensitized solar cells", *Phys. Chem. Chem. Phys.* **2013**, *15*, 8409-8415.

8. Chandra, T.; Kraft, B. J.; Huffman, J. C.; Zaleski, J. M., "Synthesis and structural characterization of porphyrinic enediynes: Geometric and electronic effects on thermal and photochemical reactivity", *Inorg. Chem.* **2003**, *42*, 5158-5172.

9. Earles, J. C.; Gordon, K. C.; Stephenson, A. W. I.; Partridge, A. C.; Officer, D. L., "Spectroscopic and computational study of *β*-ethynylphenylene substituted zinc and free-base porphyrins", *Phys. Chem. Chem. Phys.* **2011**, *13*, 1597-1605.

10. Bhyrappa, P.; Sarangi, U. K.; Velkannan, V.; Ramkumar, V., "*β*-Tetrasubstituted meso-tetra(4-n-butylphenyl)porphyrins and their metal complexes: Synthesis and rtructural properties", *Eur. J. Inorg. Chem.* **2014**, 5760-5770.

11. Kumar, P. K.; Bhyrappa, P.; Varghese, B., "An improved protocol for the synthesis of antipodal-tetrabromo-tetraphenylporphyrin and the crystal structure of its Zn(II) complex', *Tetrahedron Lett.* **2003**, *44*, 4849-4851.

12. Bhyrappa, P.; Krishnan, V., "Octabromotetraphenylporphyrin and its metal derivatives: Electronic structure and electrochemical properties" *Inorg. Chem.* **1991,** *30*, 239-245.

13. Lembo, A.; Tagliatesta, P.; Guldi, D. M., "Synthesis and photophysical investigation of new porphyrin derivatives with *β*-pyrrole ethynyl linkage and corresponding dyad with [60] fullerene", *J. Phys. Chem.* A **2006**, *110*, 11424–11434.

14. Annoni, E.; Pizzotti, M.; Ugo, R.; Quici, S.; Morotti, T.; Bruschi, M.; Mussini, P., "Synthesis, electronic characterisation and significant second-order non-linear optical responses of meso-tetraphenylporphyrins and their Zn[II] complexes carrying a push or pull group in the *β*-pyrrolic position", *Eur. J. Inorg. Chem.* **2005**, 3857-3874.

15. Serra, V. V.; Andrade, S. M.; Silva, E. M. P.; Silva, A. M. S.; Neves, M. G. P. M. S.; Costa, S. M. B., "Structural effects of the *β*-vinyl linker in pyridinium porphyrins: Spectroscopic studies in organic solvents and AOT reverse micelles", *J. Phys. Chem. B* **2013**, *117,* 15023-15032.

16. Aimi, J.; Nagamine, Y.; Tsuda, A.; Muranaka, A.; Uchiyana, M.; Aida, T., "Conformational, solvatochromism: Spatial discrimination of nonpolar solvents by using a supramolecular box of a π-conjugated zinc bisporphyrin rotamer", *Angew. Chem.* **2008**, *120*, 5231-5234.

17. Nappa, M.; Valentine, J. S., "The influence of axial ligands on metalloporphyrin visible absorption spectra. Complexes of tetraphenylporphinatozinc", *J. Am. Chem. Soc.* **1978**, *100*, 5075-5080.

18. Kojima, T.; Nakanishi, T.; Honda, T.; Harada, R.; Shiro, M.; Fukuzumi, S., "Impact of distortion of porphyrins on axial coordination in (porphyrinato)zinc(II) complexes with aminopyridines as axial ligands", *Eur. J. Inorg. Chem.* **2009**, 727-734.

19. Gilday, L. C.; White, N. G.; Beer, P. D., "Halogen- and hydrogen-bonding triazole-functionalised porphyrin-based receptors for anion recognition", *Dalton Trans*. **2013**, *42*, 15766-15773.

20. Panthi, K.; Adhikari, R. M.; Kinstle, T. H., "Aromatic fumaronitrile core-based donor-linker-acceptor-linker-donor (D-π-A-π-D) compounds: Synthesis and photophysical properties", *J. Phys. Chem. A* **2010**, *114*, 4542-4549.

21. Lakowicz, J. R., "Principles of Fluorescence Spectroscopy", Springer, New York, **2006**, pp 208-213.

22. Wang, F.; Wang, L.; Chen, X.; Yoon, J., "Recent progress in the development of fluorometric and colorimetric chemosensors for detection of cyanide ions", *Chem. Soc. Rev.* **2014**, *43***,** 4312-4324.

23. Goswami, S.; Manna, A.; Paul, S.; Das, S. K.; Aich, K. l.; Nandi, P. K., "Resonance-assisted hydrogen bonding induced nucleophilic addition to hamper ESIPT: ratiometric detection of cyanide in aqueous media", *Chem. Commun.* **2013**, *49*, 2912-2914.

24. Chaudhri, N.; Sankar, M., "Colorimetric "naked eye" detection of CN⁻, F⁻, CH_3COO^- and $H_2PO_4^-$ ions by highly nonplanar electron deficient perhaloporphyrins", *RSC Adv.* **2015**, *5*, 3269-3275.

25. Yadav, P.; Sankar, M., "Synthesis, spectroscopic and electrochemical studies of phosphoryl and carbomethoxyphenyl substituted corroles, and their anion detection properties", *Dalton Trans.* **2014**, *43*, 14680-14688.

CHAPTER 5

Simple Cost-Effective Trans-A$_2$BC-Porphyrins with Various Donor Groups for Dye-Sensitized Solar Cells

Energy level diagram of Trans-A$_2$BC Zn(II)porphyrins

R = Phenyl, *p*-bromophenyl, Thienyl, *p*-^{t}Bu-Phenyl, Pyrenyl

I-V Curves
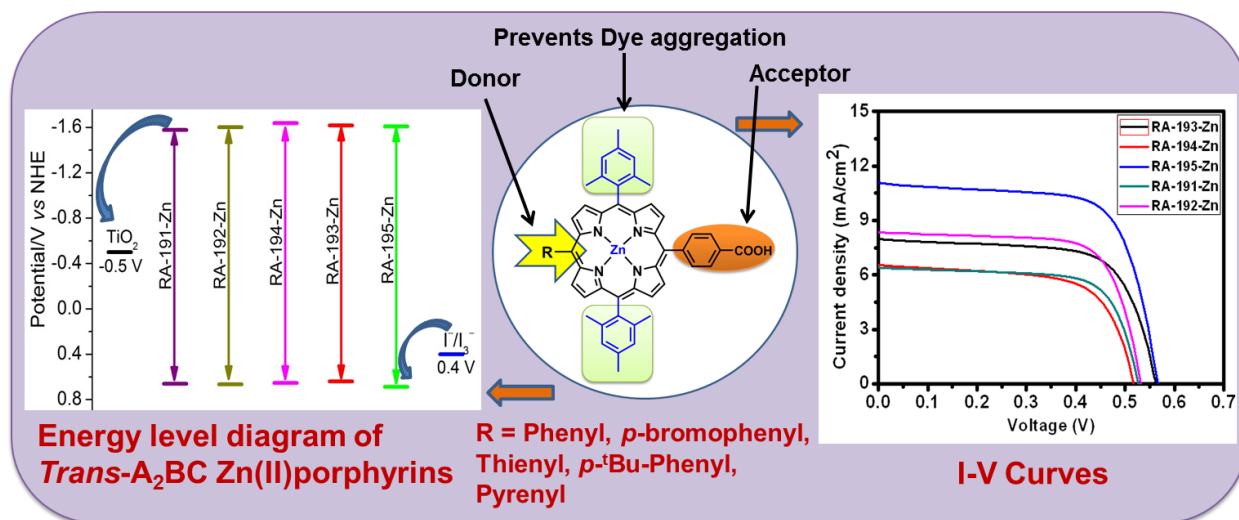
CHAPTER 5

SIMPLE COST-EFFECTIVE *TRANS*-A$_2$BC-PORPHYRINS WITH VARIOUS DONOR GROUPS FOR DYE-SENSITIZED SOLAR CELLS

5.1 INTRODUCTION

Development of a sustainable society and growing global energy consumption demand clean and renewable energy resources. Several environmental issues aroused by large consumption of fossil fuel. Artificial photosynthesis and photovoltaic technologies are desirable to harvest substantially inexhaustible solar energy. Dye-sensitized solar cells (DSSCs) [1-4], have proven their potentials as feasible energy device for solar energy conversion and are having following advantages such as low cost, easy production, flexibility, and transparency relative to traditional silicon solar cells. In this respect for the past two decades, polypyridyl ruthenium complexes [5] have been utilized to achieve electric power conversion efficiency (η) up to 11% due to their broad absorption spectrum through metal-to-ligand charge transfer (MLCT), the longer exciton lifetime, and their long-term chemical stability. Despite their overwhelming performance, Ru-polypyridyl sensitizers encounters several drawbacks such as the high cost of noble metal ruthenium, the requirement for careful synthesis, hefty purification steps, toxicity to environment and low molar extinction coefficients in the red region of visible spectrum hampers their large-scale applications. Organic dyes [6] such as coumarin, indoline, oligoene, thiophene, triarylamine, perylene, cyanine, fluorine, merocyanine and hemicyanine derivatives are of great interest owing to their modest cost, ease of synthesis and structural modification, large molar absorption coefficients, and satisfactory stability. Some organic dyes with the conversion efficiencies in a range of 5–9% have been prepared. However, porphyrins and phthalocyanines are best due to their high thermal and photochemical stability, strong absorption in visible region as well as their optical, photophysical and electrochemical properties can be tuned by peripheral substitutions [1-3,7]. The most efficient porphyrin sensitizer features push–pull D–π–A structures and/or π-extensions that made porphyrins panchromatic in visible and even near-infrared regions. Consequently, porphyrin sensitizers have exhibited power conversion efficiencies that are comparable to or even higher than those of well-established highly efficient

DSSCs based on ruthenium complexes. For example, remarkable power conversion efficiency (η) of 12.3%, was achieved by zinc porphyrin sensitizer (YD2-*o*-C8) co-sensitized with an organic dye (Y123) using a cobalt-based electrolyte which is superior to those based on Ru complexes [3]. Recently, a class of push–pull porphyrins with an electron-donating diarylamino group and an electron-withdrawing carboxyphenylethynyl anchoring group, GY50 and SM315 has revealed remarkable high efficiencies of 12% and 13% with cobalt electrolyte under standard one sun illumination [4]. However, synthesis of these bridged conjugated push–pull type porphyrin sensitizers involves multistep synthesis involving expensive metal (Pd)-catalyzed C–C and C–N coupling reactions under stringent reaction conditions leading to overall low yield of final product. All these aspects demand a simple and efficient synthetic methodology to address the practical future applications of porphyrin-based DSSCs. He and co-workers [8] reported a power conversion efficiency of 5.1% using a simple architecture having *trans*-mesityl groups and *meso*-acrylic acid substituted zinc porphyrin sensitizer.
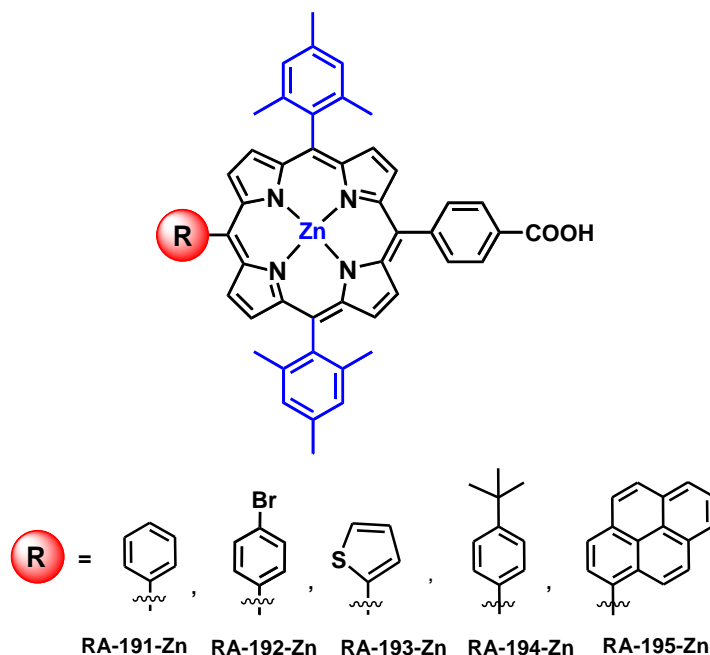
Chart 1. Molecular structures of synthesized porphyrin dyes.

However, synthesis of *meso*-bromo substituted porphyrin followed by Pd[0]-catalyzed Heck coupling to introduce the acrylic acid anchoring group involves multistep synthesis under inert and dry environment leading to high cost DSSCs. These findings prompted us to develop simple, efficient sensitizers involving fever synthetic steps. Herein, we report, five simple *trans-*

dimesityl A$_2$BC-Zn(II)porphyrins having different donor groups and carboxylic acid as the anchoring group. The benzene ring between the carboxylic acid and porphyrin ring serves as a spacer. To prevent dye aggregation alkyl and/or alkoxy groups have been introduced in *meso*-phenyl rings of porphyrinic sensitizers leading to high cell performance [3,4]. Recently, Zhang *et al* [9] reported *trans*-AB-porphyrin dyes with alkoxy chains at different positions of *meso*-phenyl ring to avoid dye aggregation. Bulky *trans*-*meso*-dimesityl groups were introduced to provide the oxidative stability to the porphyrins and to suppress the self-quenching by dye aggregation between the neighboring molecules adsorbed onto the TiO$_2$ surface by the steric hindrance around the porphyrin core. This leads to an increase of electron injection efficiency (ϕ_{inj}). It has been established that two mesityl groups lie parallel to TiO$_2$ surface thus widens the distance between two dye molecules as well as provides an effective shielding to electron recombination with the electrolyte.

To tackle these problems, herein, we designed A$_2$BC porphyrinic dyes with bulky *trans*-dimesityl groups. Further, different donor (phenyl, bromophenyl, *p-tert*-butylphenyl, thienyl and pyrenyl) groups and 4-carboxyphenyl moiety as acceptor were introduced to other *trans-meso*-positions of the porphyrin ring to establish proper push-pull design (D-π-A).The overall power conversion efficiencies (η) of DSSCs based on these dyes are in the range of 2.2 to 4.3% and highly dependent upon their donor moiety. Among all, pyrenyl appended Zn(II) porphyrin has exhibited higher power conversion efficiencies of 4.3% under 1 sun illumination which is attributed to extended π-conjugation of pyrene [11,12] with porphyrin π-system. To the best our knowledge, facile two-step synthesis of *trans*-A$_2$BC porphyrin and their subsequent application to DSSCs have not been reported so far.

5.2 EXPERIMENTAL SECTION

5.2.1 Chemicals and Instrumentation

All chemicals obtained from Alfa Aesar and used as received. The solvents were purified by distillation. The spectroscopic characterization was carried out as described in chapter 2.

5.2.2 The fabrication of DSSCs

Fluorine-doped SnO$_2$ glass (TEC-15, 2.2 mm thickness, Solaronix) was used for transparent conducting electrodes. The substrate was first cleaned in an ultrasonic bath using a detergent

solution, acetone, and ethanol, respectively (each step was 20 min long). The FTO glass plates were immersed into a 40 mM aqueous TiCl$_4$ solution at 70 °C for 30 min and washed with water and ethanol. A screen-printed double layer film of interconnected TiO$_2$ particles were used as mesoporous negative electrode. A 7 μm thick film of 20-nm-sized TiO$_2$ particles was first printed on the fluorine-doped SnO$_2$ conducting glass electrode and further coated by a 5 μm thick second layer of 400-nm sized light scattering anatase particles.

The TiO$_2$-coated electrodes (active area 0.16 cm^2) were gradually heated under air flow at 325 °C for 5 min, at 375 °C for 5 min, at 450 °C for 15 min, and 500 °C for 15 min. After the sintering process, the TiO$_2$ film was treated with 40 mM TiCl$_4$ solution, then rinsed with water and ethanol. The electrodes were heated at 500 °C for 30 min and after cooling (80 °C) were immersed for 16 h into sensitizing baths containing EtOH / THF (volume ratio: 1/1) solutions of the porphyrin in 0.2 mM concentration and when required with 0.4 mM of 3a,7a-dihydroxy-5b-cholic acid (CDCA) (Solaronix, Switzerland) was added. After washing with THF and drying by air flow, electrolyte (AN-50, Solarnix, Switzerland) solution was introduced into the space between the photoanodes and Pt-sheet counter electrode.

5.2.3 Synthesis of 5-Mesityldipyrromethane:
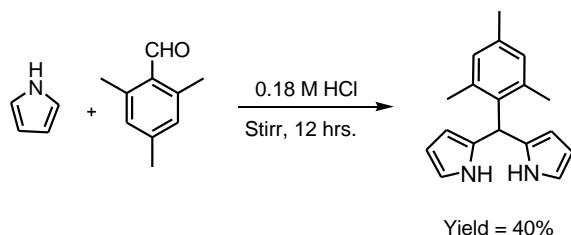
Scheme 1. Synthesis of 5-mesityl dipyrromethane.

5g of mesitaldehyde (0.034 mol) was taken in 300 mL of 0.18 M aqueous HCl. To this, 7 ml of pyrrole (0.101mol) was added. The reaction mixture was purged with argon and then stirred in dark for overnight at room temperature. At the end of this period, the reaction mixture was extracted with CHCl$_3$, washed with water and dried over anhydrous sodium sulphate. The product was purified by silica column using CHCl$_3$ as eluent. The yield was found to be 3 g, (0.013 mol) 40% (Scheme 1).

5.2.4 General procedure for the synthesis of 1:

5-Mesityldipyrromethane (3.78mmol), 4-formylbenzoate (1.89 mmol) and the corresponding aromatic aldehyde (1.89 mmol) were taken in a two-neck RB flask containing 800 ml of distilled CHCl$_3$. The reaction mixture was purged with argon for 20 minutes followed by addition of trifluoroacetic acid (2.26 mmol). The resulting reaction mixture was stirred in dark for 3 hours.
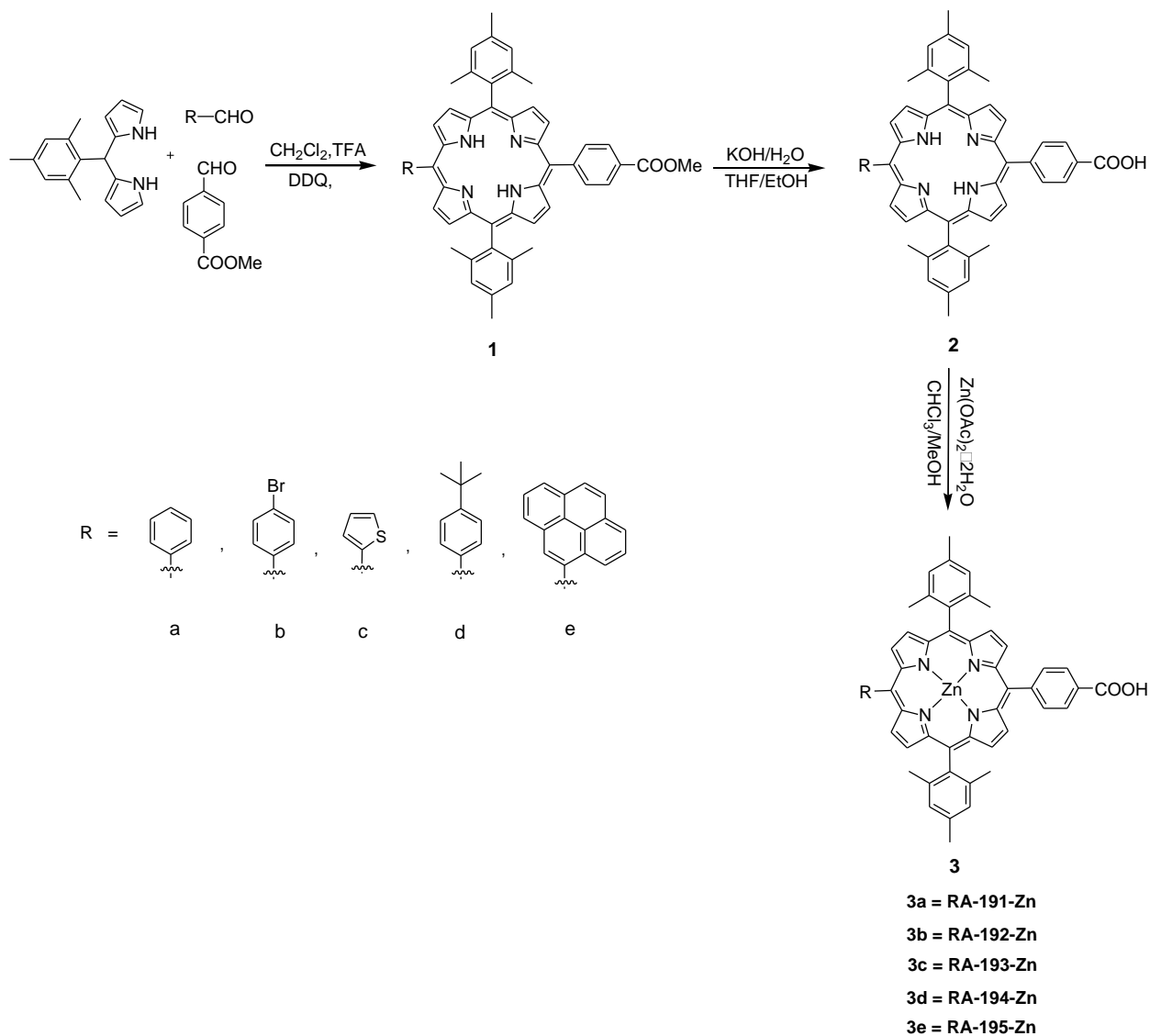
Scheme 2. Synthetic route for preparation of Zn-porphyrinic dyes *via* MacDonald [2+2] condensation.

At the end of this period DDQ (3.78 mmol) was added and allowed to stir for 1 hour. The reaction mixture was neutralized with triethylamine, concentrated to small volume and loaded on silica column, eluted using 1:1 hexane/chloroform mixture. The desired product was obtained as

second fraction (Scheme 2) which was further recrystallized from $CHCl_3$/CH_3OH mixture (1:3, v/v).The yield was found to be 10-12%.

5-(4'-carbomethoxyphenyl)-10,20-(dimesityl)-15-phenyl-porphyrin (1a): ^{1}H NMR in CDCl_3: δ (ppm) 8.80 (d, 2H, J = 4.5 Hz, β-pyrrole-H), 8.74 (d, 2H, J = 4.5 Hz, β-pyrrole-H), 8.70 (t, 4H,J = 4.5 Hz, β-pyrrole-H), 8.42 (d, 2H, J = 8.5 Hz, *meso-o*-carbomethoxyphenyl-H), 8.31 (d, 2H, J = 8.5 Hz, *meso-m*-carbomethoxyphenyl-H), 8.22 (dd, 2H, J = 8.5 Hz, *meso-o*-phenyl-H), 7.79-7.72 (m, 3H, ,*meso-m and p*-phenyl-H), 7.28 (s, 4H, *meso-m*-mesityl-H), 4.10 (s, 3H, OCH₃), 2.63 (s, 6H, *meso-p*-CH₃ mesityl-H), 1.84 (s, 12H, *meso-o*-CH₃ mesityl-H), -2.64 (s, 2H, N-H).

5-(4'-carbomethoxyphenyl)-10,20-(dimesityl)-15-(4'-bromophenyl)-porphyrin (1b): ^{1}H NMR in CDCl₃: δ (ppm) 8.78 (d, 2H, J = 4.5 Hz, β-pyrrole-H), 8.74 (d, 2H, J = 5 Hz, β-pyrrole-H), 8.71 (asym t, 4H, J = 4.5 Hz, β-pyrrole-H), 8.43 (d, 2H, J = 8.5 Hz, *meso-o*-carbomethoxyphenyl-H), 8.31 (d, 2H, J = 8.5 Hz, *meso-m*-carbomethoxyphenyl-H), 8.09 (d, 2H, J = 8.5 Hz, *meso-o*-bromophenyl-H), 7.88 (d, 2H, J = 8.5 Hz, *meso-m*-bromophenyl-H), 7.29 (s, 4H, *meso-m*-mesityl-H), 4.11 (s, 3H, OCH₃), 2.63 (s, 6H, *meso-p*-CH₃ mesityl-H), 1.83 (s, 12H, *meso-o*-CH₃ mesityl-H), -2.66 (s, 2H, N-H).

5-(4'-carbomethoxyphenyl)-10,20-(dimesityl)-15-(2'-thienyl)-porphyrin (1c): ^{1}H NMR in CDCl₃: δ (ppm) 9.01 (d, 2H, J = 4.5 Hz,β-pyrrole-H), 8.73 (d, 2H, J = 4.5 Hz, β-pyrrole-H), 8.72-8.67 (m, 4H, β-pyrrole-H), 8.42 (d, 2H, J = 7.5 Hz, *meso-o*-carbomethoxyphenyl-H), 8.31 (d, 2H, J = 8 Hz, *meso-m*-carbomethoxyphenyl-H), 7.91 (d, 1H, J = 3 Hz, *a*-thienyl-H), 7.82 (d, 1H, J = 5 Hz, γ-thienyl-H), 7.49 (t, 1H, J = 4 Hz, β-thienyl-H), 7.28 (s, 4H, *meso-m*-mesityl-H), 4.11 (s, 3H, OCH₃), 2.63 (s, 6H, *meso-p*-CH₃ mesityl-H), 1.84 (s, 12H, *meso-o*-CH₃ mesityl-H), -2.58 (s, 2H, N-H).

5-(4'-carbomethoxyphenyl)-10,20-(dimesityl)-15-(4'-ᵗbutylphenyl)-porphyrin (1d): ^{1}H NMR in CDCl₃: δ (ppm) 8.85 (d, 2H, J = 4.5 Hz, β-pyrrole-H), 8.72 (d, 2H, J = 4.5 Hz, β-pyrrole-H), 8.69 (t, 4H, J = 4 Hz, β-pyrrole-H), 8.42 (d, 2H, J = 8 Hz, *meso-o*-carbomethoxyphenyl-H), 8.31 (d, 2H,J = 8 Hz, *meso-m*-carbomethoxyphenyl-H), 8.14 (d, 2H,J = 8 Hz, *meso-o*-ᵗbutylphenyl-H), 7.75 (d, 2H, J = 8.5 Hz, *meso-m*-ᵗbutylphenyl-H), 7.28 (s, 4H, *meso-m*-mesityl-H), 4.10 (s, 3H, OCH₃), 2.63 (s, 6H, *meso-p*-CH₃ mesityl-H), 1.84 (s, 12H, *meso-o*-CH₃ mesityl-H), 1.60(s, 12H, CH₃-ᵗbutylphenyl-H), -2.62 (s, 2H, N-H).

5-(4'-carbomethoxyphenyl)-10,20-(dimesityl)-15-(2'-pyrenyl)-porphyrin (1e): ^{1}H NMR in CDCl₃: δ (ppm) 8.80 (d, 1H, J = 5 Hz, β-pyrrole-H), 8.77 (d, 2H, J = 5 Hz, β-pyrrole-H), 8.73 (d, 2H, J = 5 Hz,β-pyrrole-H), 8.59 (d, 2H, J = 5 Hz, β-pyrrole-H), 8.51 (d, 1H, J = 6 Hz, β-pyrrole-H), 8.47-8.43 (m, 4H, *meso-o-*and *m*-carbomethoxyphenyl-H), 8.40 (d, 1H, J = 9 Hz, pyrenyl- H), 8.37-8.30 (m, 4H, pyrenyl- H), 8.15-8.05 (m, 2H, pyrenyl- H), 7.72 (d, 1H, J = 9 Hz, pyrenyl-H), 7.51 (d, 1H, J = 9.5 Hz, pyrenyl- H), 7.26 (s, 4H, *meso-m*-mesityl-H), 4.12 (s, 3H, OCH₃), 2.60 (s, 6H, *meso-p*-CH₃ mesityl-H), 1.89 (s, 6H, *meso-o*-CH₃ mesityl-H), 1.84 (s, 6H, *meso-o*-CH₃mesityl-H), -2.42 (s, 2H, N-H).

5.2.5 General procedure for the synthesis of 2:

Monoester porphyrin (0.10 mmol) (**1a**-**1e**) was dissolved in 20 ml of THF. To this, KOH (10 mmol) in 0.5 ml water was added and heated at 80 °C for 24 h. At the end of this period, THF was removed under vacuum. The crude porphyrin was treated with 15 ml of 2N HCl affording green precipitate which was filtered and washed with excess of water thrice and dried. The product was purified by silica gel column chromatography using 3% methanol in chloroform as eluent. The yield of the product was found to be quantitative.

5-(4'-carboxyphenyl)-10,20-(dimesityl)-15-phenyl-porphyrin (2a): ^{1}H NMR in CDCl₃: δ (ppm) 8.81 (d, 2H, J = 4.5 Hz, β-pyrrole-H), 8.77 (d, 2H, J = 4.5 Hz, β-pyrrole-H), 8.73 (d, 2H, J = 4.5 Hz, β-pyrrole-H), 8.71 (d, 2H, J = 4.5 Hz, β-pyrrole-H), 8.54 (d, 2H, J = 8 Hz, *meso-o*-carbomethoxyphenyl-H), 8.38 (d, 2H, J = 8 Hz, *meso-m*-carbomethoxyphenyl-H), 8.23 (d, 2H, J = 7 Hz, *meso-o*-phenyl-H), 7.79-7.73 (m, 3H, *meso-m*- and *p*-phenyl-H), 7.30 (s, 4H, *meso-m*-mesityl-H), 2.64 (s, 6H, *meso-p*-CH₃ mesityl-H), 1.86 (s, 12H, *meso-o*-CH₃ mesityl-H), -2.61 (s, 2H, N-H). ESI-MS (m/z): found 743.33 [M+H]⁺, calcd. 743.33

5-(4'-carboxyphenyl)-10,20-(dimesityl)-15-(4'-bromophenyl)-porphyrin (2b): ^{1}H NMR in CDCl₃: δ (ppm) 8.78 (t, 4H, J = 4 Hz, β-pyrrole-H), 8.73 (t, 4H, J = 4 Hz, β-pyrrole-H), 8.54 (d, 2H, J = 8 Hz, *meso-o*-carbomethoxyphenyl-H), 8.38 (d, 2H, J = 8 Hz, *meso-m*-carbomethoxyphenyl-H), 8.10 (d, 2H, J = 8 Hz, *meso-o*-bromophenyl-H), 7.90 (d, 2H, J = 8 Hz, *meso-m*-bromophenyl-H), 7.30 (s, 4H, *meso-m*-mesityl-H), 2.64 (s, 6H, *meso-p*-CH₃ mesityl-H), 1.85 (s, 12H, *meso-o*-CH₃mesityl-H), -2.64 (s, 2H, N-H). ESI-MS (m/z): found 823.23 [M+H]⁺, calcd. 823.23.

5-(4'-carboxyphenyl)-10,20-(dimesityl)-15-(2'-thienyl)-porphyrin (2c): ^{1}H NMR in CDCl$_3$: δ (ppm) 9.03 (d, 2H,*J* = 4.5 Hz,*β*-pyrrole-H), 8.77 (d, 2H, *J* = 4.5 Hz, *β*-pyrrole-H), 8.72 (d, 4H, *J*= 4.5 Hz, *β*-pyrrole-H), 8.55 (d, 2H, *J* = 8 Hz, *meso-o*-carbomethoxyphenyl-H), 8.38 (d, 2H, *J* = 8 Hz, *meso-m*-carbomethoxyphenyl-H), 7.93 (d, 1H, *J* = 8 Hz*, a*-thienyl-H), 7.85 (d, 1H, *J* = 5 Hz, *γ*-thienyl-H), 7.50 (t, 1H, *β*-thienyl-H), 7.30 (s, 4H, *meso-m*-mesityl-H), 2.65 (s, 6H, *meso-p*-CH$_3$ mesityl-H), 1.86 (s, 12H, *meso-o*-CH$_3$ mesityl-H), -2.55 (s, 2H, N-H). ESI-MS (m/z): found 749.28 [M+H]$^+$, calcd. 749.29

5-(4'-carboxyphenyl)-10,20-(dimesityl)-15-(4'-ᵗbutylphenyl)-porphyrin (2d): ^{1}H NMR in CDCl$_3$: δ (ppm) 8.86 (d, 2H, *J* = 4 Hz*, β*-pyrrole-H), 8.75 (d, 2H,*J* = 4 Hz, *β*-pyrrole-H), 8.71 (asym t, 4H, *β*-pyrrole-H), 8.49 (d, 2H, *J* = 8 Hz, *meso-o*-carbomethoxyphenyl-H), 8.36 (d, 2H, *J* = 8 Hz, *meso-m*-carbomethoxyphenyl-H), 8.14 (d, 2H, *J* = 8 Hz, *meso-o*-ᵗbutylphenyl-H), 7.75 (d, 2H,*J* = 8 Hz, *meso-m*-ᵗbutylphenyl-H), 7.29 (s, 4H, *meso-m*-mesityl-H), 2.63 (s, 6H, *meso-p*-CH$_3$ mesityl-H), 1.84 (s, 12H, *meso-o*-CH$_3$ mesityl-H), 1.61(s, 9H, CH$_3$-ᵗbutylphenyl-H), -2.62 (s, 2H, N-H). ESI-MS (m/z): found 799.38 [M+H]$^+$, calcd. 799.39.

5-(4'-carboxyphenyl)-10,20-(dimesityl)-15-(2'-pyrenyl)-porphyrin (2e): ^{1}H NMR in CDCl$_3$: δ (ppm) 8.81 (s, 1H, *β*-pyrrole-H), 8.78 (d, 2H, *J* = 4.5 Hz, *β*-pyrrole-H), 8.74 (d, 2H, *J* = 4 Hz, *β*-pyrrole-H), 8.59 (d, 2H, *J* = 4.5 Hz, *β*-pyrrole-H), 8.51 (s, 1H, *β*-pyrrole-H), 8.50 (d, 2H, *J* = 8 Hz,*meso-o*-carbomethoxyphenyl-H), 8.45 (d, 2H, *J* = 8 Hz,*meso-m*-carbomethoxyphenyl-H), 8.41-8.38 (m, 2H, pyrenyl- H), 8.37-8.30 (m, 3H, pyrenyl- H), 8.13-8.03 (m, 2H, pyrenyl- H), 7.73 (d, 1H, *J* = 8 Hz,pyrenyl- H), 7.51 (d, 1H, *J* = 8 Hz,pyrenyl- H), 7.26 (s, 4H, *meso-m*-mesityl-H), 2.60 (s, 6H, *meso-p*-CH$_3$ mesityl-H), 1.89 (s, 6H, *meso-o*-CH$_3$ mesityl-H), 1.84 (s, 6H, *meso-o*-CH$_3$ mesityl-H), -2.44 (s, 2H, N-H). ESI-MS (m/z): found 867.35 [M]$^+$, calcd. 867.37

5.2.6 General procedure for the synthesis of 3:

2a-2e (0.066 mmol) was dissolved in 15 mL CHCl$_3$. To this, 10 equivalent of Zn(OAc)•2H$_2$O (0.66 mmol) in methanol was added and refluxed on water bath for 30 minutes. At the end of this period, the reaction mixture was cooled to room temperature and the solvent was removed by rotary evaporation. The residue was dissolved in CHCl$_3$, washed with water, dried over anhydrous sodium sulphate. The crude product was purified by column chromatography on silica

column using CHCl$_3$ as eluent. The product was recrystallized from CHCl$_3$/CH$_3$OH mixture (1:3, v/v) to give a purple solid 92-95%.

Zn(II)-5-(4'-carboxyphenyl)-10,20-(dimesityl)-15-phenyl-porphyrin (RA-191-Zn): ^{1}H NMR in CDCl$_3$: δ (ppm) 8.89 (s, 2H, β-pyrrole-H), 8.84 (s, 2H, β-pyrrole-H), 8.77 (t, 4H, J = 4 Hz, β-pyrrole-H), 8.50 (d, 2H, J = 7.5 Hz, *meso-o*-carbomethoxyphenyl-H), 8.38 (d, 2H, J = 7.5 Hz, *meso-m*-carbomethoxyphenyl-H), 8.24 (d, 2H, J = 6.5 Hz, *meso-o*-phenyl-H), 7.80-7.72 (m, 3H, ,*meso-m-* and *p*-phenyl-H), 7.29 (s, 4H, *meso-m*-mesityl-H), 2.64 (s, 6H, *meso-p*-CH$_3$ mesityl-H), 1.84 (s, 12H, *meso-o*-CH$_3$ mesityl-H). ESI-MS (m/z): found 803.53 [M-H]$^+$, calcd. 804.24

Zn(II)-5-(4'-carboxyphenyl)-10,20-(dimesityl)-15-(4'-bromophenyl)-porphyrin (RA-192-Zn): ^{1}H NMR in CDCl$_3$: δ (ppm) 8.86 (d, 4H, J = 4.5 Hz, β-pyrrole-H), 8.82 (s, 4H, β-pyrrole-H), 8.51 (d, 2H, J = 7.5 Hz, *meso-o*-carbomethoxyphenyl-H), 8.38 (d, 2H, J = 8 Hz, *meso-m*-carbomethoxyphenyl-H), 8.12 (d, 2H, J = 7.5 Hz, *meso-o*-bromophenyl-H), 7.89 (d, 2H, J = 7.5 Hz, *meso-m*-bromophenyl-H), 7.29 (s, 4H, *meso-m*-mesityl-H), 2.64 (s, 6H, *meso-p*-CH$_3$ mesityl-H), 1.84 (s, 12H, *meso-o*-CH$_3$ mesityl-H). ESI-MS (m/z): found 884.14 [M]$^+$, calcd. 884.15.

Zn(II)-5-(4'-carboxyphenyl)-10,20-(dimesityl)-15-(2'-thienyl)-porphyrin (RA-193-Zn): ^{1}H NMR in CDCl$_3$: δ (ppm) 9.10 (d, 2H,J = 4 Hz,β-pyrrole-H), 8.84 (d, 2H, J = 3.5 Hz, β-pyrrole-H), 8.79 (d, 4H, J = 3.5 Hz, β-pyrrole-H), 8.50 (d, 2H, J = 7.5 Hz, *meso-o*-carbomethoxyphenyl-H), 8.37 (d, 2H, J = 7.5 Hz, *meso-m*-carbomethoxyphenyl-H), 7.93 (s, 1H, *a*-thienyl-H), 7.83 (d, 1H, J = 5.5 Hz, γ-thienyl-H), 7.5 (s, 1H, β-thienyl-H), 7.29 (s, 4H, *meso-m*-mesityl-H), 2.64 (s, 6H, *meso-p*-CH$_3$ mesityl-H), 1.84 (s, 12H, *meso-o*-CH$_3$ mesityl-H). ESI-MS (m/z): found 810.19 [M]$^+$, calcd. 810.20.

Zn(II)-5-(4'-carboxyphenyl)-10,20-(dimesityl)-15-(4'-^{t}butylphenyl)-porphyrin (RA-194-Zn): ^{1}H NMR in CDCl$_3$: δ (ppm) 8.94 (d, 2H, J = 4 Hz*, β-pyrrole-H), 8.83 (d, 2H,J = 4 Hz, β-pyrrole-H), 8.78 (t, 4H, J = 4 Hz, β-pyrrole-H), 8.48 (d, 2H, J = 8 Hz, *meso-o*-carbomethoxyphenyl-H), 8.37 (d, 2H, J = 8 Hz, *meso-m*-carbomethoxyphenyl-H), 8.16 (d, 2H, J = 8 Hz, *meso-o*-^{t}butylphenyl-H), 7.75 (d, 2H,J = 8 Hz, *meso-m*-^{t}butylphenyl-H), 7.29 (s, 4H, *meso-m*-mesityl-H), 2.64 (s, 6H, *meso-p*-CH$_3$ mesityl-H), 1.83 (s, 12H, *meso-o*-CH$_3$ mesityl-H), 1.61(s, 9H, CH$_3$-^{t}butylphenyl-H). ESI-MS (m/z): found 862.30 [M+H]$^+$, calcd. 862.30.

Zn(II)-5-(4'-carboxyphenyl)-10,20-(dimesityl)-15-(2'-pyrenyl)-porphyrin (RA-195-Zn): ^{1}H NMR in CDCl$_3$: δ (ppm) 8.88 (bs, 2H, *β*-pyrrole-H), 8.84-8.78 (m, 3H, *β*-pyrrole-H), 8.66 (d, 2H, *J* = 3.5 Hz, *β*-pyrrole-H), 8.51 (d, 1H, *J* = 4.5 Hz, *β*-pyrrole-H), 8.50-8.45 (m, 4H, *meso-o-* and *m*-carbomethoxyphenyl-H), 8.41 (d, 1H pyrenyl- H), 8.38-8.29 (m, 4H, pyrenyl- H), 8.15-8.05 (m, 2H, pyrenyl- H), 7.71 (d, 1H, *J* = 8.5 Hz,pyrenyl- H), 7.53 (d, 1H, *J* = 8.5 Hz,pyrenyl- H), 7.26 (s, 4H, *meso-m*-mesityl-H), 2.60 (s, 6H, *meso-p*-CH$_3$ mesityl-H), 1.89 (s, 6H, *meso-o*-CH$_3$ mesityl-H), 1.82 (s, 6H, *meso-o*-CH$_3$ mesityl-H). ESI-MS (m/z): found 930.28 [M+H]$^+$, calcd. 930.29.

5.3 RESULT AND DISCUSSION

5.3.1 Synthesis and characterisation

Trans-A$_2$BC-esterporphyrins (**1a**-**1e**) were synthesized *via* MacDonald [2+2] condensation between 5-mesityldipyrromethane and two different types of aromatic aldehydes viz. aryl aldehyde having different donor groups (R-CHO) and 4-carbomethoxybenzaldehyde. Ester porphyrins (**1a**-**1e**) were further subjected to base hydrolysis to afford carboxyporphyrins (**2a**-**2e**) (Scheme 1) in quantitative yield. Subsequent metallation using Zn(OAc)$_2$•2H$_2$O yields the target porphyrinic dyes **RA-191-Zn**, **RA-192-Zn**, **RA-193-Zn**, **RA-194-Zn** and **RA-195-Zn** in 90-92% yield. Detailed synthetic procedures are given in the experimental section. All the intermediates and final Zn porphyrin dyes were characterized by UV-Vis, ^{1}H NMR spectroscopic techniques and HRMS spectrometry. Further structural, electronic, photophysical properties and computational studies of these dyes were investigated by electronic absorption and fluorescence spectroscopic techniques, density functional theory (DFT), cyclic voltammetry and photocurrent–voltage measurements.

5.3.2 Optical Absorption and Emission Spectral Properties

The UV-Vis spectra of the synthesized zinc porphyrin dyes were recorded in distilled CH$_2$Cl$_2$ at 298 K and the absorption data is listed in Table 1. Representative absorption spectra of dyes **RA-191-Zn** and **RA-195-Zn** are shown in Figure 1. All these synthesized dyes exhibited an intense Soret band in the range 400−450 nm and moderate absorbing two Q bands in the range 525−625nm, which are attributed to the π−π* electronic transitions. Dyes containing thienyl and

133
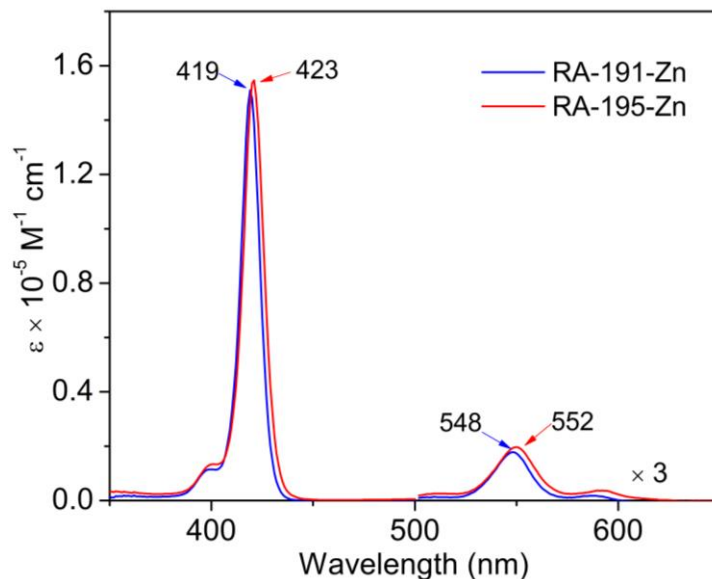
Figure 1. Electronic absorption spectra of dyes **RA-191-Zn** and **RA-195-Zn** in CH$_2$Cl$_2$ at 298 K.

pyrenyl as donor groups (**RA-Zn-193** and **RA-Zn-195**) showed marginal red shift (3-4 nm) in Soret and Q bands than those of **RA-191-Zn, RA-192-Zn** and **RA-194-Zn**. When these zinc porphyrin dyes were adsorbed onto the TiO$_2$ nanoparticle films, the absorption spectra became broader and shifted toward longer wavelengths, which may be ascribed to the electronic coupling between porphyrin dyes and the TiO$_2$ semiconductor.
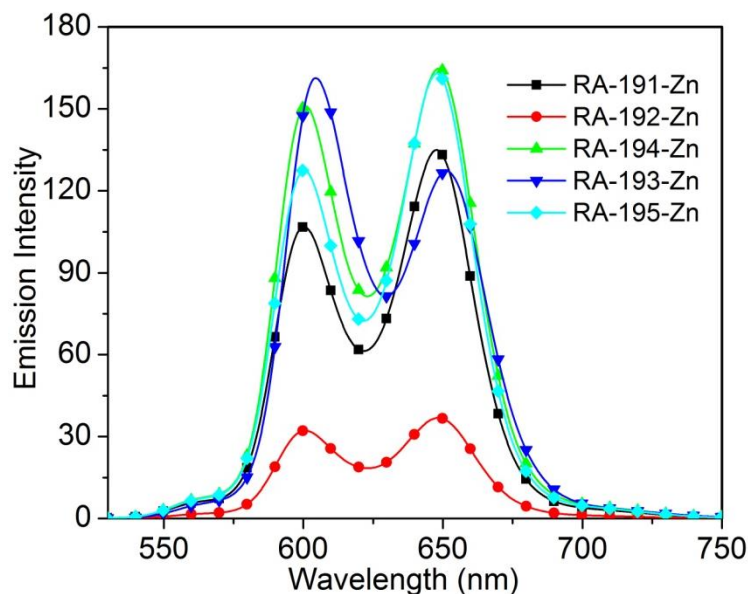
Figure 2. Fluorescence spectra of zinc porphyrin dyes in CH$_2$Cl$_2$ at 298 K.

Table 1. Optical absorption and emission spectral data of synthesized dyes in CH$_2$Cl$_2$ at 298 K. Values in parentheses refer to log ε (ε in Mol^{-1} cm^{-1}).

Porphyrin	B band(s), nm	Q band(s), nm	Emission	Φ_f^b
RA-191-Zn	419(5.17)	548(4.77), 587(4.00)	600, 648	0.037
RA-192-Zn	420(5.24)	549(4.86), 588(4.04)	600, 648	0.019
RA-194-Zn	420(5.23)	549(4.85), 588(4.03)	600, 648	0.031
RA-193-Zn	421(5.18)	550(4.80), 592(4.04)	604, 652	0.041
RA-195-Zn	423(5.17)	552(4.76), 593(4.01)	601, 649	0.041

The synthesized dyes were also characterized by fluorescence spectroscopy to elucidate the role of different donor groups. Figure 2 represents the steady state emission spectra of zinc porphyrin dyes in CH$_2$Cl$_2$ at 298 K and the emission data is listed in Table 1. No significant shifts in emission bands were observed for these dyes except **RA-193-Zn** which exhibited a red shift of 4 nm in emission bands as compared to **RA-191-Zn**. However, fluorescence quenching was observed for **RA-192-Zn** which leads to the decrement in the quantum yield. This fluorescence quenching is ascribed to the heavy atom effect of bromo group.

5.3.3 Cyclic Voltammetric Studies

The electrochemical properties of these porphyrinic dyes were investigated by cyclic voltammetry in CH$_2$Cl$_2$ containing 0.1 M TBAPF$_6$ with a scan rate of 0.1 V/s at 298 K as shown in Figure 3 and the data is listed in Table 2. The reduction potentials of these Zn(II) dyes are 20-80 mV cathodically shifted indicating the influence of electron donor moieties as compared to ZnTPP whereas oxidation potentials are anodically shifted (10-40 mV). Among all, *tert*-butyl and pyrenyl appended porphyrins showed larger cathodic shift 50-80 mV in their reduction potentials indicating their effective donor ability. Among all, pyrenyl appended porphyrin (**RA-195-Zn**) showed 40 mV cathodic shift (marginal effect) indicating the possibility of extended conjugation from pyrenyl moiety to porphyrin π-system [10,11]. Figure 4 depicts the HOMO-LUMO energy levels of Zn porphyrin dyes and compared with conduction band of TiO$_2$ and electrolyte which clearly indicate that the feasibility of electron transfer (down-hill process).
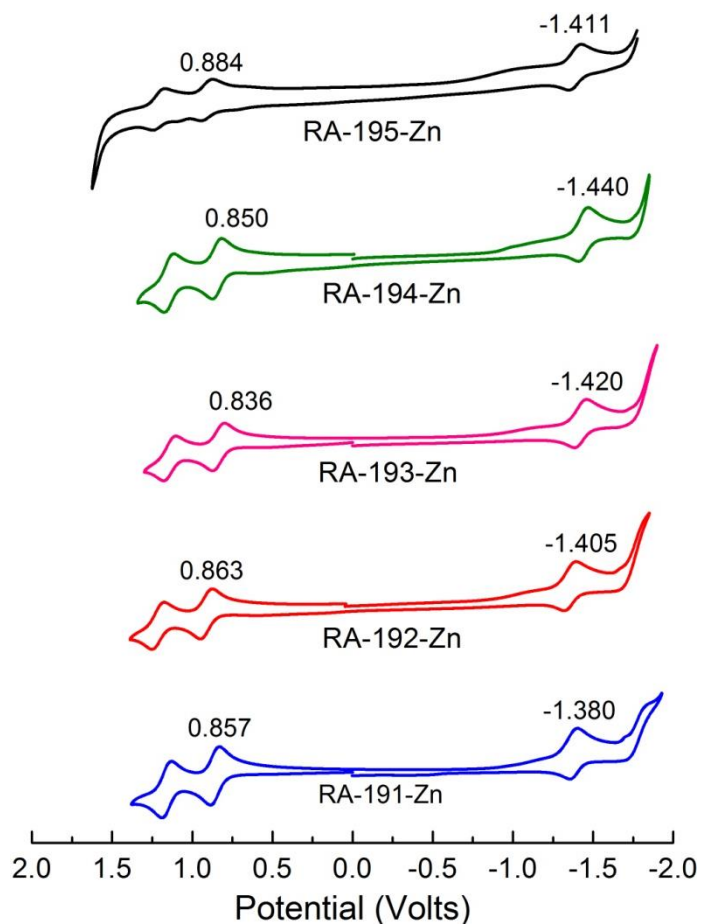
Figure 3. Cyclic voltammograms of zinc porphyrin dyes (~ 1 mM) in CH$_2$Cl$_2$ containing 0.1 M TBAPF$_6$ using Ag/AgCl as reference electrode with a scan rate of 0.10 V/s at 298 K.

Table 2. Electrochemical redox potentials (in V vs Ag/AgCl) of zinc porphyrin dyes in CH$_2$Cl$_2$ containing 0.1 M TBAPF$_6$ with a scan rate of 0.1 V/s at 298 K.

Porphyrin	Oxidation (V)		Reduction (V)		ΔE(V)
	I	II	I	II	
RA-191-Zn	0.857	1.157	-1.380	-1.775	2.237
RA-192-Zn	0.863	1.163	-1.405	-	2.268
RA-194-Zn	0.850	1.148	-1.440	-	2.287
RA-193-Zn	0.836	1.141	-1.420	-	2.256
RA-195-Zn	0.884	1.183	-1.411	-	2.295
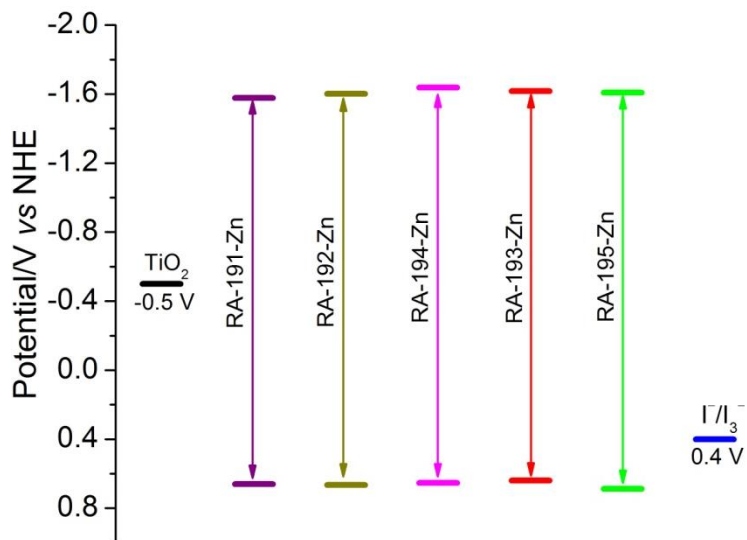
Figure 4. Energy level diagram of dyes and compared with nanocrystalline TiO$_2$ and iodide/triiodide electrolyte.

5.3.4 Photovoltaic studies

Dye-sensitized solar cells (DSSCs) were prepared using *trans*-A$_2$BC porphyrin-dyed 18 μm thick titanium dioxide photoanodes (0.16 cm^2) assembled into standard sealed sandwiched cells with a platinum counter electrode and vacuum back filled iodide/triiodide electrolyte. Figure 5 shows the typical I-V characteristics of the dye-sensitized solar cells using various porphyrin dyes using iodide/triiodide electrolyte. Figure 5 represents the typical I-V characteristics of the DSSCs using various Zn(II) porphyrin dyes. Table 3 lists the photovoltaic parameters of Zn dyes under AM 1.5 sun illumination (power 100 mW cm^{-2}) with an active area of 0.16 cm^2. We have obtained the photon-to-current efficiency (PCE) in the range of 2.2 to 4.2%. Among all, the best performance of was obtained with **RA-195-Zn** after soaking for 20 hours. **RA-195-Zn** exhibited V$_{oc}$, J$_{sc}$ and fill factor values of 550 mV, 11.0 mA/cm^2 and 0.70, respectively with the PCE value of (η) 4.23% at AM1.5G full sunlight illumination. Similar open circuit voltage (V$_{oc}$) was observed for these dyes, as expected since they have similar electronic configuration whereas much higher short circuit current density (J$_{sc}$) was observed for **RA-195-Zn** due to extended π-conjugation between pyrene and porphyrin [10,11].
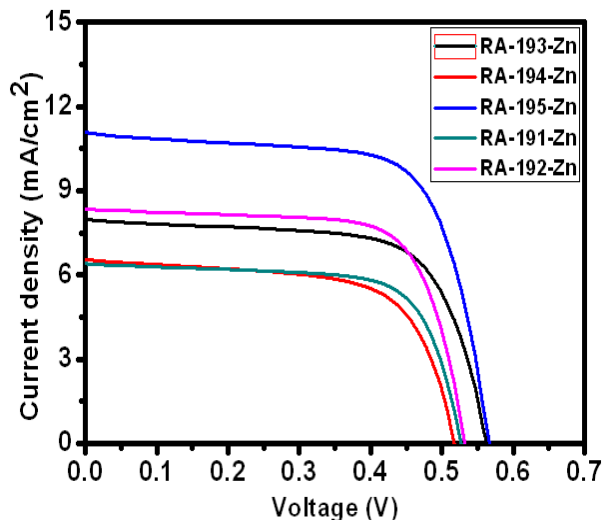
Figure 5. The typical I-V characteristics of the DSSCs using various Zn(II) porphyrin dyes.

Table 3. Photovoltaic parameters of Zn porphyrins under AM 1.5G sun illumination (power 100 mW cm^{-2}) with an active area of 0.16 cm^2.

Zn-Porphyrin	V_{oc} (V)	J_{sc} (mA/cm^2)	FF (%)	η (%)
RA-193-Zn	0.56	8.0	70	3.13
RA-194-Zn	0.52	6.5	65	2.19
RA-195-Zn	0.55	11.0	70	4.23
RA-191-Zn	0.53	5.7	70	2.11
RA-192-Zn	0.53	8.3	70	3.07

The PCE values for these dyes are highly dependent on donor groups and aligns the following order: RA-195-Zn (pyrenyl) > RA-193-Zn (2-thienyl) > RA-192-Zn (*p*-Br-phenyl) > RA-194-Zn (*p*-^{t}Bu-phenyl) > RA-191-Zn (phenyl).

This trend clearly indicates the effect of donor moiety on the efficiency of the device. Further, we are trying to probe for possibility of enhanced charge separation and broad absorption of pyrenyl dye (**RA-195-Zn**) on TiO$_2$ surface.

5.3.5 DFT Studies

We have optimized the geometries of synthesized Zn(II) porphyrin dyes using B3LYP functional and LanL2DZ basis set. All these porphyrin are exhibiting planar confirmation of the porphyrin core. The *mes*o-substituents (mesityl, different donor moieties and carboxyphenyl) are nearly

perpendicular to the porphyrin plane. Figures 5 and 6 depict the frontier molecular orbitals (FMOs) of synthesized Zn(II) porphyrin dyes having various donor moieties. In general, these porphyrins show typical TPP (having acceptor groups) type molecular orbitals a_{1u}, a_{2u} and e_g, i.e HOMO is a_{2u}, HOMO-1 is a_{1u}; LUMO and LUMO+1 are e_g orbitals (Figures 6 and 7). Further, LUMO+2 represents the acceptor carboxy phenyl moiety (Figures 6 and 7). This study clearly indicates that there could be the possibility of charge transfer from HOMO (porphyrin core) to LUMO+2 (carboxyphenyl moiety).
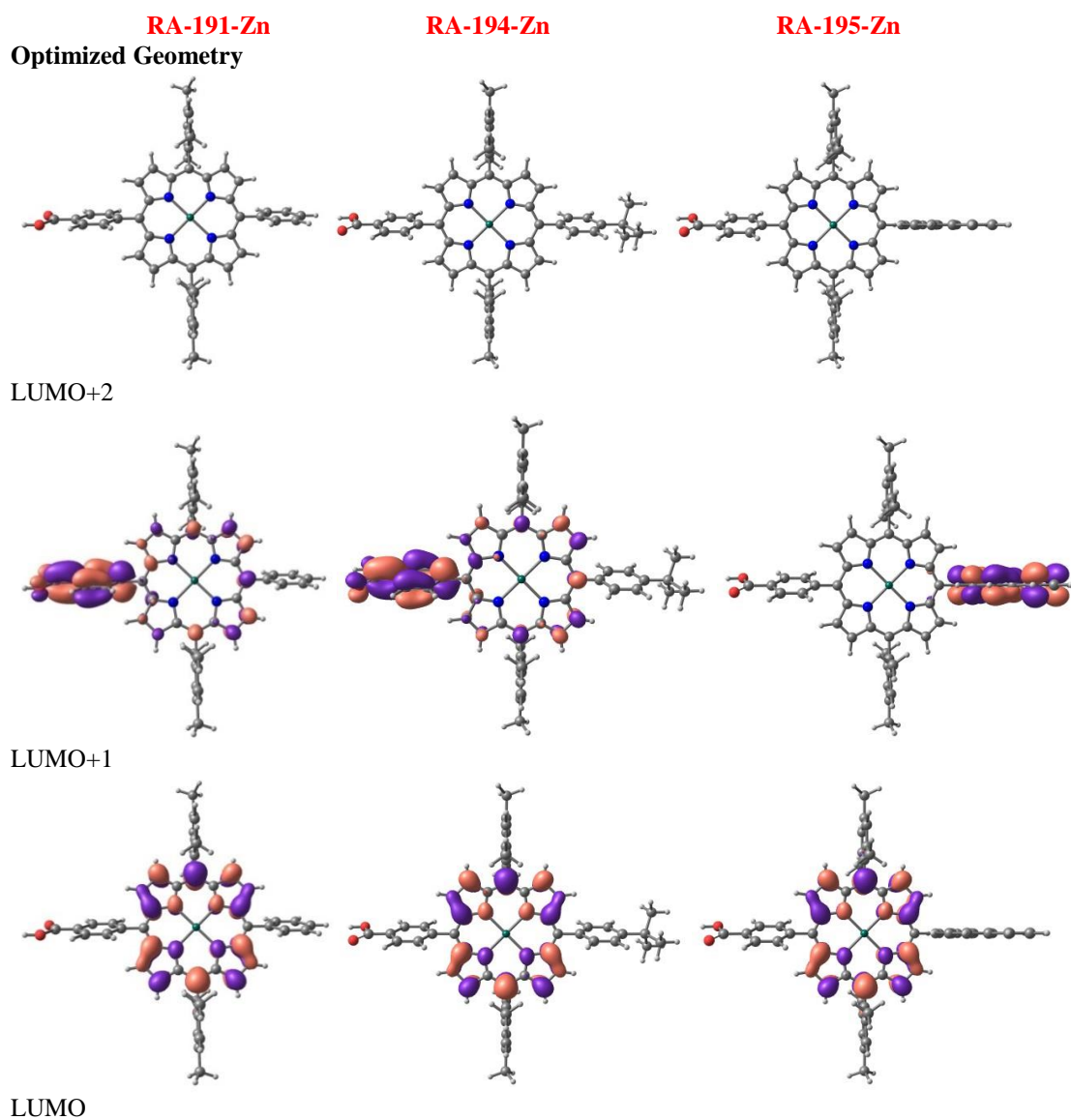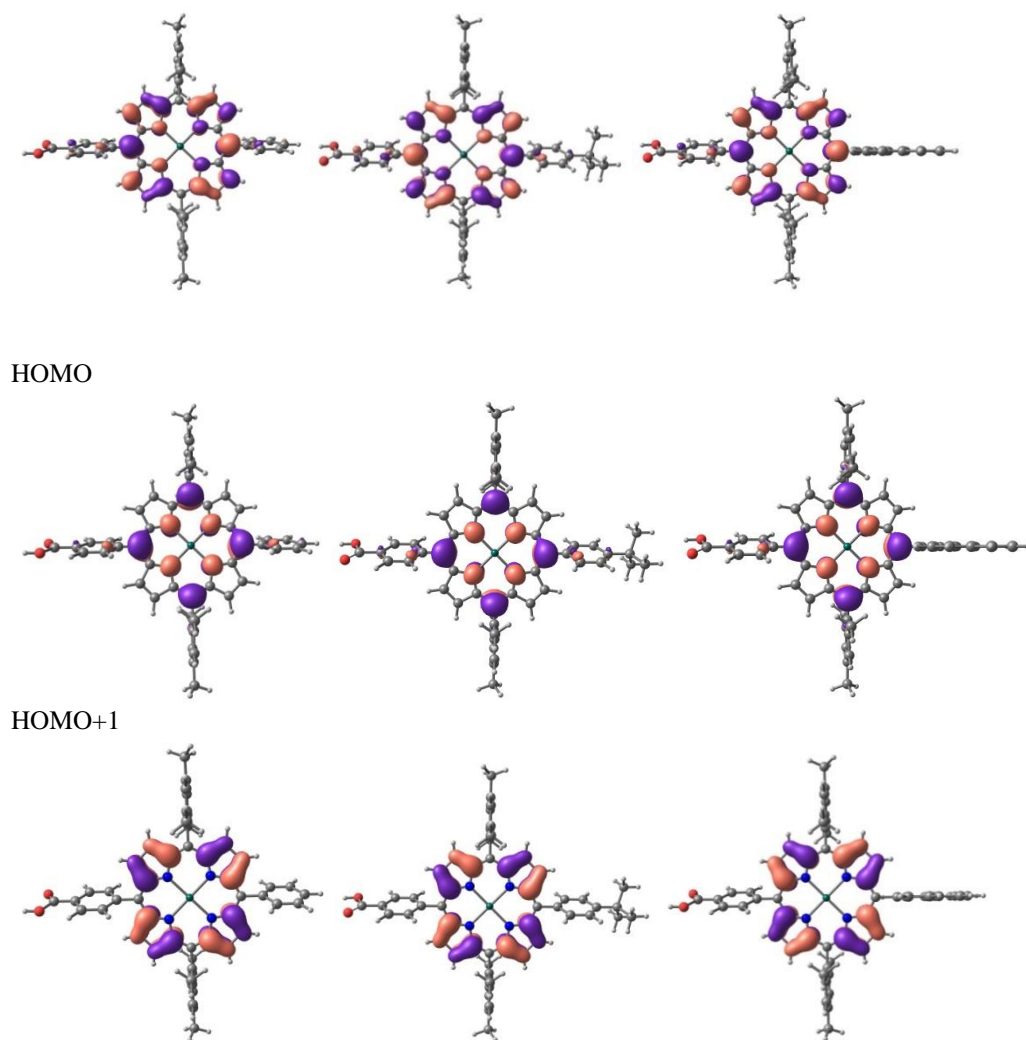
HOMO

HOMO+1

Figure 6. Frontier Molecular Orbitals (FMOs) of **RA-191-Zn, RA-194-Zn and RA-195-Zn** dyes with their optimized geometries using B3LYP/LANL2DZ basis set.

RA-192-Zn   **RA-193-Zn**

Optimized Geometry
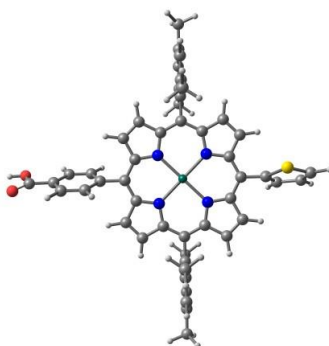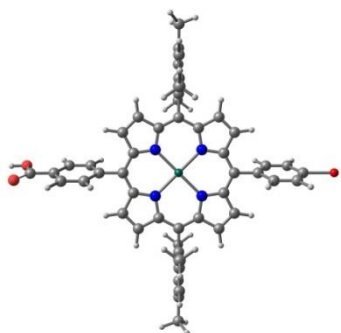
LUMO+2
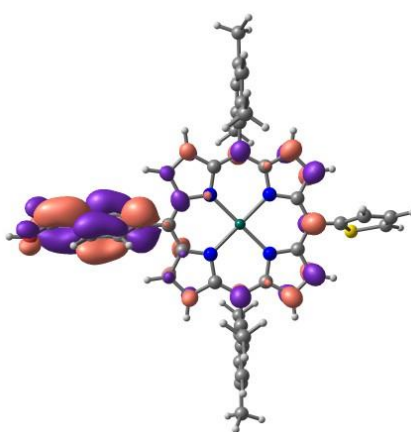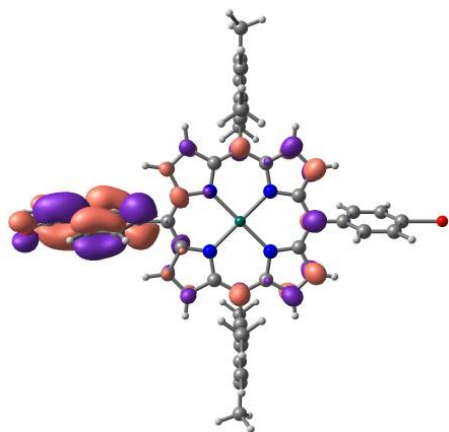
LUMO+1
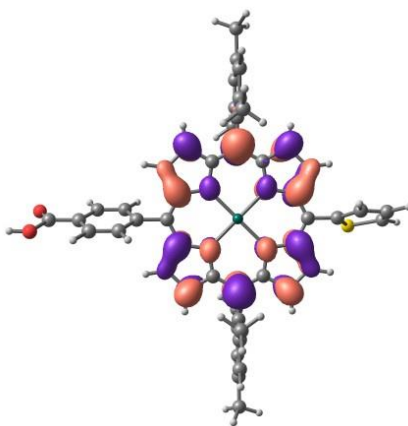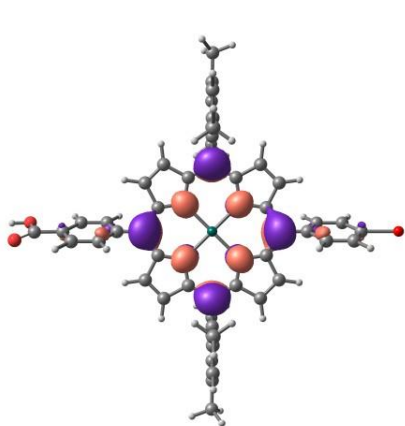
LUMO
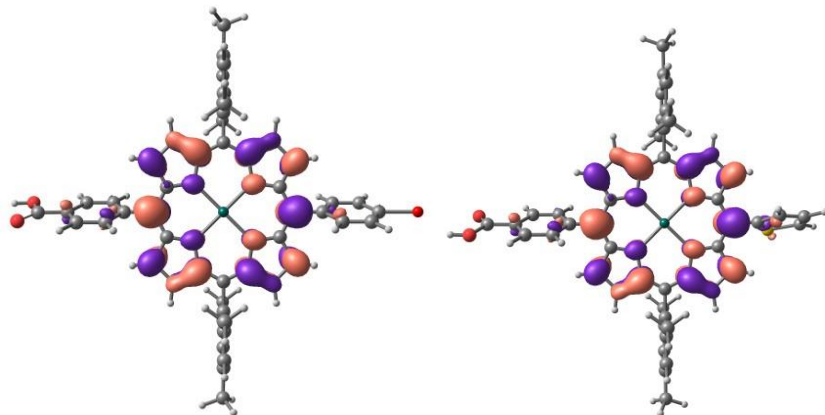
HOMO
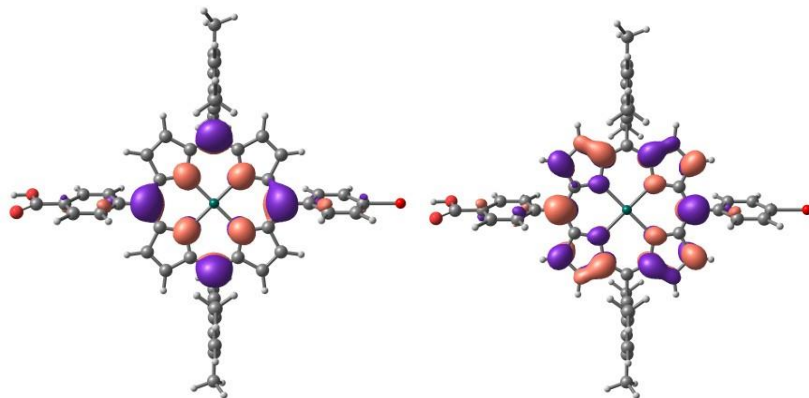
HOMO+1
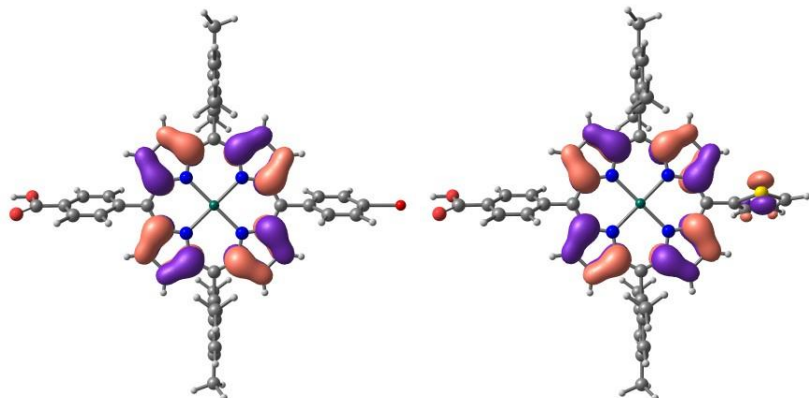
Figure 7. Frontier Molecular Orbitals (FMOs) of **RA-192-Zn** and **RA-193-Zn** dyes with their optimized geometries using B3LYP/LANL2DZ basis set.

5.4 Conclusions

We have designed and synthesized a new series of *trans*-A$_2$BC porphyrins having various donor groups in an elegant way in good yields. These porphyrins were characterized by UV-Visible, fluorescence and ^{1}H NMR spectroscopic techniques and mass spectrometry. CV studies revealed cathodic shift in reduction potentials as compared to ZnTPP indicating electron donation from R groups. These dyes exhibited the power conversion efficiency from 2.2 to 4.2% indicating highly dependent nature of electron donor moiety. Among all, pyrenyl appended porphyrin (**RA-195-Zn**) exhibited 4.2% power conversion efficiency possibly due to extended π-conjugation and enhanced charge-transfer interactions. The systematic studies to support extended π-conjugation and enhanced CT interactions are in progress.

5.5 References

1.   Higashino, T.; Imahori, H., "Porphyrins as excellent dyes for dye-sensitized solar cells: Recent developments and insights", *Dalton Trans*. **2015**, *44*, 448-463.

2.   Urbani, M.; Gratzel, M.; Nazeeruddin, M. K.; Torres, T., "*Meso*-substituted porphyrins for dye-sensitized solar cells", *Chem. Rev.* **2014**, *114*, 12330-12396.

3.   Yella, A.; Lee, H. W.; Tsao, H. N.; Yi, C.; Chandiran, A. K.; Nazeeruddin, M. K.; Diau, E. W.-G.; Yeh, C. Y.; Zakeeruddin, S. M.; Grätzel, M., "Porphyrin-sensitized solar cells with cobalt (II/III)-based redox electrolyte exceed 12 percent efficiency", *Science* **2011**, *334*, 629-634

4.   Mathew, S.; Yella, A.; Gao, P.; Humphry-Baker, R.; CurchodBasile, F. E.; Ashari-Astani, N.; Tavernelli, I.; Rothlisberger, U.; Nazeeruddin, M. K.; Grätzel, M., "Dye-sensitized solar cells with 13% efficiency achieved through the molecular engineering of porphyrin sensitizers", *Nat. Chem.* **2014**, *6*, 242-247.

5.   Wang, P.; Zakeeruddin, S. M.; Moser, J. E.; Nazeeruddin, M. K.; Sekiguchi, T.; Grätzel, M., "A stable quasi-solid-state dye-sensitized solar cell with an amphiphilic ruthenium sensitizer and polymer gel electrolyte", *Nat. Mater*. **2003**, *2*, 402-407.

6.   Lee, C.-P.; Lin, R. Y.-Y.; Lin, L.-Y.; Li, C.-T.; Chu, T.-C.; Sun, S.-S.; Lin, J. T.; Ho, K.-C., "Recent progress in organic sensitizers for dye sensitized solar cells", *RSC Adv.* **2015**, *5*, 23810-23825 and references therein.

7.   Subbaiyan, N. K.; D'Souza, F., "Light-to-electron converting panchromatic supramolecular solar cells of phthalocyanine-porphyrin heterodimers adsorbed onto nanocrystalline SnO_2 electrodes", *Chem. Commun.* **2012**, *48*, 3641-3643.

8.   He, H.; Gurung, A.; Si, L.; Sykes, A. G., "A simple acrylic acid functionalized zinc porphyrin for cost-effective dye-sensitized solar cells", *Chem. Commun.*, **2012**, *48*, 7619-7621.

9.   Zhang, N.-N.;Feng, Y.-Q.;. Li, Y.-C;Peng, X.Gu, C.-Z.;Xue, X.-D.; Yan, J.-Y.; Chen, Q.-L.; Li,X.-G.;Zhang, B., "Synthesis and characterization of simple trans-AB-porphyrins for dye-sensitized solar cells", *New J. Chem.,* **2013***, 37,* 1134-1141.

10.   Li, L.-L.; Diau, E. W.-G., "Porphyrin-sensitized solar cells", *Chem. Soc. Rev.* **2013**, *42*, 291-304.

11.   Lu, J.; Liu,S.; Li, H.; Shen, Y.; Xu, J.; Cheng, Y; Wang, M., "Pyrene-conjugated porphyrins for efficient mesoscopic solar cells: the role of spacer", *J. Mater. Chem. A*, **2014**, *2*, 17495-17501.

CHAPTER 6

Electron Deficient Nonplanar β-Octachlorovanadylporphyrin as Highly Efficient and Selective Epoxidation Catalyst for Olefins

Highly Nonplanar electron deficient β-Octachlorovanadylporphyrin catalyst

VOTPPCl$_8$ (1)

Olefins

0.002 mol% 1
2 equiv. H$_2$O$_2$
0.4 equiv. NaHCO$_3$
CH$_3$CN/H$_2$O
60 °C, 0.5 h

Epoxides

85 - 100% Conversion
100% Selectivity

<div align="center">
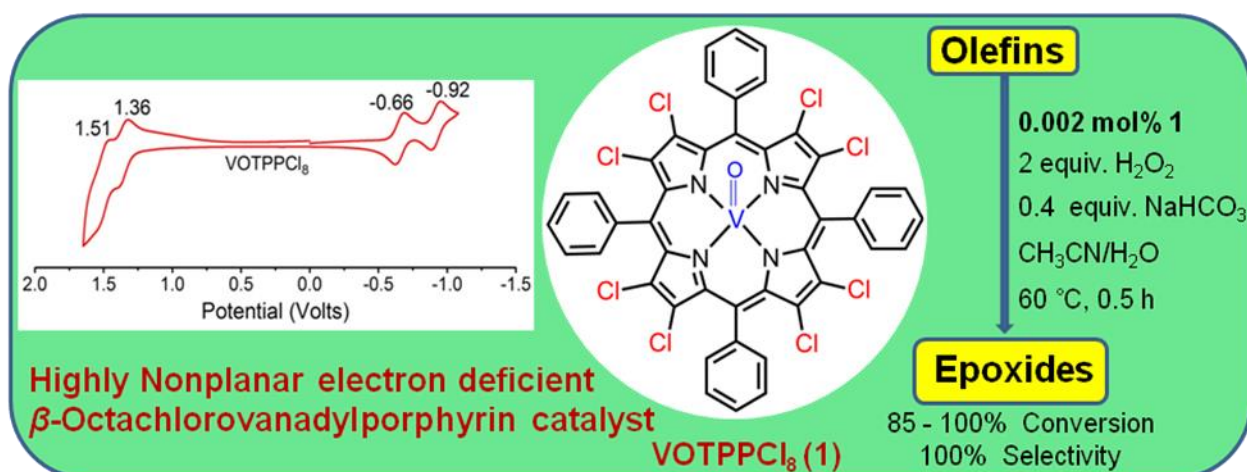
CHAPTER 6

ELECTRON DEFICIENT NONPLANAR β-OCTACHLOROVANADYLPORPHYRIN AS HIGHLY EFFICIENT AND SELECTIVE EPOXIDATION CATALYST FOR OLEFINS

</div>

6.1 INTRDUCTION

Selective oxidation of olefins to epoxy compounds has always been an interesting area of research for the chemists owing to their great importance in the production of highly valued commodity chemicals such as polyurethanes, unsaturated resins, glycols, surfactants, and other products [1,2]. Transition metal complexes play a vital catalytic role in various organic transformations e.g. epoxidation, hydroxylation, C-H activation, hydrogenation, polymerisation, carbon-carbon coupling reactions, halogenation, dehalogenation and so on in homogeneous and heterogeneous media [3-5]. Among them, metalloporphyrins have been found to be efficient catalysts for alkene epoxidation using various oxygen atom donors [6-8] due to their high chemical and thermal stability, interesting physicochemical properties and flexible architectural modification to tailor redox properties and conformational features. The β-functionalization of *meso*-tetraphenylporphyrin (TPP) is of great interest since the electronic properties of the porphyrin π-system can be altered by tuning the size, shape and electronic nature of the β-substituents.

Iron and manganese porphyrin complexes were widely utilized as effective homogenous catalysts for such oxygenation reactions in last few decades [6-9]. The major drawbacks of homogenous MTPP-based catalysts are (i) the macrocyclic ring is liable for oxidative self-destruction; (ii) aggregation of metalloporphyrins through π-π interactions; (iii) lower turnover frequency (TOF) and; (iv) poor product selectivity. Recently, highly efficient and stable Mn^{III}porphyrinic framework (MOF) was demonstrated for selective epoxidation of olefins in heterogeneous media [10]. Among various metalloporphyrins, vanadyl (V^{IV}O) porphyrins merit special attention owing to their use as anti-HIV agents [11] as compared to other vanadium complexes as potential therapeutics, 3D supramolecular assemblies [12] and catalysts for oxidation

reactions [13-14]. Notably, VOTPP was utilised for oxidation of cyclohexene under homogeneous [13] and heterogeneous conditions [14], respectively, leading to mixture products (viz. epoxide, alcohol and ketone) with very low TOF. So, there is a quest for highly efficient vanadylporphyrin catalyst for selective oxidation of olefins. To the best of our knowledge, there is no report on selective epoxidation of olefins in almost quantitative yields catalyzed by oxidovanadium porphyrin complexes in homogenous media. Herein, we present the selective epoxidation of olefins using biologically important oxidant (i.e., H_2O_2) catalyzed by robust VOTPPCl$_8$ using NaHCO$_3$ as promoter with very high TOF.
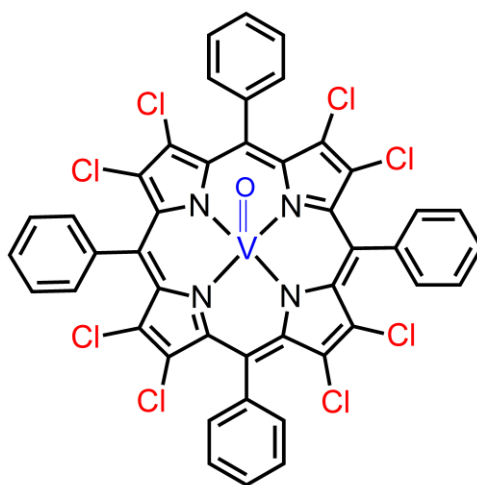
Figure 1. Molecular structure of *β*-octachlorovanadylporphyrin (VOTPPCl$_8$) employed in this study.

6.2 EXPERIMENTAL SECTION

6.2.1 Chemicals and materials

CH$_3$CN and DMF employed in the present work were of analytical grade and distilled before use. VOSO$_4$ and NaHCO$_3$ were purchased from HiMedia, India and used as received. Various alkenes used in this study were purchased from Alfa Aesar and used as received. TBAPF$_6$ was received from Alfa Aesar, India and recrystallized twice from ethanol followed by drying under vacuum at 60 °C for 10 h.

6.2.2 Instrumentation and methods

IR spectra were recorded in the mid IR range of 4000-400 cm^{-1} on a Perkin-Elmer spectrophotometer by making KBr pellets. ^{51}V NMR spectra were recorded on JEOL ECX 400 MHz spectrometer using DMSO-d$_6$ as a solvent containing 0.03% TMS (v/v). Electron

paramagnetic resonance (EPR) spectra were obtained on a Bruker EMX EPR spectrometer in toluene solvent at 120 K. The spin Hamiltonian parameters were obtained from simulated EPR spectrum. Thermal analyses were performed with SII EXSTAR 6300 instrument. DFT studies were carried out using B3LYP functional with LANLD2Z basis set. The oxidation products were quantified using a Shimadzu 2010 plus gas-chromatograph equipped with an Rtx-1 capillary column (30 m × 0.25 mm × 0.25 μm) and an FID detector. GC-MS analyses were carried out using Perkin-Elmer GC-MS (Clarus 500). Other spectroscopic methods used in this study as described in chapter 2.

6.2.3 Synthesis of 2,3,7,8,12,13,17,18-octachloro-*meso*-tetraphenylporphyrinato vanadium(IV) (VOTPPCl$_8$):

H$_2$TPPCl$_8$ (0.18 g, 0.202 mmol) was dissolved in 40 mL of DMF. To this, 10 equiv. of VOSO$_4$ (0.518 g, 2.02 mmol) was added and refluxed for 16 hours under argon atmosphere. At the end of this period the reaction mixture was cooled to room temperature and then 120 mL of distilled water was added. Porphyrin was precipitated out and filtered through G-4 crucible. The crude product was purified on silica column using CHCl$_3$ as eluent. Yield was found to be 0.152g (0.16 mmol, 79%).

UV-Vis (CH$_2$Cl$_2$): λ$_{max}$ (nm) (logε) 354 (4.01), 452 (5.15), 578 (4.00), 618 (sh); IR (KBr, cm^{-1}) 1003 (ν$_{V=O}$); MALDI-TOF-MS (m/z): found 954.95 [M]$^+$, calcd. 954.96; elemental analysis calcd. for C$_{44}$H$_{20}$N$_4$Cl$_8$VO: C, 55.32%; H, 2.11%; N, 5.87% and found: C, 55.23%; H, 2.28%; N, 5.98%.

6.2.4 Catalytic activity studies

The catalytic efficiency of VOTPPCl$_8$ was tested for the oxidation of various alkenes. In a typical catalytic experiment, 5 mmol (0.410 g) cyclohexene, 10 mmol 30 % H$_2$O$_2$ (1.13 g), 1 mmol NaHCO$_3$ (0.084 g) and 5.23×10^{-4} M (0.0005 g) of VOTPPCl$_8$ were added into a 5 mL of CH$_3$CN in a round bottom flask fitted with a condenser. The flask was placed in an oil bath and the temperature was kept 60 °C throughout the reaction time with 500 rpm mechanical stirring. After the reaction was finished, reaction mixture was filtered and its 1 mL portion was subjected to multiple hexane extraction. The extract was concentrated and its 0.2 μL was injected to the GC/GC-MS. The oxidation products were quantified using a Shimadzu 2010 plus gas-chromatograph equipped with an Rtx-1 capillary column (30 m × 0.25 mm × 0.25 μm)

and an FID detector. The product identities were confirmed by a Perkin-Elmer GC-MS (Clarus 500).

6.3 RESULTS AND DISCUSSION

6.3.1 Synthesis and Characterisation

We have synthesised free base *β*-octachloro-*meso*-tetraphenylporphyrin (H$_2$TPPCl$_8$) using reported procedure [15].VOTPPCl$_8$ was prepared by reacting H$_2$TPPCl$_8$ with 10 equivalents VOSO$_4$ in refluxing DMF for 16 hours under argon atmosphere. Then the porphyrin was precipitated by adding excess water, filtered and air dried. The crude porphyrin was purified on silica column using CHCl$_3$ as eluent. The yield was found to be 79%. In general, our vanadium metallation procedure is much simpler as compared to reported literature methods so far [12,16,17]. VOTPPCl$_8$ was characterised by optical absorption, IR and EPR spectroscopic techniques, mass spectrometry and elemental analysis. Figure 2 represents the UV-Vis spectrum of VOTPPCl$_8$ in CH$_2$Cl$_2$. VOTPPCl$_8$ exhibited a characteristic UV-Vis spectrum for a metalloporphyrin which is blue shifted as compared to that of H$_2$TPPCl$_8$. The IR spectrum of H$_2$TPPCl$_8$ exhibited a characteristic peak at ν ~3328 cm^{-1} for NH stretching frequency which disappeared upon metallation and appearance of a new peak at ~1003 cm^{-1} for V=O stretching confirmed the insertion of VO into the porphyrin core [12].
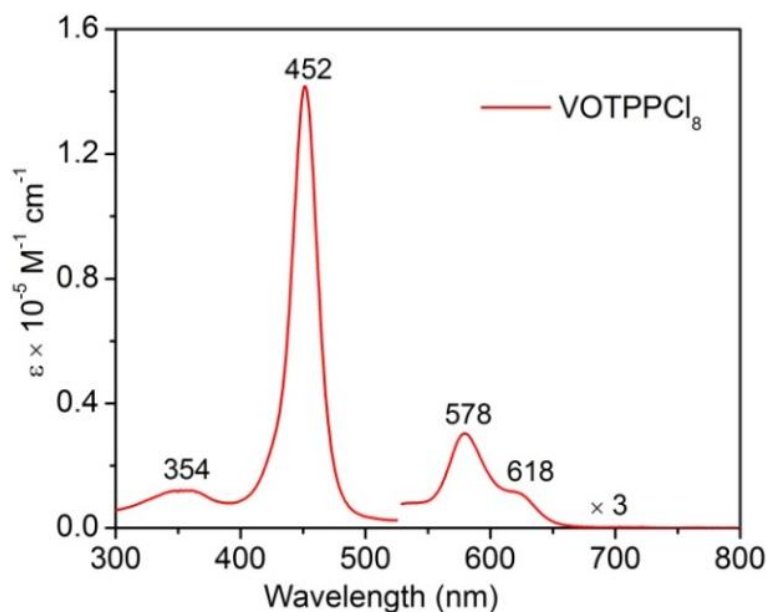
Figure 2. Electronic absorption spectrum of VOTPPCl$_8$ in CH$_2$Cl$_2$ at 298 K.

Further, the MALDI-TOF mass analysis showed a molecular ion peak at 954.95 (m/z) which is in agreement with the corresponding calculated mass number (m/z = 954.96). Our attempts to obtain X-ray quality single crystals were failed. So, we have carried out DFT studies using B3LYP functional with LANLD2Z basis set. Figure 3 represent the top and side views of optimised geometries of VOTPPCl$_8$ in gas phase. V^{IV} ion is present in square pyramidal geometry with axial oxo ligand. From the side view, it is clear that VOTPPCl$_8$ adopts nonplanar saddle shape conformation due to steric hindrance between peripheral β-chloro and *meso*-phenyl groups [15].The selected average bond angles and bond lengths of VOTPPCl$_8$ are listed in table 1. Herein, V^{IV} ion resides 0.54 Å above the porphyrin mean plane formed by 24 atoms core. V=O distance is shorter (1.59 Å) than β-octaethylvanadylporphyrin (1.62 Å) [18]. Further, VOTPPCl$_8$ exhibited a large deviation of 24 atoms core ($\Delta 24$ = 0.53 Å) and β-pyrrole carbons, ($\Delta C_\beta \pm 1.115$ Å) from the porphyrin mean plane (Table 1 and figure 3 (b)).This is further supported by longer C$_\beta$-C$_\beta$ bond length (1.376 Å) and the increment in C$_\beta$-C$_\alpha$-C$_m$ angle (~128°) with the concomitant decrement in the N-C$_\alpha$-C$_m$ angle (~123.8°) as compared to reported quasi planar vanadyl porphyrin.
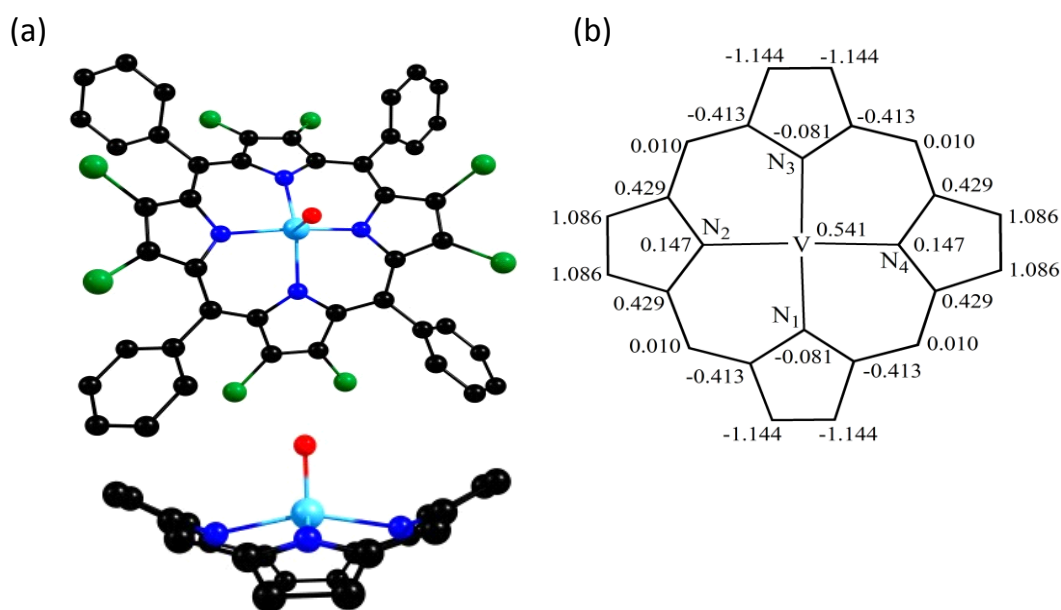
Figure 3. B3LYP/LANLD2Z optimised geometry of VOTPPCl$_8$ showing (a) top view (top) and side view (bottom)(b) the deviation of atoms from the porphyrin mean plane formed by 24 atoms core. In side view, β-chloro and *meso*-phenyl substituents are omitted for clarity.

Table 1. Selected bond lengths (Å) and bond angles (°) using the B3LYP/6-311G(d,p) basis set for optimised geometry of $VOTPPCl_8$.
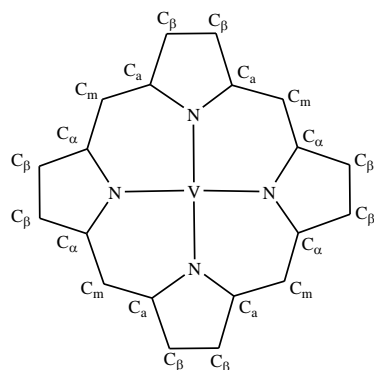
Bond Length (Å)		Bond Angle (°)	
V-N	**2.071**	**M-N-C_α**	**125.87**
V-O	1.593	N-M-N	145.03
N-C_α	1.402	**N-C_α-C_m**	**124.49**
C_α-C_β	1.452	N-C_α-C_β	107.93
C_β-C_β	**1.375**	**C_β- C_α-C_m**	**127.37**
C_α-C_m	1.416	C_α-C_β-C_β	107.85
ΔC_β (Å)^a	**1.115**	C_α-N-C_α	107.76
$\Delta 24$ (Å)^b	**0.530**		
ΔVanadium(IV) (Å)^c	**0.541**		

^{a}Deviation of β-pyrrole carbons from porphyrin mean plane formed by 24-atom core; ^{b}Deviation of 24 atoms from the porphyrin mean plane; ^{c}deviation of metal atom (V^{IV}) from the porphyrin mean plane.
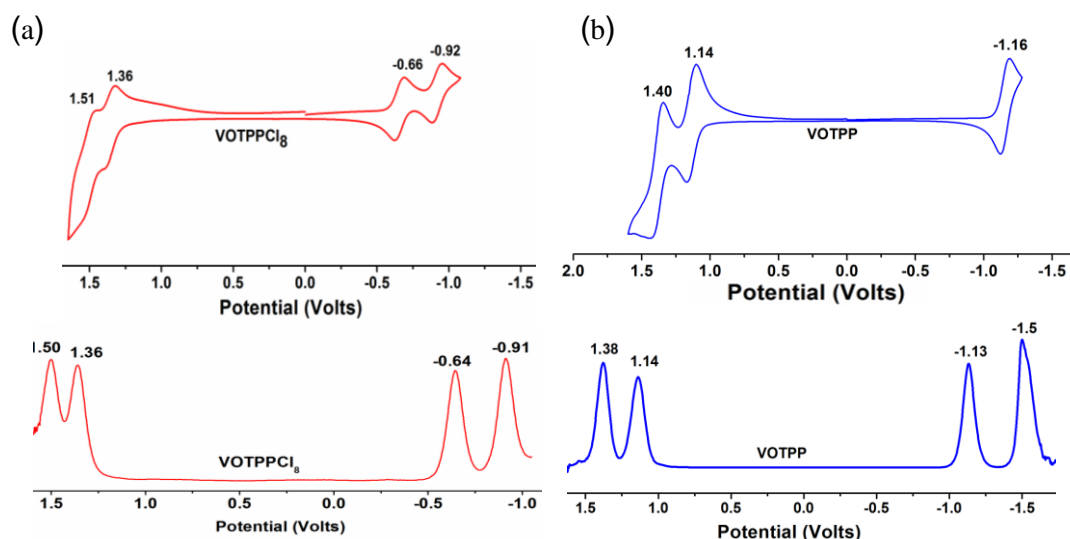
Figure 4. CV of $VOTPPCl_8$ (1 mmol) in dichloromethane containing 0.1 M $TBAPF_6$ at 298 K. Potentials are measured with respect to Ag/AgCl electrode.

Figure 4 represents the cyclic voltammograms (CVs) of $VOTPPCl_8$ and VOTPP which is measured in dichloromethane containing $TBAPF_6$ as supporting electrolyte at 298 K. It exhibited ring-centered two one electron oxidations and reductions which are further supported by the differential pulse voltammogram (DPV) of $VOTPPCl_8$ by showing four redox peaks with almost same amplitude (Figure 4).
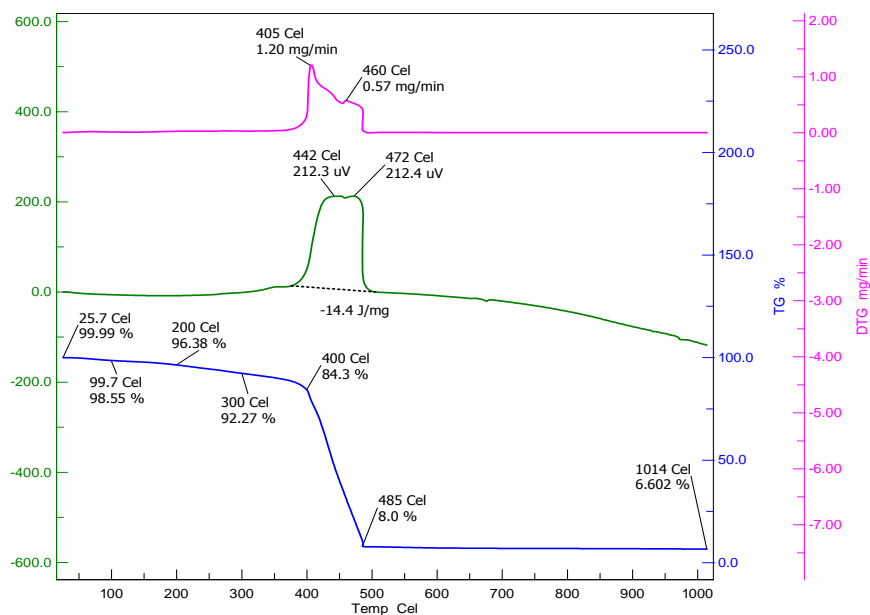
Figure 5. Thermogram (TG), Differential thermal analysis (DTA) and Differential thermogram (DTG) of VOTPPCl$_8$ at the heating rate of 10 °C/minute scanned from 25 °C to 1000 °C.
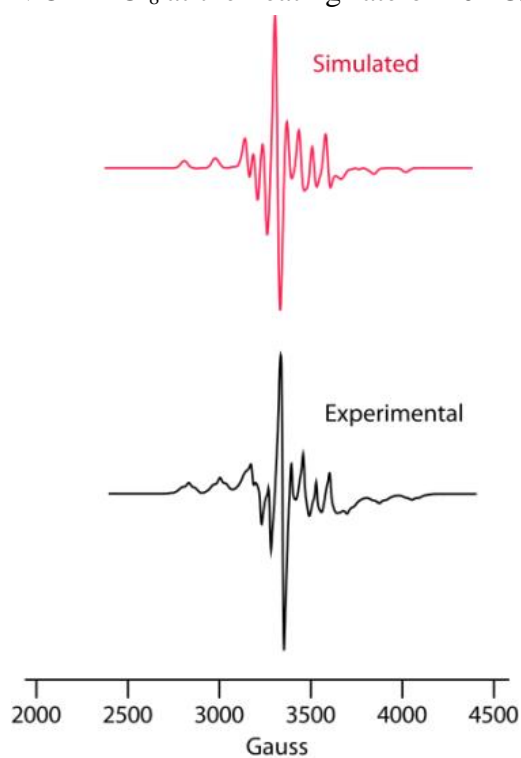
Figure 6. X-Band EPR spectrum of VOTPPCl$_8$ was recorded in toluene at 120 K (bottom). EPR parameters: microwave frequency, 9.453 GHz; incident microwave power, 0.189 mW; modulation frequency, 100.0 kHz; modulation amplitude, 5.0 G; receiver gain, 1×10^4. Simulated EPR spectrum of VOTPPCl$_8$ is shown at the top.

Notably, VOTPPCl$_8$ exhibited a remarkable anodic shift (ΔE_{red} = 500 mV) in the first ring reduction as compared to VOTPP whereas in oxidation only 220 mV anodic shift was observed due to nonplanar conformation of macrocycle which destabilizes the HOMOs and makes oxidation easier relative to reduction (Figure 4) as explained chapter 2. The anodic shift in redox potentials is due to the strong electron withdrawing effect of eight β-chloro groups.

The thermogram of VOTPPCl$_8$ exhibited almost a flat line till 390 °C indicating the high thermal stability of this porphyrin (Figure 5). The high stability of VOTPPCl$_8$ is possibly due to sterically hindered porphyrin periphery (nonplanar saddle shape conformation) and electron withdrawing β-chloro groups which prevent the oxidative decomposition. To the best our knowledge, this is the first example of metalloporphyrin showing very high thermal stability (till 390 °C) which prompted us to do catalytic oxidation studies using this vanadylporphyrin complex.

We have recorded the X-band EPR spectrum of VOTPPCl$_8$ in toluene (Figure 6). VOTPPCl$_8$ has exhibited axial EPR spectrum with well resolved ^{51}V hyperfine lines at 120 K. The spin Hamiltonian parameters were obtained from simulated EPR spectrum which is in close agreement with experimentally observed one. The obtained g_{II} and $g_{\perp}$ values are 1.965 and 1.985, respectively and A_{II} and $A_{\perp}$ values are 172×10^4 cm^{-1} and 61×10^4 cm^{-1}, respectively. The $g_{II} < g_{\perp}$ and $A_{II} >> A_{\perp}$ relationships are normal for the axially compressed d^1_{xy} configuration [17]. These results clearly indicate that vanadium is in IV oxidation state.

Further, we couldn't observe well resolved superhyperfine splitting from porphyrin N atoms since the unpaired electron resides on a σ-non-bonding orbital pointing away from these N atoms which is present in the equatorial (xy) plane [19].These results clearly indicate that vanadium is in IV oxidation state.

6.3.2 Catalytic Studies

To explore the catalytic potential of synthesized vanadium porphyrin complex (VOTPPCl$_8$), we conducted a series of experiments. Catalytic oxidation of cyclohexene by VOTPPCl$_8$ using H$_2$O$_2$ as oxidant and NaHCO$_3$ as co-catalyst gave

three products: cyclohexene epoxide (**1**), 2-cyclohexen-1-ol (**2**) and 2-cyclohexen-1-one (**3**).
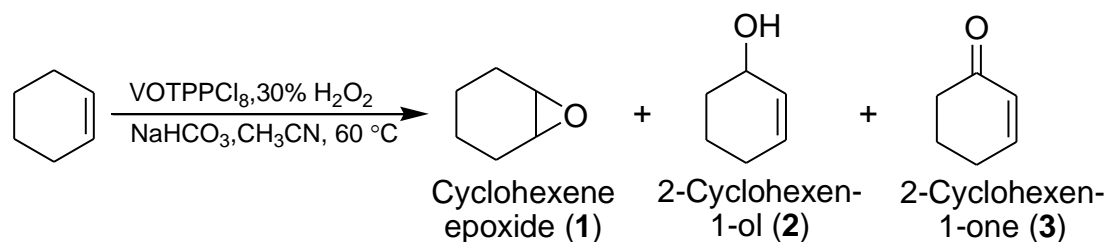
Scheme 1 Oxidation of cyclohexene catalyzed by VOTPPCl$_8$.

The catalytic activity of VOTPPCl$_8$ was initially investigated for cyclohexene as a representative oxidation substrate and different reaction parameters were optimized for 5 mmol (0.410 g) of cyclohexene in 6 h of reaction time. All the catalytic experiments were carried out in a 50 mL round bottom flask containing cyclohexene (0.410 g, 5 mmol), appropriate amount of aqueous 30% H$_2$O$_2$, NaHCO$_3$ in 5mL of desired solvent and fitted with a condenser. At first, the effect of different types of solvents *viz.* acetonitrile, methanol, dichloromethane and toluene (5 mL each), on the oxidation of 5 mmol (0.410 g) of cyclohexene was studied using 10 mmol (1.13 g) of 30% H$_2$O$_2$ and 1 mmol (0.084 g) of NaHCO$_3$ as promoter at 60 ^{o}C. CH$_3$CN was found to be the most suitable solvent with the maximum of 61% conversion followed by 57% conversion of cyclohexene using methanol as a solvent (data not shown). The possible reason for the increased conversion is due to the enhanced formation of oxidohydroperoxido- or oxidoperoxidovanadium(V) species. Therefore, CH$_3$CN was used as a solvent for the optimization of remaining reaction conditions.

The catalyst amount was optimized by taking three different amounts of catalyst (0.0005 g, 0.0010 g and 0.0015 g) while keeping other reaction parameters constant such as 30% H$_2$O$_2$ (1.13 g, 10 mmol), NaHCO$_3$ (0.084 g, 1 mmol), acetonitrile (5 mL) and reaction temperature (60 ^{o}C). The conversion increased from 61% to 73% by increasing the catalyst amount from 0.0005 g to 0.0010 g as presented in Table 1 (entry 2). Thereafter, no considerable improvement in conversion was obtained (77%) upon increasing the catalyst amount up to 0.0015 g and hence catalyst amount 0.0010 g (1.04 µmol) was considered as optimized catalyst amount.

The effect of oxidant amount i.e. aq. 30% H$_2$O$_2$ was measured by varying its amount. For this purpose, three different oxidant amount viz. 5, 10 and 15 mmol were chosen

and reactions were carried out by taking 1.04 µmol of catalyst, 1 mmol of promoter (i.e. NaHCO$_3$) and 5 mL of CH$_3$CN at 60 ^{o}C. The cyclohexene conversion was lowest (59 %) for 5 mmol of 30% H$_2$O$_2$ and comparable conversions were obtained while increasing H$_2$O$_2$ amount up to 10 mmol (77 %) and 15 mmol (78 %). Considering these observations, 10 mmol of 30% H$_2$O$_2$ was concluded best for the maximum oxidation of cyclohexene (entry 2, Table 1).

Table 2. Oxidation of cyclohexene (0.41 g, 5 mmol) using VOTPPCl$_8$ as a catalyst in 6 hour time scale under different reaction conditions.

Entry No.	Catalyst (mg, µmol)	30 % H$_2$O$_2$ (g, mmol)	NaHCO$_3$ (g, mmol)	CH$_3$CN(mL)	Temp. (^{o}C)	Conv. %
1	0.5, 0.52	1.13, 10	0.084, 1	5	60	61
2	1.0, 1.04	1.13, 10	0.084, 1	5	60	73
3	1.5, 1.57	1.13, 10	0.084, 1	5	60	77
4	1.0, 1.04	1.69, 15	0.084, 1	5	60	78
5	1.0, 1.04	0.57, 5	0.084, 1	5	60	59
6	**1.0, 1.04**	**1.13, 10**	**0.168, 2**	**5**	**60**	**82**
7	1.0, 1.04	1.13, 10	0.252, 3	5	60	85
8	1.0, 1.04	1.13, 10	0.168, 2	7	60	68
9	1.0, 1.04	1.13, 10	0.168, 2	3	60	81
10	1.0, 1.04	1.13, 10	0.168, 2	5	70	86
11	1.0, 1.04	1.13, 10	0.168, 2	5	50	51
12	1.0, 1.04	1.13, 10	0.168, 2	5	30[a]	35
13	1.0, 1.04	1.13, 10	–	5	60	58
14	–	1.13, 10	0.168, 2	5	60	16
15	–	1.13, 10	–	5	60	5

The solvent (CH$_3$CN) amount is also an important factor in terms of percentage conversion of cyclohexene. The effect of different amounts of solvent is shown in Table 2 under above optimized conditions i.e. catalyst (0.0010 g, 1.04 µmol), 30% H$_2$O$_2$ (1.31 g, 10 mmol), NaHCO$_3$(0.168 g, 2 mmol) at 60 °C reaction temperature. While using 5 mL of acetonitrile

82% of cyclohexene conversion was obtained which was reduced to 68% for 7 mL of CH$_3$CN possibly due to the dilution effect. The conversion was slightly decreased (81%) when 3 mL of solvent amount was employed. Considering all these facts, 5 mL of CH$_3$CN was chosen as optimal solvent amount for cyclohexene oxidation.

To understand the dependence of cyclohexene oxidation over reaction temperature, reactions have been carried out at different temperatures *i.e.* room temperature (30 ^{o}C), 50, 60 and 70 ^{o}C temperature under the optimized conditions for 6 hours. The oxidation of cyclohexene was found to be slowest at room temperature (30 ^{o}C) with only 35 % conversion. The catalytic activity of the catalyst VOTPPCl$_8$ increased significantly on increasing temperature from room temperature to 70 ^{o}C. A conversion of 51 % was obtained for 50 ^{o}C which was also further increased up to 82 % and 86 % for 60 ^{o}C and 70 ^{o}C, respectively (Table 2).

Table 3. Product distribution for the oxidation of cyclohexene (5 mmol) using VOTPPCl$_8$ as catalyst (1 μmol) and 10 mmol of 30% H$_2$O$_2$ as an oxidant under different reaction conditions.
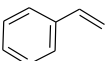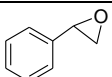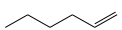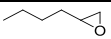
Entry No.	Solvent (mL, v/v)	NaHCO$_3$ (g, mmol)	Temp. (^{o}C)	Time (h)	Conv. %	TOF (h^{-1})	Product selectivity		
							-Oxide (**1**)	-Ol (**2**)	-One (**3**)
1	CH$_3$CN (5)	0.168, 2	60	6	82	653	22	42	36
2	CH$_3$CN (5)	–	60	6	58	462	13	58	29
3	**CH$_3$CN/H$_2$O (3/2)**	**0.168, 2**	**60**	**0.5**	**100**	**9560**	**99**	**–**	**–**
4	CH$_3$CN/H$_2$O(3/2)	0.168, 2	30^{a}	2	51	1219	30	44	26
5	CH$_3$OH (5)	0.168, 2	60	6	80	637	3	11	86
6	CH$_3$OH (5)	–	60	6	56	446	1	43	57
7	CH$_3$OH/H$_2$O(3/2)	0.168, 2	60	0.5	97	9273	7	52	41
8	CH$_3$OH/H$_2$O(3/2)	0.168, 2	30^{a}	2	45	1076	18	42	40

Details of all experimental conditions are presented in Table 2. Thus, the optimized reaction conditions for the oxidation of 5 mmol of cyclohexene are (entry no. 6, Table

1): catalyst [VOTPPCl$_8$] (0.0010 g, 1.04 µmol), 30% aqueous H$_2$O$_2$ (1.13 g, 10 mmol), CH$_3$CN (5 mL) and temperature 60 °C. The selectivity of different oxidation products under the optimized reaction condition is: 22% cyclohexene epoxide (**1**), 42% 2-cyclohexen-1-ol (**2**) and 36% 2-cyclohexen-1-one (**3**). To investigate the effect of both catalyst (VOTPPCl$_8$) and promoter (NaHCO$_3$) on the oxidation of cyclohexene, three types of controlled experiments were performed under the optimized conditions (Table 2): (i) The control experiment in the absence of catalyst (VOTPPCl$_8$) but with promoter NaHCO$_3$ under optimized conditions gave 16% of conversion (entry no. 14), (ii) The control experiment in the absence of promoter NaHCO$_3$ but with catalyst (VOTPPCl$_8$) under optimized conditions gave 58% of conversion (entry no. 13) and, (iii) The control experiment in the absence of both promoter NaHCO$_3$ and catalyst (VOTPPCl$_8$) under optimized conditions gave only 5% of conversion after 6 hours of

Table 4. Oxidation of different olefins using 1.04 µmol of VOTPPCl$_8$ as catalyst, 30% H$_2$O$_2$ as terminal oxidant and sodium bicarbonate as promoter using CH$_3$CN/H$_2$O solvent mixture under the optimized reaction conditions.

$$\text{Olefins} \xrightarrow[\text{0.4 equiv. NaHCO}_3\text{, CH}_3\text{CN/H}_2\text{O, 60 °C}]{\text{0.002 mol% VOTPPCl}_8\text{, 2 equiv. 30% H}_2\text{O}_2} \text{Epoxides}$$
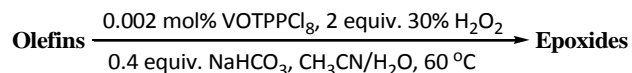
Entry No.	Substrate (5 mmol)	Product	Time (h)	Conv. %	% Selectivity	TOF (h^{-1})
1			0.5	100	99	9560
2			0.5	92	98	8884
3			0.5	98	100	9463
4			0.5	85	100	8208

reaction time (entry no. 16). These control experiments demonstrate that the catalyst itself is moderately efficient in catalytic oxidation of cyclohexene using 30% H$_2$O$_2$ as an oxidant with adequate conversion of 58% even in the absence of any promoter. But the product selectivity for cyclohexene epoxide decreased from 22% to 13% (Table 3,

entry no. 2), whereas, only 5% of cyclohexene was converted in the absence of both catalyst and promoter showing their catalytic roles in the oxidation (entry 15, Table 2).

However, 16% of cyclohexene conversion was observed using NaHCO$_3$ alone in the reaction. Surely the use of NaHCO$_3$ as promoter activated the oxidant H$_2$O$_2$ and resulted in the increased catalytic efficiency of the catalyst (VOTPPCl$_8$) towards oxidation of cyclohexene in respect of both the conversion and selectivity of epoxide [20,21].

Bhattacharyya *et al* [21] have reported that HCO$_3^-$, which is an essential component in such systems, forms a peroxymonocarbonate ion, HCO$_4^-$ and exists as following equillibria and is more active (more nucleophilicity) oxidant than H$_2$O$_2$.

$$H_2O_2 + HCO_3^- \rightleftharpoons HCO_4^- + H_2O$$
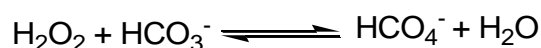
Later, this bicarbonate-activated peroxide (BAP) system, was adopted for olefin epoxidation using H$_2$O$_2$ as terminal oxidant in CH$_3$CN solvent and in water/co-solvent mixture. All these facts and our previous results showing respectable amount of selectivity towards epoxide (i.e. 22 %, Table 3, entry no. 1) under the optimized conditions led us to investigate that how the solvent mixture of water with CH$_3$CN or CH$_3$OH (as we have stated previously that comparable results were obtained with methanol) affects the cyclohexene conversion and epoxide selectivity?

To understand the effect of these solvent mixtures, the experiments were conducted under above stated optimized condition. The use of CH$_3$CN/H$_2$O (3 mL/2 mL, v/v) at 60 ^{o}C mixture dramatically improved the catalytic efficiency of the catalyst (VOTPPCl$_8$) and almost all cyclohexene was converted into epoxide (99% selectivity) within half an hour of reaction time (Table 3, entry no. 3). Using CH$_3$CN/H$_2$O (3mL/2mL, v/v) mixture at room temperature yielded 51% of conversion in 2 hours of reaction time with reduced 30% selectivity for cyclohexene epoxide (**1**) and increased 44% and 26% selectivity for the allylic oxidation products 2-cyclohexen-1-ol (**2**) and 2-cyclohexen-1-one (**3**), respectively. Similarly, in methanol/water (3 mL/2 mL, v/v) mixture 97% conversion was obtained in 0.5 hour time scale at 60 ^{o}C but with poor cyclohexane epoxide (**1**) selectivity i.e. 7% (Table 3, entry no.7) and a maximum of

45% conversion was obtained at room temperature with 18% selectivity towards epoxide. The similar trend of epoxide selectivity for acetonitrile and methanol was observed throughout the series of experiments (i.e. the epoxide selectivity is always higher if CH_3CN is used as solvent alone or with water).

Finally, an optimized condition both in the respect of percentage conversion and epoxide selectivity was achieved for the cyclohexene oxidation as follows: catalyst (VOTPPCl₈) (0.0010 g, 1.04μmol), 30% aqueous H_2O_2 (1.13 g, 10 mmol), CH_3CN/H_2O (3mL/2mL, v/v) and temperature 60 °C. Under this optimized condition, we have carried out the epoxidation reactions of various olefins and the results are summarized in Table 4.

6.3.3 Catalytic Mechanism
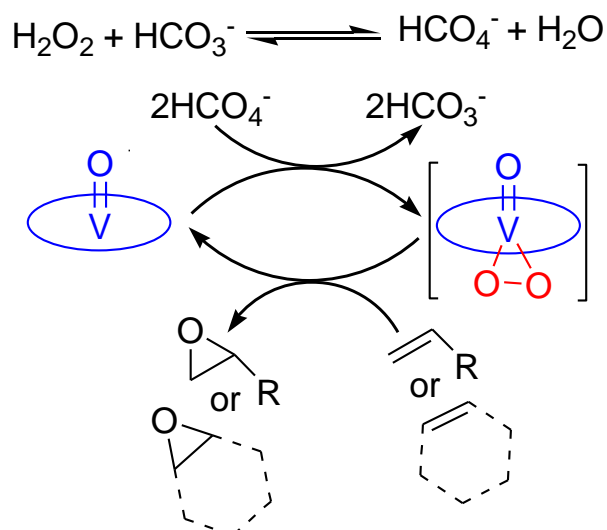
Scheme 2 Plausible catalytic mechanism for the conversion olefins to epoxides using VOTPPCl₈ catalyst.

We tried UV-Visible spectral titration of VOTPPCl₈ in presence of $H_2O_2/NaHCO_3$ in CH_3CN/H_2O mixture and found no spectral changes are observed. So, we have carried out ^{51}V NMR experiments in order to ascertain the intermediate formed during the catalytic reaction. H_2O_2 and HCO_3^- are used together to increase the activity of H_2O_2 by the *insitu* generation of HCO_4^- which is more nucleophilic than H_2O_2 and thus attributes to the enhanced oxidizing activity of the metal complexes and to speed-up the reaction. Hence, in the presence of H_2O_2 and $NaHCO_3$, the solution of VOTPPCl₈

in DMSO-d$_6$ is converted into oxidoperoxidovanadium(V), [VO(O$_2$)TPPCl$_8$]$^-$ with a resonance at -618.4 ppm and remains stable for two days as shown in the Figure 7. The addition of cyclohexene decreases the peak intensity at -618.4 ppm by heating to 50 °C for 5 minutes (Figure 7c). Further, the peak at -618.4 ppm is completely diminished by adding excess of cyclohexene and heating at 50 °C for 10 minutes (Figure 7d). The peak appeared at -618.4 ppm in ^{51}V NMR indicates the formation ofoxidoperoxidovanadium(V) species [22,23]. In general, oxidoperoxidovanadium(V) species [22,23], [VO(O$_2$)TPPCl$_8$]$^-$ is more stable as compared to oxidohydroperoxidovanadium(V), [VO(O-OH)TPPCl$_8$]$^-$ species [24] in which hydroperoxide ion binds in side-on mode. Hence, the 100% selectivity for epoxide formation with very good conversion (85-100%) from olefin to epoxide by VOTPPCl$_8$ catalyst is possibly due to the formation of oxidoperoxidovanadium(V) intermediate, [VO(O$_2$)TPPCl$_8$]$^-$ which converts olefin to expoxide selectively [20-23].
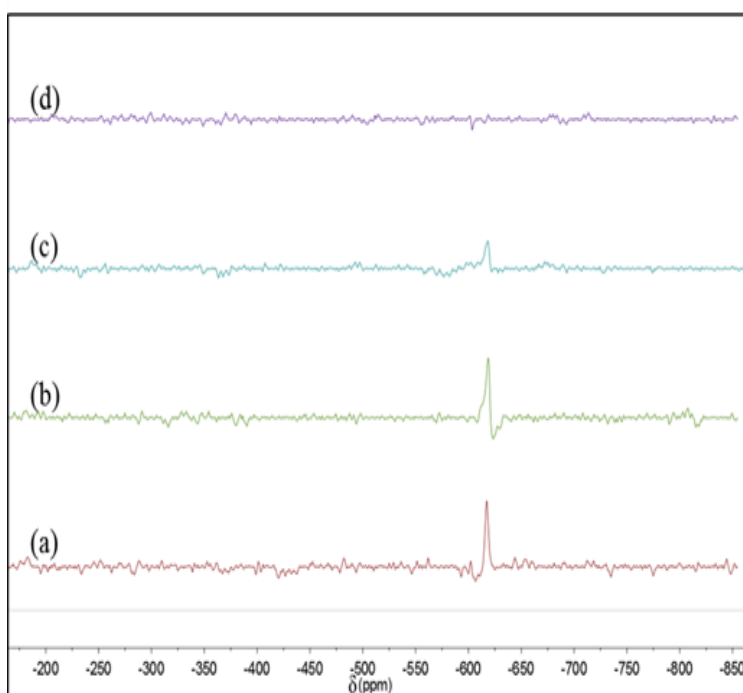
Figure 7. ^{51}V NMR spectra of VOTPPCl$_8$ (5.2 µmol) in DMSO-d$_6$ in the presence of: (a) 0.36 mmol of 30% aq. H$_2$O$_2$ and 0.3 mmol of NaHCO$_3$, 10 minutes after addition, a peak appeared at -618.4 ppm; (b) after 48 hours; (c) 1.2 mmol of cyclohexene was added and heated for 5 minutes at 50 °C; (d) large excess of cyclohexene was added and heated for10 minutes at 50 °C.
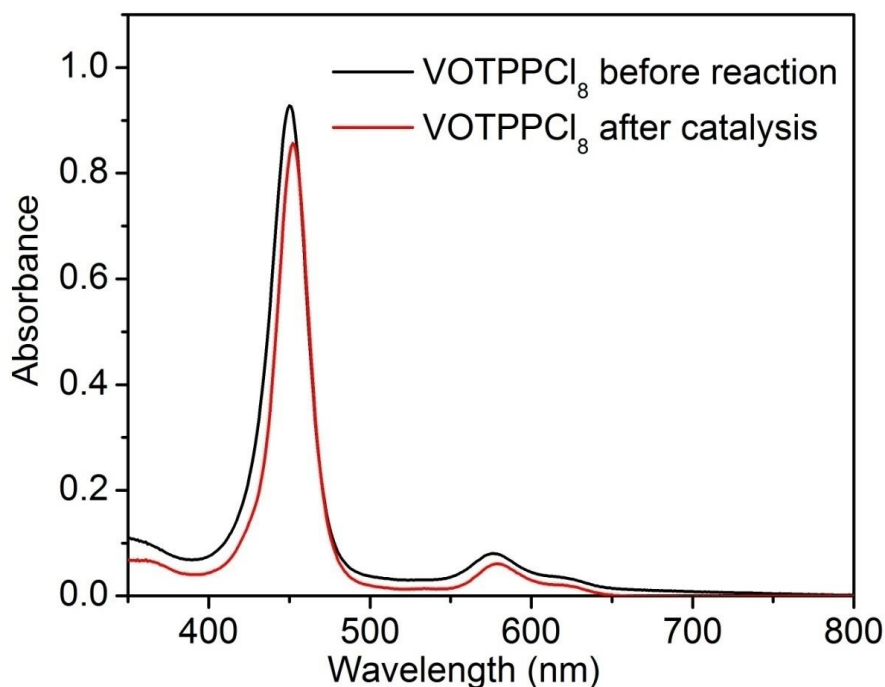
Figure 8. UV-Visible spectra of VOTPPCl$_8$ in CH$_2$Cl$_2$ (before catalysis) and in CH$_3$CN (after catalytic reaction) at 298 K.

The reason for very high TOF numbers is due to high thermal and chemical stability of VOTPPCl$_8$ which resist for thermal as well as chemical oxidative degradation and further bulkiness prevents bimolecular attack [26-28]. At the end, the obtained epoxide product was distilled off and catalyst was recovered. The UV-Vis absorption spectral features of VOTPPCl$_8$ didn't change before and after catalytic reaction indicating its high thermal and chemical stability as shown in Figure 8.

6.4 CONCLUSIONS

We have synthesized VOTPPCl$_8$ in good yield and characterized by various spectroscopic techniques. DFT optimized structure of VOTPPCl$_8$ exhibited severe nonplanar saddle shape conformation and the oxidation state of metal ion (V^{IV}) was confirmed by EPR spectroscopy. CV studies revealed the electron deficient nature of porphyrin π-system by showing remarkable anodic shift in redox potentials as compared to VOTPP. VOTPPCl$_8$ showed very high thermal stability till 390 °C due to electron deficient nonplanar porphyrin core. Further, VOTPPCl$_8$ was utilized for the selective epoxidation of various olefins in almost quantitative yield in presence of H$_2$O$_2$/NaHCO$_3$ in CH$_3$CN/H$_2$O mixture. The formation of oxidoperoxidovanadium(V)

intermediate during catalytic cycle was probed by ^{51}V NMR studies. This porphyrin catalyst (VOTPPCl$_8$) has higher thermochemical stability and recyclability. However, anchoring of these catalysts in polymers or mesoporous materials (heterogenization) in high concentrations would be important for the commercial applications. Currently, we are working on the said topic and the results will be reported in the near future.

6.5 REFERENCES

1. Weissemel, K.; Arpe, H. J., "Industrial Organic Chemistry", 3rd Ed., VCH: Weinheim, Germany, **1997**.

2. Rao, A. S., In "Comprehensive Organic Synthesis" Trost, B. M.; Fleming, I.; Ley, S. V., Eds.; Pergamon: Oxford, **1991**; Vol. 7, pp 357-436.

3. Gupta, K. C.; Sutar, A. K., "Catalytic activities of Schiff base transition metal complexes", *Coord. Chem. Rev.* **2008**, *252*, 1420-1450.

4. Bauer, I.; Knölker, H. J., "Iron Catalysis in Organic Synthesis", *Chem. Rev.* **2015**, *115*, 3170-3387.

5. Conte, V.; Coletti, A.; Floris, B.; Licini, G.; Zonta, C., "Mechanistic aspects of vanadium catalysed oxidations with peroxides", *Coord. Chem. Rev.* **2011**, *255*, 2165-2177.

6. Sheldon, R. A.; "Metalloporphyrins in Catalytic Oxidations", Marcel Dekker,Inc., New York, **1994**.

7. Meunier, B., "Biomimetic Oxidation Catalyzed by Transition Metal Complexes", Imperial College Press, London, **1999**.

8. Montanari, F.; Casella, L., "Metalloporphyrin Catalyzed Oxidations", Kluwer Academic Publishers, Boston, **1994**.

9. Peng, S.-H.; Mahmood, M. HR.; Zou, H.-B.; Yang S.-B.; Liu, H.-Y., "The first manganese N-confused porphyrins catalyzed oxidation of alkene", *J. Mol. Catal. A* **2014**, *395*, 180-185.

10. Yang, X. L.; Wu, C. D., "Metalloporphyrinic Framework Containing Multiple Pores for Highly Efficient and Selective Epoxidation", *Inorg. Chem.* **2014**, *53*, 4797-4799 and references therein.

11. Wong, S. Y.; Sun, R. W.-Y.; Chung, N. P.-Y.; Lin C.-L.; Che, C.-M., "Physiologically stable vanadium(IV) porphyrins as a new class of anti-HIV agents**",** *Chem. Commun*. **2005**, 3544-3546.

12. Chen, W.; Suenobu, T.; Fukuzumi, S., "A Vanadium Porphyrin with Temperature-Dependent Phase Transformation: Synthesis, Crystal Structures, Supramolecular Motifs and Properties*", Chem. Asian J*. **2011**, *6,* 1416-1422.

13. Mansour, E. M. K.; Maillard, P.; Krausz, P.; Gaspard S.; Giannotti, C., "Photochemically induced olefin oxidation by titanyl and vanadyl porphyrins", *J. Mol. Catal*. **1987**, *41*, 361-366.

14. Rehiman, A. K.; Bharathi, K. S.; Sreedaran, S.; Rajesh, K.; Narayanan, V., "Cationic vanadyl porphyrin-encapsulated mesoporous Al/V-MCM-41 as heterogeneous catalysts for the oxidation of alkenes", *Inorg. Chim. Acta* **2009**, *362*, 1810-1818.

15. Spyroulias, G. A.; Despotopoulos, A. P.; Raptopoulou, C. P.;Terzis, A. ;de Montauzon, D.; Poilblanc, R.; Coutsolelos, A. G., "Comparative study of structure-properties relationship for novel *β*-halogenated lanthanide porphyrins and their nickel and free bases precursors, as a function of number and nature of halogens atoms", *Inorg. Chem.* **2002**, *41*, 2648-2659

16. Harada, R.;Okawa H.; Kojima, T., "Synthesis, characterization, and distortion properties of vanadyl complexes of octaphenylporphyrin and dodecaphenylpor-phyrin", *Inorg. Chim. Acta* **2005**, *358*, 489-496.

17. Ghosh, S. K.; Patra R.; Rath, S. P., "Axial ligand coordination in sterically strained vanadyl porphyrins: Synthesis, structure, and properties", *Inorg. Chem.* **2008**, *47*, 9848-9856.

18. Molinaro; F. S.; Ibers, J. A., "Crystal and molecular structure of 2,3,7,8,12,13,17,18-octaethylporphinatooxovanadium(IV)", *Inorg. Chem.* **1976**, *15*, 2278-2283.

19. Smith II, T. S.; LoBrutto R.; Pecoraro,V. L., "Paramagnetic spectroscopy of vanadyl complexes and its applications to biological systems", *Coord. Chem. Rev.* **2002**, *228*, 1-18.

20. Bagherzadeh, M.; Amini, M.; Parastar, H.; Heravi, M. J.; Ellern A.; Woo, L. K., "Synthesis, X-ray structure and oxidation catalysis of a oxido-peroxido molybdenum(VI) complex with a tridentate Schiff base ligand", *Inorg. Chem. Commun.* **2012**, *20*, 86-89.

21. Maiti, S. K.; Dinda, S.; Banerjee, S.; Mukherjee A. K.; Bhattacharyya, R., "Oxidoperoxidotungsten(VI) complexes with secondary hydroxamic acids: synthesis, structure and catalytic uses in highly efficient, selective and ecologically benign oxidation of olefins, alcohols, sulfides and amines with H$_2$O$_2$ as a terminal oxidant", *Eur. J. Inorg. Chem.* **2008**, 2038-2051.

22. Maurya, M. R.; Chaudhary, N.; Avecilla, F.; Adao, P.; Costa Pessoa, J., "Oxidovanadium(IV) and dioxidovanadium(V) complexes of hydrazones of 2-benzoylpyridine and their catalytic applications", *Dalton Trans*. **2015**, *44*, 1211–1232.

23. Pettersson, L.; Andersson I.; Gorzsás, A., "Speciation in peroxovanadate systems", *Coord. Chem. Rev.,* **2003**, *237*, 77–87.

24. Schneider, C. J.; Penner-Hanh, J. E.; Pecoraro, V. L., "Elucidating the Protonation Site of Vanadium Peroxide Complexes and the Implications for Biomimetic Catalysis", *J. Am. Chem. Soc.*, **2008**, *130*, 2712–2713.

25. Araghi, M.; Mirkhani, V.; Moghadam, M.; Tangestaninejad, S.; Mohammdpoor-baltork, I., "Synthesis and characterization of a new porphyrin-polyoxometalate hybrid material and investigation of its catalytic activity", *Dalton Trans*. **2012**, *41*, 3087-3094.

26. Zhang, W.; Jiang, P.; Wang, Y.; Zhang, J.; Zhang, P., "Bottom-up approach to engineer two covalent porphyrinic frameworks as effective catalysts for selective oxidation", *Catal. Sci. Technol.* **2015**, *5*, 101-104.

27.   Zhang, K.; Yu, Y.; Nguyen, S. T.; Hupp, J. T.; Broadbelt, L. J.; Farha, O. K., "Epoxidation of the commercially relevant divinylbenzene with [tetrakis-(pentafluorophenyl)porphyrinato]iron(III) chloride and its derivatives", *Ind. Eng. Chem. Res.* **2015**, *54*, 922-927.

CHAPTER 7

Facile Synthesis and Electrochemical Studies of Diethoxyphosphorylphenyl Substituted Porphyrin and its Metal Complexes

Reagents and conditions:
1. BF$_3$·Et$_2$O, DDQ, **50%**
2. M(OAc)$_2$·nH$_2$O, CHCl$_3$/MeOH or DMF, **98%**

M = 2H, Ni(II), Cu(II), Zn(II)

<div align="center">
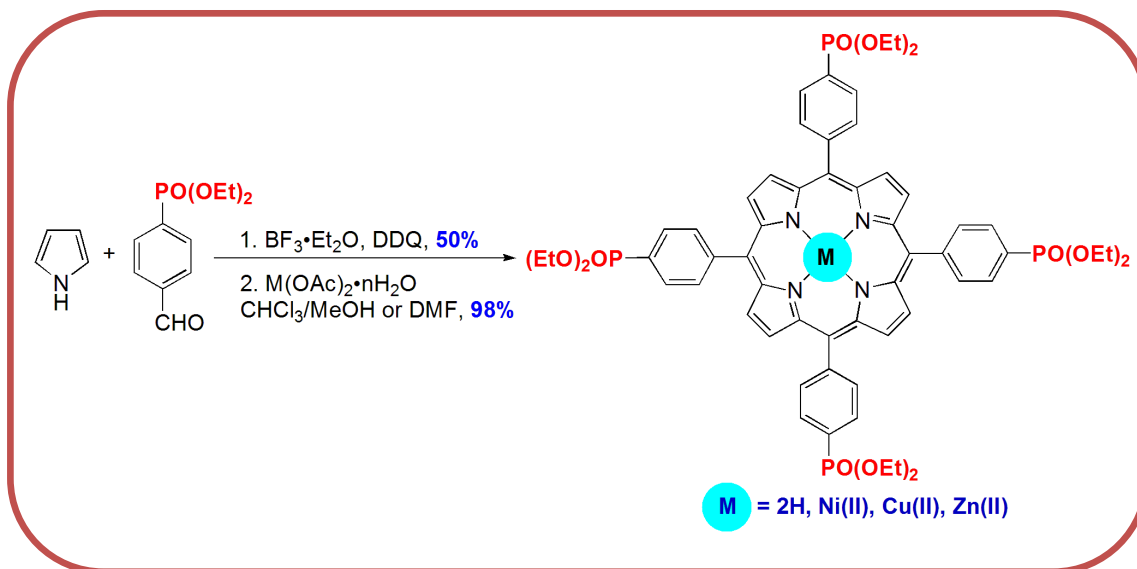
CHAPTER 7

FACILE SYNTHESIS AND ELECTROCHEMICAL STUDIES OF DIETHOXYPHOSPHORYLPHENYL SUBSTITUTED PORPHYRIN AND ITS METAL COMPLEXES

</div>

7.1 INTRODUCTION

Tetrapyrrolic macrocycles occupy a central place in bioinorganic chemistry [1]. Metalloporphyrins play a vital role in various biological processes such as hydroxylation, oxygen transport, electron transport, and oxidizing catalytic reactions [2]. Functionalization of the porphyrin periphery is one of the most convenient approaches for the synthesis of novel porphyrin-based materials to tune their structural, optical and electrochemical redox properties. Arylphosphonic acid appended porphyrins are promising candidates for DSSC applications [3] and oxidation catalysis [4]. Significant synthetic progress in this area was achieved by applying transition metal catalyzed cross-coupling methodology. Arnold *et al*. prepared phosphorus substituted porphyrins by Pd-catalyzed coupling reactions of diphenylphosphine or its oxides with bromoporphyrins [5,6]. Similarly, *meso*-phosphinylporphyrins have also been afforded from Pd and Cu catalyzed C-P cross-coupling reactions of *meso*-iodoporphyrins with diphenylphosphine [7,8]. Bujoli *et al.* have reported the synthesis of 5,10,15,20-*tetrakis*(4'-diethoxyphosphorylphenyl)porphyrin (H_2TPhPP) using Adler-Longo method [4] in 30% yield. Enakieva *et al.* and Kubat *et al.* have reported the synthesis of H_2TPhPP using bromoporphyrin precursor [9,10]. After learning about the good applicability of phosphoryl porphyrins in diverse areas, we aimed to find some straightforward synthetic procedures.

Herein, we report the modified synthesis of H_2TPhPP in higher yield (50%) and its metal derivatives (Ni(II), Cu(II) and Zn(II)). To determine the effect of phosphorylphenyl substituents on porphyrin π-system, we have carried out electrochemical studies. All synthesized porphyrins (Chart 1) were characterized by UV-visible, fluorescence, ^{1}H NMR spectroscopic techniques and mass spectrometry.
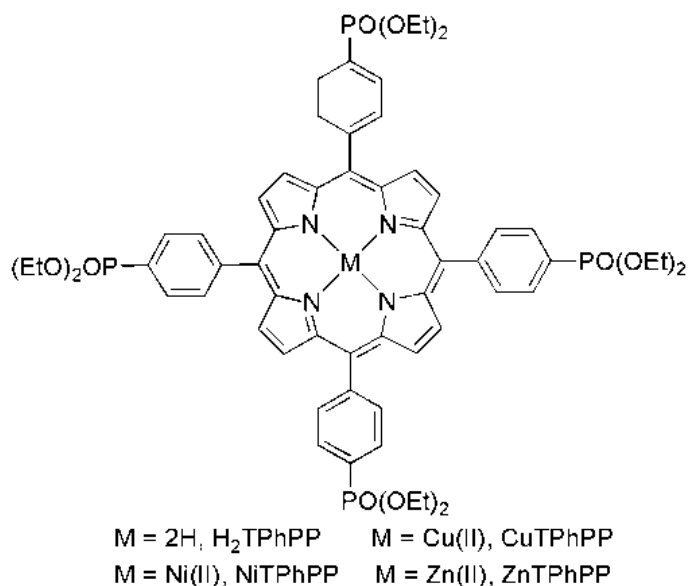
Chart 1. Molecular structure of synthesized porphyrins.

7.2 EXPERIMENTAL SECTION

7.2.1 Materials and Methods

p-Bromobenzaldehyde, *p*-chloranil, $BF_3 \cdot Et_2O$, pyrrole, phenylboronic acid and $Pd(PPh_3)_4$ were obtained from Sigma-Aldrich and used as received. Methanol, petroleum ether, anhydrous sodium sulphate, CH_3CN, NaCl, toluene, K_2CO_3, $NaHCO_3$, $CHCl_3$, ethyl acetate, metal (Ni(II), Cu(II) and Zn(II)) acetate hydrate, triethylamine and DMF were purchased from Rankem, India and used as received. Toluene and triethylamine were dried and distilled over P_2O_5 and CaH_2, respectively. Quantum yield (ϕ) was calculated with reference to H_2TPP and ZnTPP by using following formula, $\phi_{sample} = (\phi_{ref} \times A_{sample} \times \varepsilon_{ref}) / (A_{ref} \times \varepsilon_{sample})$. Mass spectra were recorded on Bruker Daltanics-microTOF ESI-mass spectrometer.

7.2.2 Synthesis of 5,10,15,20-*tetrakis*(4'-diethoxyphosphorylphenyl)porphyrin (H₂TPhPP)

A round bottom flask was charged with 150 mL of distilled $CHCl_3$. To this, diethyl(4-formylphenyl)phosphonate (1.35 g, 5.50 mmol), pyrrole (0.38 mL, 5.50 mmol) and 0.6 mL of 2.5 M $CHCl_3$ solution of $BF_3 \cdot OEt_2$ were added under argon atmosphere and allowed to stir for 2 h at RT. Then *p*-chloranil (0.32 g, 1.30 mmol) was added and allowed to reflux on water bath for

90 minutes. The crude porphyrin was purified on silica column using $CHCl_3$ and CH_3OH mixture (98.5:1.5, v/v) as eluent. The yield was found to be 0.793 g (50%).

^{1}H NMR in $CDCl_3$: δ (ppm) 8.81 (s, 8H, *β-pyrrole*-H), 8.34-8.29 (m, 8H, *o-meso*-phenyl-H), 8.21 (dd, *J* = 14 Hz, *J* = 8 Hz, 8H, *m-meso*-phenyl-H), 4.46-4.30 (m, 16H, $-OCH_2$), 1.51 (t, 24H, *J* = 8.0 Hz, $-CH_3$), -2.86 (s, 2H, -NH). ESI-MS (m/z): found 1181.35 [M+Na]$^+$, calcd. 1181.35.

7.2.3 Synthesis of MTPhPP (M = Ni(II), Cu(II) and Zn(II))

H_2TPhPP (0.2 g, 0.172 mmol) was dissolved in 150 mL of $CHCl_3$. To this, $M(OAc)_2 \bullet nH_2O$ (10 equiv.) in 20 mL of methanol was added and allowed to reflux on water bath for 50 minutes. Then, the solvent was evaporated to dryness and redissolved in minimum amount of $CHCl_3$ and washed with water (2×150 mL). The organic layer was dried over anhydrous Na_2SO_4 and purified on silica column using $CHCl_3$/methanol mixture (98.5:1.5, v/v) as eluent. The yield was found to almost quantitative.

ZnTPhPP: ^{1}H NMR in $CDCl_3$: δ (ppm) 8.81 (s, 8H, *β-pyrrole*-H), 8.21 (dd, *J* = 8 Hz, *J* = 4 Hz, 8H, *o-meso*-phenyl-H), 7.73 (dd, *J* = 12 Hz, *J* = 8 Hz, 8H, *m-meso*-phenyl-H), 4.04-3.90 (m, 16H, $-OCH_2$), 1.28 (t, 24H, *J* = 7.0 Hz, $-CH_3$,). ESI-MS (m/z): found 1245.25 [M+Na]$^+$, calcd. 1245.45. **CuTPhPP:** ESI-MS (m/z): found 1243.26 [M+Na]$^+$, calcd. 1243.60.

H_2TPhPP (0.2 g, 0.172 mmol), $Ni(OAc)_2 \bullet 4H_2O$ (0.43 g, 1.72 mmol) was dissolved in 80 mL of DMF and allowed to reflux for 90 minutes under inert atmosphere. At the end of this period, 200 ml of distilled water was added and the precipitate was filtered, washed with water and dried under vacuum. The crude porphyrin was purified on silica column using $CHCl_3$ and methanol mixture (98.5:1.5, v/v) as eluent. Yield: 0.205 g (98%).

NiTPhPP: ^{1}H NMR in $CDCl_3$: δ (ppm) 8.79 (s, 8H, *β-pyrrole*-H), 8.19-8.10 (m, 16H, *o-* and *m-meso*-phenyl-H), 4.42-4.26 (m, 16H, $-OCH_2$), 1.48 (t, 24H, *J* = 8.0 Hz, $-CH_3$). ESI-MS (m/z): found 1238.27 [M+Na]$^+$, calcd. 1238.75.

7.3 RESULT AND DISCUSSION

The synthesis of H_2TPhPP was first reported by Bujoli *et al.* in 1995 using Adler-Longo method [4] in 30% yield. But this procedure involves evaporation of propionic acid and purification of tarry reaction mixture by multiple column chromatography separations. In 2009, Enakieva *et al.* reported the synthesis of H_2TPhPP using a multi-step synthetic route as shown in Scheme [9].
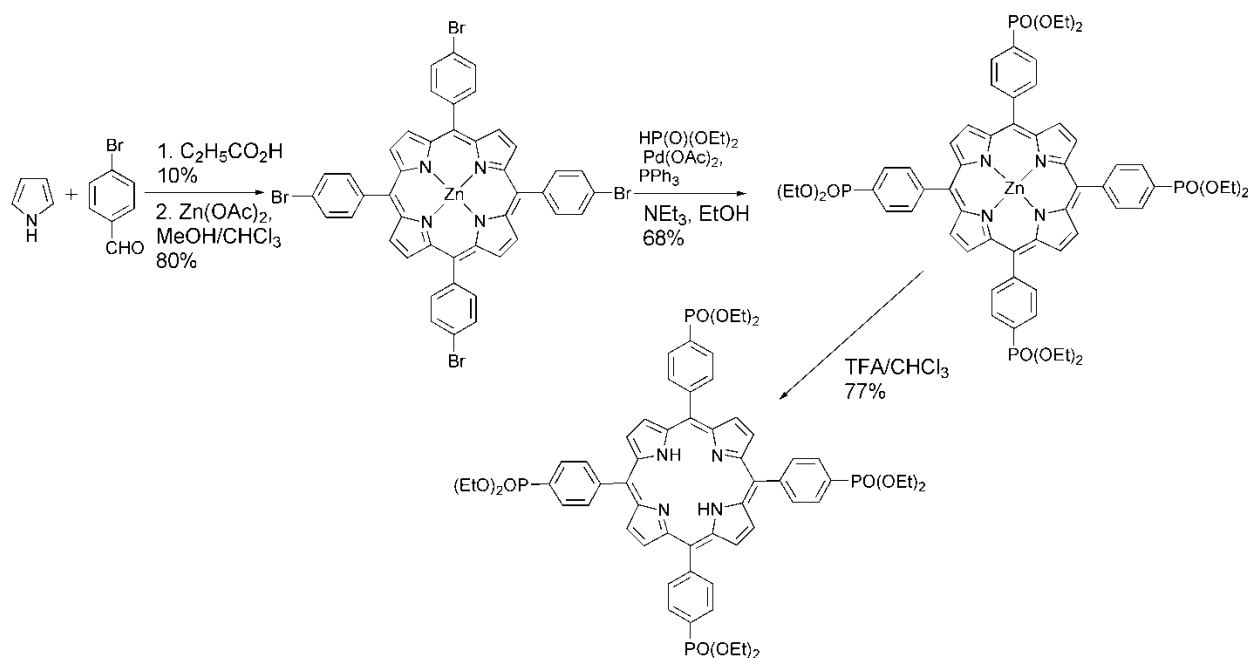
Scheme 1. Multi-step synthetic route for the preparation of H$_2$TPhPP [9].

We have synthesized H$_2$TPhPP in one step using convenient Lindsey method [11] in good yield (50%) as shown in scheme 2. First, we synthesized diethyl(4-formylphenyl) phosphonate *via* Pd-catalyzed coupling reaction of 4-bromobenzaldehyde with diethyl phosphite [12]. Subsequently, we condensed the same with pyrrole using modified Lindsey procedure to afford H$_2$TPhPP. In this mild method, we didn't get a tarry reaction mixture as observed in Adler-Longo method so that we could purify our desired product easily.CuTPhPP and ZnTPhPP were
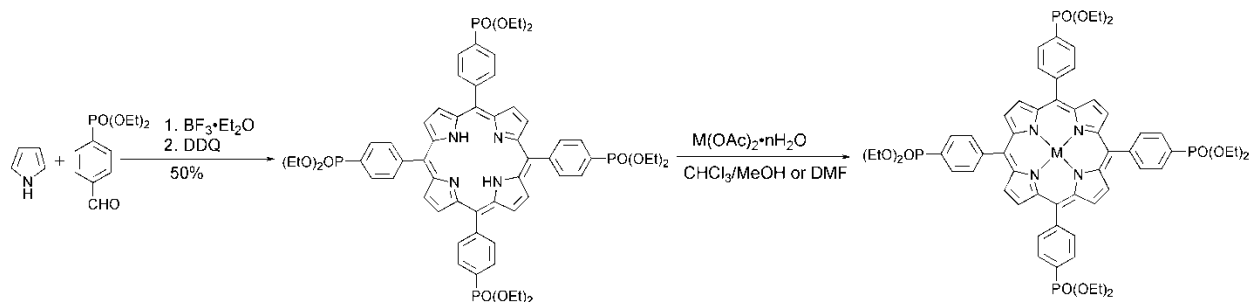
Scheme 2. Improved synthetic route *via* modified Lindsey method for H$_2$TPhPP.

prepared by refluxing 10 equiv. of M(OAc)$_2$•nH$_2$O and H$_2$TPhPP in CHCl$_3$/MeOH mixture whereas NiTPhPP was prepared by refluxing Ni(OAc)$_2$•4H$_2$O and H$_2$TPhPP in DMF for 1.5 hours under argon atmosphere.

The optical absorption spectra of H_2TPhPP and its metal complexes were recorded in CH_2Cl_2 at 298 K. Table 1 list the absorption spectral data of these porphyrins in CH_2Cl_2. H_2TPhPP exhibited a Soret band (B band) at 418 nm and four Q bands at 514, 548, 589 and 644 nm while CuTPhPP exhibited a Soret band at 415 nm and one Q band at 539 nm as shown in Figure 1. The observed spectral pattern and λ_{max} values are close to H_2TPP. We recorded the optical absorption
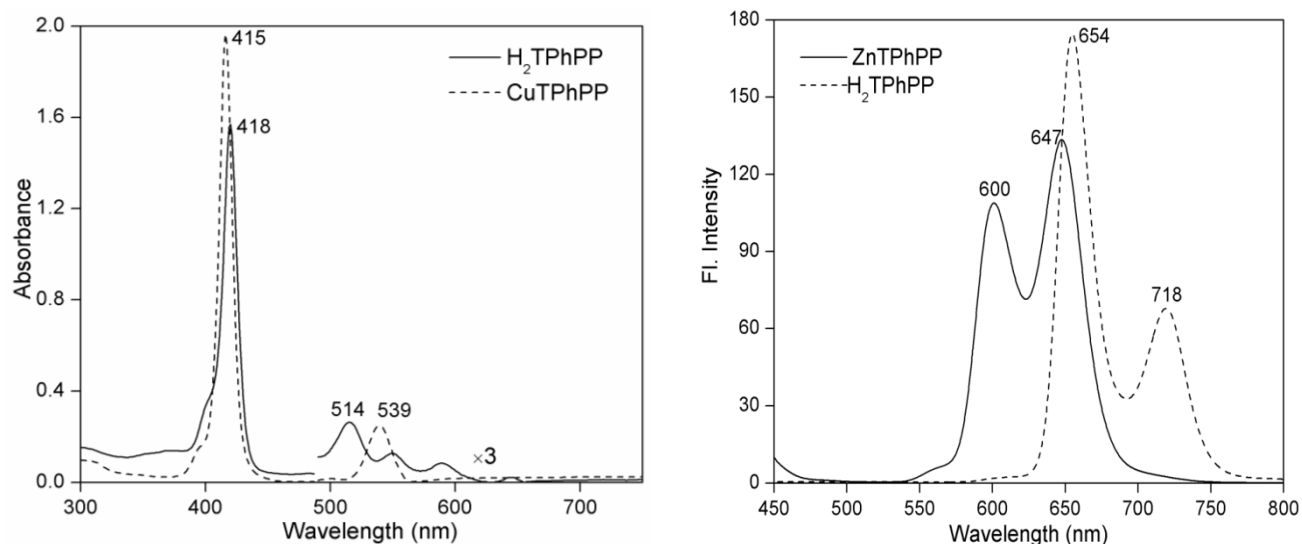
Figure 1. UV-Visible absorption spectra of H_2TPhPP and CuTPhPP in CH_2Cl_2 at 298 K (left).Fluorescence spectra of H_2TPhPP and ZnTPhPP in CH_2Cl_2 at 298 K (right).

spectra of ZnTPhPP in CH_2Cl_2 at different concentrations (10^{-5} to 10^{-6} M) and found no spectral changes indicating the non-aggregation behavior of ZnTPhPP. Emission spectra of H_2TPhPP and ZnTPhPP are shown in Figure 1 (right). H_2TPhPP exhibited λ_{em} at 654 and 718 nm whereas Zn(II) complex exhibited λ_{em} at 600 and 647 nm and corresponding quantum yields are also listed in Table 1. The observed spectral patterns and quantum yield values for MTPhPP (M = 2H and Zn(II)) match with corresponding MTPP. ^{1}H NMR spectra of NiTPhPP was recorded in $CDCl_3$ as shown in Figure 2. The β-pyrrole protons of NiTPhPP are slightly upfield shifted as compared to NiTPP.The characteristic multiplet observed for –OCH_2 group is due to 1,3-coupling of phosphorous as well as -CH_3 group. For all porphyrins, the integrated intensities match with proposed structures. ESI-mass spectra of H_2TPhPP and its metal complexes are shown in Figures 3-6.

171
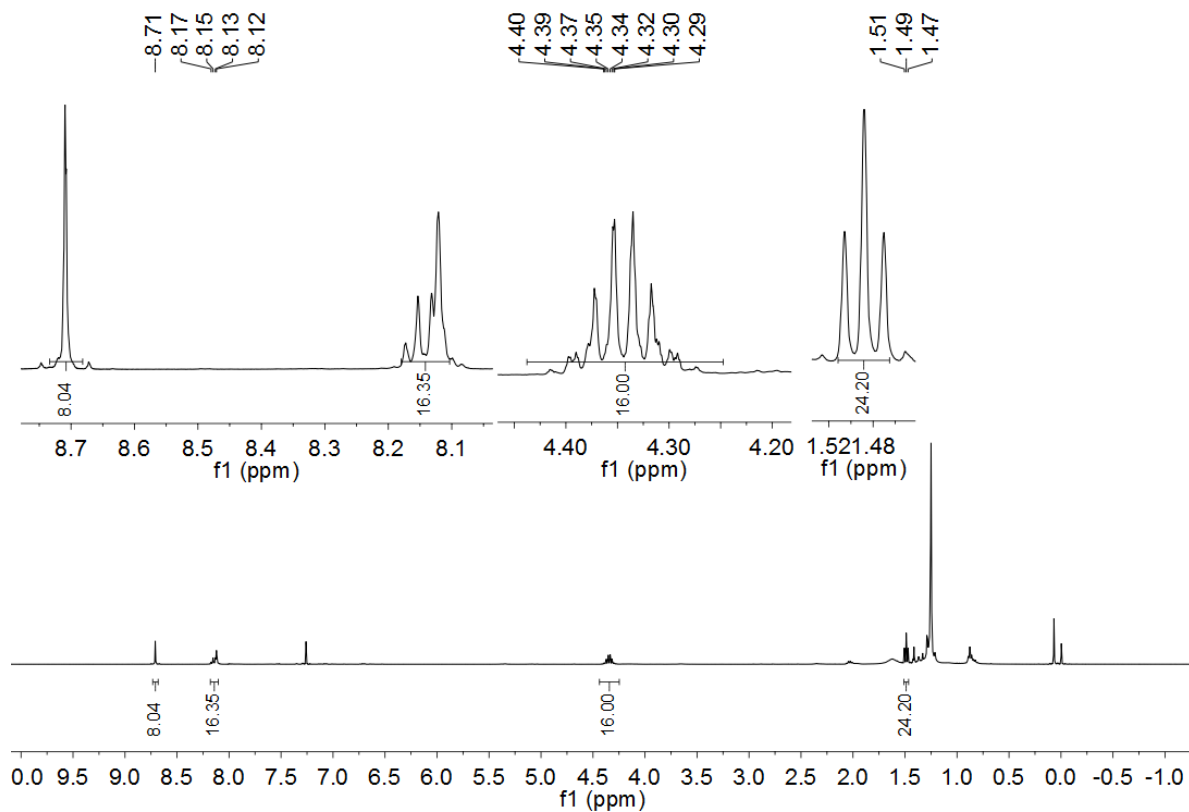
Figure 2. ^{1}H NMR spectrum of NiTPhPP in CDCl$_3$ at 298 K.
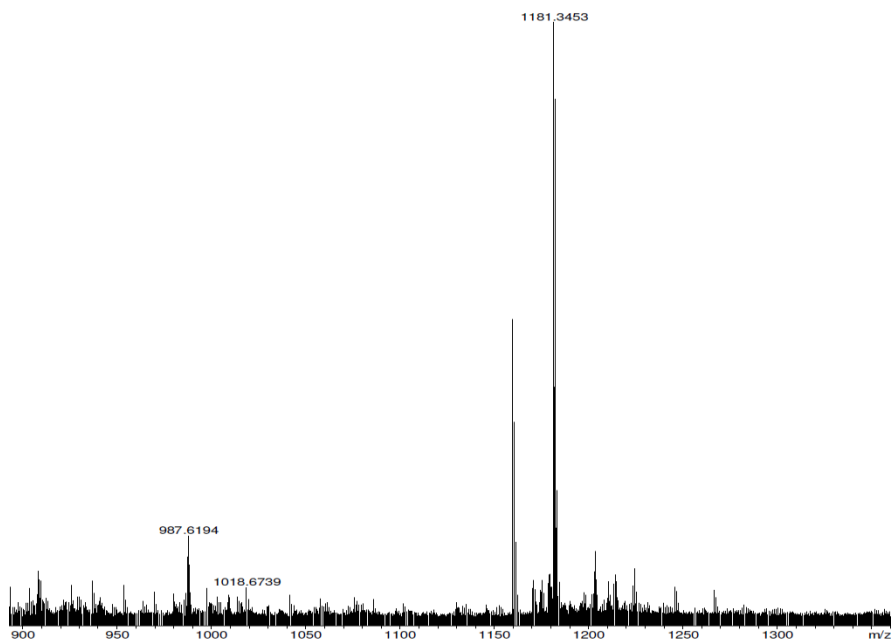
Figure 3. ESI-mass spectrum of H$_2$TPhPP in postive ion mode.
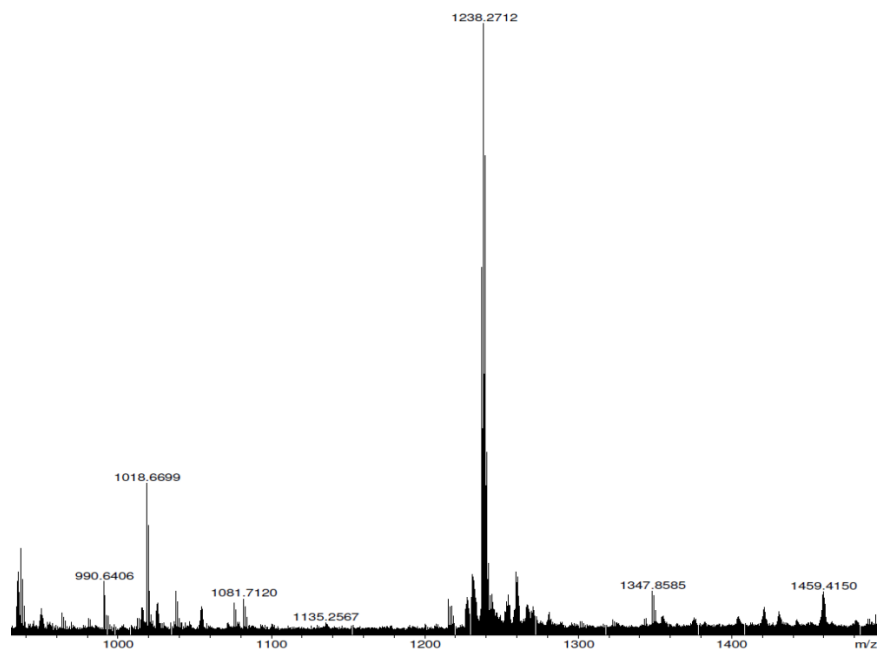
Figure 4. ESI-mass spectrum of NiTPhPP in postive ion mode.
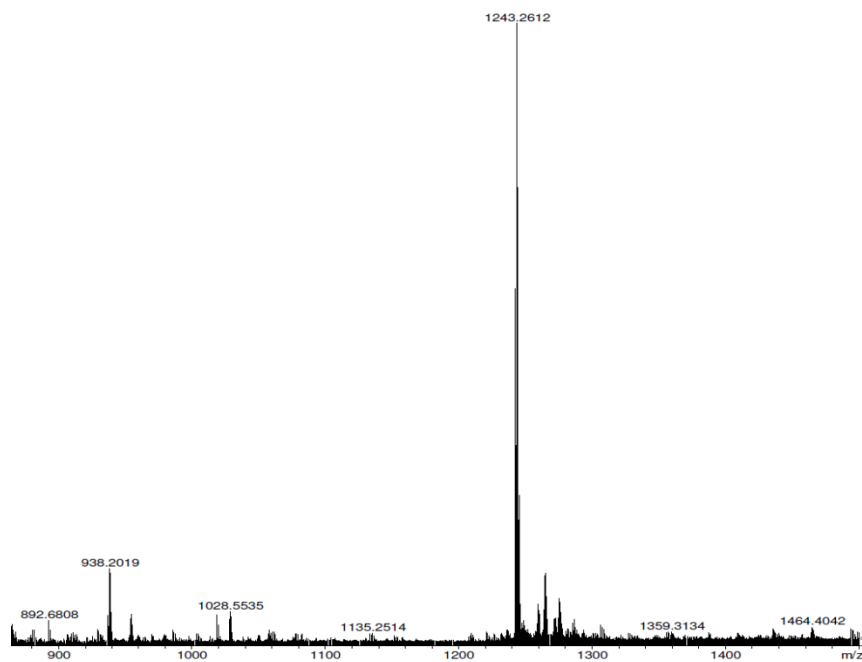
Figure 5. ESI-mass spectrum of CuTPhPP in postive ion mode.
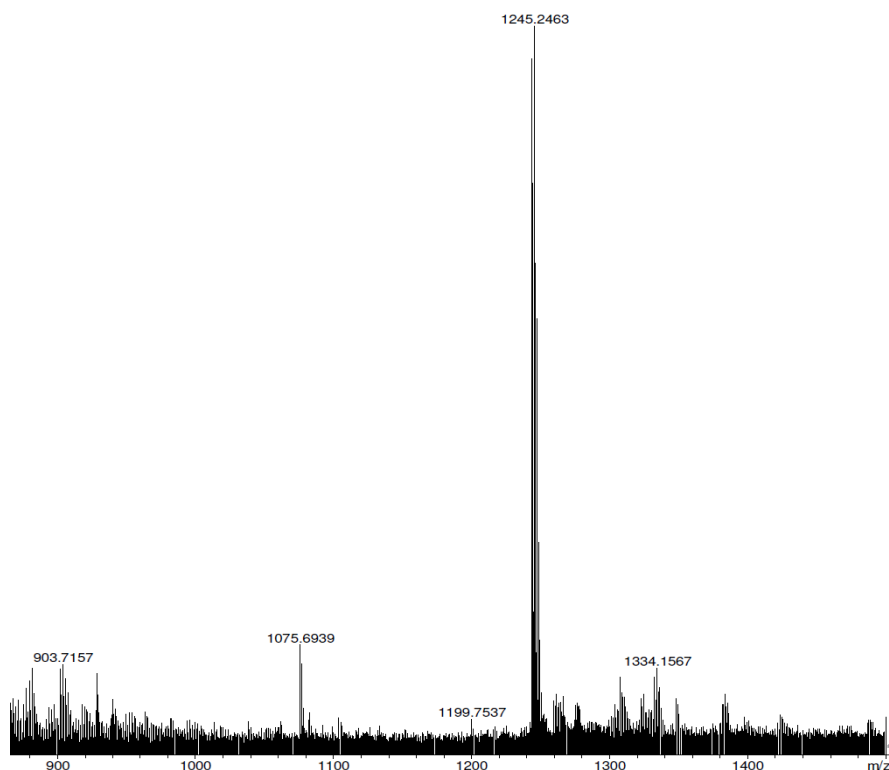
Figure 6. ESI-mass spectrum of ZnTPhPP in postive ion mode.

Table 1. Optical absorption and emission spectral data of H_2TPhPP and its metal derivatives (λ_{max},nm (logε, L mol^{-1} cm^{-1}) in CH_2Cl_2 at 298 K.

Porphyrin	B band, nm	Q band(s), nm	Emission λ_{max}, nm	ϕ_f
H_2TPhPP	418(4.87)	514(3.69), 548(3.43), 589(3.34), 644(3.18)	654, 718	0.092
NiTPhPP	414(4.83)	527(3.38)		
CuTPhPP	415(5.45)	539(4.11)		
ZnTPhPP	420(5.59)	548(4.26), 588(sh)	600, 647	0.035

ϕ_f = quantum yield

To examine the influence of diethoxyphosphoryl groups on porphyrin π-system, the electrochemical redox behavior of these porphyrins was studied by cyclic voltammetry in CH_2Cl_2 at 298 K. The cyclic voltammograms of MTPhPP (M = 2H, Ni(II), Cu(II) and Zn(II)) are shown in Figure 8. Table 2 lists the comparative electrochemical redox data of MTPhPPs and
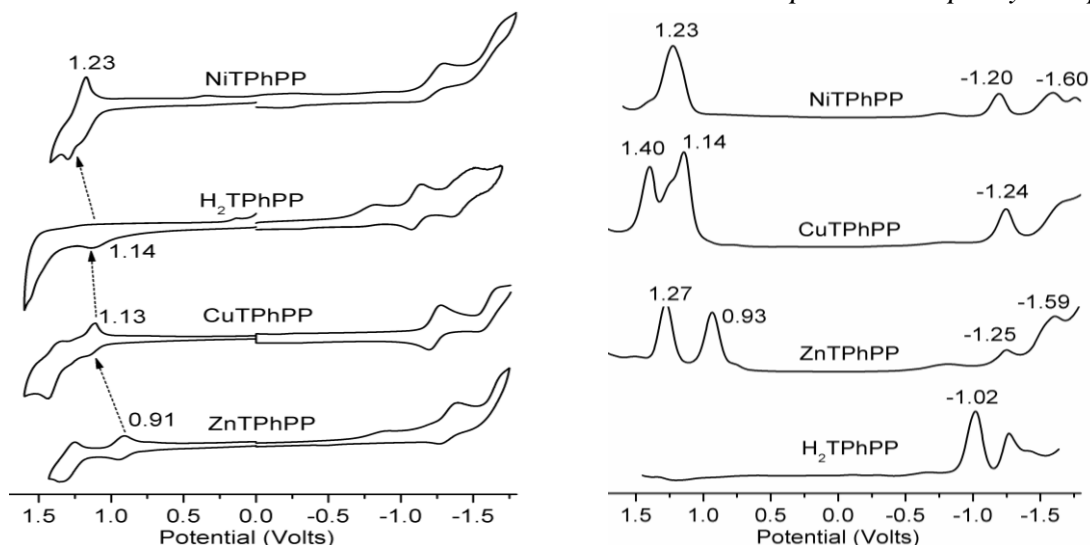
Figure 7. Cyclic Voltammograms of MTPhPPs (M = 2H, Ni, Cu and Zn) in CH_2Cl_2 containing 0.1 M $TBAPF_6$ using Ag/AgCl as reference electrode with a scan rate of 0.1 V/s at 298 K (left).Differential Pulse Voltammograms (DPVs) of MTPhPPs (M = 2H, Cu, Ni and Zn) in CH_2Cl_2 containing 0.1 $TBAPF_6$ as supporting electrolyte (right).

Table 2. Electrochemical redox data (*vs* Ag/AgCl) of H_2TPhPP and its metal derivatives in CH_2Cl_2 containing 0.1 M $TBAPF_6$ at 298 K.

Porphyrins	Oxidation (V)		Reduction (V)		ΔE (V)
	I	II	I	II	
H_2TPP	1.00	1.34	-1.23	-1.54	2.23
H_2TPhPP	1.14[i]	-	-1.11	-1.43	2.25
NiTPP	1.02	1.36	-1.28	-1.72	2.30
NiTPhPP	1.23[a]	-	-1.20[b]	-1.60[b]	2.43
CuTPP	0.97	1.35	-1.33	-1.71	2.30
CuTPhPP	1.14	1.39	-1.24	-1.61	2.37
ZnTPP	0.84	1.14	-1.36	-1.77	2.20
ZnTPhPP	0.91	1.29	-1.28[b]	-1.58[b]	2.19

[a]two electron oxidation; [i]irreversible; [b]data obtained from DPV

MTPPs. These porphyrins exhibited two reversible oxidations and two reductions [13]. However, NiTPhPP exhibited a reversible two electron oxidation which is common for electron deficient Ni(II)porphyrins and is well documented in literature [13]. Further, the current obtained for one two-electron oxidation in DPV is approximately double as that of one one-electron reduction of NiTPhPP.

The electron withdrawing nature of phosphoryl groups is reflected in cyclic voltammetric studies. H_2TPhPP exhibited 120-140 mV anodic shift in their first ring redox potentials as compared to H_2TPP. Similarly, metal derivatives exhibited 70-210 mV anodic shift in first ring oxidation potentials and 80-120 mV in first ring reduction potentials as compared to their corresponding MTPPs. The positive shift in first ring redox potentials of these porphyrins are interpreted in terms of electron withdrawing nature of diethoxyphophoryl groups. As the electronegativity of metal ion increases, the oxidation potential increases.

7.4 CONCLUSIONS

We have developed a facile one step synthetic route for H_2TPhPP *via* modified Lindsey method in good yield. Also, its metal complexes were synthesized and characterized. These porphyrins exhibited 70-210 mV anodic shift in their redox potentials that are interpreted in terms of strong electron withdrawing nature of diethoxyphosphoryl groups.

7.5. REFERENCES

1   Milgrom, L. R.; O'Neill, F., "Porphyrins*"*, Ch. 8. In "The Chemistry of Natural Products", Thomson, R. H., Ed.; Blackie Academic and Professional, London, **1993**; pp 329-376.

2   Huheey, J. E.; Keiter, E. A.; Keiter, R. L., "Inorganic Chemistry-Principles of Structure and Reactivity", 4th Ed., Harper Collins, New York, **2006**.

3   Odobel, F.; Blart, E.; Lagree, M.; Villieras, M.; Boujtita, H.; El Murr, N.; Caramori, S.; Bignozzi, C., "Porphyrin dyes for TiO_2 sensitization", *J. Mater. Chem.* **2003**, *13*, 502-510.

4   Deniaud, D.; Schollorn, B.; Mansuy, D.; Rouxel, J.; Battioni, P.; Bujoli, B., "Synthesis and catalytic properties of manganese porphyrins incorporated into phosphonate networks", *Chem. Mater.* **1995**, *7*, 995-1000.

5   Atefi, F.; McMurtrie, J. C.; Turner, P.; Duriska, M.; Arnold, D. P., "*Meso*-porphyrinylphosphine oxides: Mono- and bidentate ligands for supramolecular chemistry and the crystal structures of monomeric {[10,20-diphenylporphyrinatonickel(II)-5,15-diyl]-bis-[P(O)Ph₂] and polymeric self-coordinated {[10,20-diphenylporphyrinatozinc(II)-5,15-diyl]-bis-[P(O)Ph₂]}", *Inorg. Chem.* **2006**, *45*, 6479-6489.

6   Atefi, F.; McMurtrie, J. C.; Arnold, D. P., "Multiporphyrin coordination arrays based on complexation of magnesium(II) porphyrins with porphyrinylphosphine oxides", *Dalton Trans*. **2007**, 2163-2170.

7   Matano, Y.; Matsumoto, K.; Terasaka, Y.; Hotta, H.; Araki, Y.; Ito, O.; Shiro, M.; Sasamori, T.; Tokitoh, N.; Imahori, H., "Synthesis, structures, and properties of *meso*-phosphorylporphyrins: Self organization through P-oxo-zinc coordination", *Chem. Eur. J.* **2007,** *13*, 891-901.

8   Matano, Y.; Matsumoto, K.; Nakao, Y.; Uno, H.; Sakaki, S.; Imahori, H., "Regioselective *β*-metalation of *meso*-phosphanylporphyrins. Structure and optical properties of porphyrin dimers linked by peripherally fused phosphametallacycles", *J. Am. Chem. Soc.* **2008**, *130*, 4588-4589.

9   Enakieva, Y. Y.; Bessmertnykh, A. G.; Gorbunova, Y. G.; Stern, C.; Rousselin, Y.; Tsivadze, A. Y.; Guilard, R., "Synthesis of *meso*-polyphosphorylporphyrins and example of self-assembling", *Org. Lett*. **2009**, *11*, 3842-3845.

10   Kubat, P.; Lang, K.; Anzenbacher Jr., P., "Modulation of porphyrin binding to serum albumin by pH", *Biochim. Biophys. Acta* **2004**, *1670*, 40-48.

11   Lindsey, J. S.; Wagner, R. W., "Investigation of the synthesis of ortho-substituted tetraphenylporphyrins", *J. Org. Chem.* **1989**, *54*, 828-836.

12 Hau, S. K.; Cheng, Y. J.; Yip, H. L.; Zhang, Y.; Ma, H.; Jen, A. K. Y., "Effect of chemical modification of fullerene-based self-assembled monolayers on the performance of inverted polymer solar cells", *ACS Appl. Mater. Interfaces* **2010**, *2*, 1892-1902.

13 Ghosh, A.; Helvorsen, I.; Nilson, H. J.; Steene, E.; Wondimagegn, T.; Lie, R.; Caemelbecke, E. V.; Guo, N.; Ou Z.; Kadish, K. M., "Electrochemistry of nickel and copper *β*-octahalogeno-*meso*-tetraarylporphyrins. Evidence for important role played by saddling-induced metal (dx^2-y^2)-porphyrin ("a$_{2u}$") orbital interactions", *J. Phy. Chem.* B **2001**, *105*, 8120-8124.

CHAPTER 8

Summary and Conclusions

CHAPTER 8

SUMMARY AND CONCLUSIONS

Meso- and *β*-substituted porphyrins are of considerable importance owing to their use as catalysts, sensitizers in dye-sensitized solar cells (DSSCs) and photodynamic therapy (PDT), nonlinear optical (NLO) materials and biomimetic model compounds of tetrapyrroles. In chapter 1, we have discussed the biological importance of tetrapyrroles and applications of porphyrins in detail. The increase in number of substituents at the *β*-pyrrole positions of the TPP induces non-planar conformation of the porphyrin macrocycle and they exhibit unique physicochemical properties. Appending desired substituents at the pyrrole positions could provide control over shape, size, symmetry and tunable electronic properties, such porphyrins would permit facile entry into various possible materials applications. Syntheses of desired functionalized pyrroles for the preparation of mixed substituted porphyrins are often difficult and would result in lower yield of the products.

In chapter 2, we have synthesized two new families of porphyrins with mixed substituent pattern viz. 2-nitro-12,13-disubstituted-*meso*-tetraphenylporphyrins ($H_2TPP(NO_2)X_2$, X = Ph, phenylethynyl (PE), 2-thienyl (Th), Br and CN) and 2-nitro-7,8,12,13,17,18-hexasubstituted-*meso*-tetraphenylporphyrins ($H_2TPP(NO_2)X_6$, X = Br, Ph, PE and Th) and their metal (Co(II), Ni(II), Cu(II) and Zn(II)) complexes which are characterized by various spectroscopic techniques and single crystal X-ray structures. $H_2TPP(NO_2)X_6$ exhibited remarkable red-shift in the Soret band ($\Delta\lambda_{max}$ = 45 - 70 nm) and longest wavelength band, $Q_x(0,0)$ ($\Delta\lambda_{max}$ = 65 - 90 nm) as compared to $H_2TPP(NO_2)$. The single crystal structures of $MTPP(NO_2)X_2$ (M = Zn(II) and Ni(II); X = Br, Ph and PE) showed quasi-planar conformation whereas $H_2TPP(NO_2)Th_2$ and $NiTPP(NO_2)Br_6$ exhibited moderate and highly nonplanar saddle shape conformations, respectively. Further, DFT fully optimized geometries of $H_2TPP(NO_2)X_2$ and $H_2TPP(NO_2)X_6$ revealed moderate and severe saddle shape nonplanar conformations, respectively. These unsymmetrically substituted porphyrins exhibited dramatic red-shift in their B and $Q_x(0,0)$ bands as compared to $MTPP(NO_2)$ and MTPP. The dramatic downfield shift of NH proton resonances and the higher protonation/deprotonation constants of $H_2TPP(NO_2)X_6$ readily reflects the electronic effects of the mixed substituents (X) and nonplanarity of the macrocycle as compared

to $H_2TPP(NO_2)X_2$. The fairly broader range of first ring redox potentials (0.68 to 1.31 V for oxidation and -0.64 to -1.10 V for reduction) and σ values of $MTPP(NO_2)X_6$ clearly indicate the redox tunability achieved by means of unsymmetrical substitution. Further, the HOMO-LUMO gap considerably decreases as we increase the number of *β*-substituents from 3 to 7 i.e., $MTPP(NO_2)X_2$ to $MTPP(NO_2)X_6$. The remarkable red-shift in electronic spectral features, downfield shift of NH protons, the variation in protonation and deprotonation constants, the significant shift in redox potentials of these porphyrins are interpreted in terms of both inductive and resonance interactions of susbtituents on porphyrin π-system as well as nonplanarity of the macrocycle. The $\Delta E_{1/2}$ obtained from the redox potentials as well as from spectral data ($Q_x(0,0)$ band) suggests that the unsymmetrical tri- and hepta-substitution can compensate the effect of homo tetra- and octa-substitution of porphyrins (H_2TPPX_n, n = 4 and 8). By means of *β*-pyrrole mixed substitution on the porphyrin macrocycle, we were able to achieve a remarkable bathochromic shift in electronic spectral bands, varying degrees of nonplanarity, higher reactivity constants (ρ values) and tunable electrochemical redox properties with dramatic reduction in HOMO-LUMO gap.

In chapter 3, we have synthesised highly electron deficient *β*-substituted Ni(II) porphyrins (**1**-**5**) and utilized as novel sensors for selective rapid visual detection of CN^- ions. We have described about the single crystal X-ray structures, electronic spectral and electrochemical redox properties of these sensors. The ratiometric and colorimetric responses of these porphyrins were monitored by change in optical absorption spectra. These sensors were found to be highly selective for CN^- ions with extremely high binding constants (10^{16}- 10^8 M^{-2}) through axial ligation of CN^- ions and are able to detect < 0.11 ppm of CN^- ions. **1**-**5** were recovered from **1**-**5**•$2CN^-$ adduct by acid treatment and reused without loss of their sensing ability. CN^- binding strongly perturbs the redox properties of parent porphyrin π-system. The applicability of **1**-**5** as a practical visible colorimetric test kits for CN^- ions in aqueous and non-aqueous media have also been explored. The reversibility studies revealed that the sensors **1**-**5** can be recoverable and reusable for cyanide detection without losing their sensing ability. The mode of binding was confirmed by single crystal X-ray, spectroscopic studies and DFT calculations.

In chapter 4, *β*-phenylethynyl-substituted porphyrins were synthesized by Stille coupling reaction in shorter timescale as compared to literature methods. $H_2TPP(PE)_8$ exhibited red shift of 92 nm in Soret and 117 nm in longest wavelength, $Q_x(0,0)$ bands as compared to H_2TPP. $MTPP(PE)_n$ exhibited only marginal shift in first oxidation potentials (10 - 100 mV) whereas profound anodic shifts were found in the first ring reduction potentials (ΔE_{red} = 450 - 500 mV), which are interpreted in terms of electron withdrawing and conjugative effect of *β*-phenylethynyl substituents. Hence, we could observe substantial decrement in the HOMO-LUMO gap. The free base and Zn(II) porphyrins exhibited lower fluorescence quantum yields and lifetime values as compared to MTPPs. $MTPP(PE)_8$ display a strong solvatochromism which is reflected by a large red-shift in their absorption and emission maxima while increasing the solvent polarity. These porphyrins exhibited lower radiative rate constants (k_r) and enhanced nonradiative rate constants (k_{nr}) as compared to MTPP. The decrement in fluorescence lifetime values, quantum yields, radiative rate constants (k_r) and profound solvatochromism with enhanced nonradiative rate constants (k_{nr}) have been interpreted in terms of intramolecular charge transfer (ICT) from porphyrin core to phenylethynyl moieties. In general, these charge transfer transitions mixed with porphyrin B and Q transitions which was evidenced by large FWHM of B bands. Further, $ZnTPP(PE)_8$ was utilized for the colorimetric "naked-eye" detection of CN^-, F^-, Cl^-, Br^-, $H_2PO_4^-$ and CH_3COO^- ions through axial coordination of anion to Zn(II) metal centre. The enhanced Lewis acidity of $ZnTPP(PE)_8$ is further proved by axial ligation studies. Moreover, $ZnTPP(PE)_8$ exhibited extremely high binding constants (10^{12} - 10^7 M^{-2}) with anions as compared to ZnTPP.

In chapter 5, we have designed and synthesized a new series of *trans*-A_2BC porphyrins having various donor groups in two steps in good yields. These porphyrins were characterized by UV-Visible, fluorescence and ^1H NMR spectroscopic techniques and mass spectrometry. CV studies revealed cathodic shift in reduction potentials as compared to ZnTPP indicating electron donation from R groups. These dyes exhibited the power conversion efficiency from 2.2 to 4.2% indicating highly dependent nature of electron donor moiety. Among all, pyrenyl appended porphyrin (**RA-195-Zn**) exhibited 4.2% power conversion efficiency possibly due to extended π-conjugation and enhanced charge-transfer interactions. The systematic studies to support extended π-conjugation and enhanced CT interactions are in progress.

In chapter 6, we have synthesized $VOTPPCl_8$ in good yield and characterized by various spectroscopic techniques. DFT optimized structure of $VOTPPCl_8$ exhibited severe nonplanar saddle shape conformation and the oxidation state of metal ion (V^{IV}) was confirmed by EPR spectroscopy. CV studies revealed the electron deficient nature of porphyrin π-system by showing remarkable anodic shift in redox potentials as compared to VOTPP. $VOTPPCl_8$ showed very high thermal stability till 390 °C due to electron deficient nonplanar porphyrin core. Further, $VOTPPCl_8$ was utilized for the selective epoxidation of various olefins in almost quantitative yield in presence of H_2O_2/$NaHCO_3$ in CH_3CN/H_2O mixture. The formation of oxidoperoxidovanadium(V) intermediate during catalytic cycle was probed by ^{51}V NMR studies. This porphyrin catalyst ($VOTPPCl_8$) has higher thermochemical stability and recyclability.

We have developed a facile one step synthetic route for H_2TPhPP *via* modified Lindsey method in good yield which is described in chapter 7. Also, its metal complexes were synthesized and characterized. These porphyrins exhibited 70-210 mV anodic shift in their redox potentials that are interpreted in terms of strong electron withdrawing nature of diethoxy phosphoryl groups.

Herein, we have reported the synthesis and unique physciochemical properties of some *Meso-* and *β*-substituted porphyrins and utilized for anion sensing, catalysis and dye-sensitized solar cells (DSSCs) applications.

APPENDIX

APPENDIX 1

Synthesis, Spectral and Electrochemical Studies of Electronically Tunable *β*-Substituted Porphyrins with Mixed Substituent Pattern

Table of Contents (TOC)

Figure A1. The ORTEP diagrams showing top and side views of NiTPP(NO$_2$)(Th)$_2$(Py) (1a and 1b), ZnTPP(NO$_2$)(PE)$_2$(CH$_3$OH) (1d and 1e) and ZnTPP(NO$_2$)Br$_2$(CH$_3$OH) (1g and 1h). The solvates are not shown for clarity, and in side view, the β-substituents and *meso*-phenyl groups are not shown for clarity. The displacement of porphyrin-core atoms in Å from the mean plane are shown in figures 1c, 1f and 1i for NiTPP(NO$_2$)(Th)$_2$(Py), ZnTPP(NO$_2$)(PE)$_2$(CH$_3$OH) and ZnTPP(NO$_2$)Br$_2$, respectively.

Table A1. Crystal structure data of NiTPP(NO$_2$)(Ph)$_2$(Pyridine) (**1**), ZnTPP(NO$_2$)(PE)$_2$(CH$_3$OH) (**2**), ZnTPP(NO$_2$)Br$_2$(CH$_3$OH) (**3**), NiTPP(NO$_2$)Br$_6$ (**4**), and H$_2$TPP(NO$_2$)(Th)$_2$ (**5**).

	1	**2**	**3**	**4**	**5**
Empirical formula	C$_{61}$H$_{40}$N$_6$O$_2$Ni	C$_{61}$H$_{43}$N$_5$O$_4$Zn	C$_{45}$H$_{29}$N$_5$O$_5$Br$_2$Zn	C$_{88}$H$_{42}$N$_{10}$O$_4$Br$_{12}$Ni$_2$	C$_{53}$H$_{39}$C$_{l0}$N$_5$O$_4$S$_2$
Formula wt.	947.70	975.37	944.90	2379.66	874.01
Crystal system	Triclinic	Triclinic	Triclinic	Triclinic	Triclinic
Space group	P-1	P-1	P-1	P-1	P-1
a (Å)	11.938(5)	12.7702(6)	12.490(1)	14.211(5)	13.948(5)
b (Å)	12.248(5)	13.5976(6)	13.544(2)	14.367(5)	14.270(5)
c (Å)	17.642(5)	16.1781(7)	14.381(2)	19.651(5)	14.559(5)
α (º)	109.644(5)	66.257(2)	107.593(7)	89.091(5)	118.629(5)
β (º)	99.080(5)	79.410(2)	108.531(7)	89.869(5)	94.368(5)
γ (º)	94.664(5)	75.696(2)	103.813(8)	89.984(5)	112.334(5)
Volume (Å^3)	2373.8(15)	2480.46(19)	2042.3(5)	4012(2)	2230.5(14)
Z	2	2	2	2	2
D$_{cald}$ (mg/m^3)	1.326	1.306	1.537	1.970	1.301
Wavelength (Å)	0.71073	0.71073	0.71073	0.71073	0.71073
T (˚C)	293 K	293 K	293 K	293 K	293 K
No. of total reflns.	11581	12091	30281	16103	11007
No. of indepnt. reflns.	6207	8376	9620	9459	4083
R^a	0.0615	0.0625	0.1061	0.0585	0.1083
R$_w$^{b}	0.1337	0.1886	0.2598	0.1562	0.2415
CCDC	1018319	1018393	1019075	1019824	1018509

Table A2. Selected bond lengths and bond angles of NiTPP(NO$_2$)Ph$_2$(Py) (**1**), ZnTPP(NO$_2$)(PE)$_2$ (MeOH) (**2**), ZnTPP(NO$_2$)Br$_2$(MeOH) (**3**), NiTPP(NO$_2$)Br$_6$ (**4**) and H$_2$TPP(NO$_2$)(Th)$_2$ (**5**).

M = 2H, Zn, Ni
R = Th, Br, PE
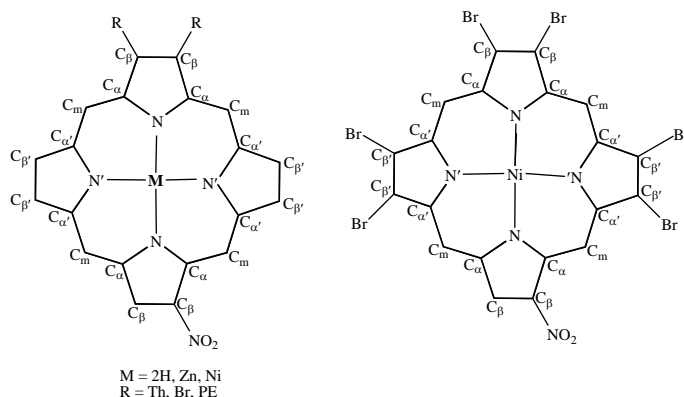
	1	**2**	**3**	**4**	**5**
	Bond Length (Å)				
M-N	**2.112(3)**	**2.088(2)**	**2.087(9)**	**1.920(6)**	-
M-N′	2.048(3)	2.042(3)	2.042(9)	1.927(6)	-
M-O/M-N	2.156(3)	2.173(3)	2.154(12)	-	-
N-C$_\alpha$	1.377(4)	1.372(4)	1.370(13)	1.384(10)	1.368(7)
N′-C$_\alpha$	1.376(4)	1.372(4)	1.349(13)	1.375(10)	1.376(6)
C$_\alpha$-C$_\beta$	1.450(5)	1.448(4)	1.453(15)	1.447(10)	1.460(7)
C$_{\alpha'}$-C$_{\beta'}$	1.439(5)	1.445(5)	1.468(15)	1.443(10)	1.422(9)
C$_\beta$-C$_\beta$	**1.349(5)**	**1.370(5)**	**1.334(15)**	**1.336(10)**	**1.340(9)**
C$_{\beta'}$-C$_{\beta'}$	1.344(5)	1.339(5)	1.298(15)	**1.349(10)**	1.358(6)
C$_\alpha$-C$_m$	1.394(4)	1.402(4)	1.404(15)	1.392(10)	1.408(9)
C$_{\alpha'}$-C$_m$	1.404(5)	1.403(4)	1.406(15)	1.399(10)	1.399(6)
ΔC$_\beta$ (Å)^a	**0.166**	**0.072**	**0.157**	**1.10**	**0.750**
Δ24 (Å)^b	**0.095**	**0.061**	**0.095**	**0.564**	**0.367**
ΔMetal (Å)	**0.397**	**0.295**	**0.237**	**0.035**	-
	Bond Angle (deg)				
M-N-C$_\alpha$	**126.2(2)**	**126.0(2)**	**125.9(8)**	**125.4(5)**	-
M-N′-C$_\alpha$	125.9(2)	126.4(2)	125.7(8)	**125.0(5)**	-
N-M-N	160.7(1)	167.9(1)	166.7(4)	169.8(3)	-
N′-M-N′	161.1(1)	166.1(1)	168.7(4)	170.2(2)	-
N-C$_\alpha$-C$_m$	**125.0(3)**	**125.2(3)**	**125.4(10)**	**123.3(7)**	**124.1(5)**
N′-C$_{\alpha'}$-C$_m$	126.4(3)	126.6(3)	127.6(10)	**122.9(7)**	125.9(5)

N-C$_\alpha$-C$_\beta$	108.8(3)	108.9(3)	108.2(10)	109.0(6)	109.7(5)
N′-C$_{\alpha'}$-C$_{\beta'}$	109.5(3)	109.2(3)	108.6(10)	108.9(6)	106.0(5)
C$_\beta$- C$_\alpha$-C$_m$	**126.1(3)**	**125.5(3)**	**126.3(10)**	**127.2(7)**	**125.9(5)**
C$_{\beta'}$- C$_{\alpha'}$-C$_m$	124.0(3)	124.2(3)	123.8(10)	**127.2(7)**	128.1(5)
C$_\alpha$-C$_m$-C$_{\alpha'}$	125.2(3)	125.0(3)	124.3(10)	120.3(7)	124.2(5)
C$_\alpha$-C$_\beta$-C$_\beta$	107.5(3)	107.0(3)	107.7(10)	107.7(7)	106.9(5)
C$_{\alpha'}$-C$_{\beta'}$-C$_{\beta'}$	107.4(3)	107.4(3)	107.5(11)	107.3(7)	108.6(6)
C$_\alpha$-N-C$_\alpha$	107.5(3)	107.9(2)	108.0(9)	106.2(6)	106.3(4)
C$_{\alpha'}$-N- C$_{\alpha'}$	106.3(3)	106.8(2)	107.8(9)	106.8(6)	110.8(4)

[a]ΔC$_\beta$ refers to the mean plane displacement of the β-pyrrole carbons

[b] Δ24 refers to the mean plane deviation of 24-atom core
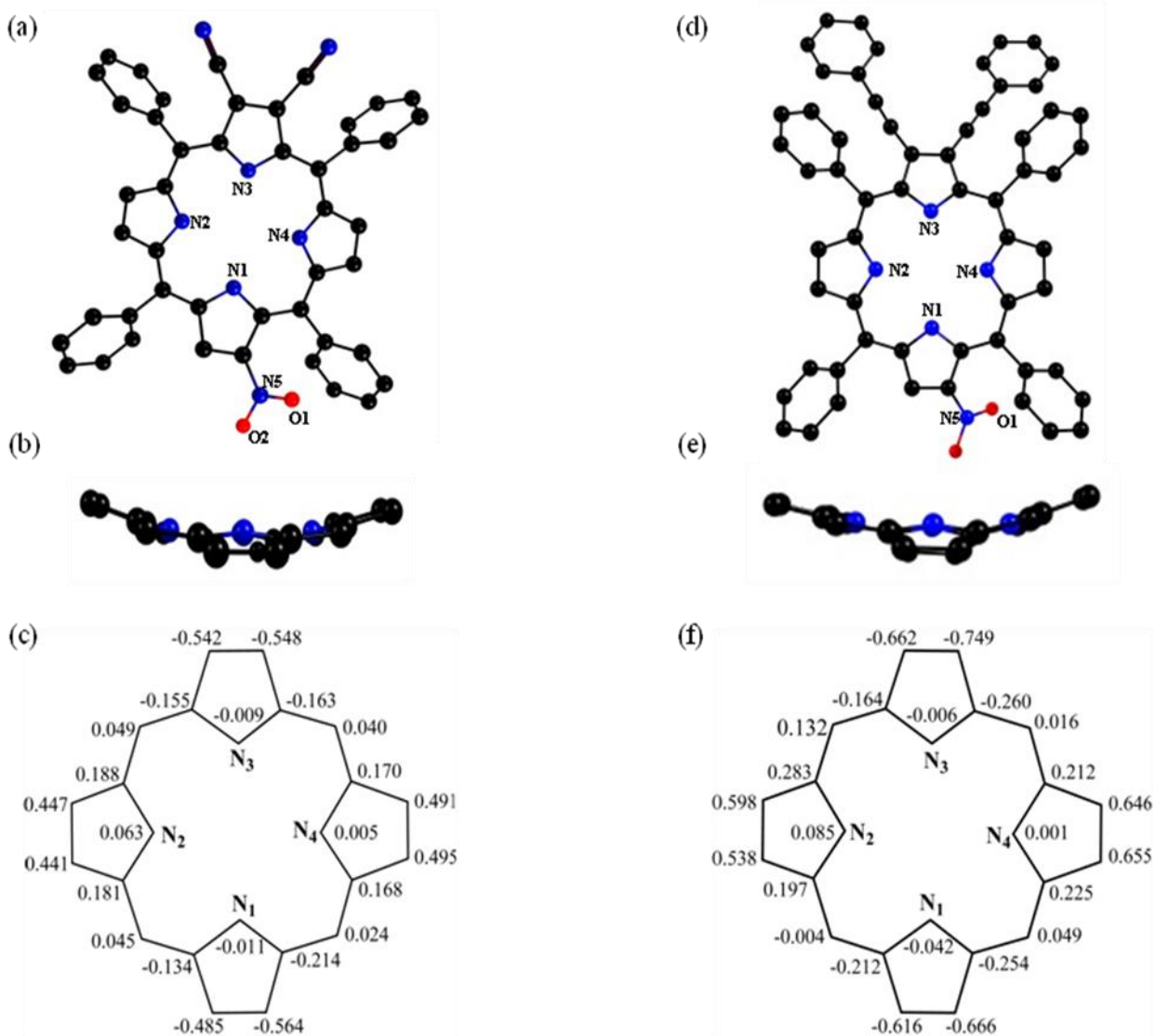
Figure A2. B3LYP/LanLD2Z optimised geometries showing top as well as side views of **H₂TPP(NO₂)(CN)₂** (**1a** and **1b**) and **H₂TPP(NO₂)(PE)₂** (**1d** and **1e**), respectively. In side view, the *β*-substituents and *meso*-phenyl groups are not shown for clarity. The displacement of porphyrin-core atoms in Å from the mean plane are shown in figures **1c** and **1f** for **H₂TPP(NO₂)(CN)₂** and **H₂TPP(NO₂)(PE)₂**, respectively. Color codes for atoms: C (black), N (blue) and O (red).
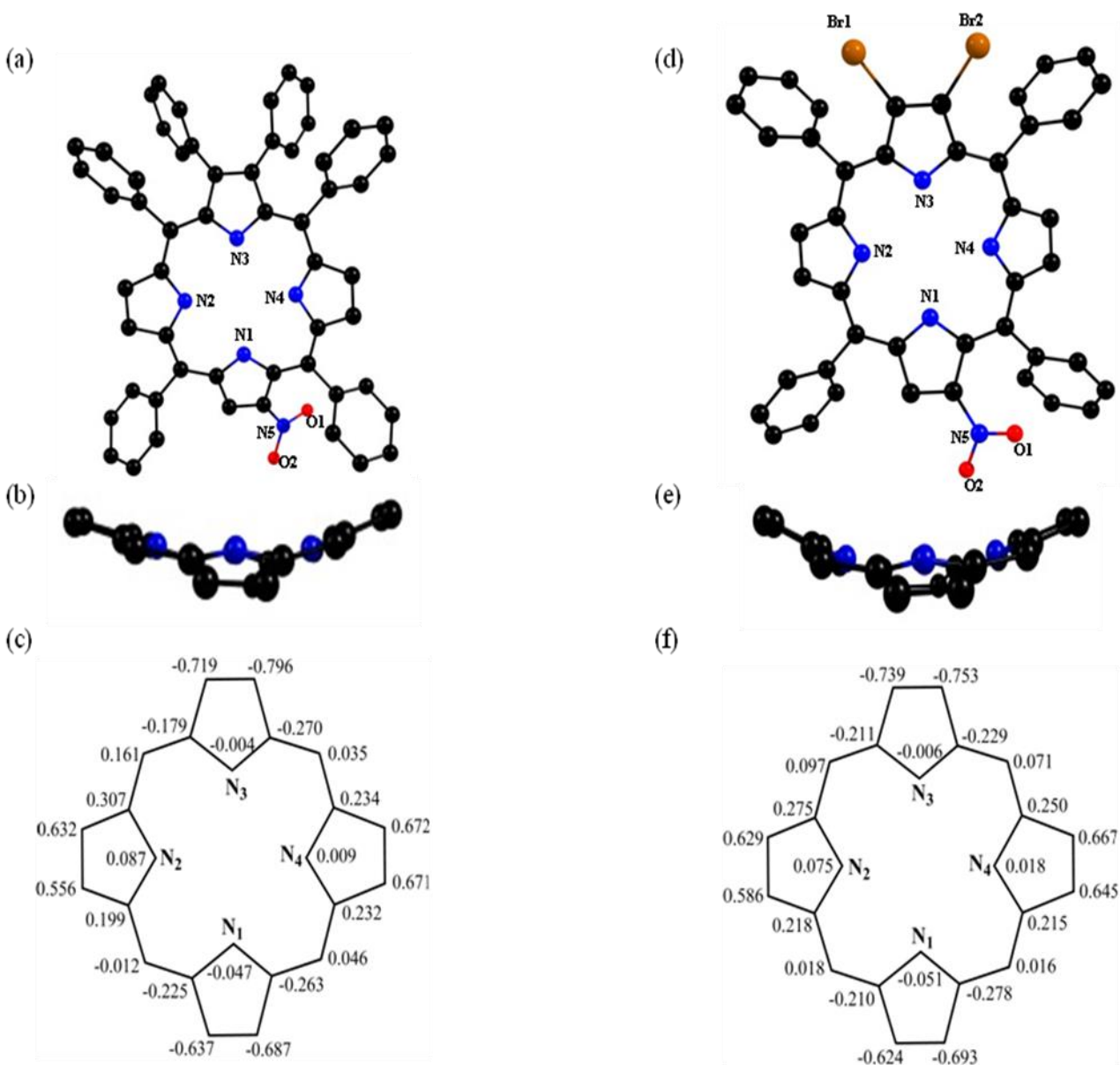
Figure A3. B3LYP/LanLD2Z optimised geometries showing top as well as side views of **H₂TPP(NO₂)Ph₂** (**1a** and **1b**) and **H₂TPP(NO₂)Br₂** (**1d** and **1e**), respectively. In side view, the *β*-substituents and *meso*-phenyl groups are not shown for clarity. The displacement of porphyrin-core atoms in Å from the mean plane are shown in figures **1c** and **1f** for **H₂TPP(NO₂)Ph₂** and **H₂TPP(NO₂)Br₂**, respectively. Color codes for atoms: C (black), N (blue), O (red) and Br (brown).
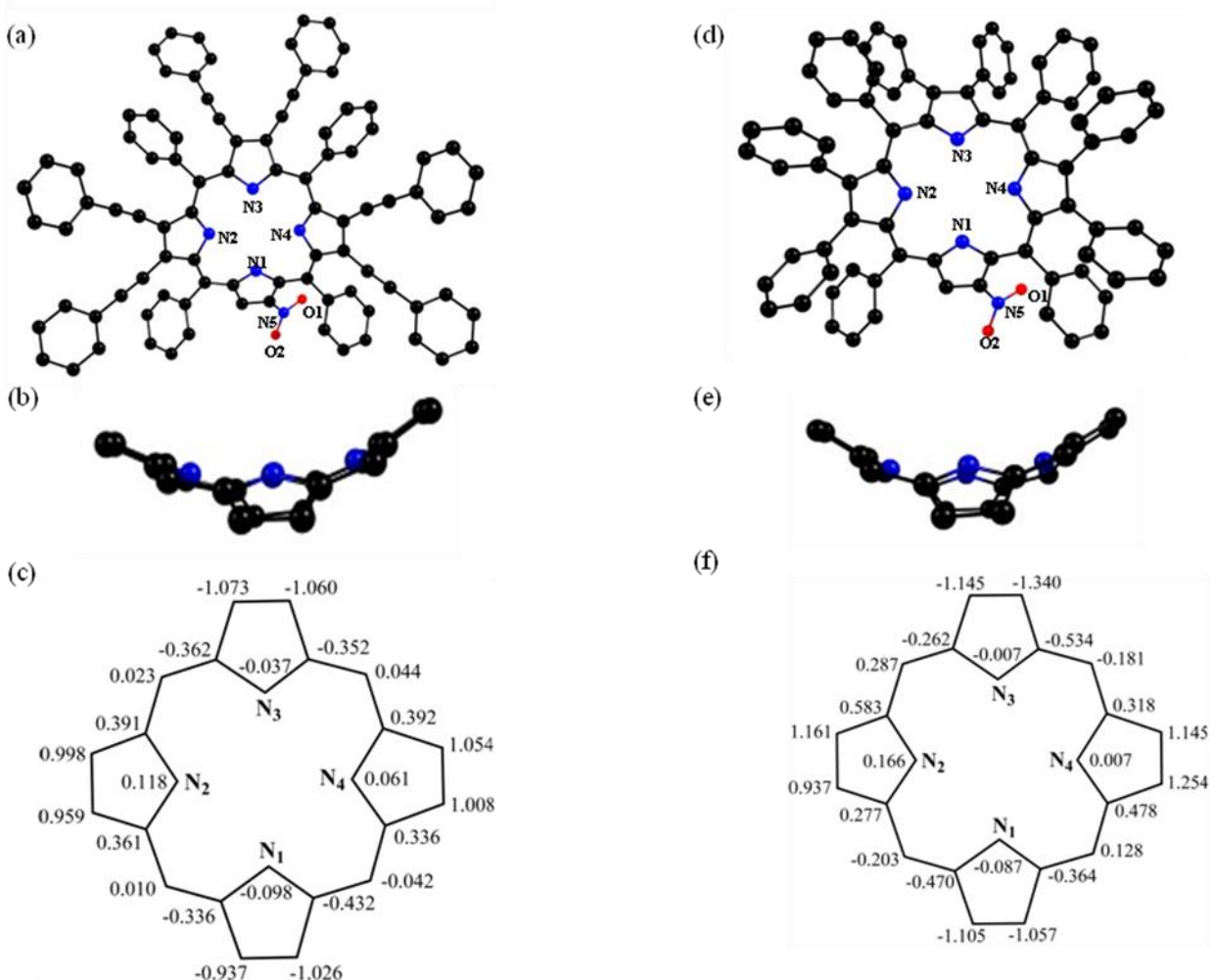
Figure A4. B3LYP/LanLD2Z optimised geometries showing top as well as side views of **H₂TPP(NO₂)(PE)₆** (**1a** and **1b**) and **H₂TPP(NO₂)Ph₆** (**1d** and **1e**), respectively. In side view, the *β*-substituents and *meso*-phenyl groups are not shown for clarity. The displacement of porphyrin-core atoms in Å from the mean plane are shown in figures **1c** and **1f** for **H₂TPP(NO₂)(PE)₆** and **H₂TPP(NO₂)Ph₆**, respectively. Color codes for atoms: C (black), N (blue) and O (red).

Table A3. Selected bond lengths (Å) and bond angles (º) for the B3LYP/LanLD2Z optimised geometries of $H_2TPP(NO_2)X_2$ (X = CN, PE, Br, Ph and Th).
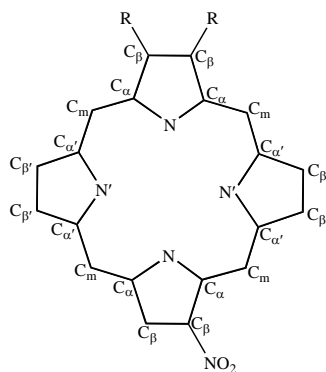
R = CN, PE, Br, Ph and **Th**

	$H_2TPP(NO_2)$ (CN)$_2$	$H_2TPP(NO_2)$ (PE)$_2$	$H_2TPP(NO_2)$ Br$_2$	$H_2TPP(NO_2)$ (Ph)$_2$	$H_2TPP(NO_2)$ (Th)$_2$
Bond Length (Å)					
N-C_α	1.386	1.387	1.389	1.388	1.387
N′-C_α	1.392	1.393	1.392	1.392	1.392
C_α-C_β	1.467	1.471	1.460	1.472	1.471
$C_{\alpha'}$-$C_{\beta'}$	1.447	1.447	1.394	1.447	1.447
C_β-C_β	1.382	1.390	1.375	1.380	1.384
$C_{\beta'}$-$C_{\beta'}$	1.380	1.380	1.380	1.381	1.381
C_α-C_m	1.423	1.423	1.420	1.424	1.425
$C_{\alpha'}$-C_m	1.411	1.413	1.413	1.412	1.413
ΔC_β (Å)[a]	**0.501**	**0.641**	**0.667**	**0.671**	**0.727**
$\Delta 24$ (Å)[b]	**0.234**	**0.294**	**0.315**	**0.320**	**0.344**
Bond Angle (deg)					
N-C_α-C_m	**125.7**	**124.7**	**124.7**	**124.6**	**124.5**
N′-$C_{\alpha'}$-C_m	127.2	127.1	127.0	126.7	126.6
N-C_α-C_β	109.5	109.8	109.2	109.9	109.9
N′-$C_{\alpha'}$-$C_{\beta'}$	106.5	106.4	106.4	106.4	106.3
C_β- C_α-C_m	**124.7**	**125.3**	**125.9**	**125.3**	**125.4**
$C_{\beta'}$- $C_{\alpha'}$-C_m	126.3	126.5	126.6	126.9	127.1
C_α-C_m-$C_{\alpha'}$	124.0	123.9	123.8	123.8	123.5
C_α-C_β-C_β	106.8	106.6	107.0	106.6	106.6
$C_{\alpha'}$-$C_{\beta'}$-$C_{\beta'}$	108.3	108.3	108.2	108.2	108.3
C_α-N-C_α	107.1	106.9	107.2	106.5	106.7
$C_{\alpha'}$-N- $C_{\alpha'}$	110.4	110.5	110.6	110.6	110.6

[a]ΔC_β refers to the mean plane displacement of the β-pyrrole carbons

[b] $\Delta 24$ refers to the mean plane deviation of 24-atom core

Table A4. Selected bond lengths (Å) and bond angles (º) for the B3LYP/LanLD2Z optimised geometries of $H_2TPP(NO_2)X_6$ (X = PE, Br, Ph and Th).

R = PE, Br, Ph and **Th**
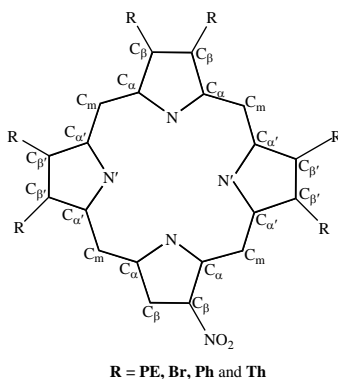
	$H_2TPP(NO_2)(PE)_6$	$H_2TPP(NO_2)Br_6$	$H_2TPP(NO_2)Ph_6$	$H_2TPP(NO_2)(Th)_6$
	Bond Length (Å)			
$N-C_\alpha$	1.387	1.388	1.386	1.385
$N'-C_\alpha$	1.389	1.391	1.387	1.386
$C_\alpha-C_\beta$	1.470	1.470	1.473	1.473
$C_{\alpha'}-C_{\beta'}$	1.453	1.451	1.457	1.456
$C_\beta-C_\beta$	1.388	1.375	1.382	1.385
$C_{\beta'}-C_{\beta'}$	1.417	1.391	1.404	1.410
$C_\alpha-C_m$	1.425	1.425	1.427	1.428
$C_{\alpha'}-C_m$	1.415	1.419	1.419	1.421
ΔC_β (Å)	**1.014**	**1.152**	**1.143**	**1.240**
$\Delta 24$ (Å)	**0.479**	**0.542**	**0.562**	**0.581**
	Bond Angle (deg)			
$N-C_\alpha-C_m$	**124.6**	**124.0**	**123.8**	**123.4**
$N'-C_{\alpha'}-C_m$	**124.5**	**123.8**	**123.2**	**123.1**
$N-C_\alpha-C_\beta$	109.7	109.2	109.8	109.6
$N'-C_{\alpha'}-C_{\beta'}$	106.1	105.2	106.3	106.2
$C_\beta-C_\alpha-C_m$	**125.5**	**126.5**	**126.2**	**126.7**
$C_{\beta'}-C_{\alpha'}-C_m$	**129.2**	**130.8**	**130.3**	**130.6**
$C_\alpha-C_m-C_{\alpha'}$	123.0	122.2	122.3	121.7
$C_\alpha-C_\beta-C_\beta$	106.1	107.0	106.6	106.6
$C_{\alpha'}-C_{\beta'}-C_{\beta'}$	107.7	108.4	107.8	107.7
$C_\alpha-N-C_\alpha$	107.0	107.3	106.8	107.8
$C_{\alpha'}-N-C_{\alpha'}$	111.9	112.2	111.5	111.8

[a] ΔC_β refers to the mean plane displacement of the β-pyrrole carbons

[b] $\Delta 24$ refers to the mean plane deviation of 24-atom core

Table A5. Optical absorption spectral data of metal complexes of mixed substituted porphyrins

Porphyrin	B band(s), nm	Q band(s), nm
CoTPP(NO$_2$)	382(sh), 420(5.08)	540(4.03), 578(3.94)
CoTPP(NO$_2$)Br$_2$	383(sh), 431(5.04)	551(3.94), 595(4.02)
CoTPP(NO$_2$)Ph$_2$	388(sh), 434(4.98)	553(3.96), 593(3.98)
CoTPP(NO$_2$)(PE)$_2$	441(5.16)	609(4.30)
CoTPP(NO$_2$)Th$_2$	435(5.07)	602(4.13)
CoTPP(NO$_2$)(CN)$_2$	431(5.18)	609(4.39)
CoTPP(NO$_2$)Br$_6$	453(5.11)	567(4.07)
CoTPP(NO$_2$)Ph$_6$	400(sh), 454(5.01)	570(4.00), 611(3.96)
CoTPP(NO$_2$)(PE)$_6$	487(5.29)	597(4.39)
CoTPP(NO$_2$)Th$_6$	464(5.00)	580(4.13), 627(3.96)
NiTPP(NO$_2$)	386(sh), 428(5.14)	539(4.07), 583(3.97)
NiTPP(NO$_2$)Br$_2$	385(sh), 437(5.17)	548(4.02), 597(4.11)
NiTPP(NO$_2$)Ph$_2$	389(sh), 440(5.10)	550(4.04), 598(4.07)
NiTPP(NO$_2$)(PE)$_2$	446(5.23)	561(4.06), 614(4.94)
NiTPP(NO$_2$)Th$_2$	323(4.26), 441(5.12)	555(4.03), 605(4.17)
NiTPP(NO$_2$)(CN)$_2$	435(5.25)	612(4.47)
NiTPP(NO$_2$)Br$_6$	348(4.36), 454(5.22)	565(4.16), 603(3.90)
NiTPP(NO$_2$)Ph$_6$	456(5.04)	569(4.03), 621(3.99)
NiTPP(NO$_2$)(PE)$_6$	489(5.30)	598(4.43), 638(4.16)
NiTPP(NO$_2$)Th$_6$	466(5.09)	580(4.17), 631(4.09)
CuTPP(NO$_2$)	380(sh), 422(5.26)	547(4.15), 589(3.96)
CuTPP(NO$_2$)Br$_2$	430(5.23)	556(4.02), 600(4.05)
CuTPP(NO$_2$)Ph$_2$	384(sh), 432(5.18)	556(4.06), 601(4.00)
CuTPP(NO$_2$)(PE)$_2$	442(5.28)	565(4.05), 613(4.30)
CuTPP(NO$_2$)Th$_2$	433(5.23)	561(4.07), 608(4.14)
CuTPP(NO$_2$)(CN)$_2$	434(5.41)	571(3.99), 618(4.58)
CuTPP(NO$_2$)Br$_6$	361(4.34), 461(5.01)	584(4.07), 625(3.80)
CuTPP(NO$_2$)Ph$_6$	450(5.01)	582(4.02), 630(3.90)
CuTPP(NO$_2$)(PE)$_6$	493(5.28)	610(4.43)
CuTPP(NO$_2$)Th$_6$	460(4.81)	596(3.93), 639(3.72)
ZnTPP(NO$_2$)	426(5.23)	556(4.07), 599(3.90)

ZnTPP(NO$_2$)Br$_2$	340(4.29), 433(5.36)	562(4.12), 606(4.10)
ZnTPP(NO$_2$)Ph$_2$	435(5.27)	561(4.12), 607(4.00)
ZnTPP(NO$_2$)(PE)$_2$	446(5.38)	573(4.16), 620(4.35)
ZnTPP(NO$_2$)Th$_2$	437(5.25)	564(4.07), 612(4.08)
ZnTPP(NO$_2$)(CN)$_2$	442(5.42)	634(4.47)
ZnTPP(NO$_2$)Br$_6$	377(4.38), 476(5.00)	600(sh), 682(4.11)
ZnTPP(NO$_2$)Ph$_6$	379(4.37), 467(5.07)	595(3.90), 648(3.86)
ZnTPP(NO$_2$)(PE)$_6$	494(5.35)	613(4.35), 696(sh)
ZnTPP(NO$_2$)Th$_6$	476(5.06)	607(4.01), 663(3.92)

Values in parentheses refer to log ε (ε in Mol^{-1} cm^{-1}).

Table A6. Fluorescence Spectral data of mixed substituted porphyrins in CH$_2$Cl$_2$ at 298 K.

Porphyrin	λ_{Ex}nm	$\lambda_{fl,max}$nm	Quantum Yield, ϕ_f	Stoke shift (nm)	Stokes shift (cm^{-1})
H$_2$TPP(NO$_2$)Ph$_2$	439	756	0.0167	70	1350
H$_2$TPP(NO$_2$)(PE)$_2$	444	746	0.0180	59	1151
H$_2$TPP(NO$_2$)Th$_2$	440	768, 805(sh)	0.0092	73	1367
H$_2$TPP(NO$_2$)(CN)$_2$	440	728	0.0582	26	509
H$_2$TPP(NO$_2$)(PE)$_6$	494	813	0.0023	62	1016
ZnTPP(NO$_2$)Ph$_2$	435	709	0.0110	102	2370
ZnTPP(NO$_2$)(PE)$_2$	446	687	0.0160	67	1573
ZnTPP(NO$_2$)Th$_2$	437	712	0.0100	100	2295
ZnTPP(NO$_2$)(CN)$_2$	442	662	0.0334	28	667
ZnTPP(NO$_2$)(PE)$_6$	494	737	0.0051	41	799
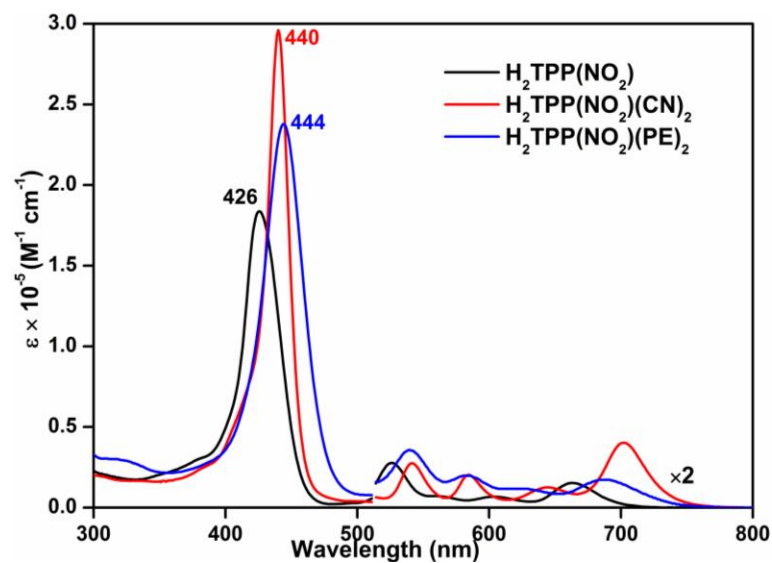
Figure A5. Electronic absorption spectra of $H_2TPP(NO_2)X_2$ (X = H, CN, PE) derivatives in CH_2Cl_2 at 298 K. Q bands are magnified 3 times.
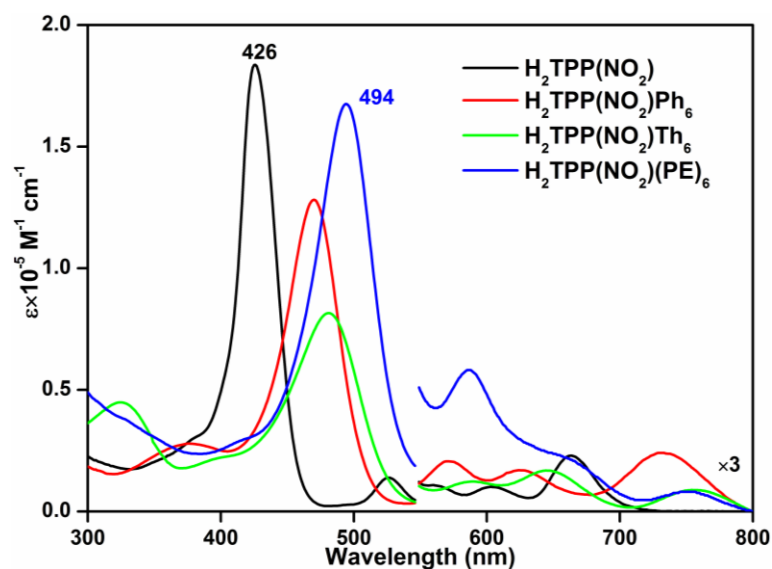
Figure A6. UV- Visible spectra of $H_2TPP(NO_2)X_6$ (X = H, Ph, Th, PE) derivatives in CH_2Cl_2 at 298 K. Q bands are magnified 3 times.
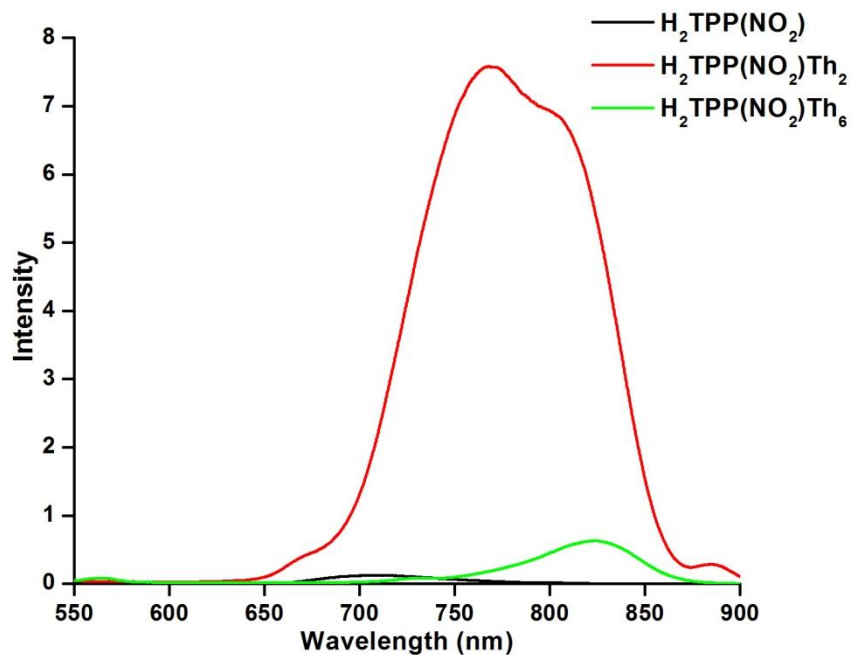
Figure A7.Fluorescence spectra of $H_2TPP(NO_2)Th_n$ (n = 0, 2, 6) in CH_2Cl_2 at 298 K.

(a)   **(b)**
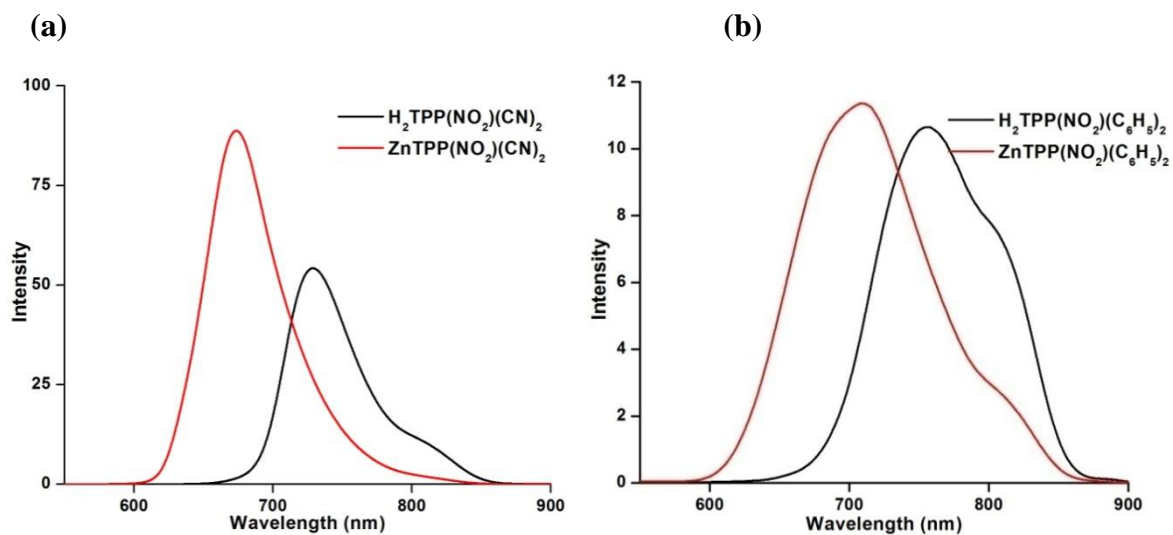
Figure A8. Emission spectra of (a) $MTPP(NO_2)(CN)_2$ and (b) $MTPP(NO_2)(C_6H_5)_2$, where M = 2H and Zn(II) in CH_2Cl_2 at 298 K.

Figure A9. Fluorescence spectra of (a) MTPP(NO$_2$)(PE)$_2$ and (b) MTPP(NO$_2$)(PE)$_6$ (M = 2H, Zn(II)) in CH$_2$Cl$_2$ at 298 K.

(a) (b)
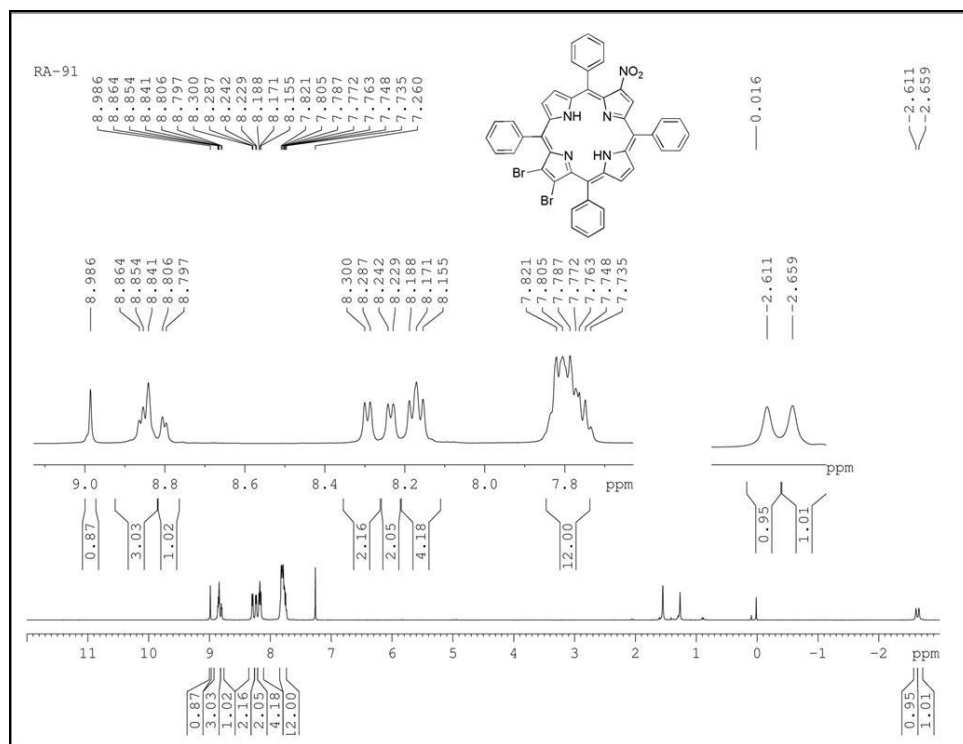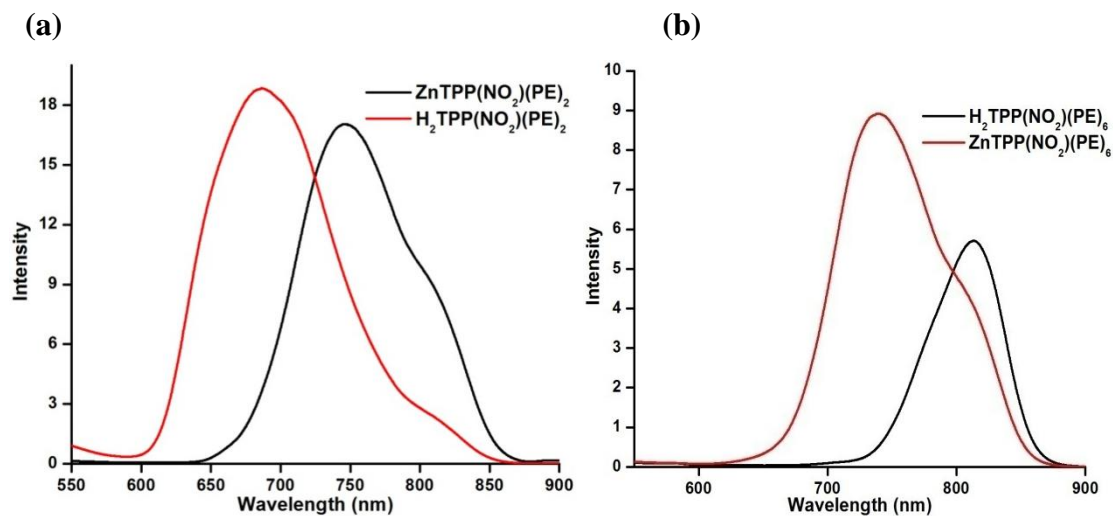
Figure A10.^{1}H NMR spectrum of H$_2$TPP(NO$_2$)Br$_2$ in CDCl$_3$at 298 K.

Figure A11. ^{1}H NMR spectrum of NiTPP(NO$_2$)Br$_2$ in CDCl$_3$.

Figure A12. ^{1}H NMR spectrum of ZnTPP(NO$_2$)Br$_2$ in CDCl$_3$.
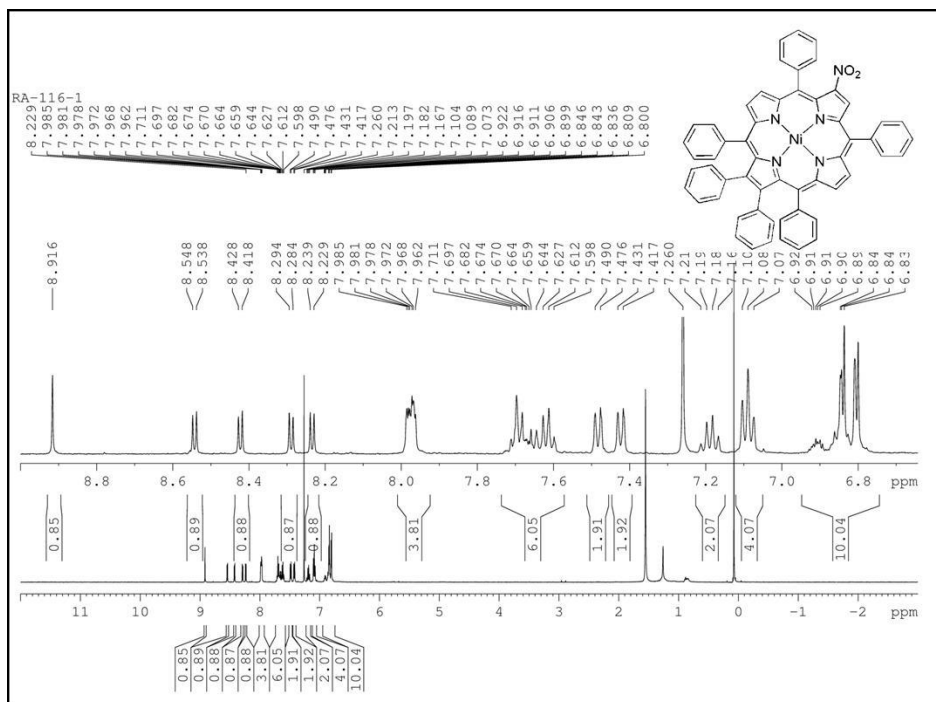
Figure A13. ^{1}H NMR spectrum of NiTPP(NO$_2$)Ph$_2$ in CDCl$_3$.
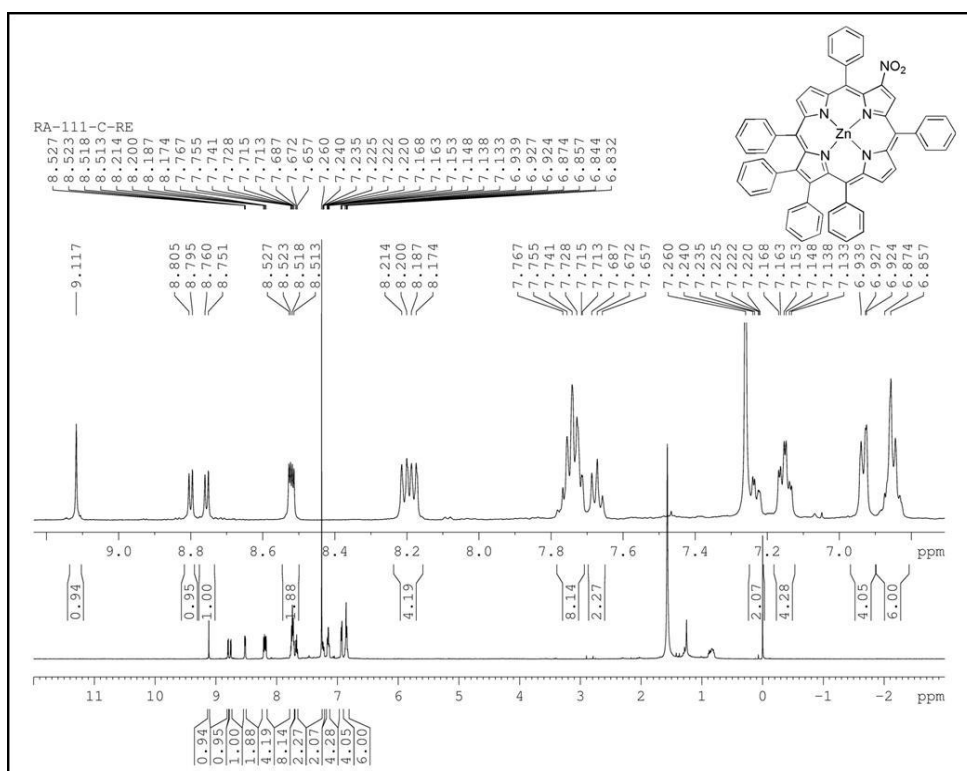
Figure A14. ^{1}H NMR spectrum of ZnTPP(NO$_2$)Ph$_2$ in CDCl$_3$.

Figure A15. ^{1}H NMR spectrum of $H_2TPP(NO_2)(PE)_2$ in $CDCl_3$.

Figure A16. ^{1}H NMR spectrum of $H_2TPP(NO_2)Th_2$ in $CDCl_3$.

Figure A17. ^{1}H NMR spectrum of NiTPP(NO$_2$)Th$_2$ in CDCl$_3$.

Figure A18. ^{1}H NMR spectrum of ZnTPP(NO$_2$)Th$_2$ in CDCl$_3$.
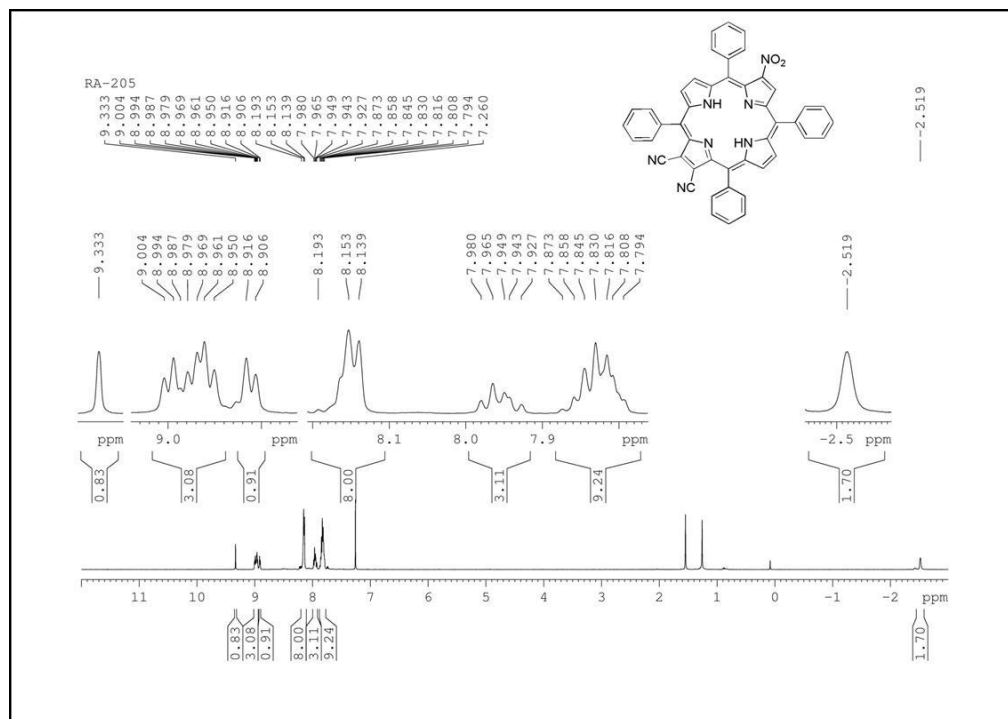
Figure A19. ^{1}H NMR spectrum of $H_2TPP(NO_2)(CN)_2$ in $CDCl_3$.
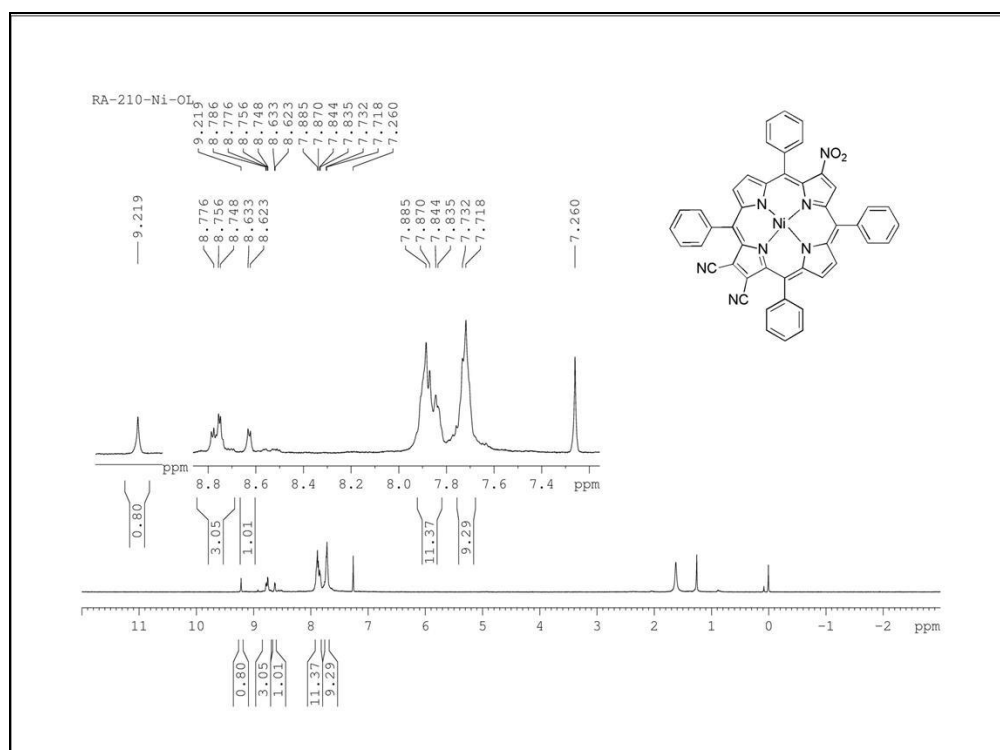
Figure A20. ^{1}H NMR spectrum of $NiTPP(NO_2)(CN)_2$ in $CDCl_3$.
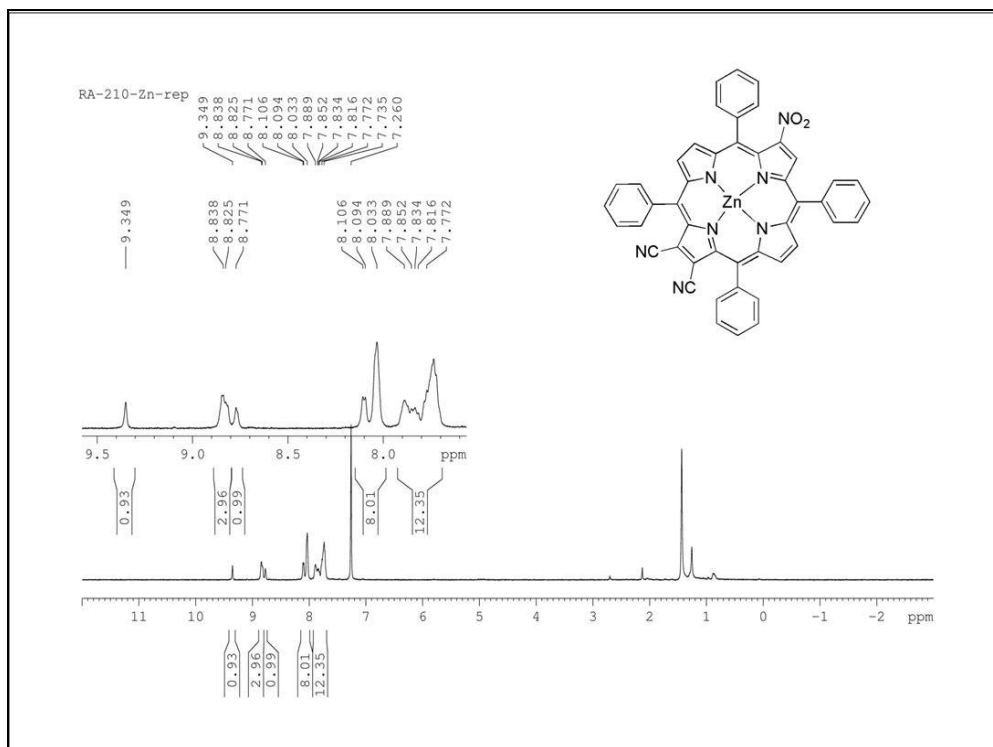
Figure A21. 1H NMR spectrum of ZnTPP(NO$_2$)(CN)$_2$ in CDCl$_3$.
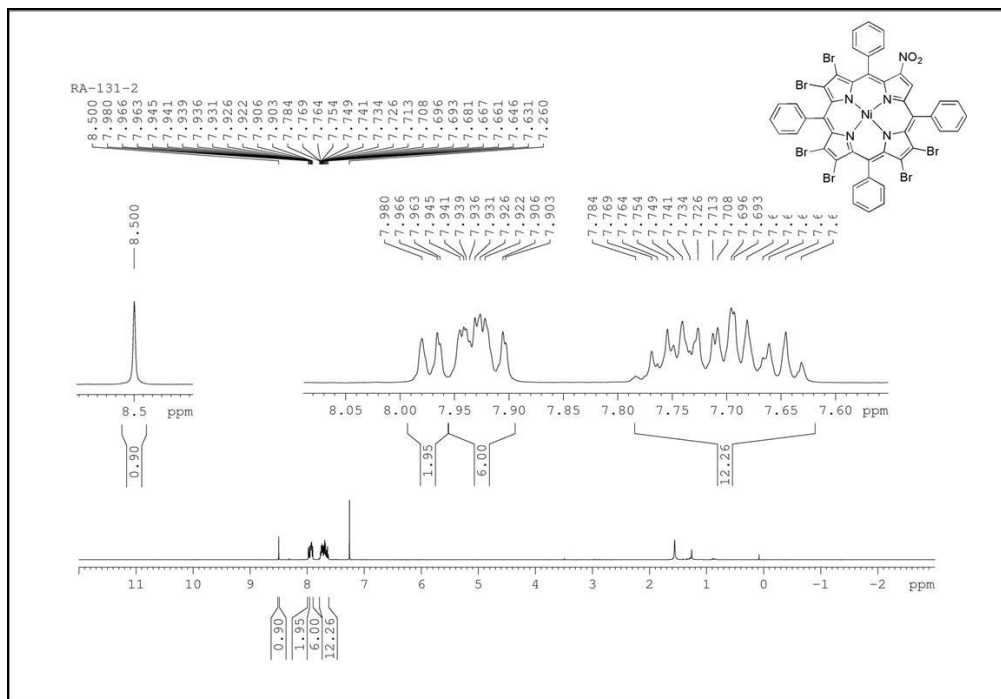
Figure A22. ^{1}H NMR spectrum of NiTPP(NO$_2$)Br$_6$ in CDCl$_3$.
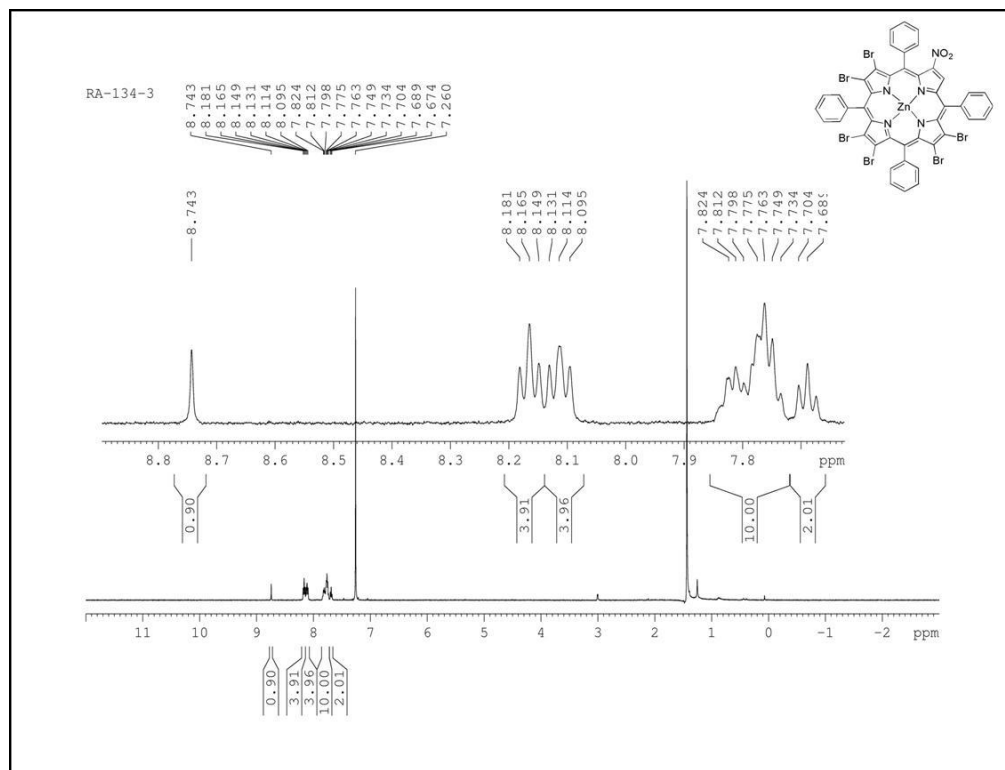
Figure A23. ^{1}H NMR spectrum of ZnTPP(NO$_2$)Br$_6$ in CDCl$_3$.
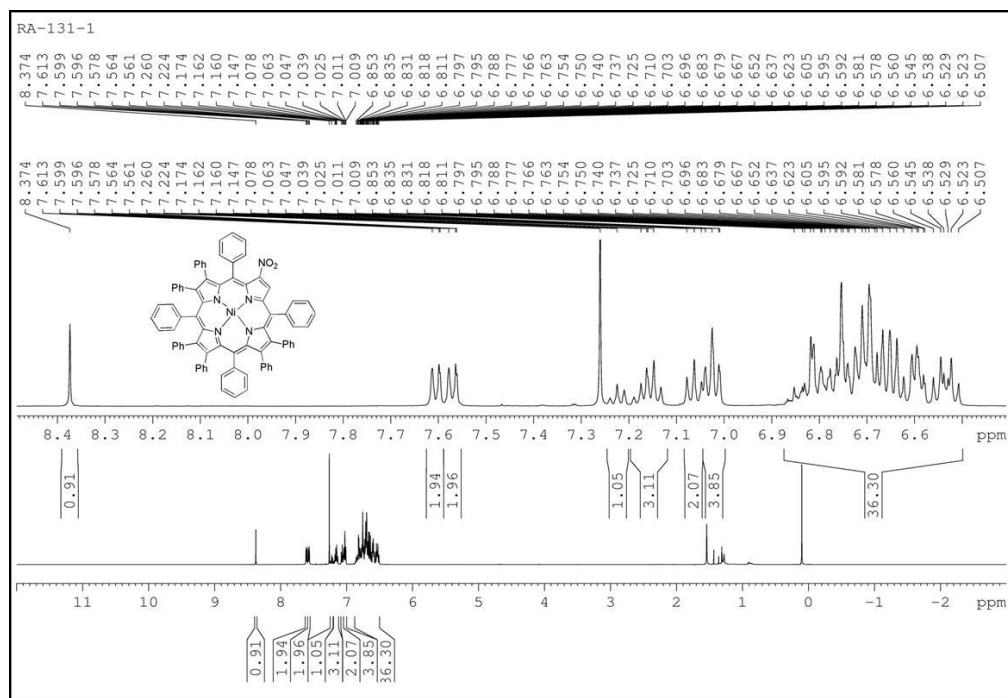
Figure A24. ^{1}H NMR spectrum of NiTPP(NO$_2$)Ph$_6$ in CDCl$_3$.

Figure A25. ^{1}H NMR spectrum of ZnTPP(NO$_2$)Ph$_6$ in CDCl$_3$.

Figure A26. 1H NMR spectrum of NiTPP(NO$_2$)(PE)$_6$ in CDCl$_3$

Figure A27. 1H NMR spectrum of ZnTPP(NO$_2$)(PE)$_6$ in CDCl$_3$

(a). H$_2$TPP(NO$_2$)(PE)$_6$ (2)

(b). H$_2$TPP(NO$_2$)Th$_6$ (3)
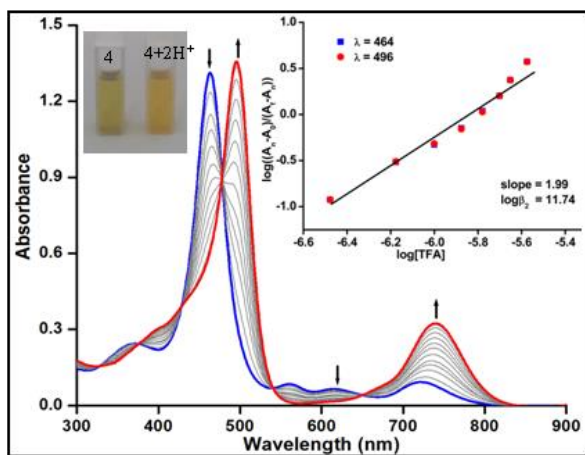
(c). $H_2TPP(NO_2)Ph_6$ (4)

(d). $H_2TPP(NO_2)Br_2$ (5)
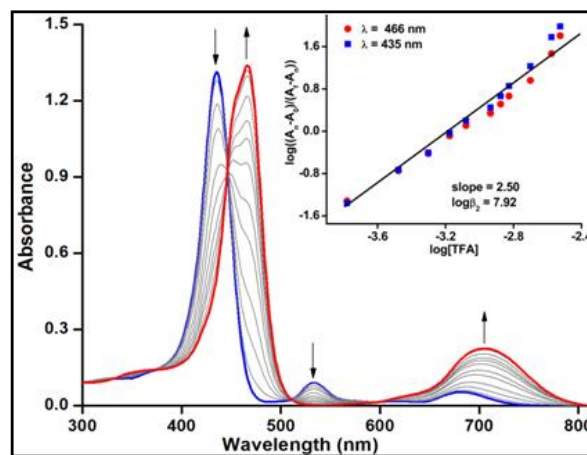
(e). $H_2TPP(NO_2)(PE)_2$ (6)
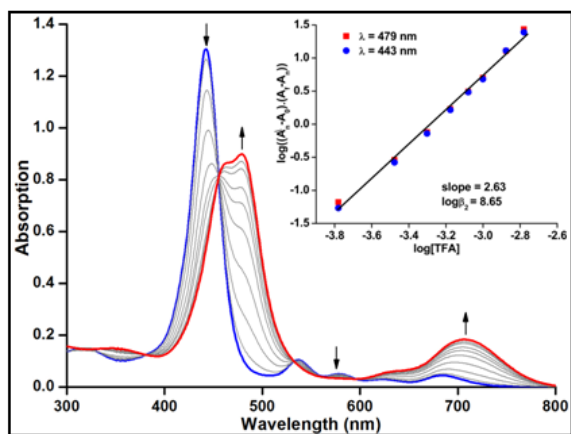
(f). $H_2TPP(NO_2)Ph_2$ (7)
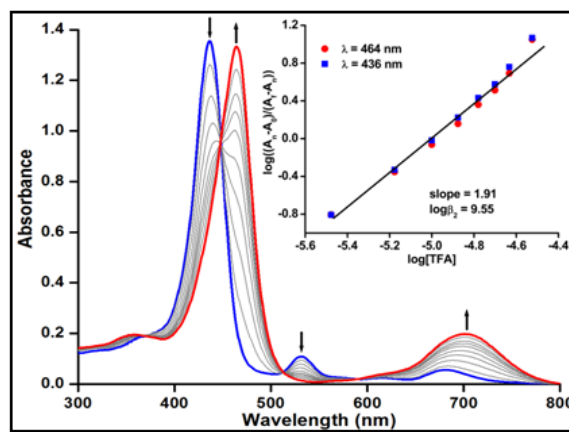
(g). $H_2TPP(NO_2)Th_2$ (8)
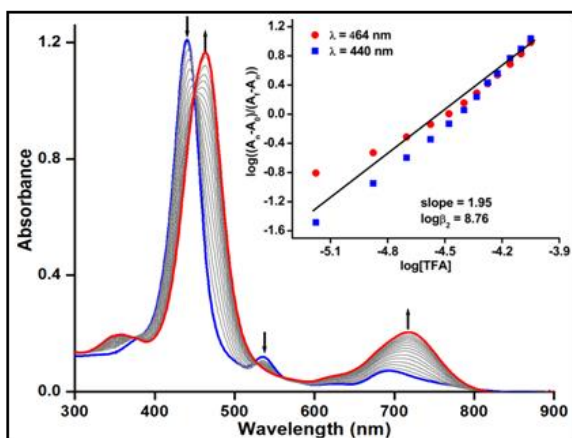
(h). $H_2TPP(NO_2)CN_2$ (9)
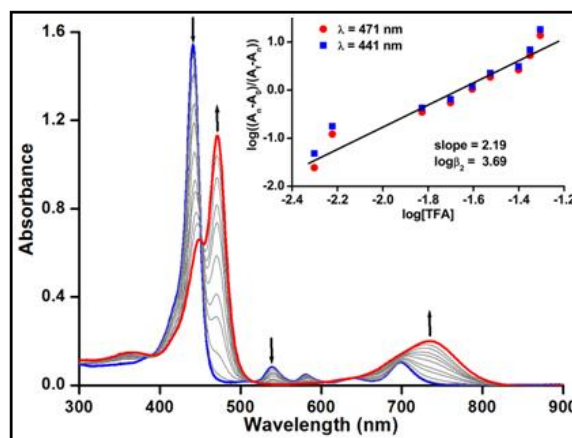
Figure A28. UV-Visible spectral changes during titration of **2-9** while increasing [TFA], insets show the corresponding Hill plots.

(a). $H_2TPP(NO_2)(PE)_6$ (2)
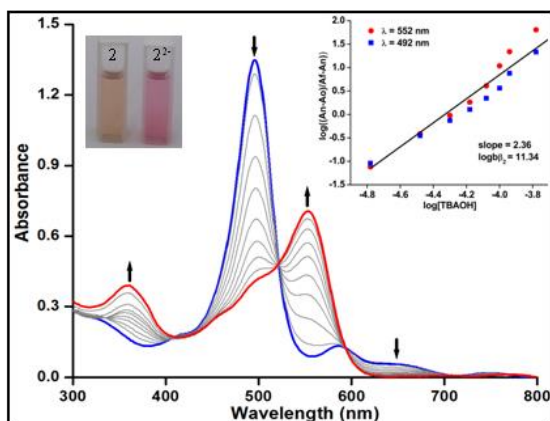
(b). $H_2TPP(NO_2)Th_6$ (3)
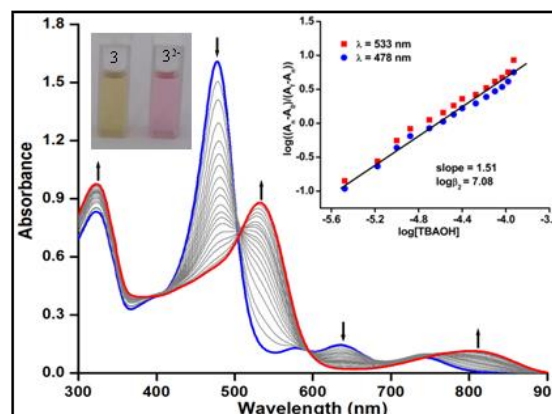
(c). $H_2TPP(NO_2)Ph_6$ (4)
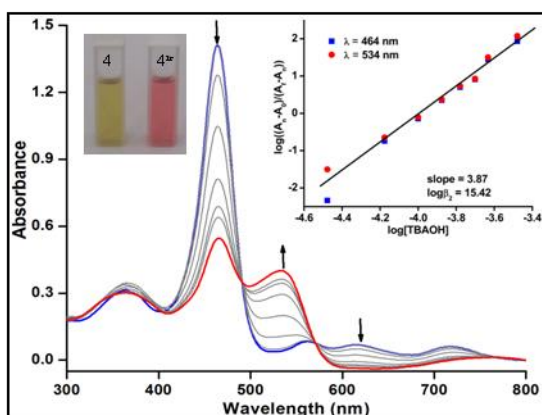
Figure A29. UV-Visible spectral changes during titration of TBAOH, insets show Hill plots.

Table A7. Electrochemical redox data of various metal complexes of mixed substituted porphyrins in CH_2Cl_2 containing 0.1 M $TBAPF_6$ with a scan rate of 0.1 V/s at 298 K.

Porphyrin	Oxidation (mV)		Reduction (mV)			Metal Centred		ΔE (mV)
						Oxdn.	Redn.	
	I	II	I	II	III	I	II	
CoTPP	1060	1315	-1380			850	-860	2440
CoTPP(NO$_2$)	1175	1421	-1298			910	-661	2473
CoTPP(NO$_2$)Br$_2$	1223	1442	-1208			922	-515	2431
CoTPP(NO$_2$)Ph$_2$	1134	1348	-1292			886	-644	2426
CoTPP(NO$_2$)(PE)$_2$	1212	1414	-1187			957	-545	2399
CoTPP(NO$_2$)Th$_2$	1117	1317	-1260			881	-585	2377
CoTPP(NO$_2$)(CN)$_2$	1267	1391	-1147			965	-380	2414

CoTPP(NO$_2$)Br$_6$	1377	1513	-1103			1012	-269	2480	
CoTPP(NO$_2$)Ph$_6$	1082	1192	-1382			801	-638	2463	
CoTPP(NO$_2$)(PE)$_6$	1273	1397	-1073			1009	-337	2346	
CoTPP(NO$_2$)Th$_6$	1158	-	-1253			884	-472	2411	
NiTPP	1020	1315	-1280	-1720				2300	
NiTPP(NO$_2$)	1187	1316	-948	-1212				2136	
NiTPP(NO$_2$)Br$_2$	1242[a]	-	-829	-1061				2071	
NiTPP(NO$_2$)Ph$_2$	1116	1241	-939	-1200				2055	
NiTPP(NO$_2$)(PE)$_2$	1193	1306	-818	-1032				2011	
NiTPP(NO$_2$)Th$_2$	1119	1238	-908	-1137				2027	
NiTPP(NO$_2$)(CN)$_2$	1296[a]	-	-734	-966				2030	
NiTPP(NO$_2$)Br$_6$	1305[a]	-	-703	-950				2008	
NiTPP(NO$_2$)Ph$_6$	956	1183	-988	-1275				1944	
NiTPP(NO$_2$)(PE)$_6$	1244[a]	-	-732	-943				1976	
NiTPP(NO$_2$)Th$_6$	1018	1266	-902	-1165				1920	
CuTPP	970	1350	-1325	-1705				2295	
CuTPP(NO$_2$)	1076	1442	-979	-1229				2055	
CuTPP(NO$_2$)Br$_2$	1072	1491	-856	-1074				1928	
CuTPP(NO$_2$)Ph$_2$	962	1320	-967	-1214				1929	
CuTPP(NO$_2$)(PE)$_2$	1061	1456	-847	-1055				1908	
CuTPP(NO$_2$)Th$_2$	956	1402	-911	-1140				1867	
CuTPP(NO$_2$)(CN)$_2$	1331	1599	-626	-1049				1957	
CuTPP(NO$_2$)Br$_6$	1066	1609	-693	-922				1753	
CuTPP(NO$_2$)Ph$_6$	698	1213	-985	-1288				1683	
CuTPP(NO$_2$)(PE)$_6$	1013	1498	-749	-944	-1421			1762	
CuTPP(NO$_2$)Th$_6$	780	1305	-864	-1163				1644	
ZnTPP	835	1140	-1360	-1765				2195	
ZnTPP(NO$_2$)	913	1217	-1048[i]	-1192	-1500			1961	
ZnTPP(NO$_2$)Br$_2$	948	1182	-939[i]	-1080				1887	
ZnTPP(NO$_2$)Ph$_2$	850	1074	-1064[i]	-1204	-1498			1914	
ZnTPP(NO$_2$)(PE)$_2$	933	1181	-953[i]	-1085				1886	
ZnTPP(NO$_2$)Th$_2$	875	1106	-993[i]	-1126	-1376			1868	
ZnTPP(NO$_2$)(CN)$_2$	1069	1429	-698	-1089				1767	
ZnTPP(NO$_2$)Br$_6$	931	1192	-839[i]	-977	-1227			1770	
ZnTPP(NO$_2$)Ph$_6$	686	853	-1076[i]	-1377[i]				1762	
ZnTPP(NO$_2$)(PE)$_6$	925	1176	-858[i]	-976				1783	
ZnTPP(NO$_2$)Th$_6$	754	985	-931[i]	-1106	-1496			1685	[a]refers

two electron oxidation and [i]refers to irreversibl
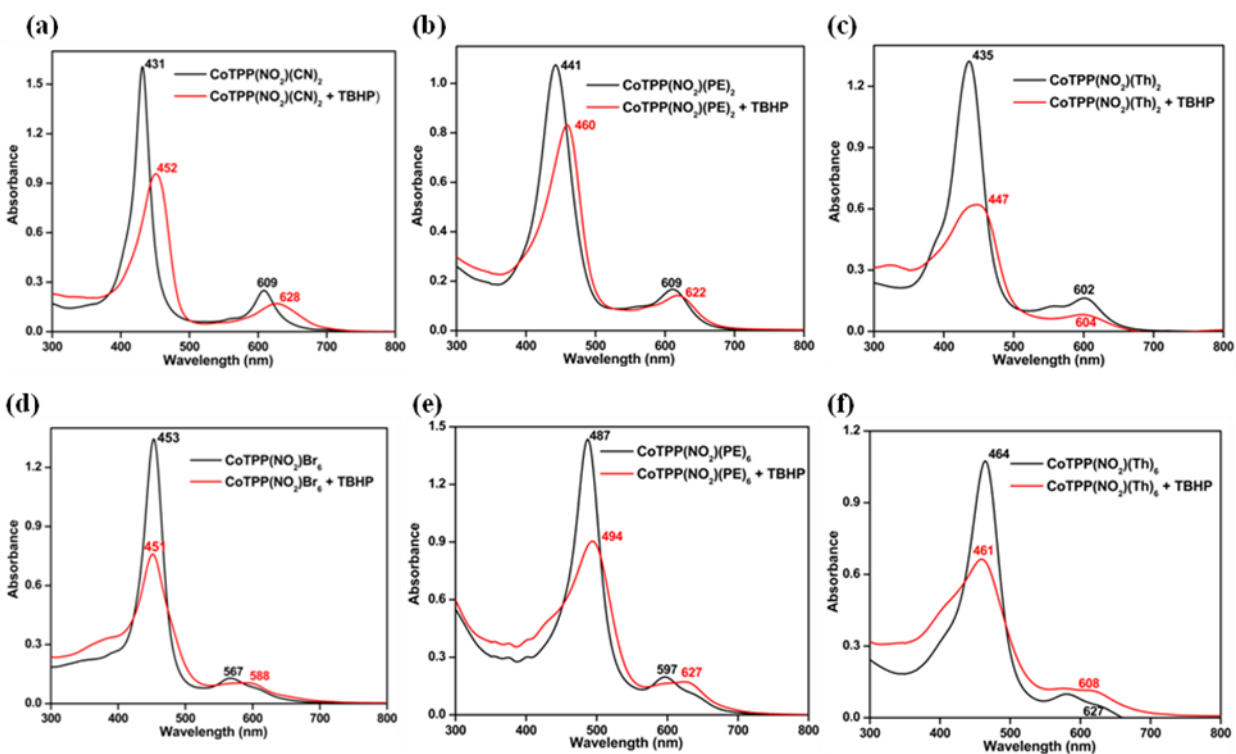
Figure A30. UV-Visible spectral changes of Co(II) porphyrins upon addition of *tert*-butyl hydroperoxide (conversion of Co(II) to Co(III) porphyrins) in CH_2Cl_2 at 298 K.

Table A8. UV-Visible spectral data of Co(II) and Co(III) porphyrins in CH_2Cl_2 at 298 K.

Porphyrin	Without TBHP (Co^{II})		With TBHP (Co^{III})	
	B band, nm	Q band(s), nm	B band, nm	Q band(s), nm
$CoTPP(NO_2)$	420	540, 578	442	557
$CoTPP(NO_2)Br_2$	431	551, 595	450	597
$CoTPP(NO_2)Ph_2$	434	553, 593	430	588
$CoTPP(NO_2)(PE)_2$	441	609	460	620
$CoTPP(NO_2)Th_2$	435	602	447	604
$CoTPP(NO_2)(CN)_2$	431	609	452	628
$CoTPP(NO_2)Br_6$	453	567	451	588
$CoTPP(NO_2)Ph_6$	454	570, 611	446	604
$CoTPP(NO_2)(PE)_6$	487	597	494	627
$CoTPP(NO_2)Th_6$	464	580, 627	461	608
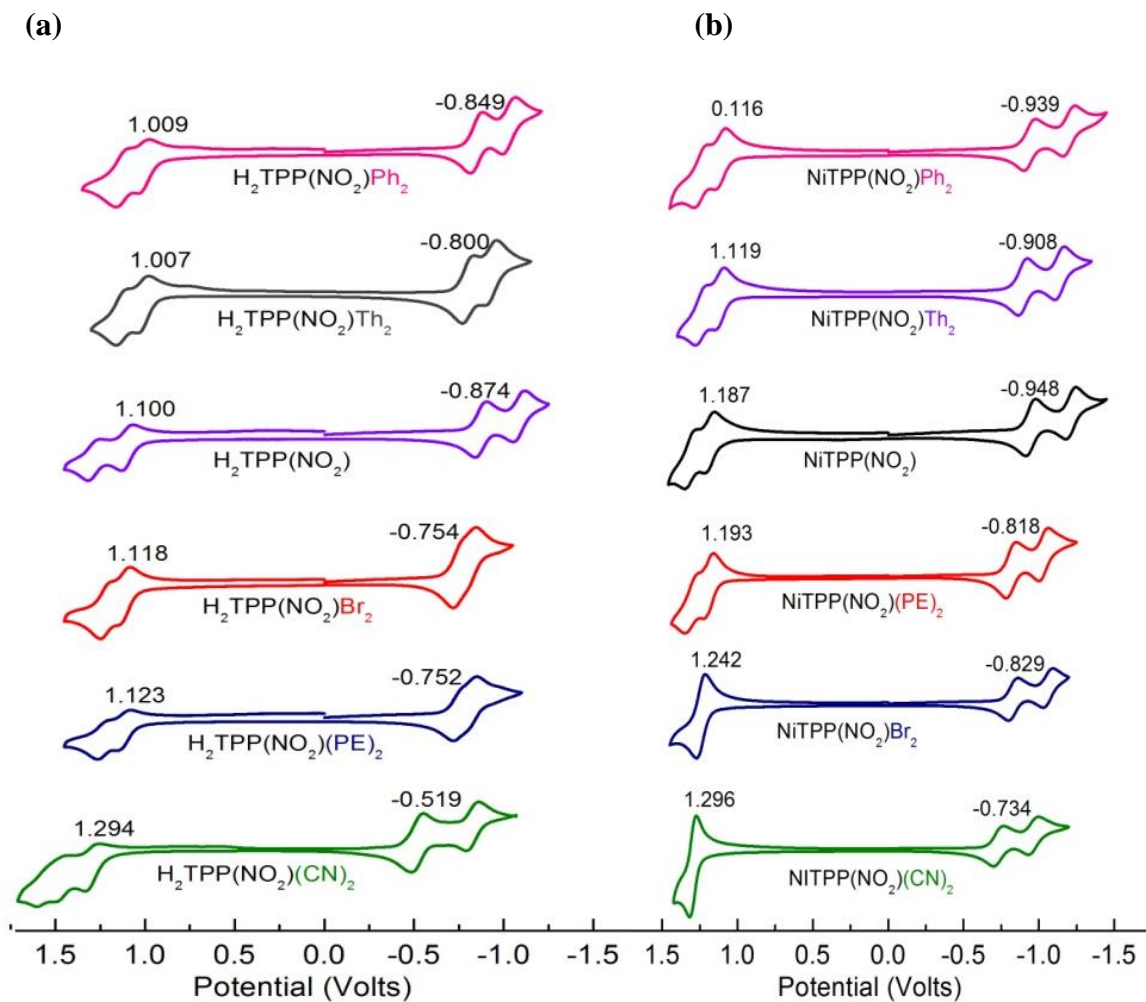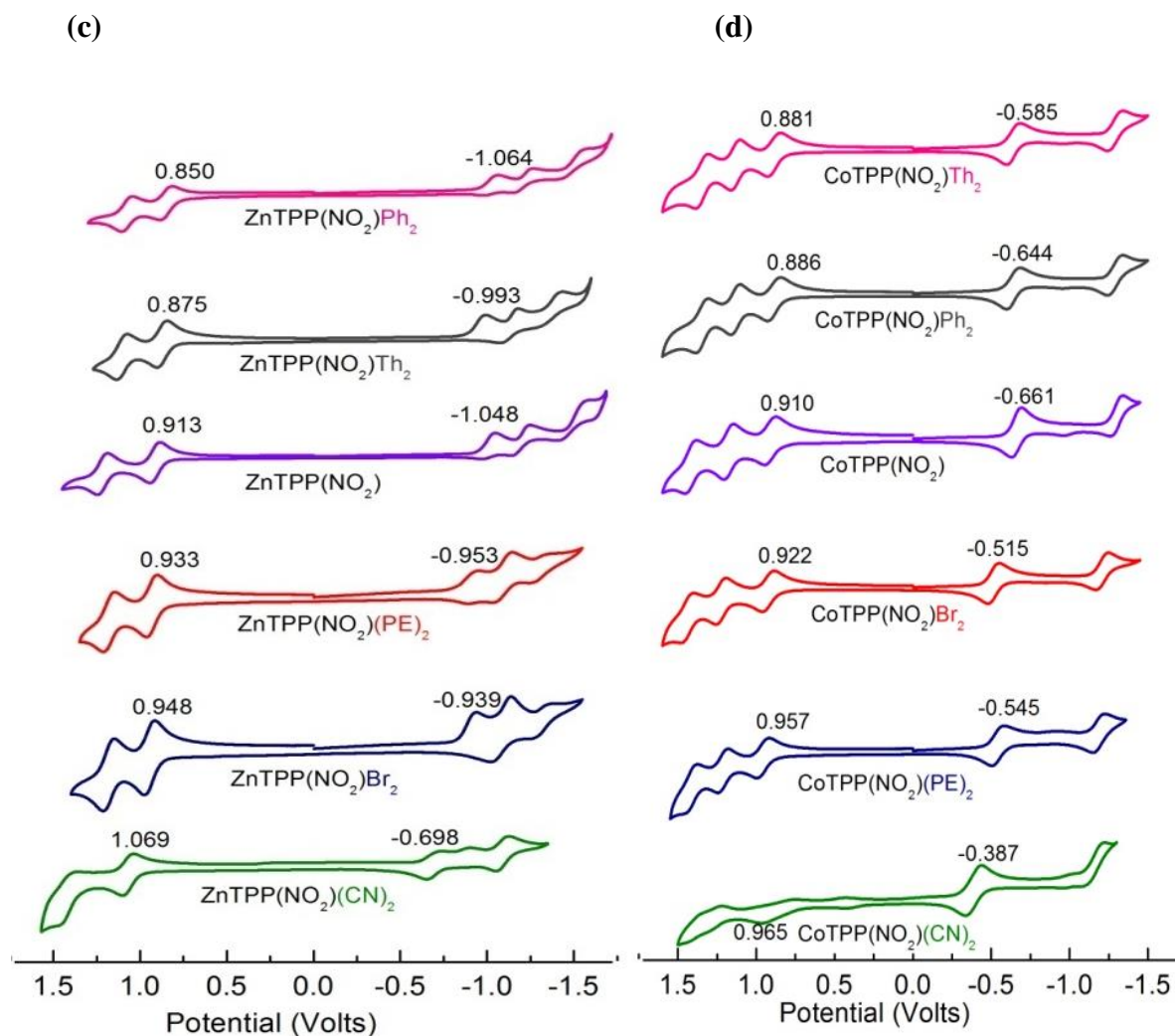
Figure A31. Cyclic voltammograms of (a) $H_2TPP(NO_2)X_2$, (b) $NiTPP(NO_2)X_2$, (c) $ZnTPP(NO_2)X_2$, (d) $CoTPP(NO_2)X_2$ (where X = H, Br, CN, PE, Th and Ph) complexes in CH_2Cl_2[a].

[a]Containing 0.1M $TBAPF_6$ with a scan rate of 0.1 V/s. Pt Working electrode, Ag/AgCl Reference electrode and Pt wire counter electrode were used.

(a)

(b)

(c)　　　　　　　　　　　　　　　　　**(d)**
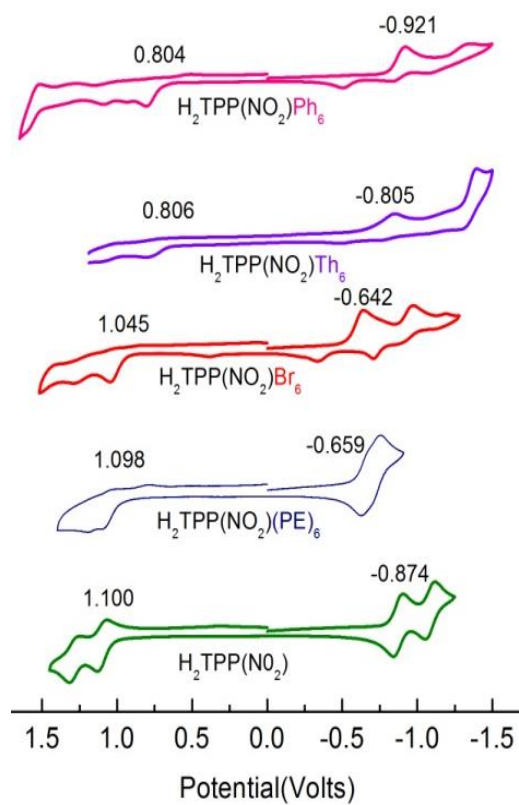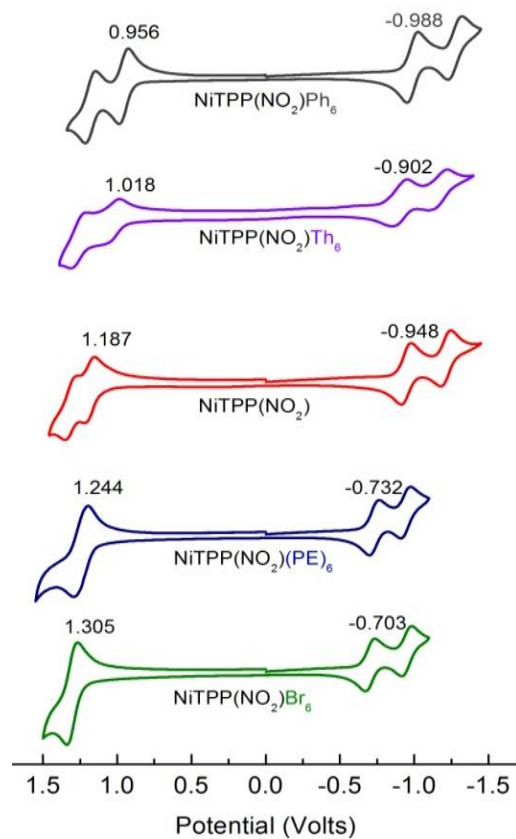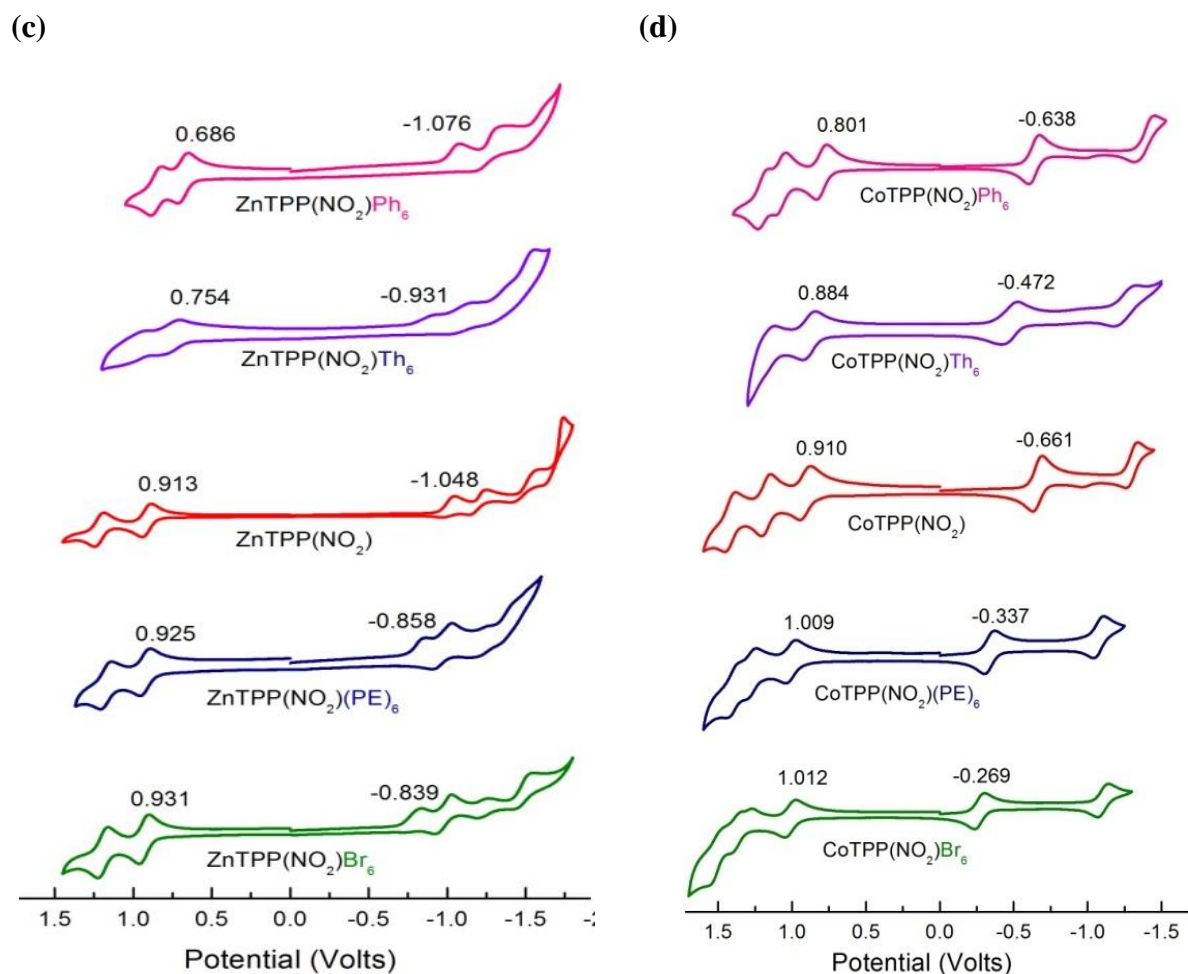
Figure A32. Cyclic voltammograms of (a) $H_2TPP(NO_2)X_6$, (b) $NiTPP(NO_2)X_6$, (c) $ZnTPP(NO_2)X_6$, (d) $CoTPP(NO_2)X_6$ (where X = H, Br, PE, Th and Ph) complexes in CH_2Cl_2. [a]Containing 0.1M TBAPF6 with a scan rate of 0.1 V/s. Pt Working electrode, Ag/AgCl Reference electrode and Pt wire counter electrode were used.

(a)   **(b)**
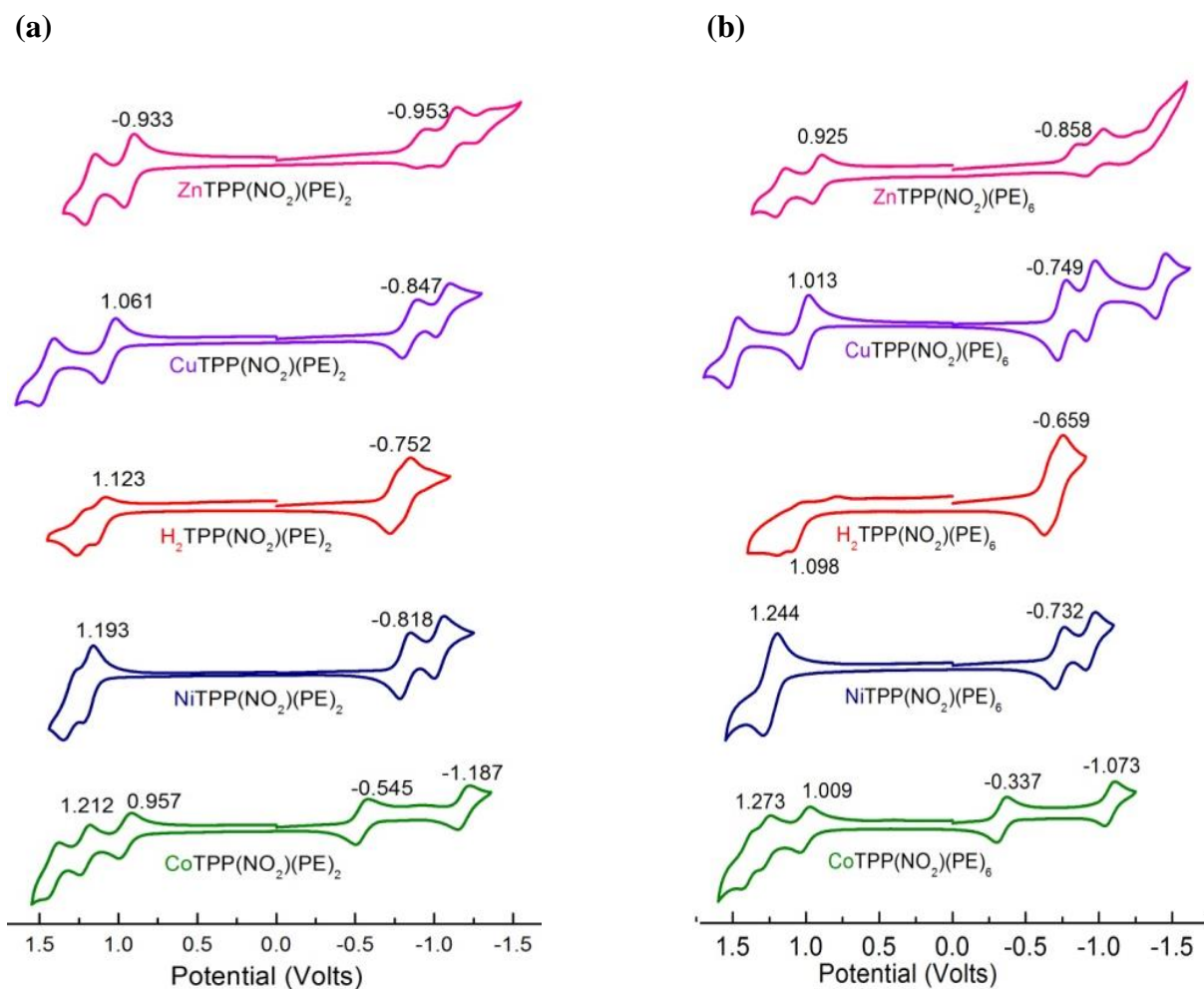
Figure A33. Cyclic voltammograms of (a) MTPP(NO$_2$)(PE)$_2$, (b) MTPP(NO$_2$)(PE)$_6$ where M = 2H, Cu(II), Zn(II), Ni(II), and Co(II) in CH$_2$Cl$_2$[a].

[a]Containing 0.1M TBAPF6 with a scan rate of 0.1 V/s. Pt Working electrode, Ag/AgCl Reference electrode and Pt wire counter electrode were used.
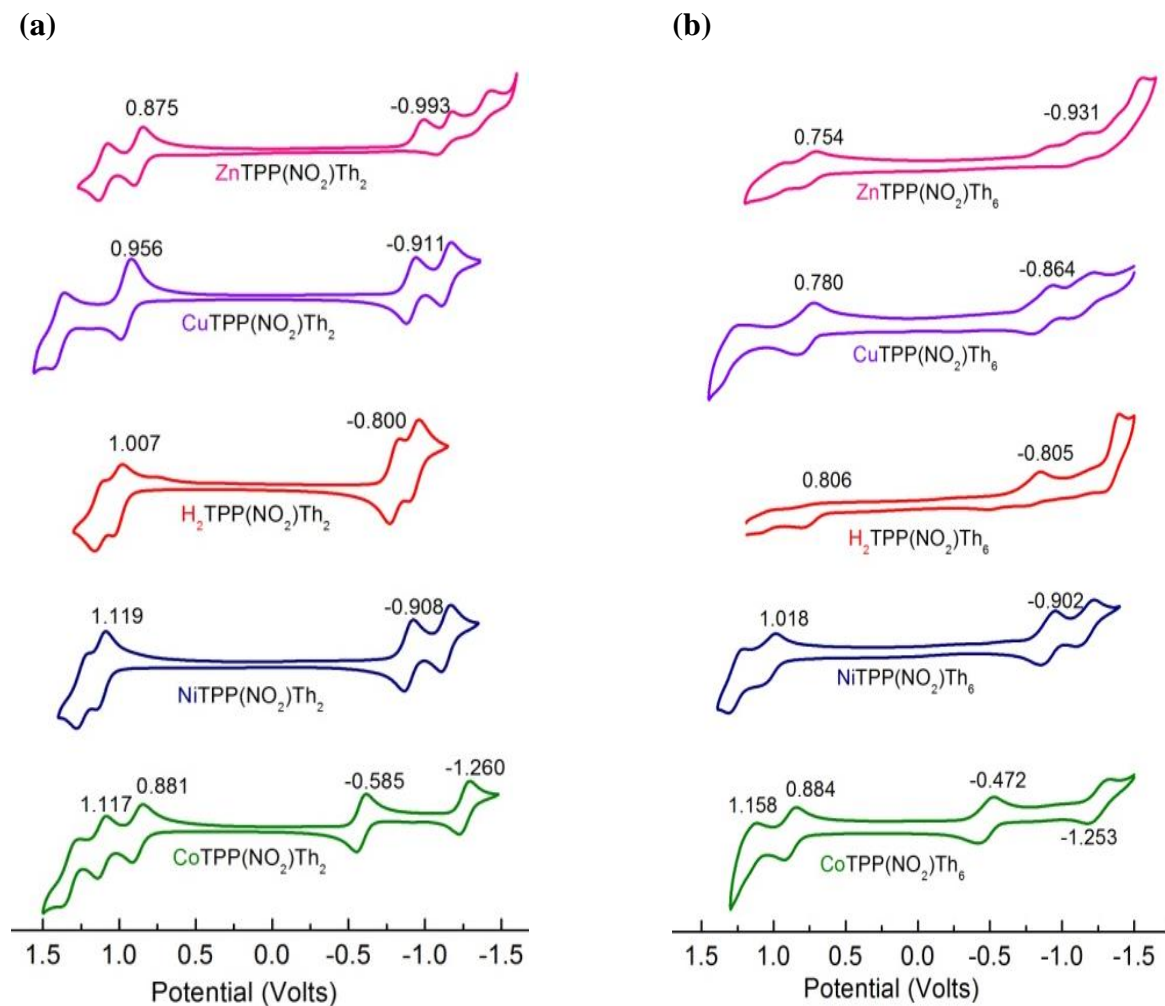
Figure A34. Cyclic voltammograms of (a) MTPP(NO$_2$)Th$_2$, (b) MTPP(NO$_2$)Th$_6$ where M = 2H, Cu(II), Zn(II), Ni(II), and Co(II) in CH$_2$Cl$_2$[a].

[a]Containing 0.1M TBAPF6 with a scan rate of 0.1 V/s. Pt Working electrode, Ag/AgCl Reference electrode and Pt wire counter electrode were used.
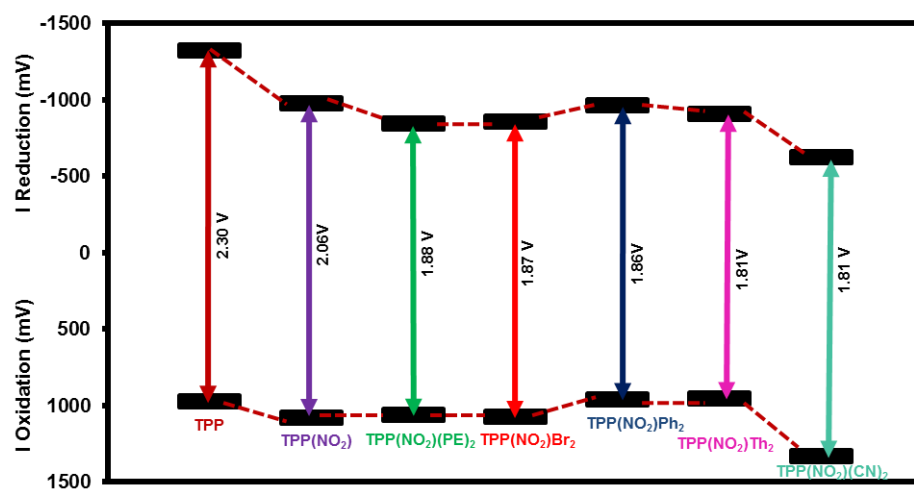
Figure A35. The HOMO-LUMO variation of CuTPP(NO$_2$)X$_2$ where X = PE, Br, Ph and Th in comparison to CuTPP(NO$_2$) and CuTPP.

(a) H$_2$TPP(NO$_2$)X$_2$
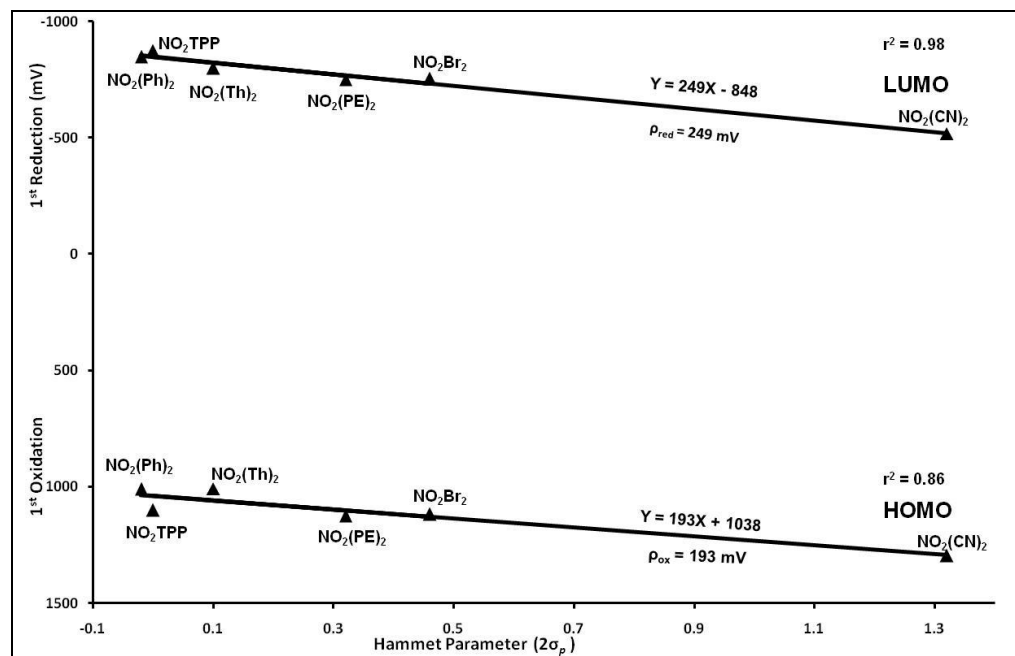
(b) CuTPP(NO$_2$)X$_2$
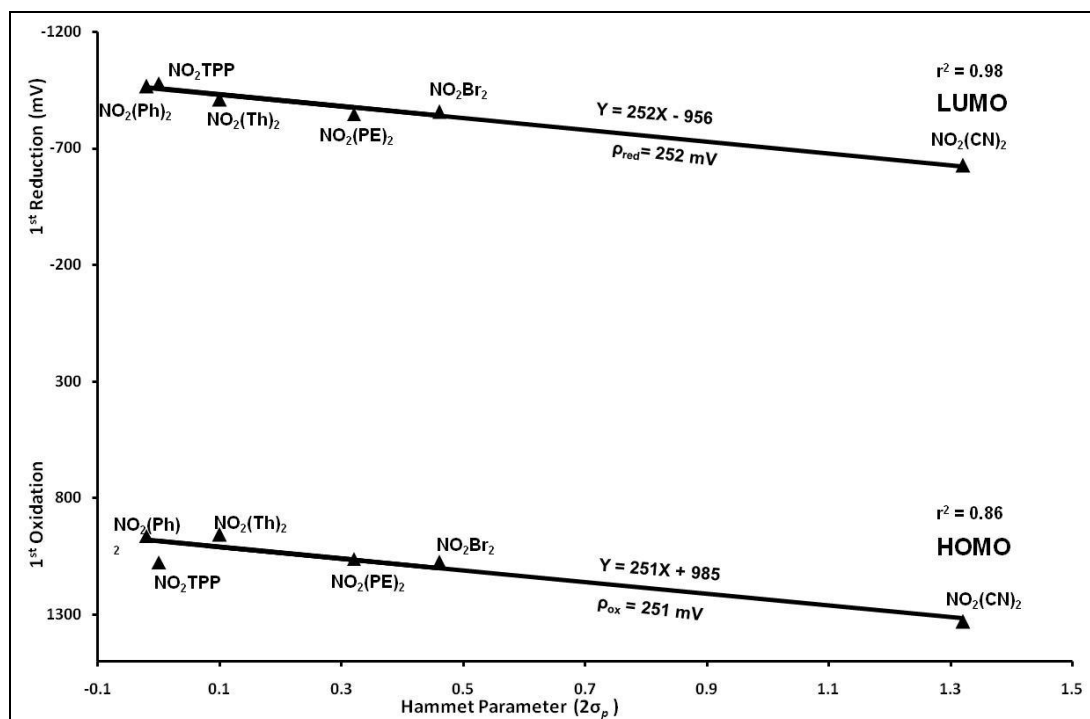
(c) NiTPP(NO$_2$)X$_2$
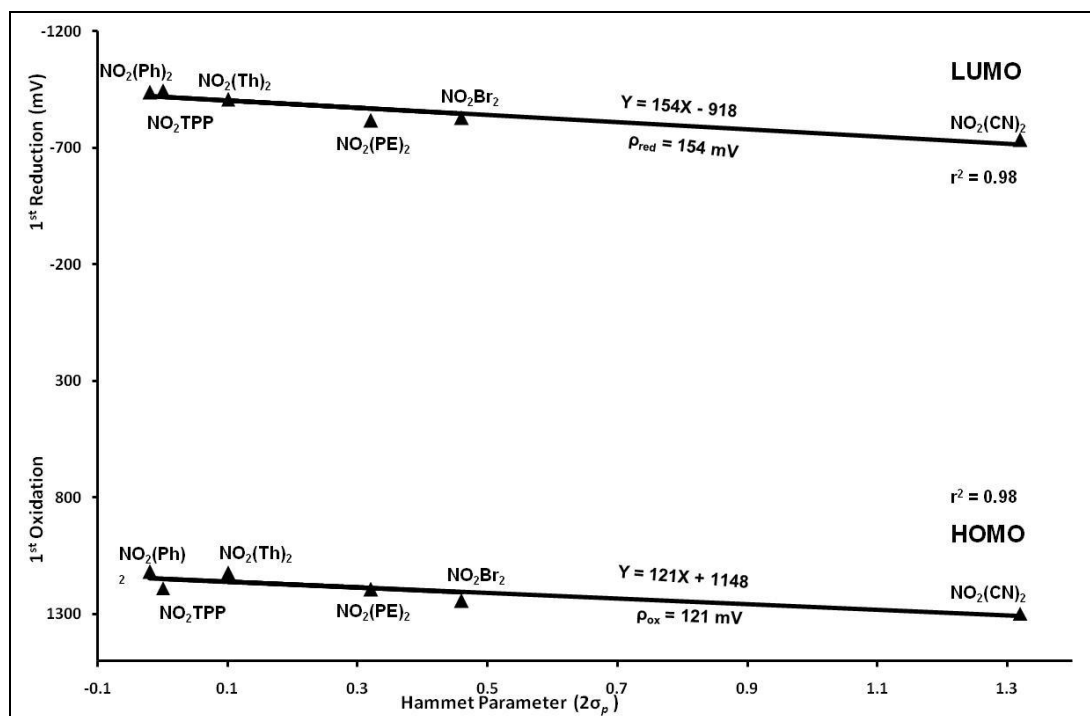
(d) ZnTPP(NO$_2$)X$_2$
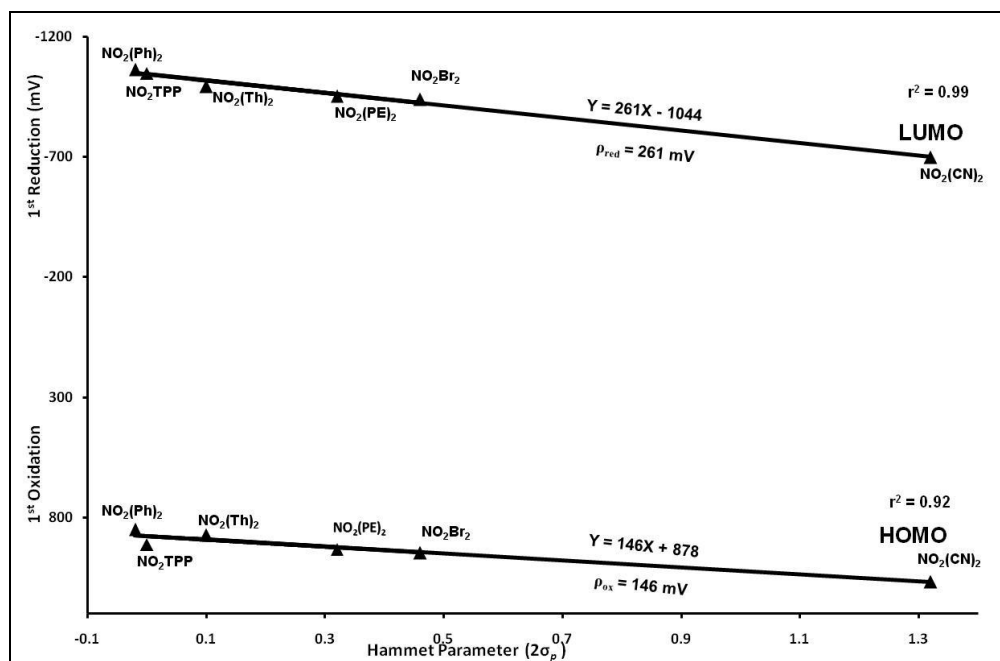
(e) $H_2TPP(NO_2)X_6$
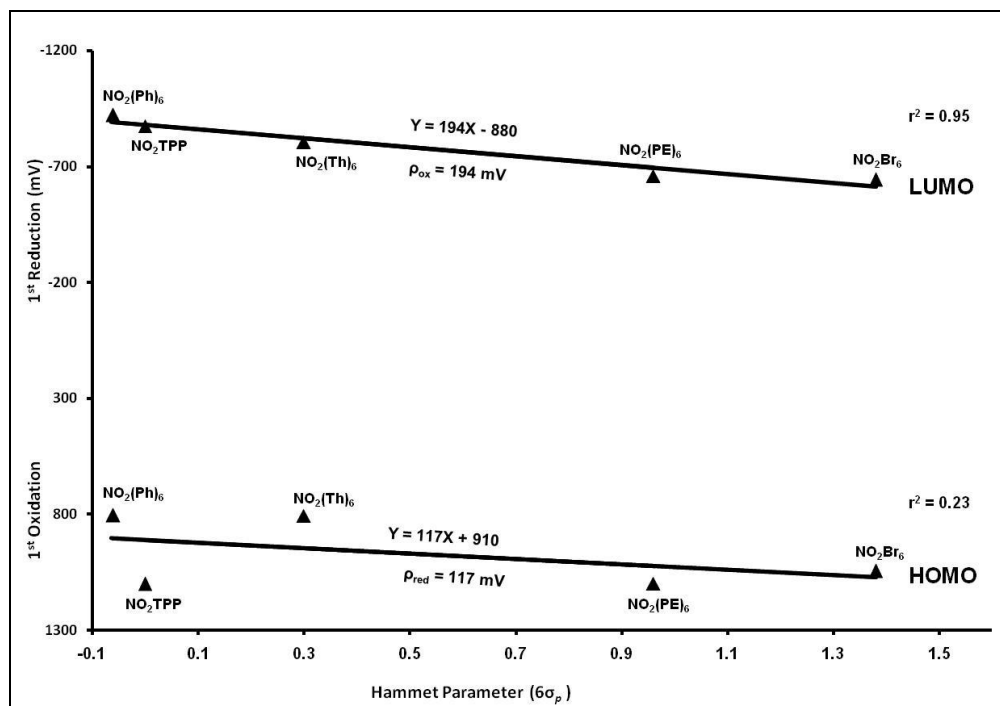
(f) $NiTPP(NO_2)X_6$
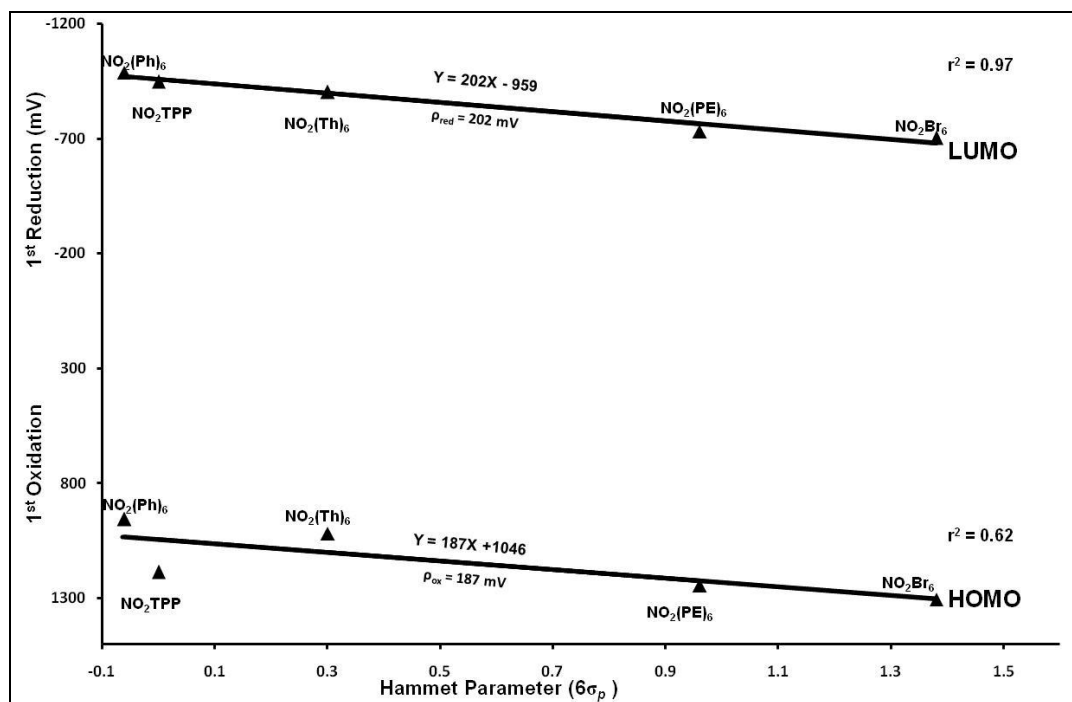
(g) CuTPP(NO$_2$)X$_6$
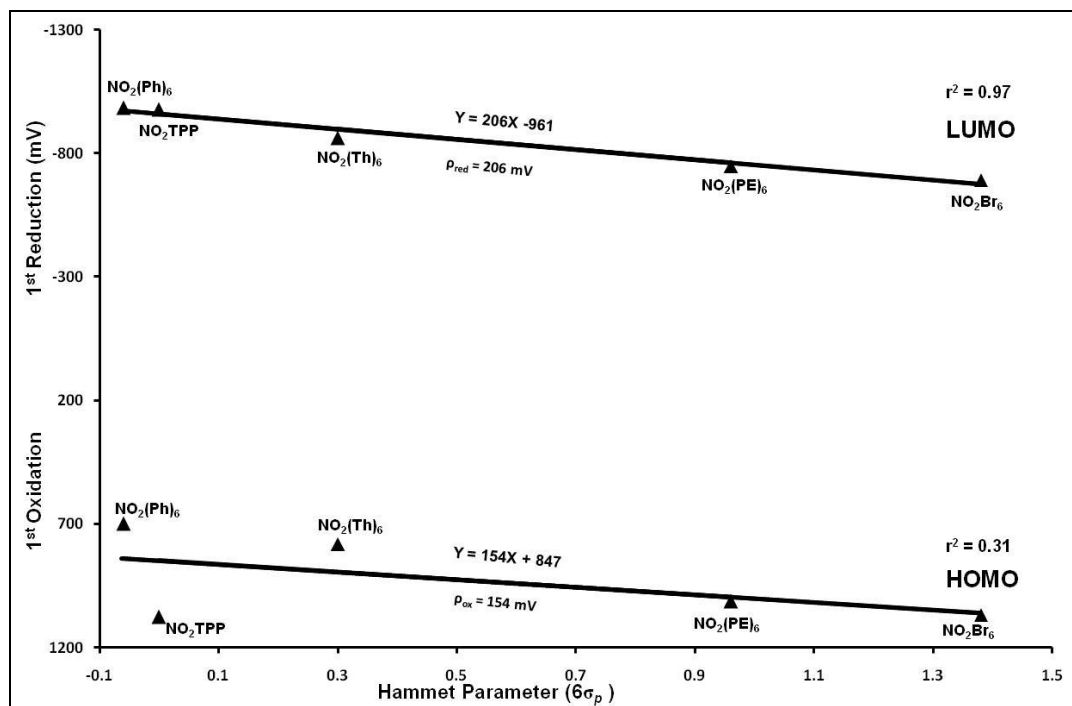
(h) ZnTPP(NO$_2$)X$_6$
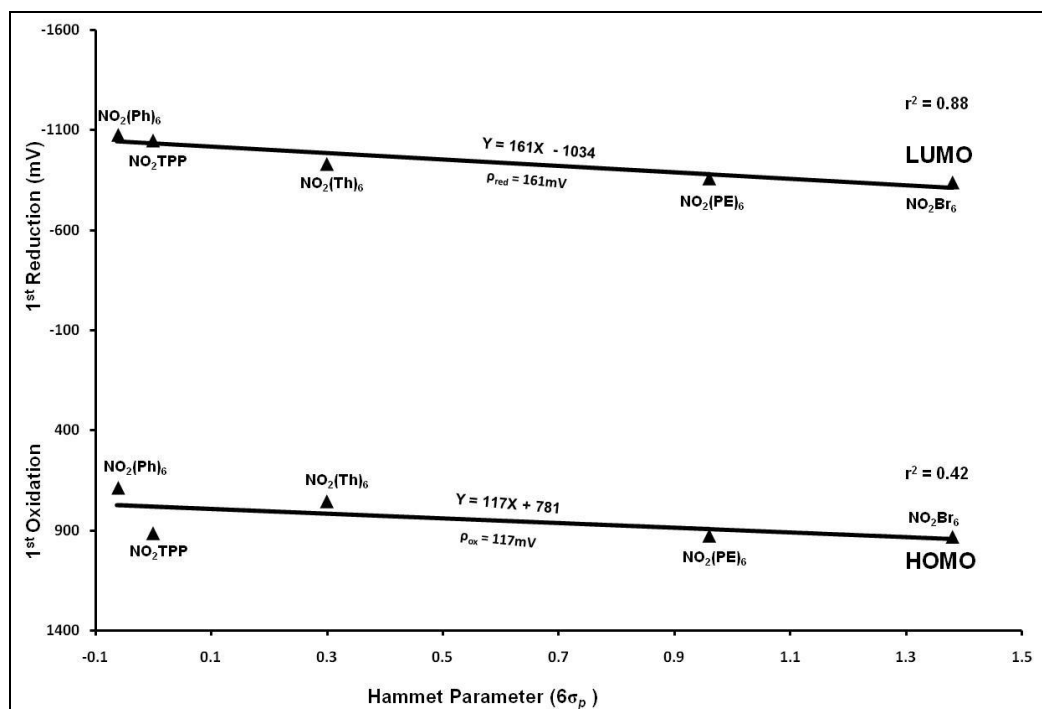
(i) CoTPP(NO$_2$)X$_6$ (metal centered)
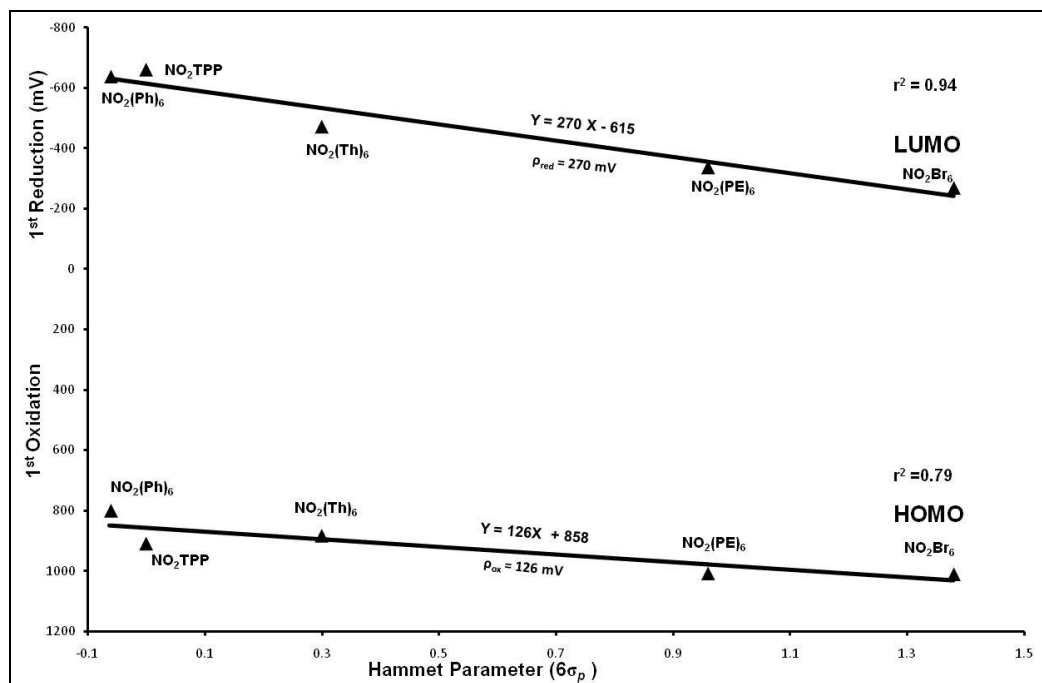
(j) CoTPP(NO$_2$)X$_6$ (ring centered)
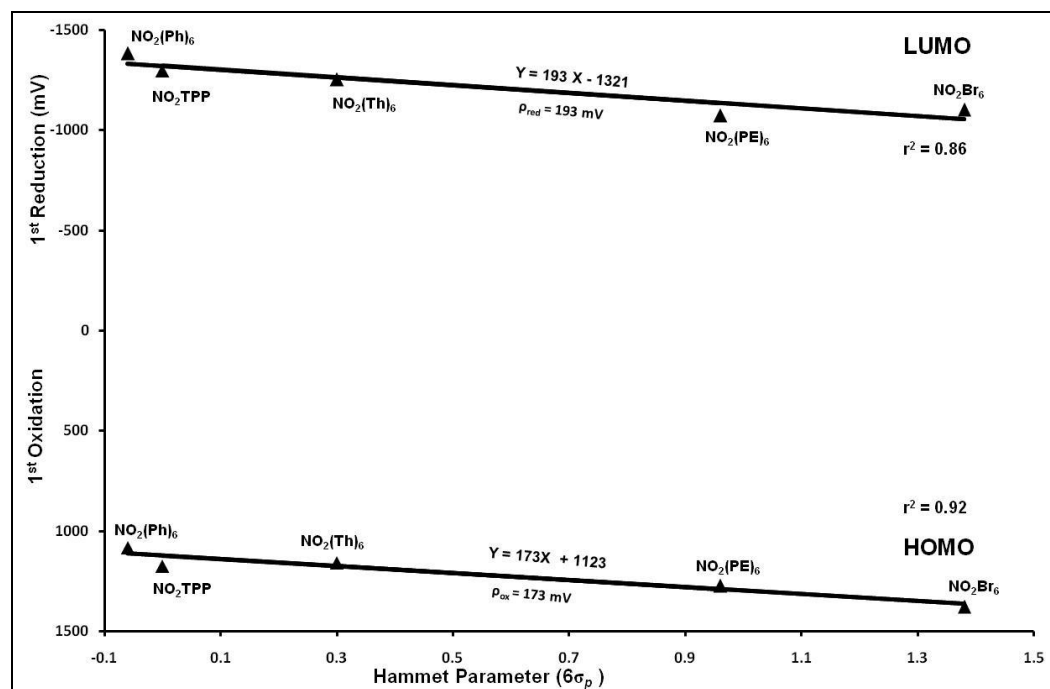
Figure A36. Plot of 1st ring redox potentials *versus* the Hammett parameter (σ_p) of various Mixed substituted Porphyrins.

Appendix 2

Ratiometric Colorimetric "Naked eye" Selective Detection of CN⁻ ions by Electron Deficient Ni(II) Porphyrins and their Reversibility Studies

Table of Contents

NiTPP(NO₂)

NCS, TCE
reflux, 2.5 hrs.

R = NO₂, NiTPP(NO₂)Cl₇, **4** (Yield = 23%)
R = Cl, NiTPPCl₈, **5** (Yield = 19%),

Scheme 1. Synthetic route to *β*-substituted electron deficient Ni(II) perhaloporphyrins (**4-5**).

Table A1. UV-Visible spectral data of **1-5** in CH₂Cl₂ at 298 K.

Porphyrin	B band, nm	Q band(s), nm
1	440(5.10)	630(4.50)
2	445(5.13)	632(4.47)
3	450(5.07)	636(4.54)
4	448(5.12)	562(4.04), 604(3.80)
5	439(5.28)	554(4.18), 591(sh)

The values in parentheses refer to logε.
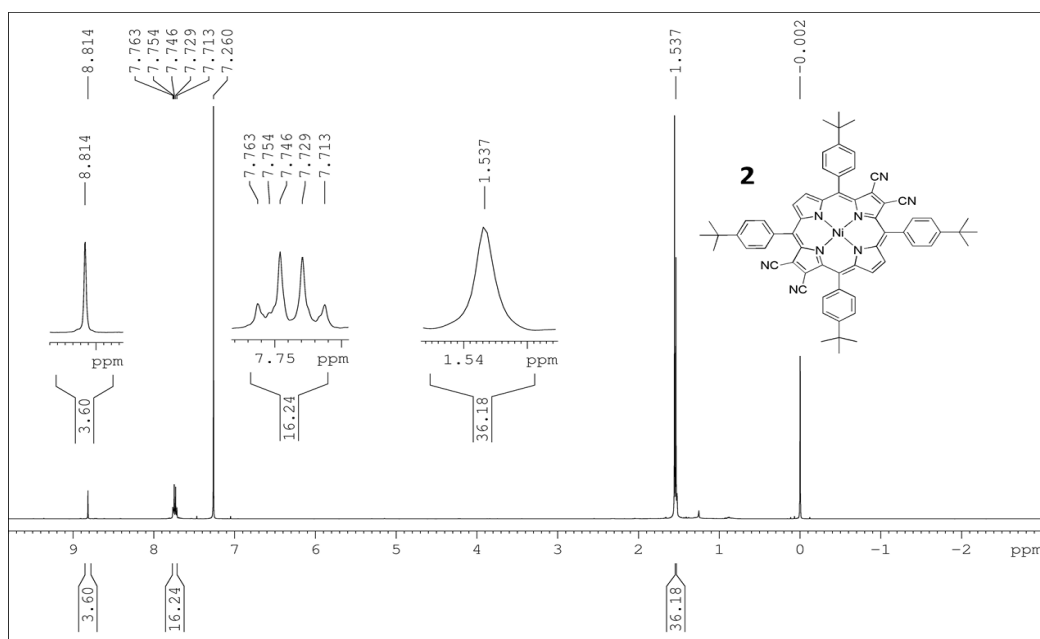
Figure A1. ¹H NMR spectrum of **2** in CDCl₃ at 298 K.
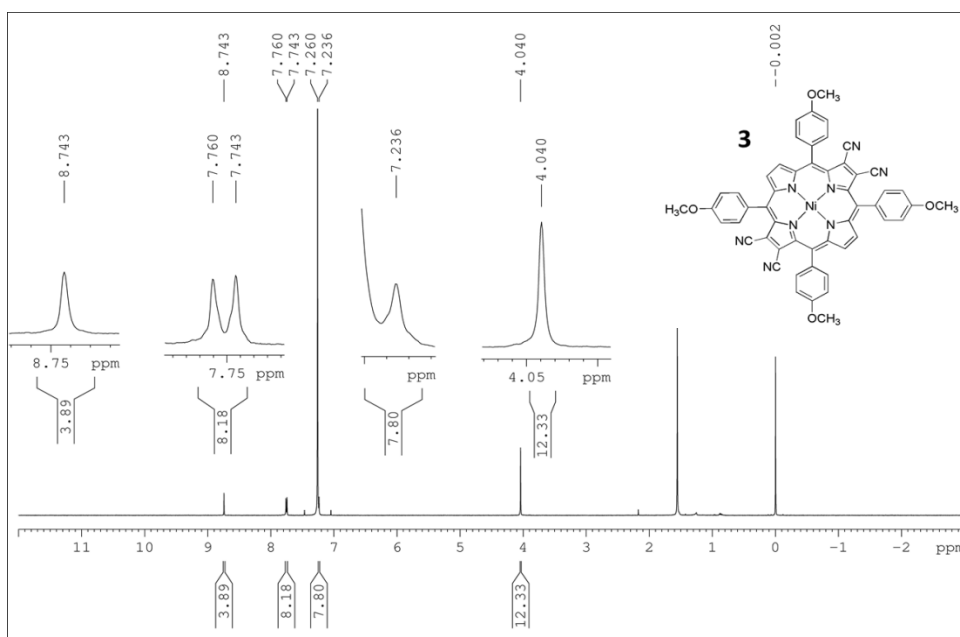
Figure A2. ^{1}H NMR spectrum of **3** in CDCl$_3$ at 298 K.

Table A2. Electrochemical redox potentials^a of **1-5** in CH$_2$Cl$_2$ at 298 K.

Porphyrin	Oxidation(volts)	Reduction(volts)		$\Delta E_{1/2}$ (I_{ox}-I_{red}) (Volts)
	I	I	II	
1	1.44	-0.38	-0.81	1.82
2	1.40	-0.44	-0.84	1.84
3	1.32	-0.43	-0.85	1.75
4	1.33	-0.64	-0.88	1.97
5	1.26	-0.82	-1.14	2.08

^{a}*vs* Ag/AgCl

231
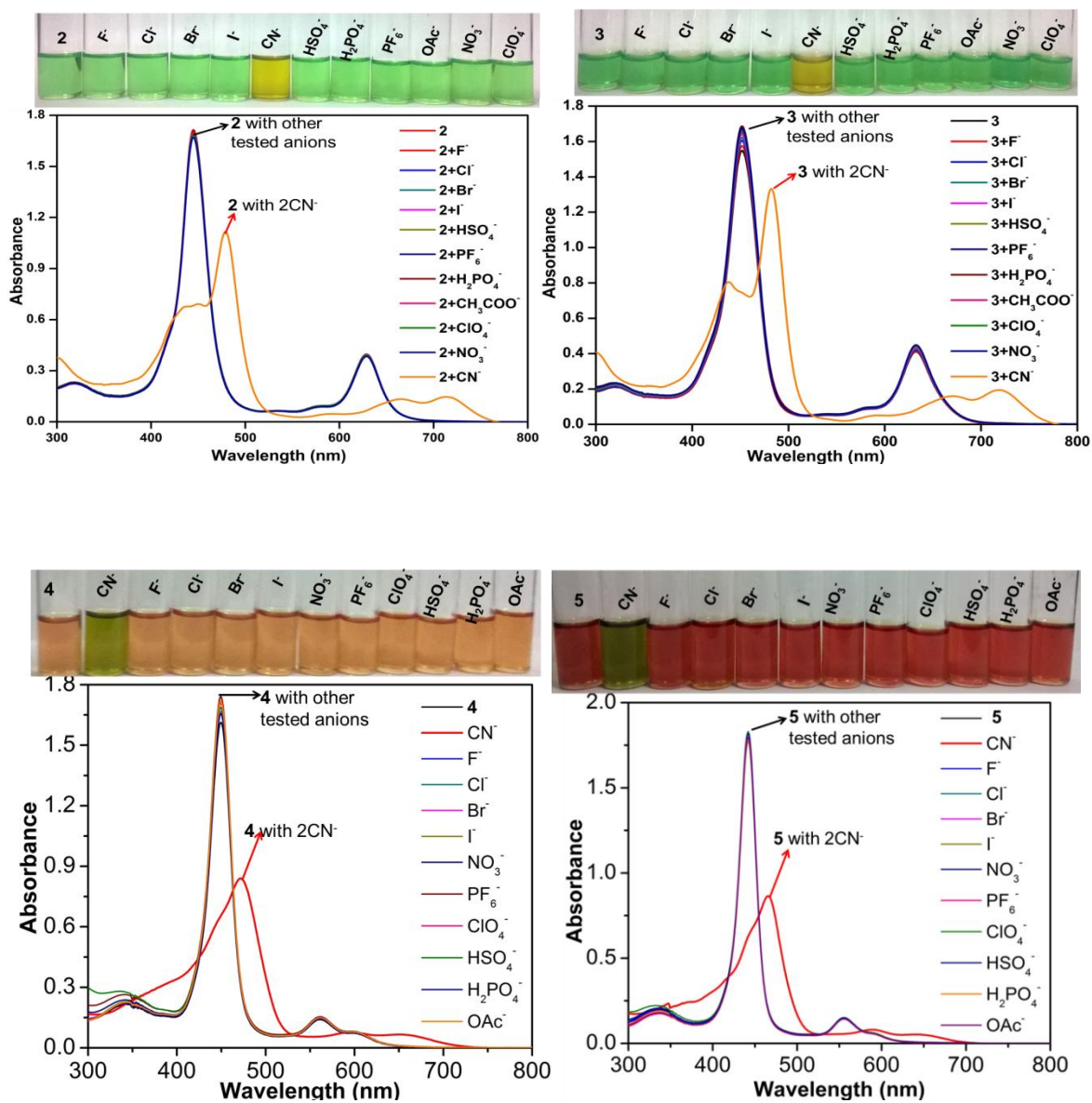
Figure A3. Colorimetric responses and corresponding absorption spectral changes of **2-5** while adding of excess of anions in toluene at 298 K.
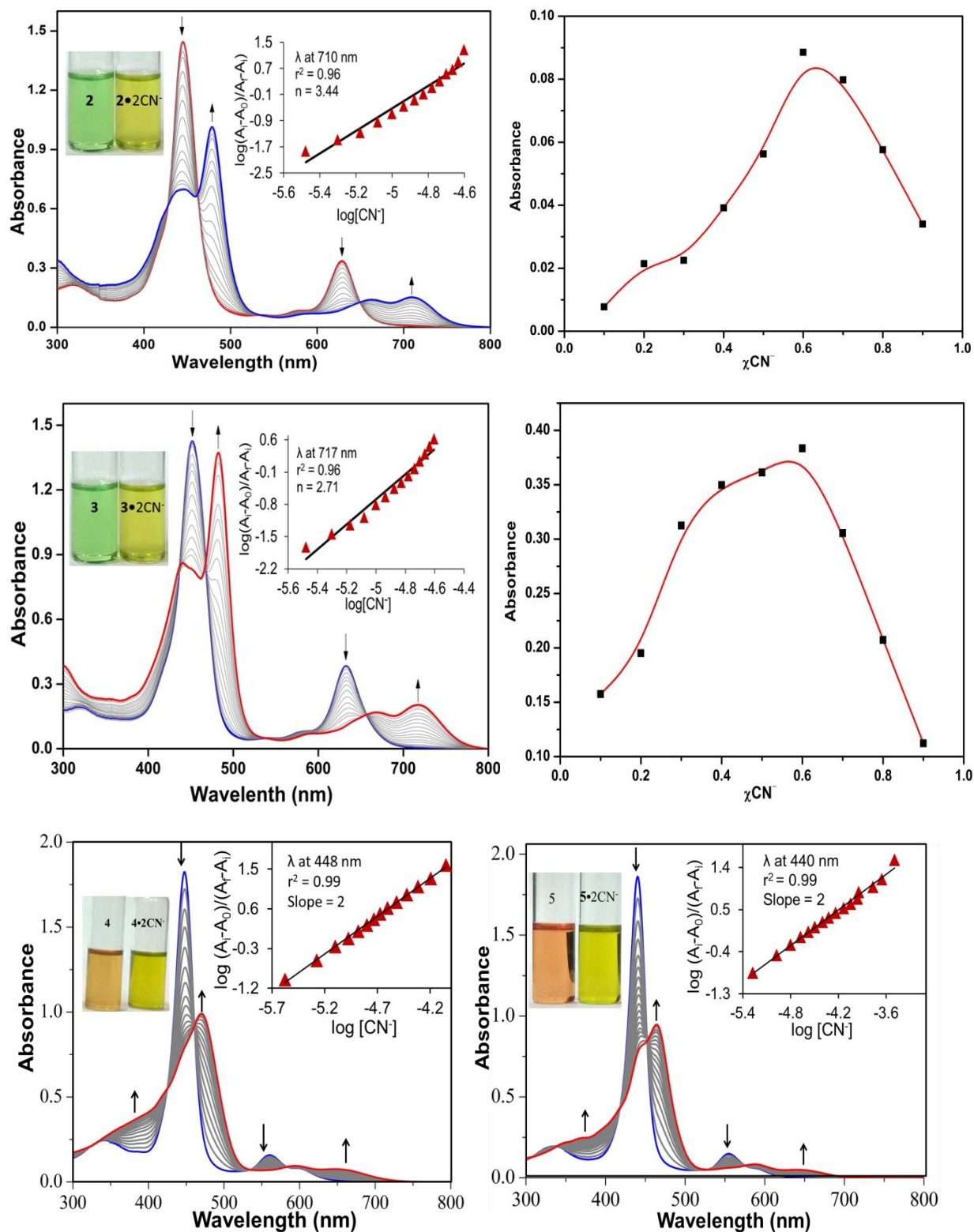
Figure A4. UV-Vis spectral titrations of **2**-**5** with TBACN in toluene and insets show their corresponding Hill plots. The stoichiometry of **2**-**3** was established using Job's plot.

233
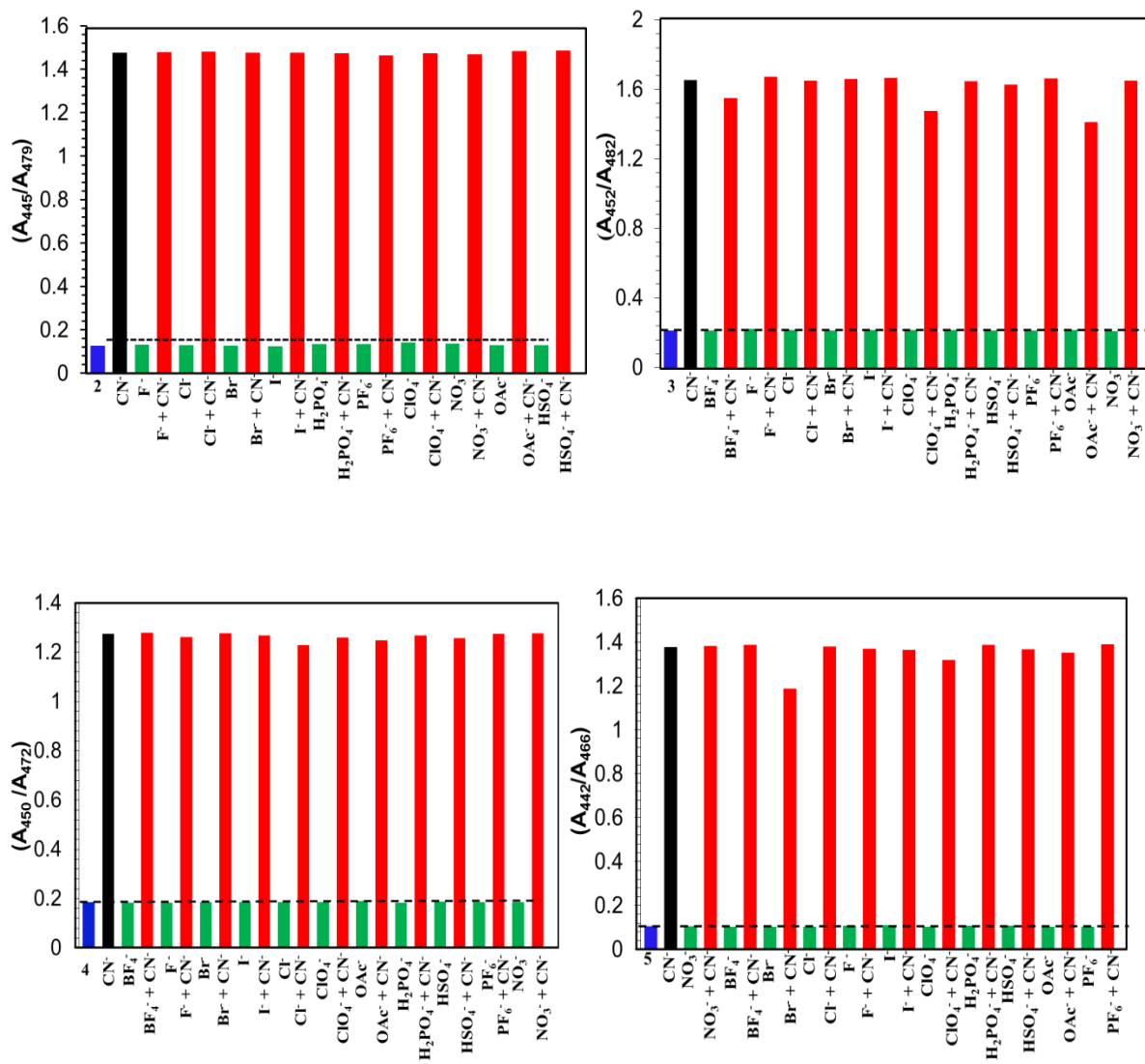
Figure A5. Ratiometric response of **2**-**5** on addition of 2 equiv. of cyanide ions in presence of 10 equiv. of other interfering anions. Blue bars indicate the references, Black bars indicate only with CN⁻ ions, Green bars indicate various anions and red bar indicate the addition of cyanide ion in presence of interfering anions.
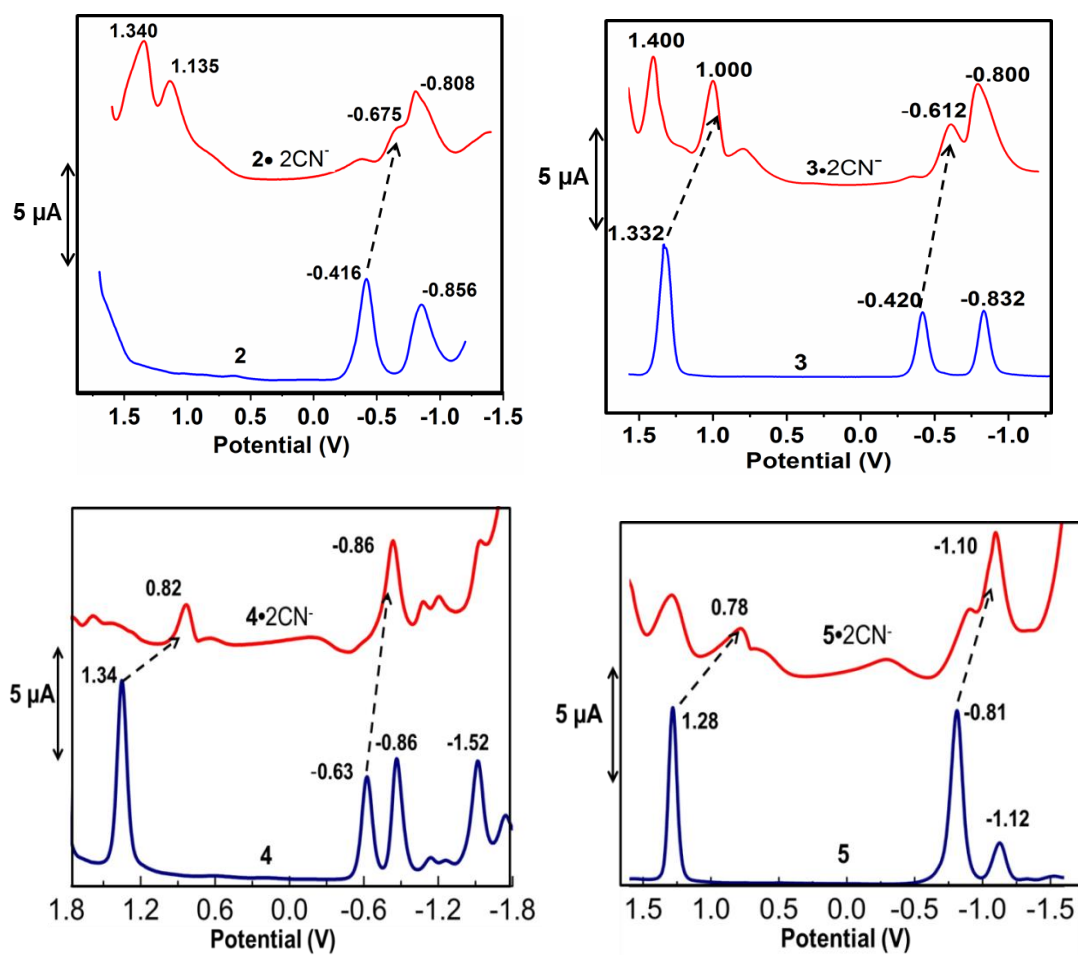
Figure A6. DPV traces of **2-5** in absence and presence of [CN⁻] in CH$_2$Cl$_2$ containing 0.1 M TBAPF$_6$ at 298 K.
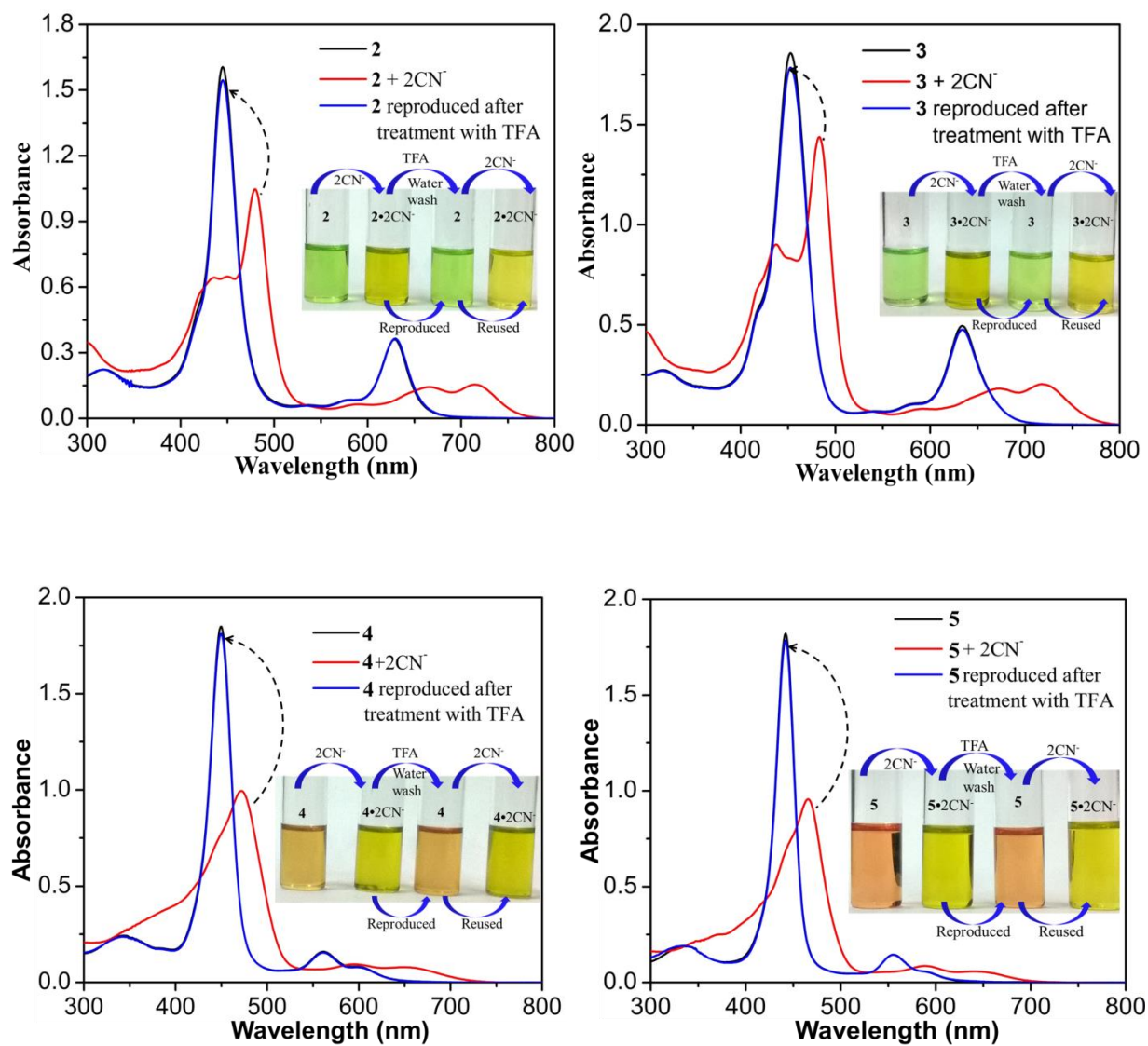
Figure A7. UV-Vis spectra of **2-5** for complexation with 2CN⁻ and reversibility test in toluene at 298 K, insets show corresponding colorimetric response for reversibility and reusability test.
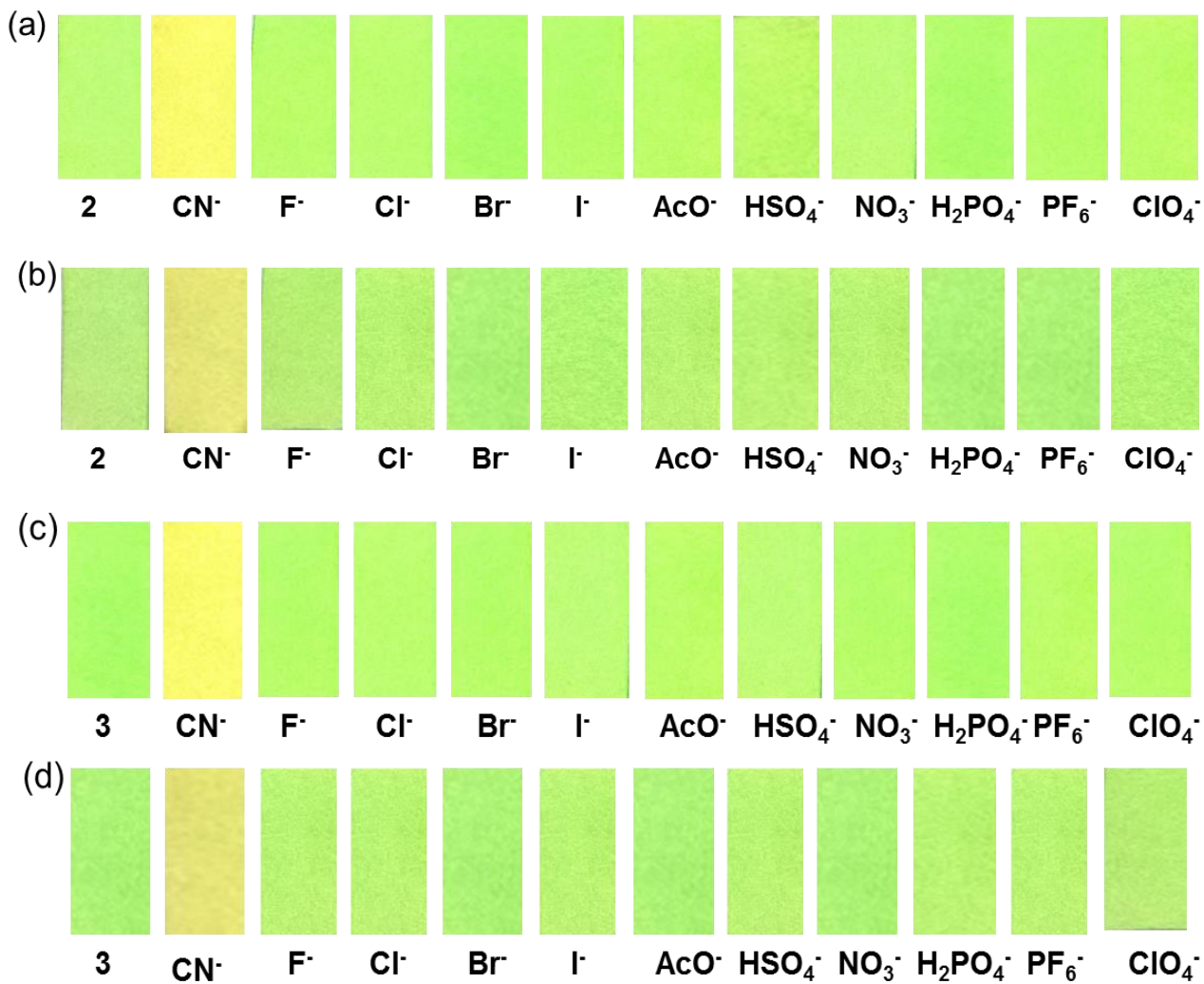
Figure A8. Colorimetric response by coated paper strips of **2** and **3** (1 mM) with various anions in toluene (a and c) and neutral aqueous solution (b and d) at 298 K.
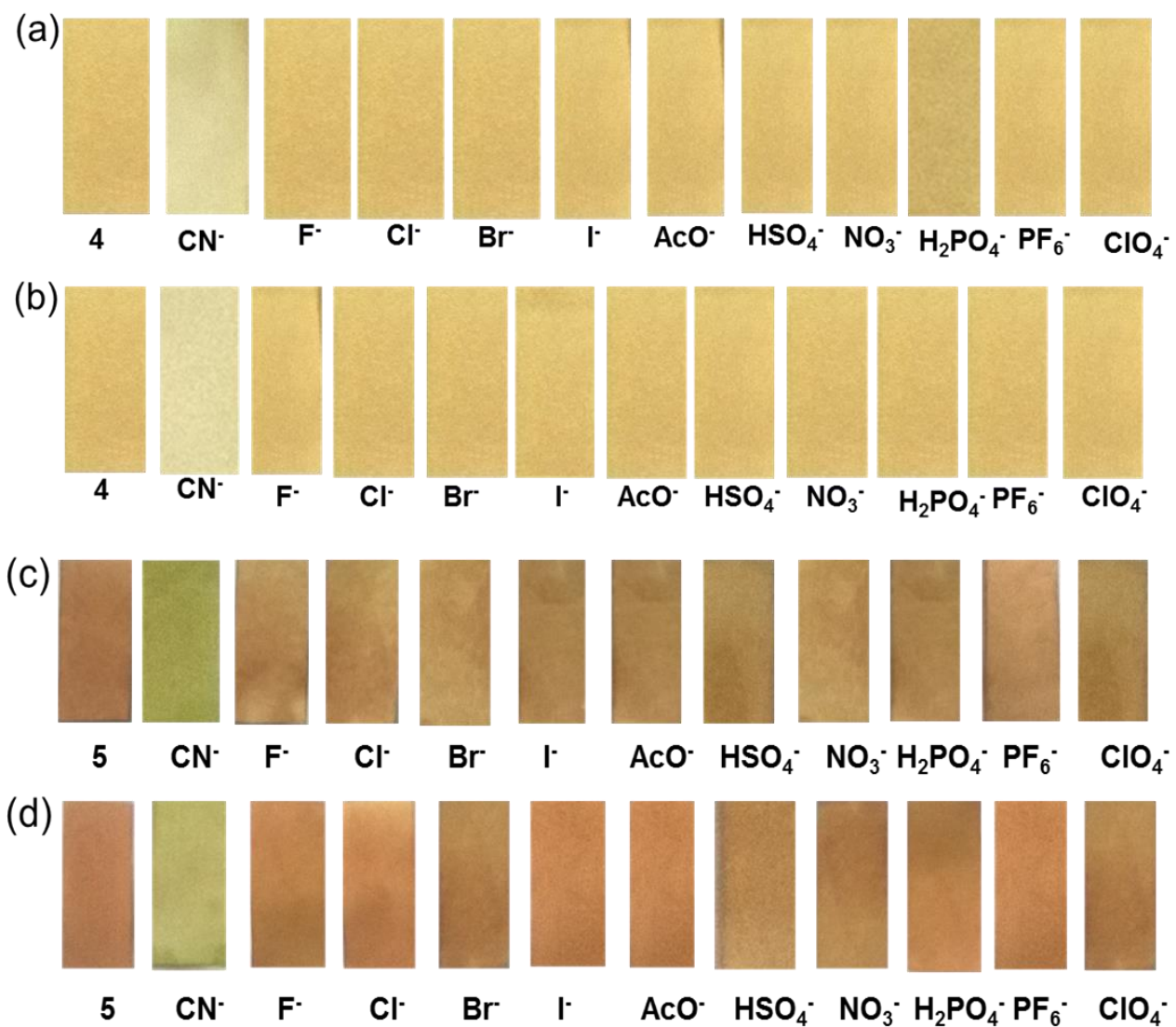
Figure A9. Colorimetric response by coated paper strips of **4** and **5** (1 mM) with various anions in toluene (a,c) and neutral aqueous solution (b,d) at 298 K.
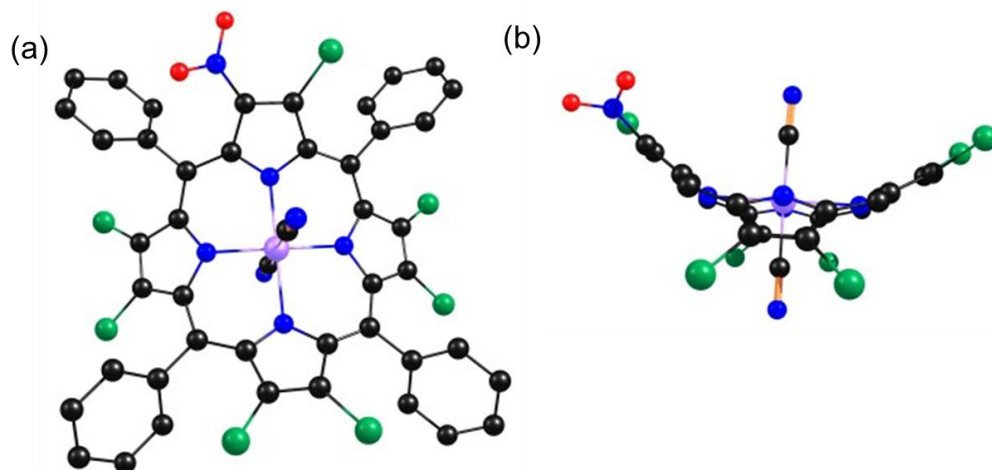
Figure A10. B3LYP/LANL2DZ optimized geometry showing top (a) as well as side views (b) of NiTPP(NO$_2$)Cl$_7$•2CN$^-$, hydrogens are omitted in both top and side views for clarity.
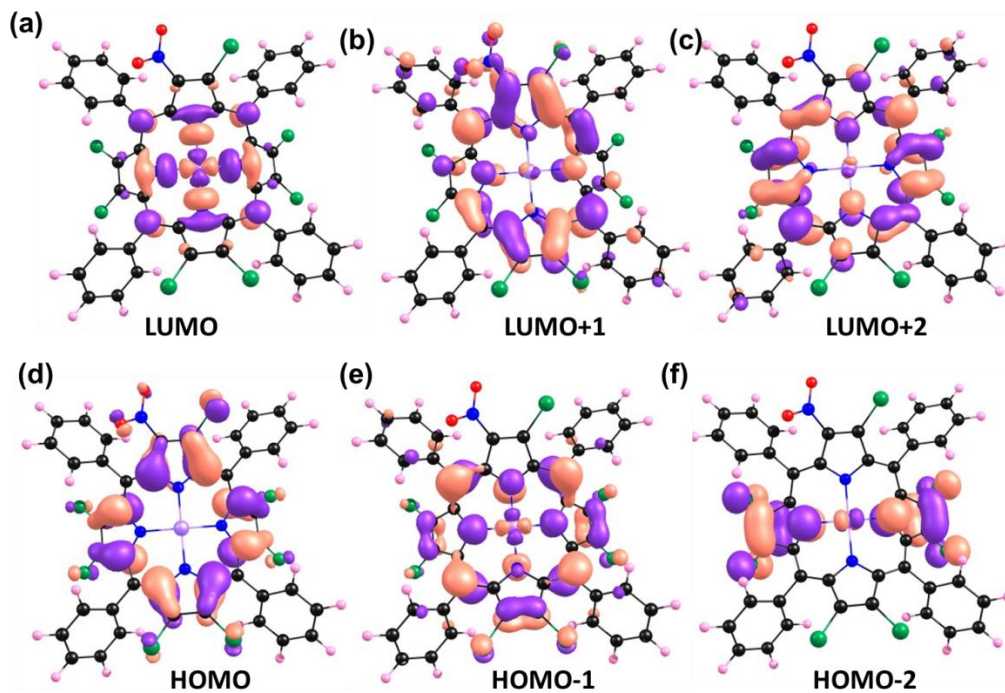
Figure A11. Pictorial representation of frontier molecular orbitals of NiTPP(NO$_2$)Cl$_7$ (**4**) obtained by DFT calculations using B3LYP as density functional with LANL2DZ basis sets in gas phase.
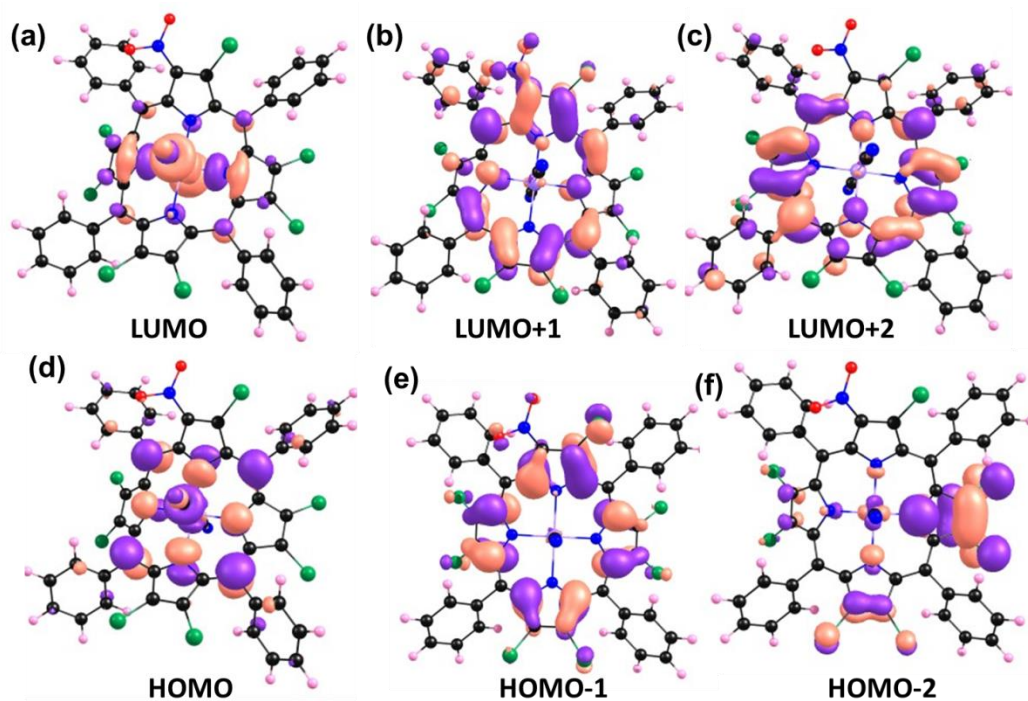
Figure A12. Pictorial representation of frontier molecular orbitals of NiTPP(NO$_2$)Cl$_7$•2CN$^-$ (**4**•2CN$^-$) obtained by DFT calculations using B3LYP as density functional with LANL2DZ basis sets in gas phase.
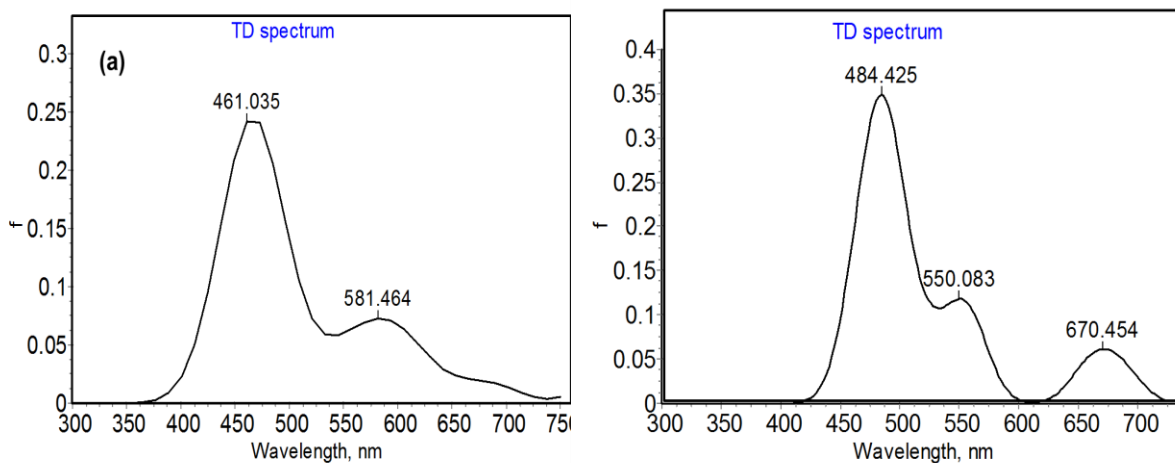
Figure A13. Theoretical UV-Visible spectra of (a) **4** and (b) **4**•2CN$^-$ obtained by TD-DFT calculations in gas phase.
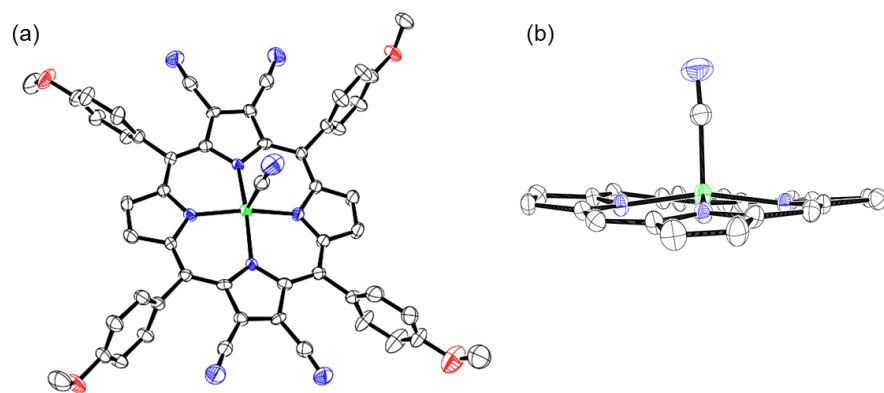
Figure A14. Single crystal X-ray structure of **3** with axial coordination of CN⁻ ion. The counter cation (tetrabutylammonium ion) was not shown for clarity.
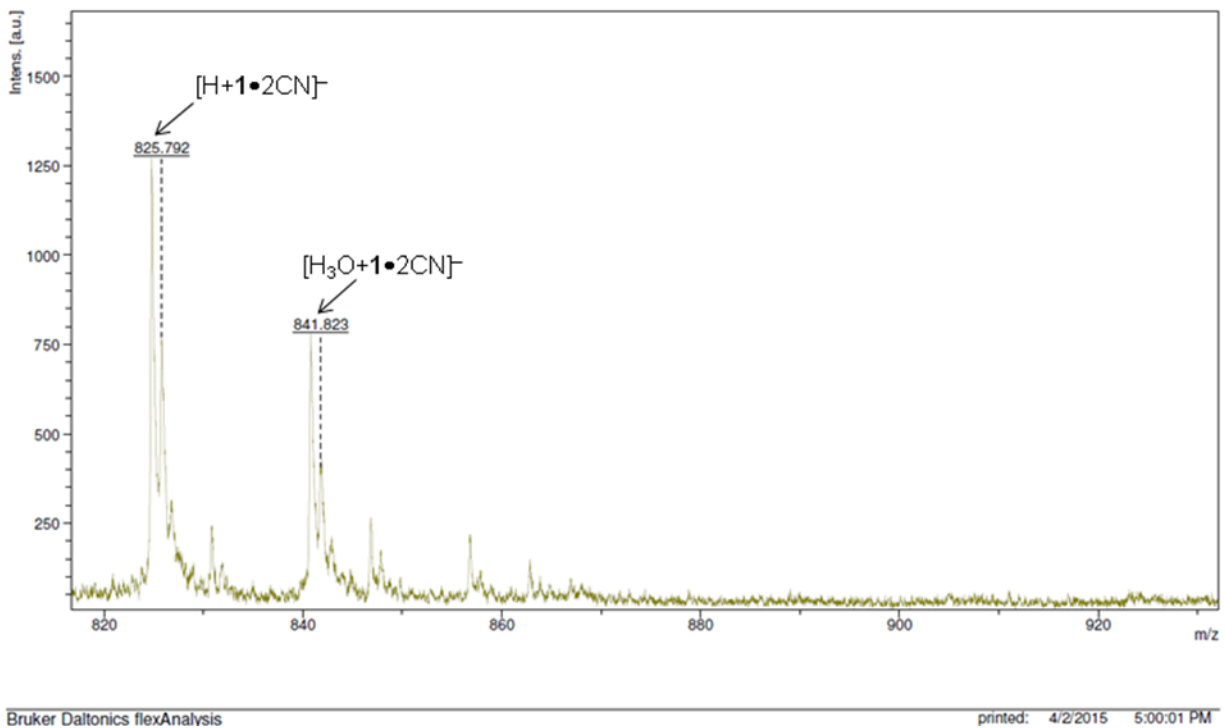
Figure A15. MALDI-TOF negative ion mode mass spectrum of **1** in presence cyanide ions using HABA matrix.
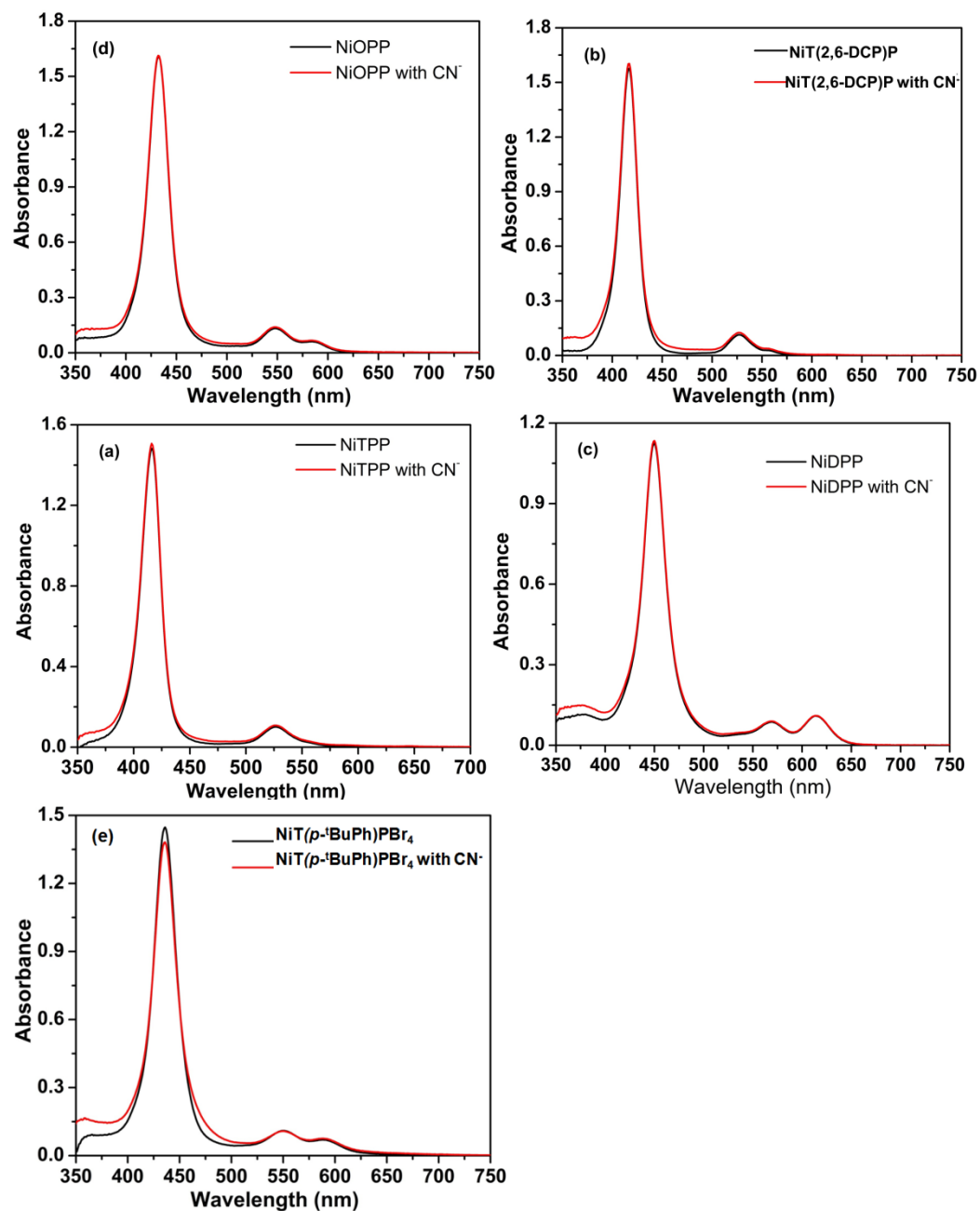
Figure A16. UV-Visible spectra of (a) *meso*-tetraphenylporphyrinato nickel(II) (NiTPP); (b) *meso-tetrakis*(2,6-dichlorophenyl)porphyrinato nickel(II) (NiT(2,6-DCP)P); (c) 2,3,5,7,8,10,12,13,15,17, 18,20-dodecaphenylporphyrinato nickel(II) (NiDPP); (d) 2,3,5,10,15,17,18,20-octaphenyl-porphyrinato nickel(II) (NiOPP); (e) *Meso-tetrakis*(*p*-[t]butylphenyl)porphyrinato nickel(II) (NiT(*p*-[t]bu-ph)P) in toluene (black lines) at 298 K and then excess addition of [CN^{-}] in toluene (red lines).

242
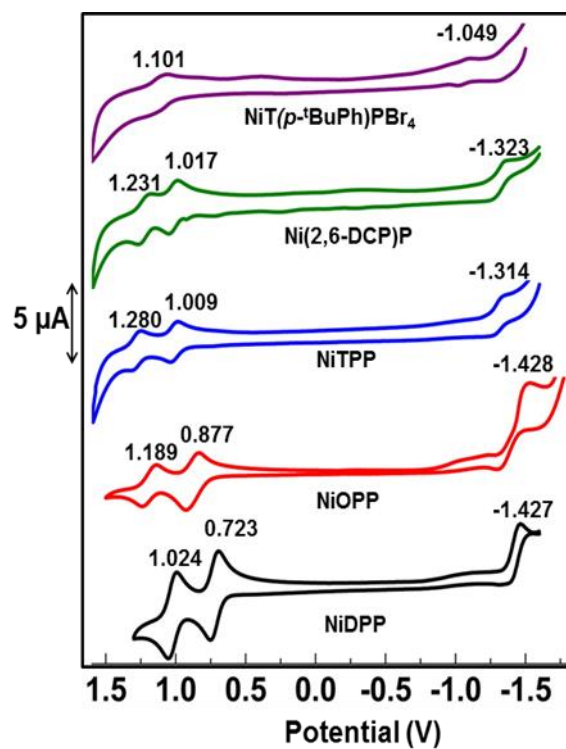
Figure A17. CVs of various planar and nonplanar Ni(II) porphyrins in CH$_2$Cl$_2$ at 298 K.

Table A3. Electrochemical redox data of various planar and nonplanar porphyrins in CH$_2$Cl$_2$ at 298 K.

Porphyrin	Oxidation (V)		Reduction (V)
	I	II	I
NiTPP	1.009	1.280	-1.314
NiOPP	0.877	1.189	-1.428
NiDPP	0.723	1.024	-1.427
NiT(2,6-DCP)P	1.017	1.231	-1.323
NiT(*p*-^{t}BuPh)PBr$_4$	1.101	-	-1.049

APPENDIX 3

SYNTHESIS, SPECTROSCOPIC, ELECTROCHEMICAL REDOX, SOLVATOCHROMISM AND ANION BINDING PROPERTIES OF *β*-TETRA- AND -OCTAPHENYLETHYNYL SUBSTITUTED *MESO*-TETRAPHENYLPORPHYRINS

Table of contents

Figure A1. ^{1}H NMR spectrum of NiTPP(PE)$_4$ in CDCl$_3$ at 298 K.

Figure A2. ^{1}H NMR spectrum of H$_2$TPP(PE)$_8$ in CDCl$_3$ at 298 K.

Figure A3. ^{1}H NMR spectrum of ZnTPP(PE)$_8$ in CDCl$_3$ at 298 K

Figure A4. ^{1}H NMR spectrum of NiTPP(PE)$_8$ in CDCl$_3$ at 298 K.
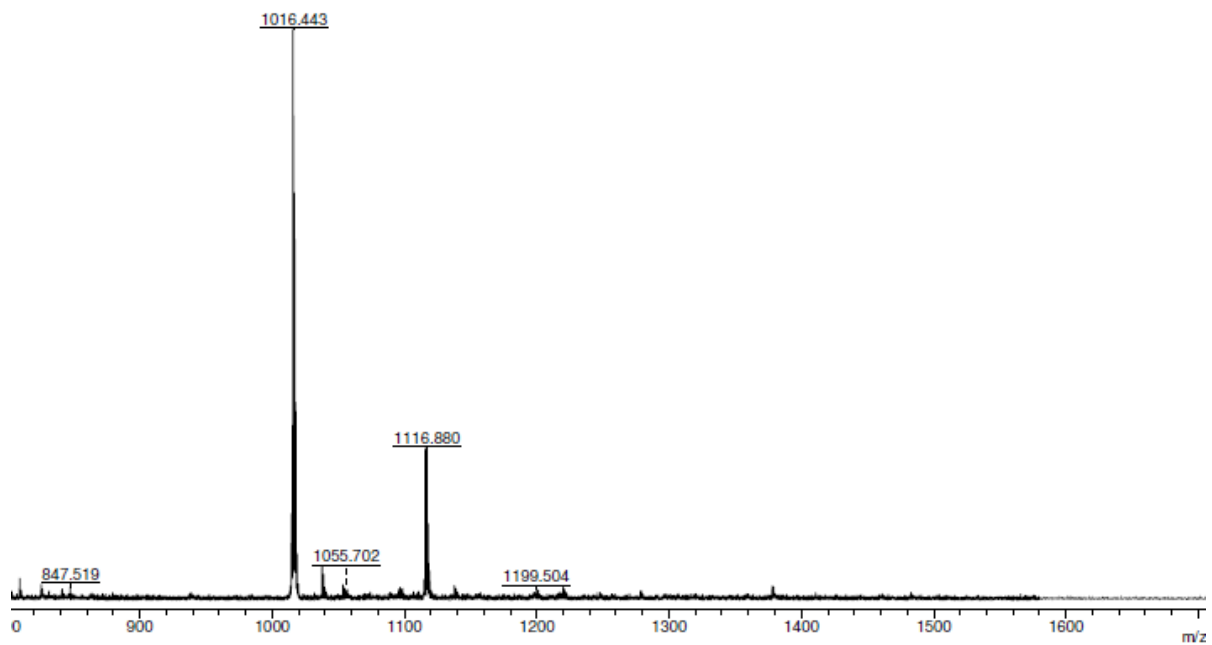
Figure A5. MALDI-TOF mass spectrum of $H_2TPP(PE)_4$
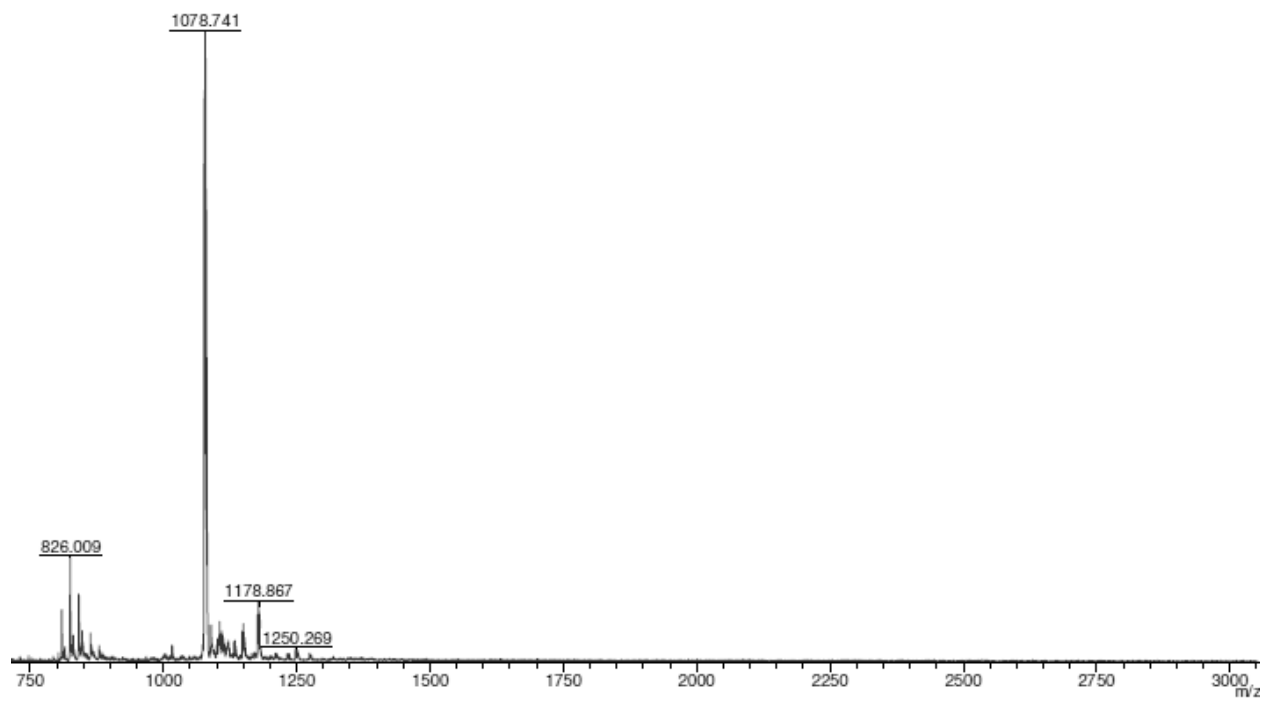
Figure A6. MALDI-TOF mass spectrum of $ZnTPP(PE)_4$
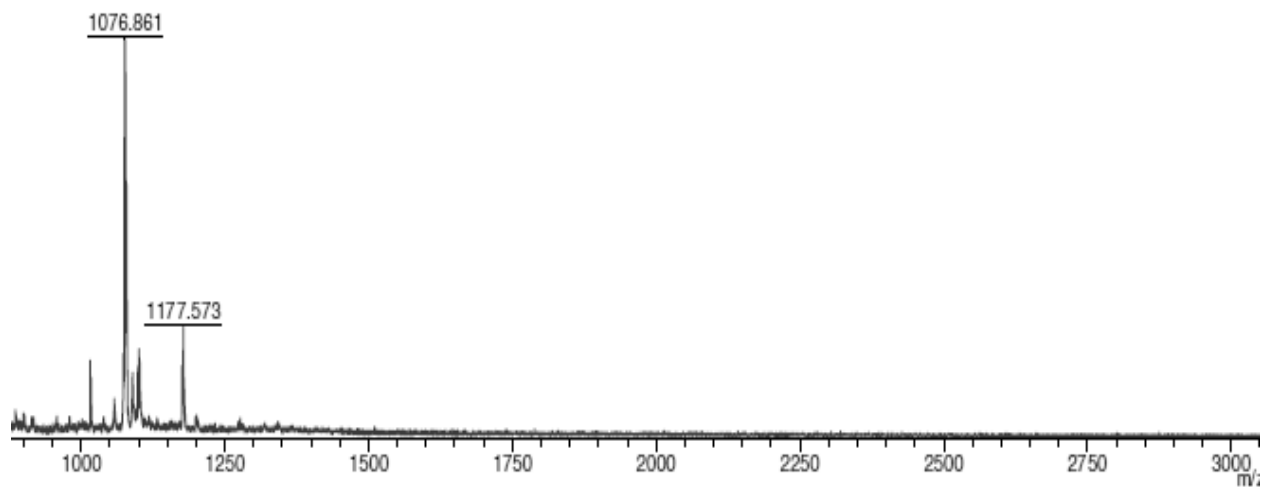
Figure A7. MALDI-TOF mass spectrum of CuTPP(PE)$_4$
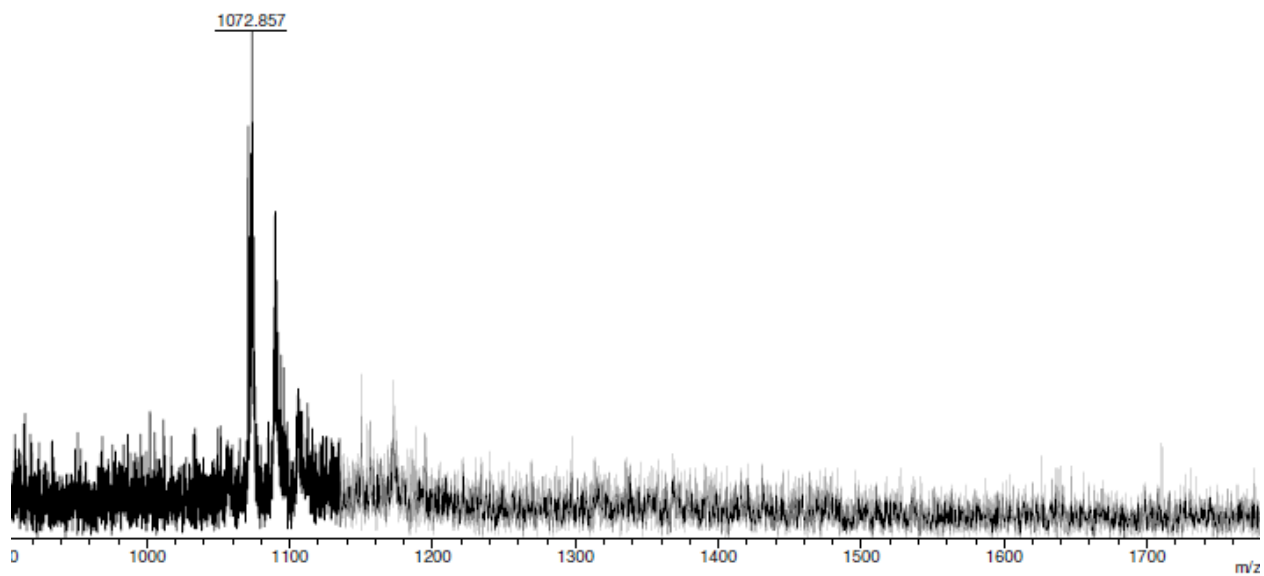
Figure A8. MALDI-TOF mass spectrum of NiTPP(PE)$_4$

249
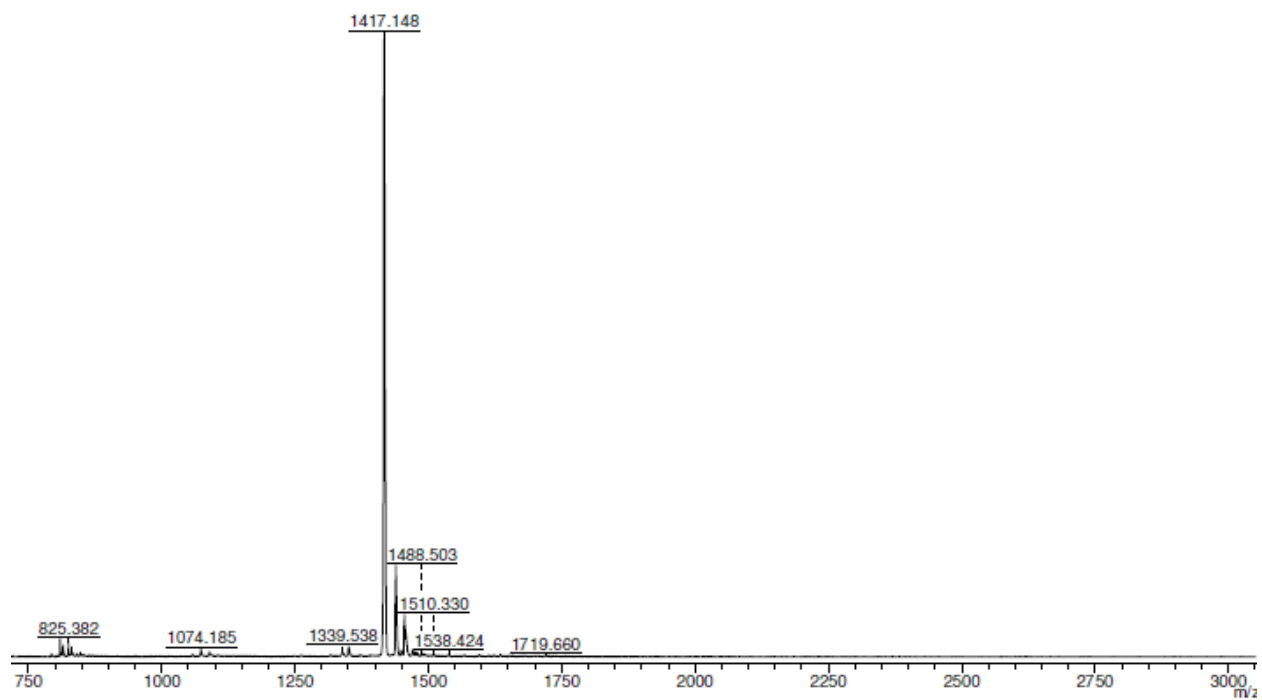
Figure A9. MALDI-TOF mass spectrum of $H_2TPP(PE)_8$
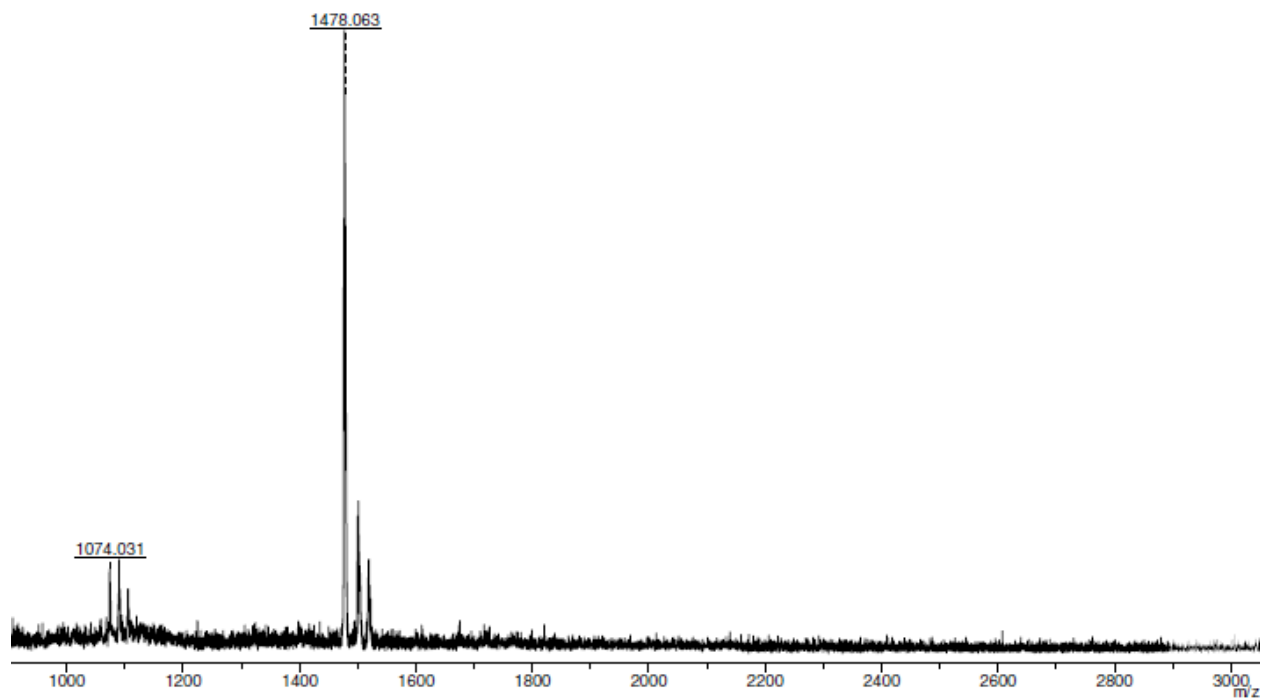
Figure A10. MALDI-TOF mass spectrum of $CuTPP(PE)_8$
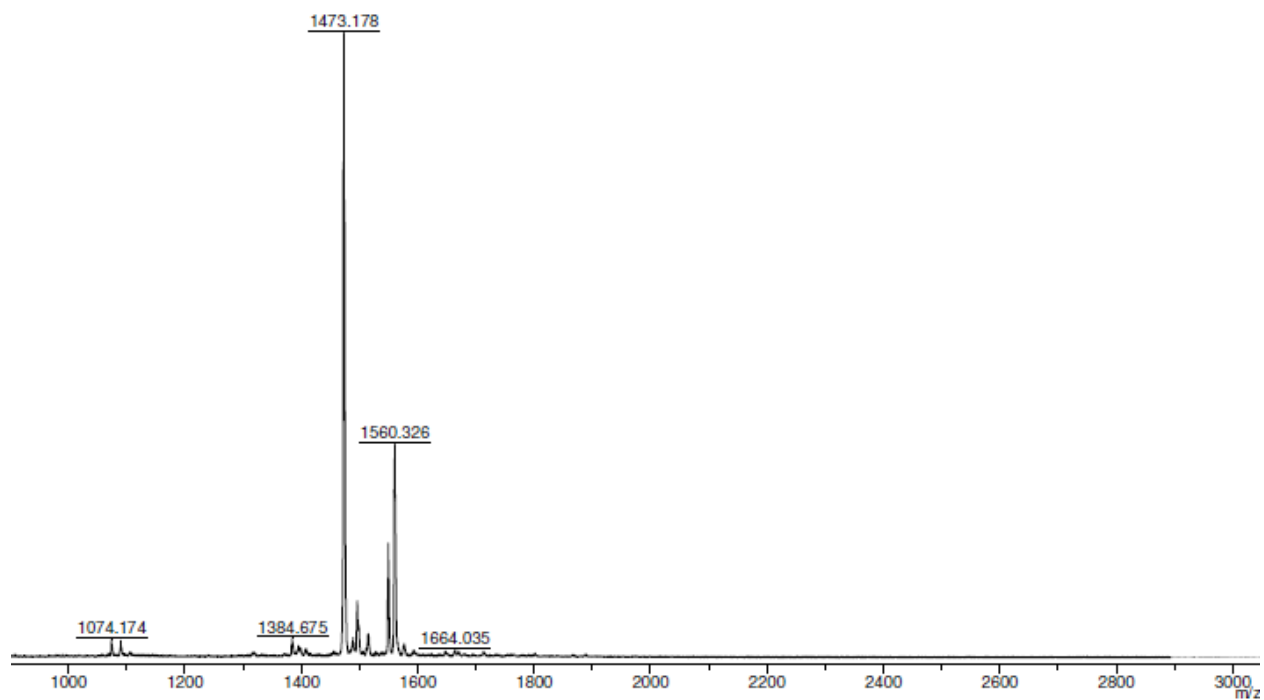
Figure A11. MALDI-TOF mass spectrum of CoTPP(PE)$_8$
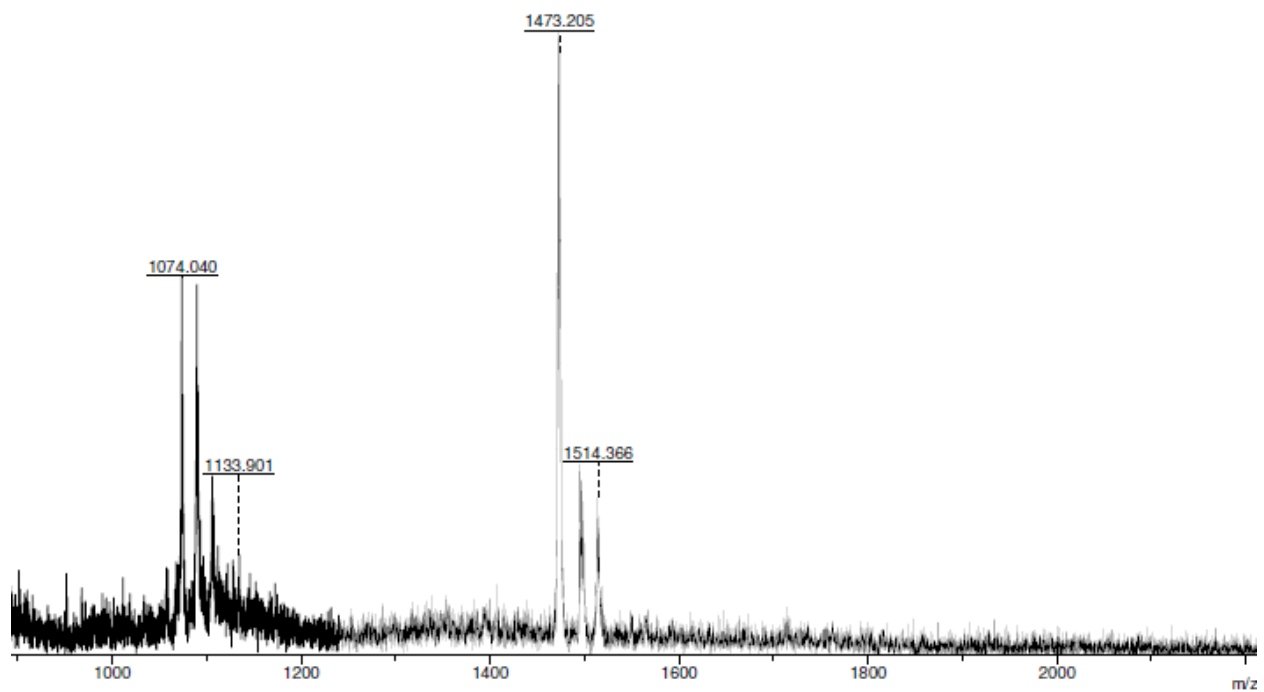
Figure A12. MALDI-TOF mass spectrum of NiTPP(PE)$_8$
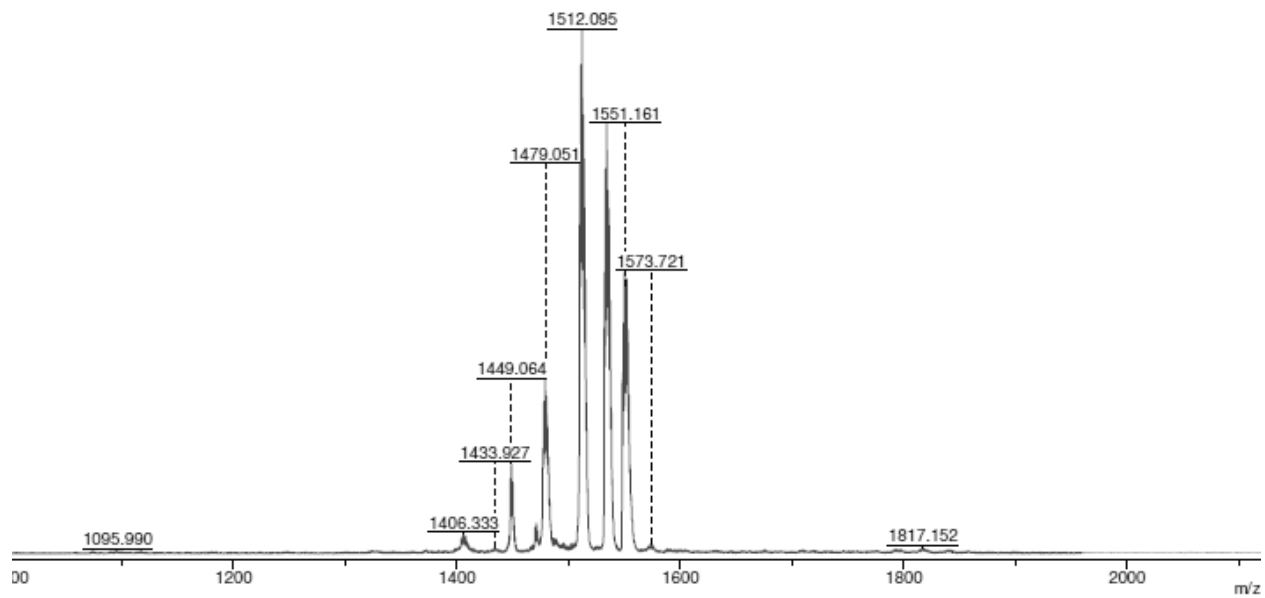
Figure A13. MALDI-TOF mass spectrum of ZnTPP(PE)$_8$.
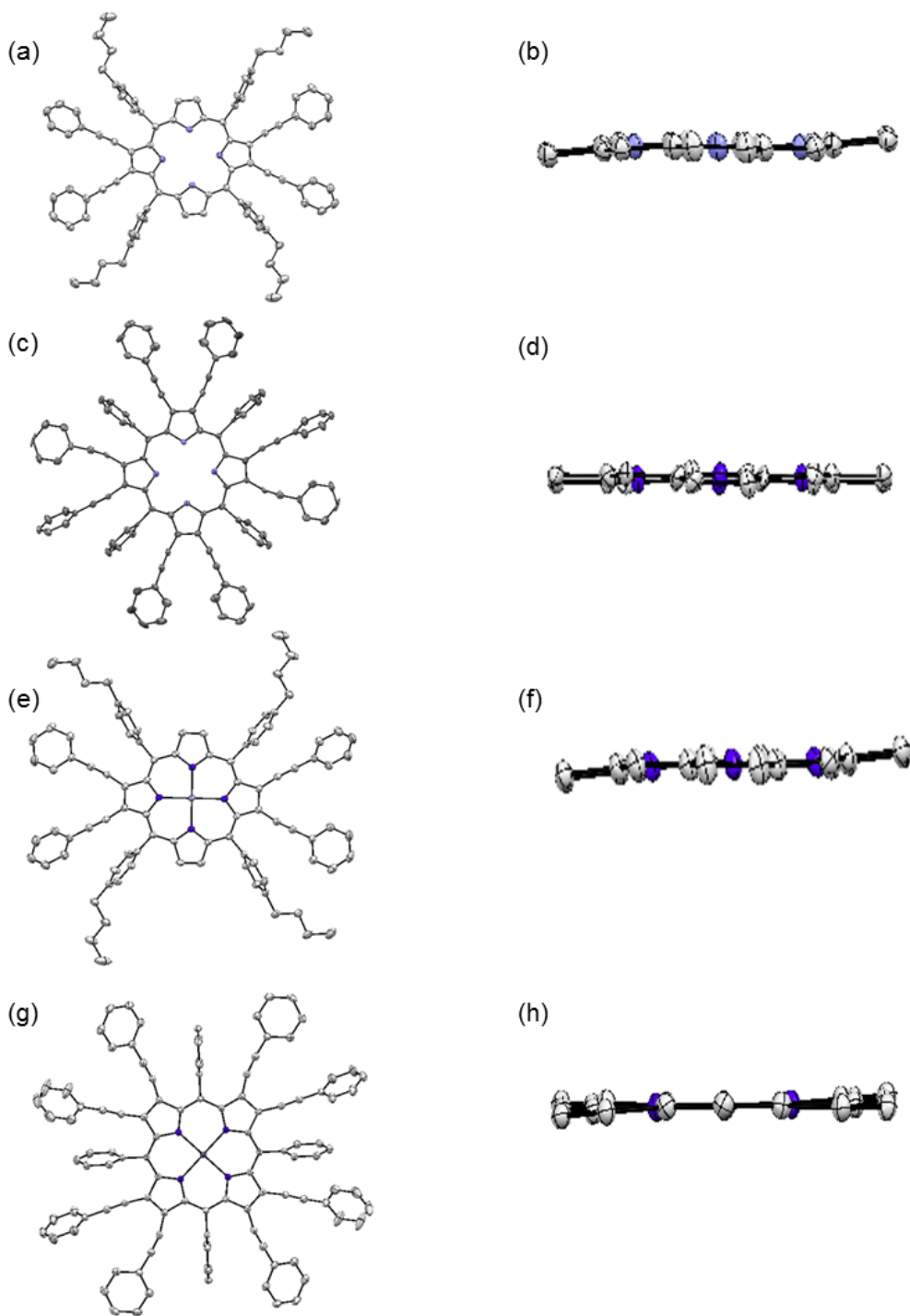
Figure A14. The ORTEP diagrams showing top and side views of $H_2T(4\text{-BuPh})P(PE)_4$ (a and b); $H_2TPP(PE)_8$ (c and d) ; $ZnTPP(PE)_4$ (e and f) and $ZnTPP(PE)_8$(g and h). The solvates are not shown for clarity, and in side view, the *β*-substituents and *meso*-phenyl groups are not shown for clarity. Crystal structures data for $H_2T(4\text{-BuPh})P(PE)_4$ is taken from P. Bhyrappa *et al.,Eur. J. Inorg. Chem.*, 2014, 5760-5770 and for $MTPP(PE)_8$ T. Chandra *et al.*, *Inorg. Chem.* 2003, **42**, 5158-5172.
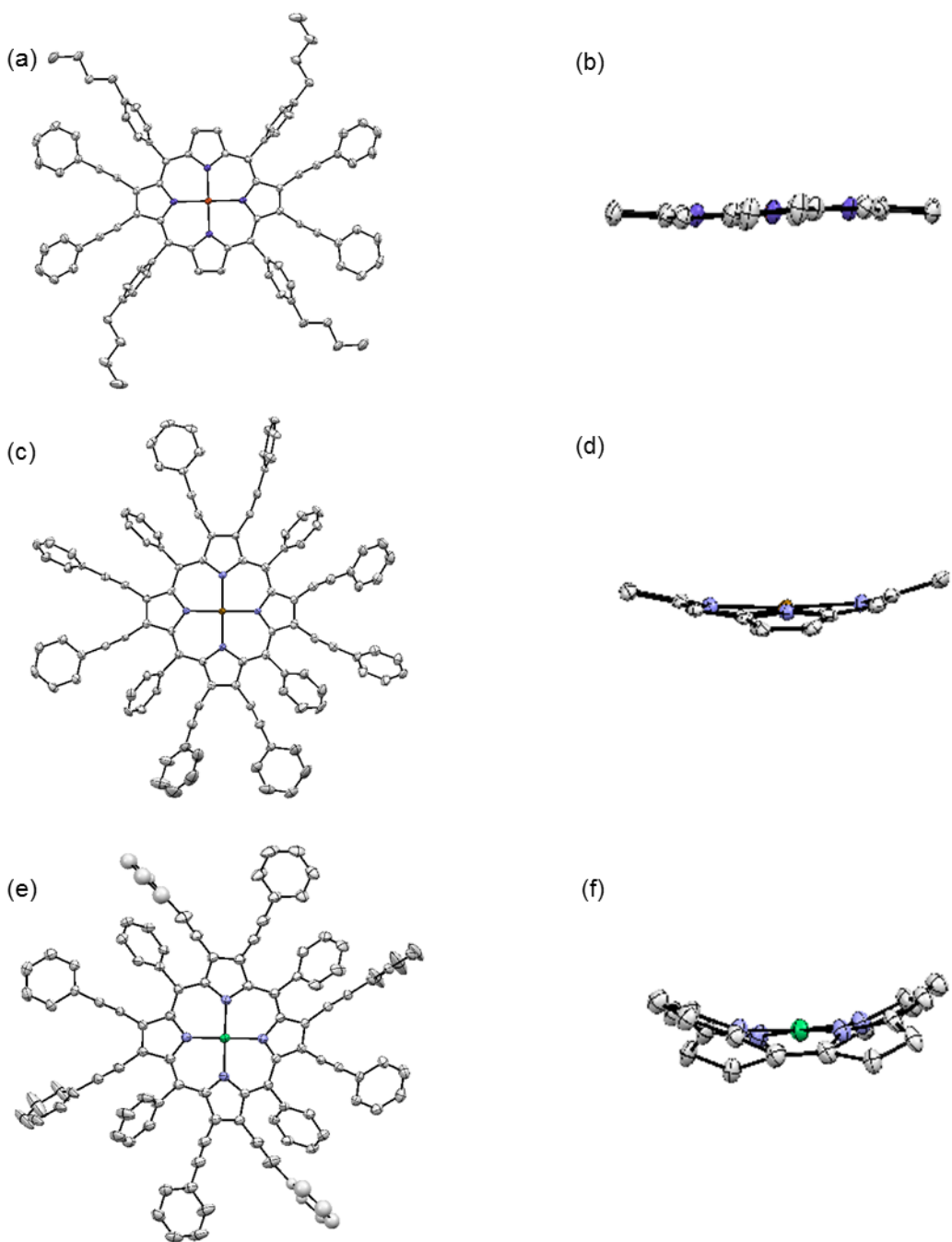
Figure A15. The ORTEP diagrams showing top and side views of CuT(4-BuPh)P(PE)$_4$ (a and b); CuTPP(PE)$_8$ (c and d) and NiTPP(PE)$_8$ (e and f). The solvates are not shown for clarity, and in side view, the *β*-substituents and *meso*-phenyl groups are not shown for clarity.Crystal structures data for H$_2$T(4-BuPh)P(PE)$_4$ is taken from P. Bhyrappa *et al.,Eur. J. Inorg. Chem.*, 2014, 5760-5770 and for MTPP(PE)$_8$ T. Chandra *et al*., *Inorg. Chem.* 2003, **42**, 5158-5172.

Table A1. Crystal structure data of β-phenylethynyl substituted porphyrins from literature.[a,b]

Porphyrin	ΔC_β	$\Delta 24$	ΔMetal	Remarks
$H_2T(4\text{-BuPh})P(PE)_4$[a]	0.058	0.086	-	Planar
$H_2TPP(PE)_8$[b]	0.094	0.068	-	Planar
$ZnT(4\text{-BuPh})P(PE)_4$[a]	0.051	0.042	0.00	Planar
$ZnTPP(PE)_8$[b]	0.040	0.032	0.00	Planar
$CuT(4\text{-BuPh})P(PE)_4$[a]	0.056	0.046	0.00	Planar
$CuTPP(PE)_8$[b]	0.578	0.287	0.008	Nonplanar
$NiTPP(PE)_8$[b]	0.700	0.470	0.011	Nonplanar

[a]Crystal structures data is taken from P. Bhyrappa, U. K. Sarangi, V. Velkannan and V. Ramkumar, *Eur. J. Inorg. Chem.*, 2014, 5760-5770; [b]Crystal structures data is taken fromT. Chandra, B. J. Kraft, J. C. Huffman, J. M. Zaleski, *Inorg. Chem.* 2003, **42**, 5158-5172.
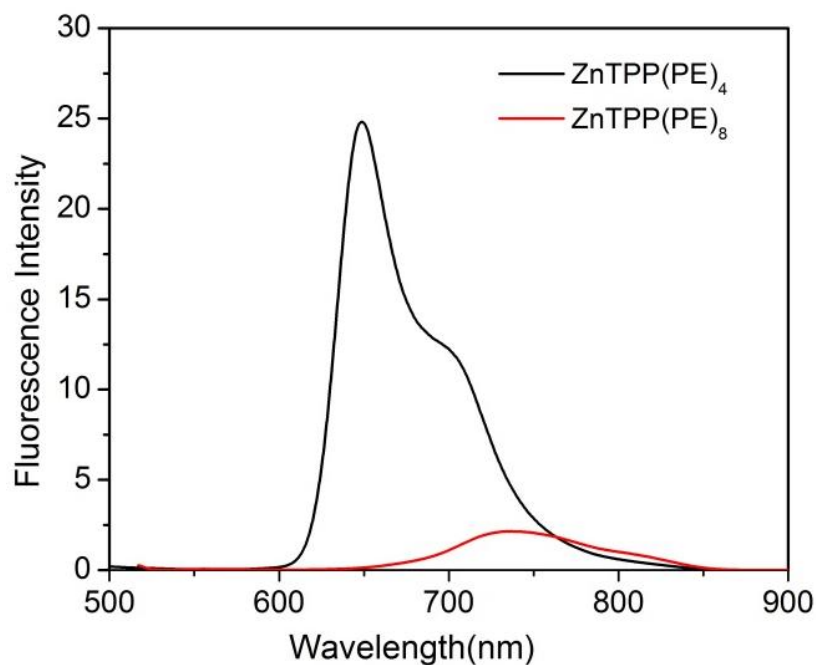
Figure A16. Fluorescence spectra of $ZnTPP(PE)_n$ (n = 4 and 8) in CH_2Cl_2 at 298 K.
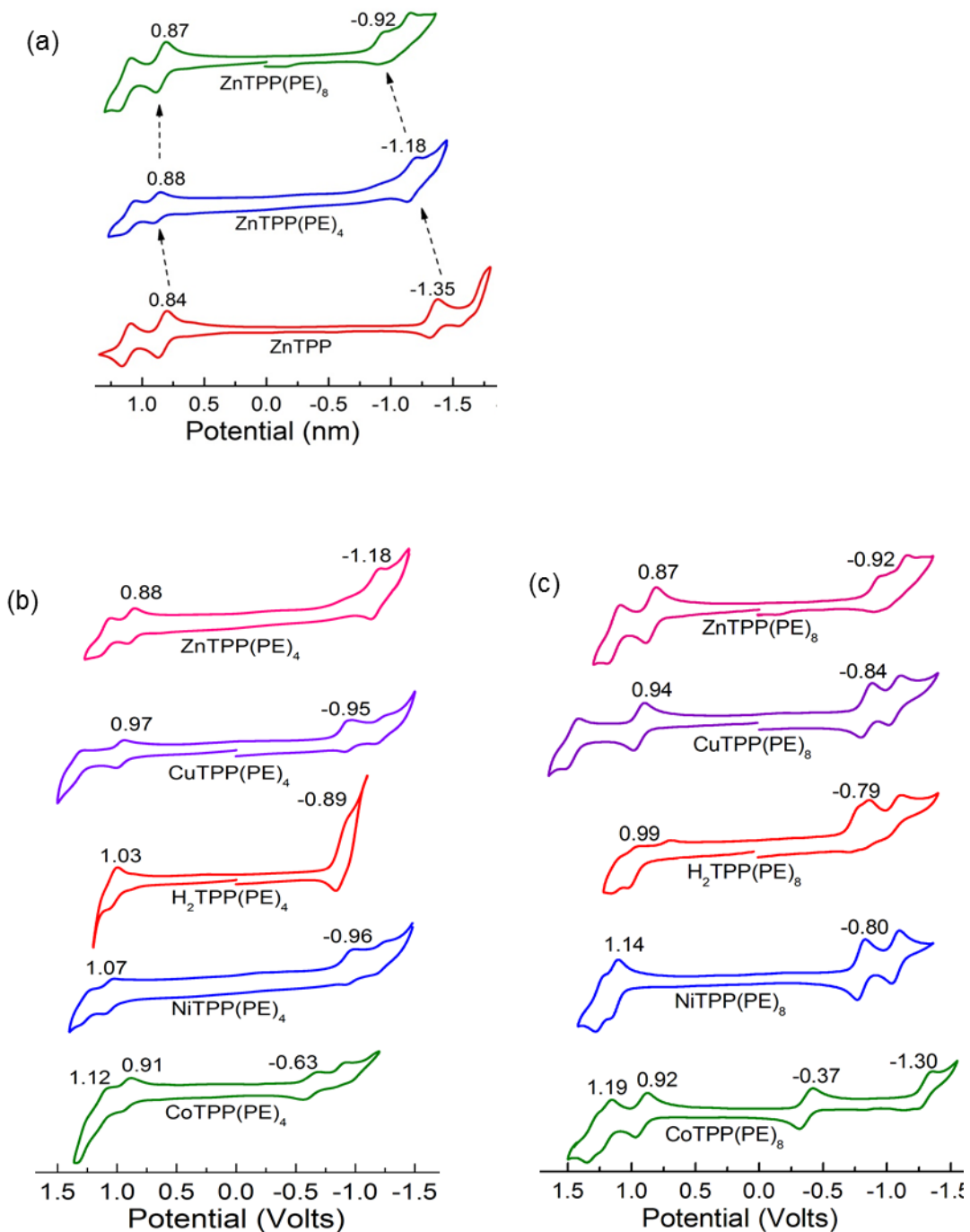
Figure A17. Cyclic Voltammograms of (a) ZnTPP(PE)$_n$ (n = 0, 4 and 8); (b) MTPP(PE)$_4$; (c) MTPP(PE)$_8$ where M = 2H, Co(II), Ni(II), Cu(II) and Zn(II); in CH$_2$Cl$_2$ containing 0.1 M TBAPF$_6$ using Ag/AgCl as reference electrode with a scan rate of 0.1 V/sat 298 K.

Table A2. Electrochemical redox data (*vs*Ag/AgCl)of CoTPP(PE)$_n$ (n = 0, 4 and 8) using 0.1 M TBAPF$_6$with a scan rate of 0.1 V/s at 298 K.

Porphyrin	Oxidation		Reduction		Metal Centered	
	I	II	I	II	Co $^{II/III}$	Co $^{II/I}$
CoTPP	1.06	1.32	-1.38	-	0.85	-0.86
CoTPP(PE)$_4$	1.12	-	-	-	0.91	-0.63
CoTPP(PE)$_8$	1.19	1.31	-1.30	-	0.92	-0.37
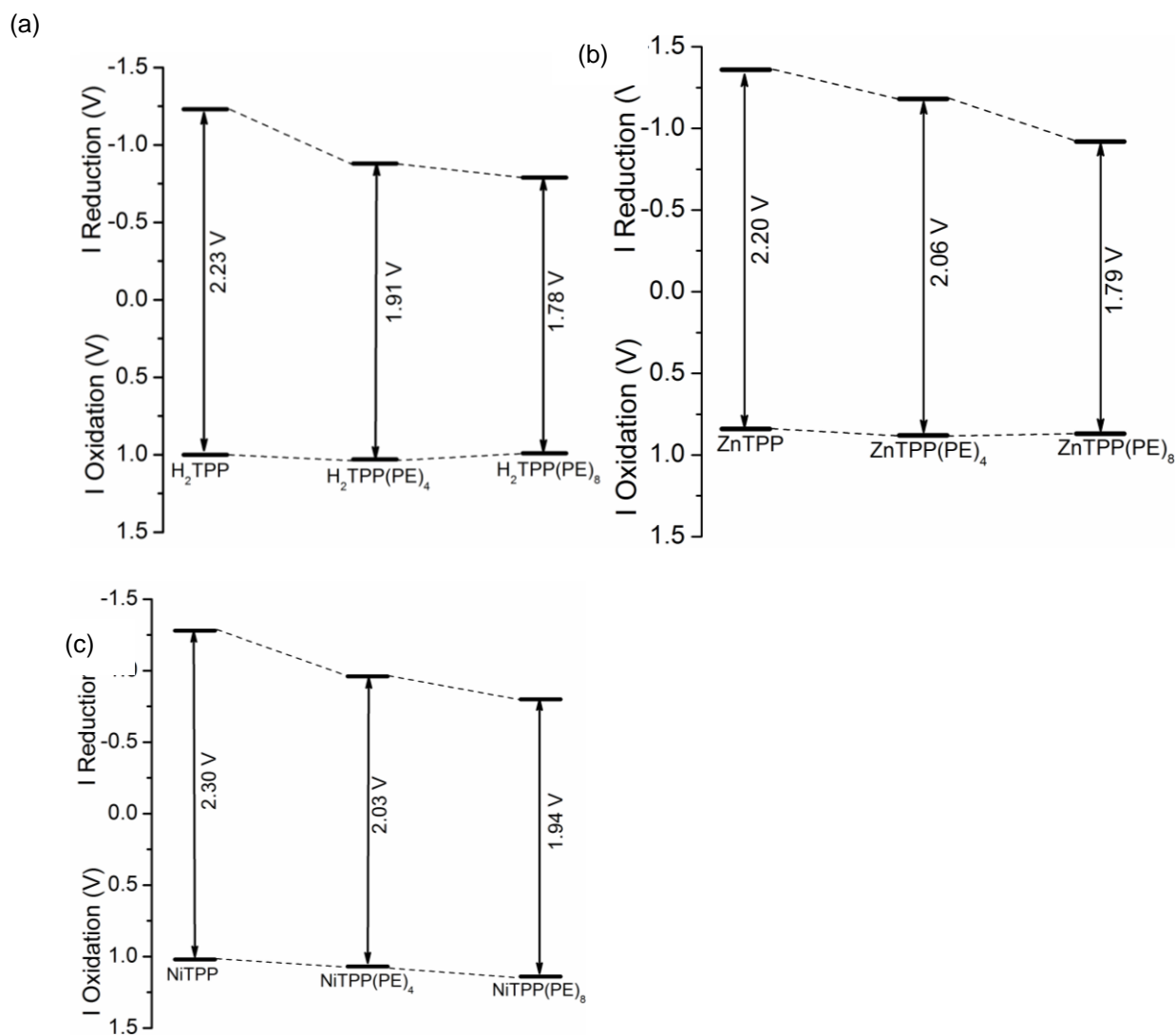
Figure A18. HOMO-LUMO gap variation in MTPP(PE)$_n$ (M = 2H, Zn(II) and Ni(II); n = 0, 4 and 8).
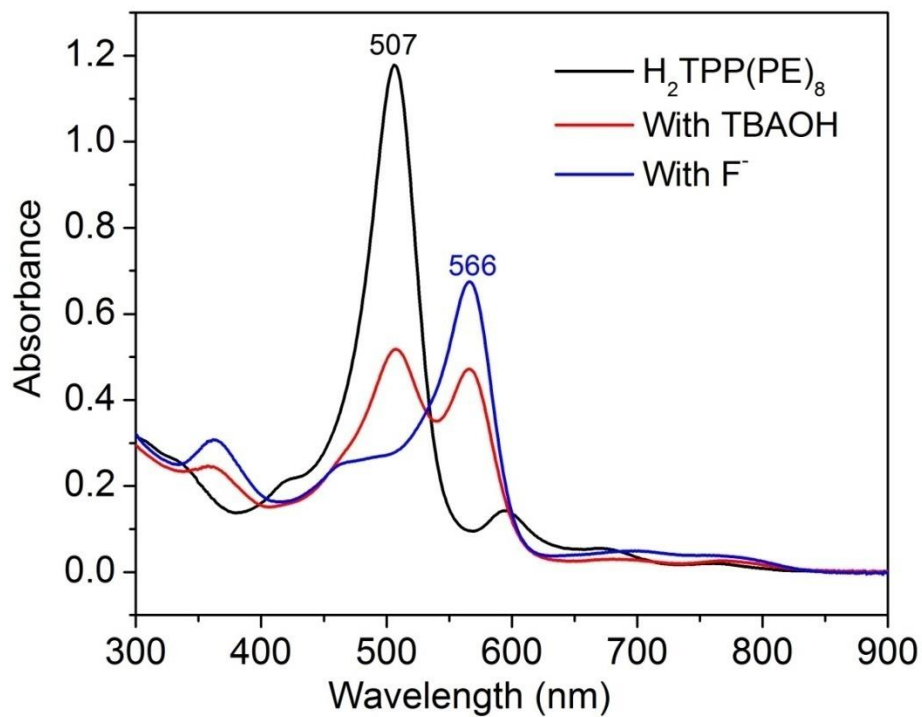
Figure A19. UV-Visible spectral changes of $H_2TPP(PE)_8$ upon addition of TBAOH and F^- ion in CH_2Cl_2 at 298 K.
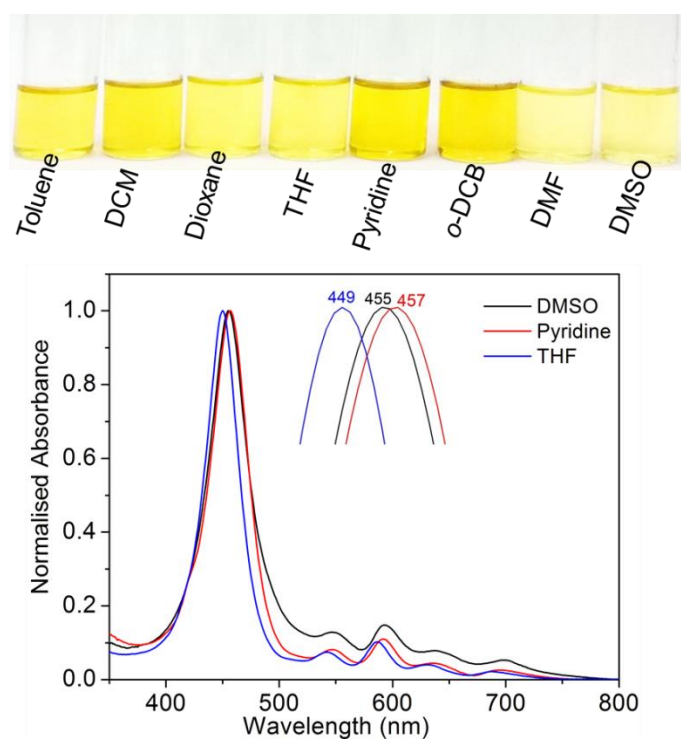

Figure A20. (top) $H_2TPP(PE)_4$ in different solvents; (bottom) UV-Visible and spectralshifts of $H_2TPP(PE)_4$ in selected solvents at 298 K.
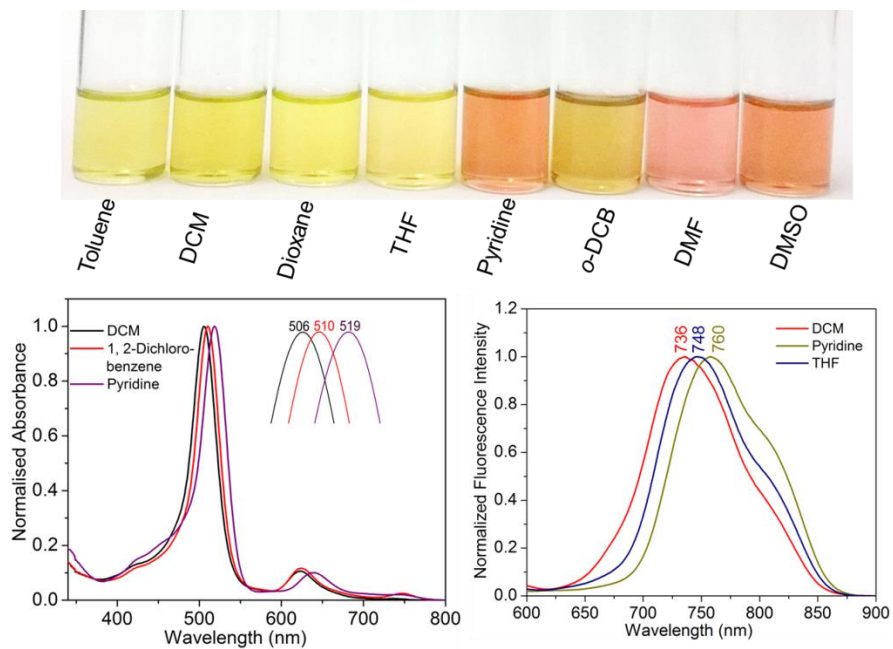
Figure A21. (top) Colorimetric response of ZnTPP(PE)$_8$ in different solvents; (bottom) UV-Visible and fluorescence spectra of ZnTPP(PE)$_8$ in different solvents at 298 K.

Table A3. Optical absorption spectral data of $H_2TPP(PE)_4$, $ZnTPP(PE)_4$ and $ZnTPP(PE)_8$ in different solvents at 298 K.

Solvent	B band, nm	Q band(s), nm	Emission, nm
$H_2TPP(PE)_4$			
Toluene	454(5.05)	544(3.93), 588(4.09), 633(3.67), 691(3.40)	729
DCM	453(5.57)	545(4.44),590(4.58), 633(4.20), 691(3.96)	739
1,4-Dioxane	452(5.07)	544(3.95), 588(4.09), 633(3.70), 690(3.47)	747
THF	450(4.92)	543(3.79), 587(3.93), 631(3.53), 689(3.26)	734
Pyridine	457(4.99)	547(3.90), 592(4.04), 637(3.64), 693(3.40)	745
o-Dichlorobenzene	458(5.02)	546(3.96), 592(4.12), 637(3.73), 694(3.48)	732
DMF	453(4.99)	545(3.98), 589(4.09), 632(3.81), 688(3.68)	793
DMSO	455(4.83)	548(3.93), 593(3.99), 639(3.72), 699(3.55)	703, 787
$ZnTPP(PE)_4$			
Toluene	463(5.37)	583(4.16), 631(4.63)	643
DCM	458(5.48)	581(4.26), 630(4.68)	644
1,4-Dioxane	466(5.41)	589(4.20), 635(4.61)	651
THF	465(5.47)	589(4.25), 636(4.67)	652, 709
Pyridine	476(5.36)	598(4.15), 645(4.56)	671, 716
o-Dichlorobenzene	464(5.30)	584(4.03), 633(4.56)	645
DMF	470(5.54)	593(4.33), 641(4.73)	663, 715
DMSO	473(5.52)	595(4.27), 642(4.71)	664, 715
$ZnTPP(PE)_8$			
Toluene	508(5.53)	624(4.58)	736
DCM	506(5.52)	623(4.54)	736
1,4-Dioxane	506(5.41)	625(4.44), 739(3.84)	743
THF	508(5.44)	628)(4.45), 740(3.77)	748
Pyridine	519(5.35)	639(4.34), 745(3.66)	759
o-Dichlorobenzene	510(5.34)	624(4.41), 747(3.73)	740
DMF	519(5.39)	641(4.37)	762
DMSO	517(5.39)	637(4.39)	761

Values in parentheses refers to $\log\varepsilon$ (ε in Mol^{-1} cm^{-1}).

Table A4. Fluorescence quantum yield and lifetime data of $H_2TPP(PE)_8$ and $ZnTPP(PE)_8$ in different solvents at 298 K.

| Porphyrin	Solvent	$\lambda_{em, nm}$	Stokes shift (cm^{-1})	Φ_f	τ (ns)	χ^2
$H_2TPP(PE)_8$	Toluene	810	829.55	3.6×10^{-3}	1.63	1.12
	DCM	814	838.35	5.2×10^{-3}	1.44	0.84
	1,4-Dioxane	820	911.04	2.7×10^{-3}	1.47	1.09
	THF	823	1007.23	1.9×10^{-3}	1.45	1.12
	Pyridine	826	965.36	2.4×10^{-3}	0.23(27.54%) 1.31(67.46%) 5.58(5.0%)	1.01
	o-DCB	809	796.95	3.5×10^{-3}	1.59	1.07
	DMF	765	1677.37	1.6×10^{-3}	0.66(73.15%) 2.26(26.85%)	1.12
	DMSO	839	2552.83	0.43×10^{-3}	1.13(64.49%) 2.96(5.97%) 0.17(29.54%)	1.09
$ZnTPP(PE)_8$	Toluene	736	2,438.68	2.2×10^{-3}	1.24	1.18
	DCM	736	2,464.41	2.4×10^{-3}	0.97	1.01
	1,4-Dioxane	743	72.84	3.1×10^{-3}	1.40	1.31
	THF	748	144.53	2.8×10^{-3}	1.01	1.19
	Pyridine	759	247.59	4.3×10^{-3}	0.77(39.70%) 1.57(60.30%)	0.99
	o-DCB	740	-126.63	2.3×10^{-3}	1.39	1.27
	DMF	762	2,477.26	3.7×10^{-3}	0.75(43.55%) 1.73(56.45%)	0.96
	DMSO	761	2,557.98	3.6×10^{-3}	0.39(24.44%) 1.45(75.56%)	0.98
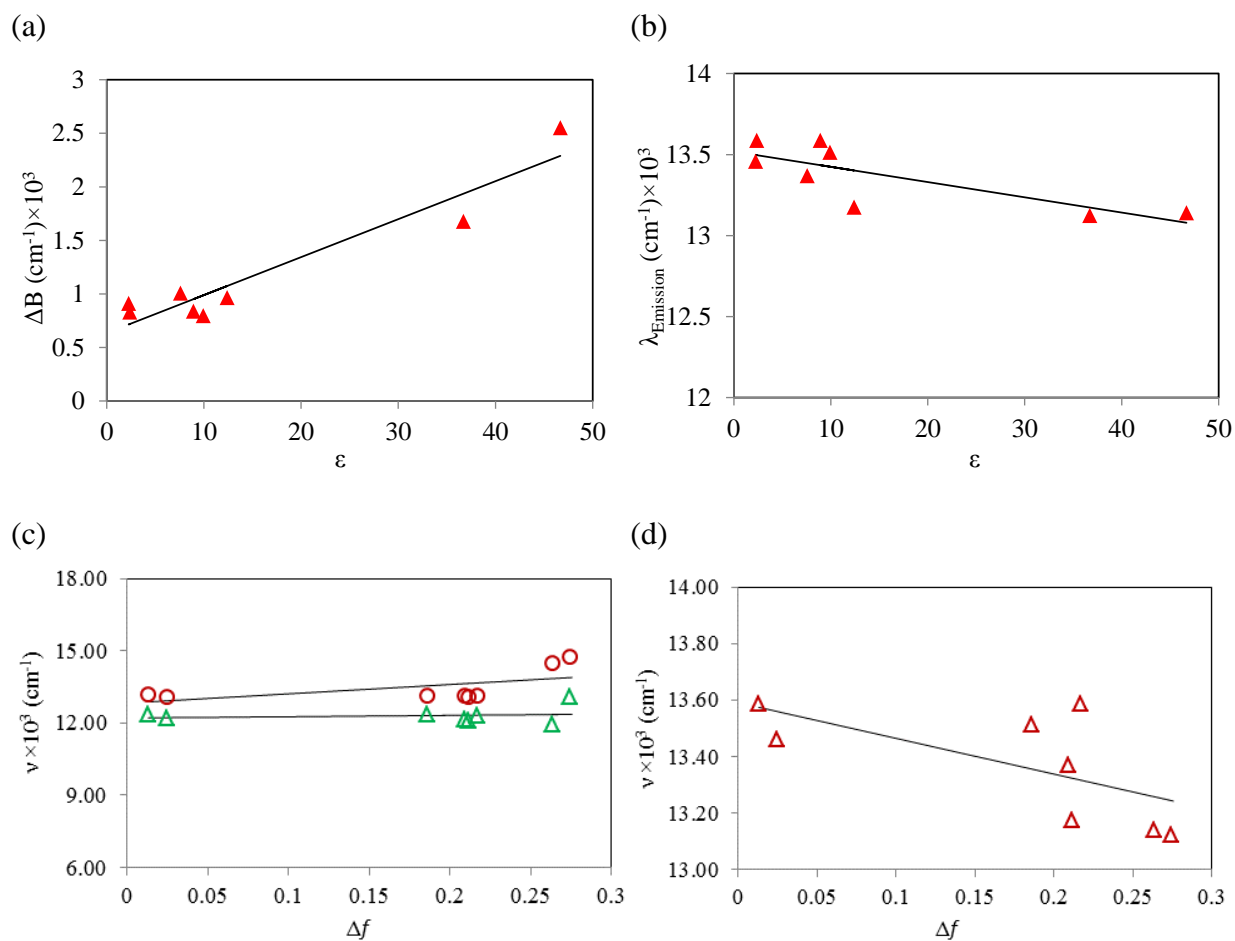
Figure   A22. (a) Stokes shift of $H_2TPP(PE)_8$ in different solvents *vs*. dielectric constant of various solvents ; (b) Emisssion wavelength (cm^{-1}) of $ZnTPP(PE)_8$ *vs*. dielectric constant of different solvent; (c) Lippert-Mataga plot showing Stokes shift as a function of solvent orientation polarisability (Δf) for $H_2TPP(PE)_8$; (d) Lippert-Mataga plot showing emisssion wavelength (cm^{-1}) as a function of solvent orientation polarisability (Δf) for $ZnTPP(PE)_8$.
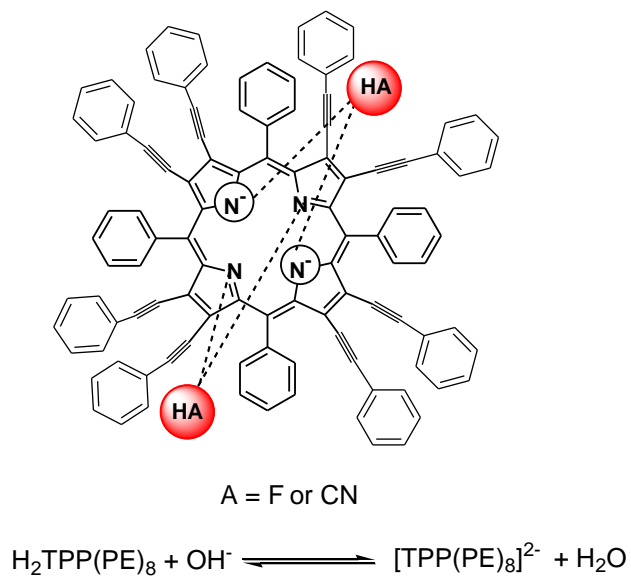
(a)

(b)

A = F or CN

$$H_2TPP(PE)_8 + OH^- \rightleftharpoons [TPP(PE)_8]^{2-} + H_2O$$
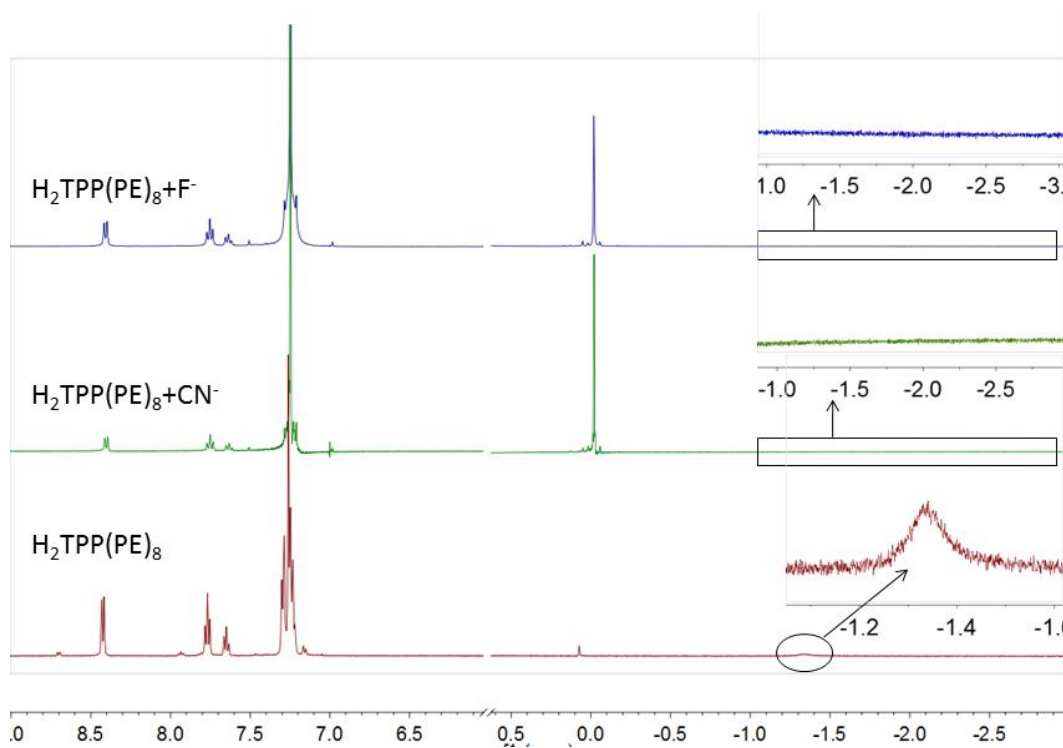
Figure A23. (a) ^{1}H NMR spectral changes of $H_2TPP(PE)_8$ upon addition of CN$^-$ (green) and F$^-$ ions (blue) in CDCl$_3$ at 298 K; (b) Proposed schematic representation of dianionic species with HA (A = F or CN) and H$_2$O.
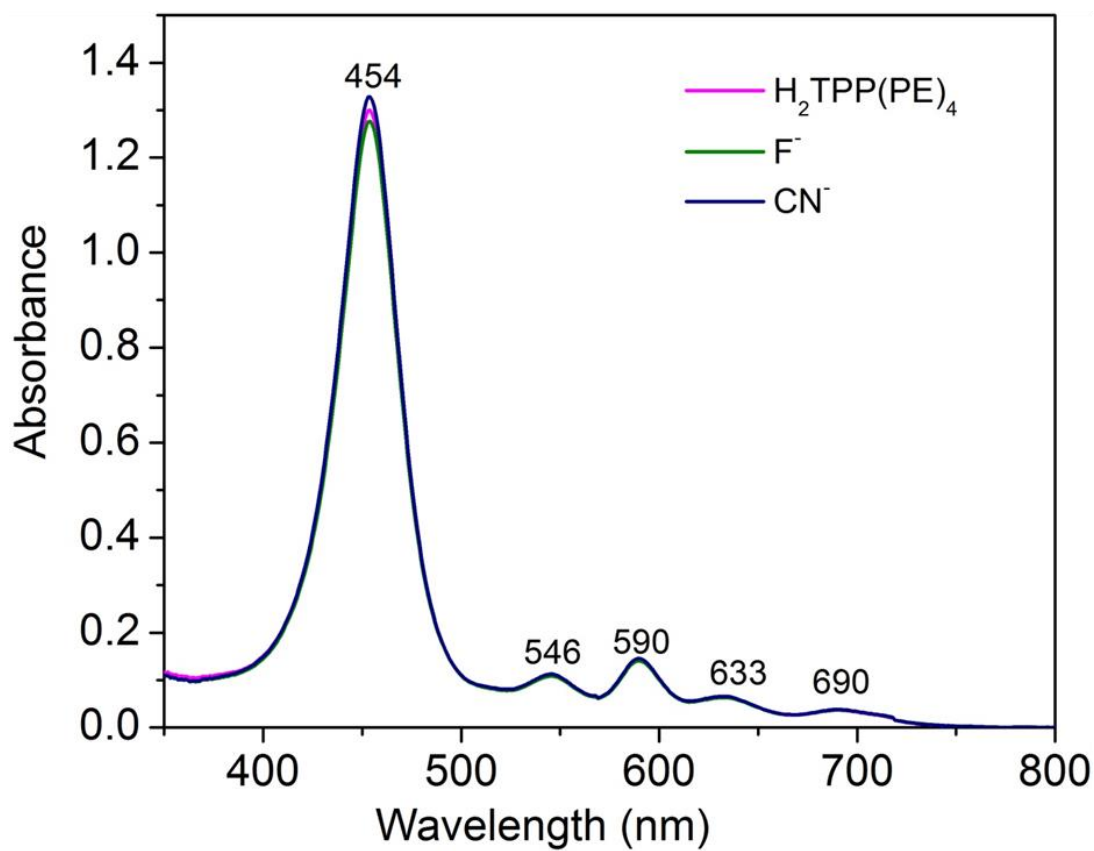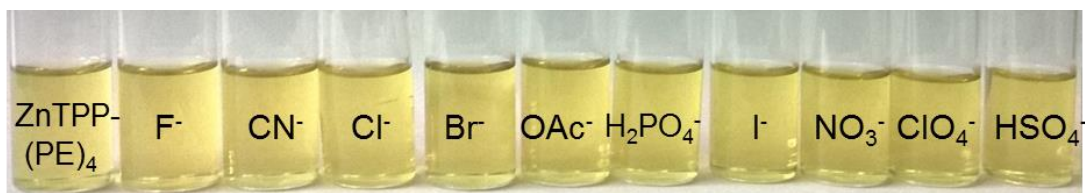
Figure A24. (top) ZnTPP(PE)$_4$ in presence of different anions in CH$_2$Cl$_2$ at 298 K; (bottom) UV-Visible of ZnTPP(PE)$_4$ in presence of F$^-$ and CN$^-$ ions in CH$_2$Cl$_2$ at 298 K.

Table A5. Optical absorption data of spectral data of $H_2TPP(PE)_8$ and $ZnTPP(PE)_4$ in presence of different anions in CH_2Cl_2 at 298 K.

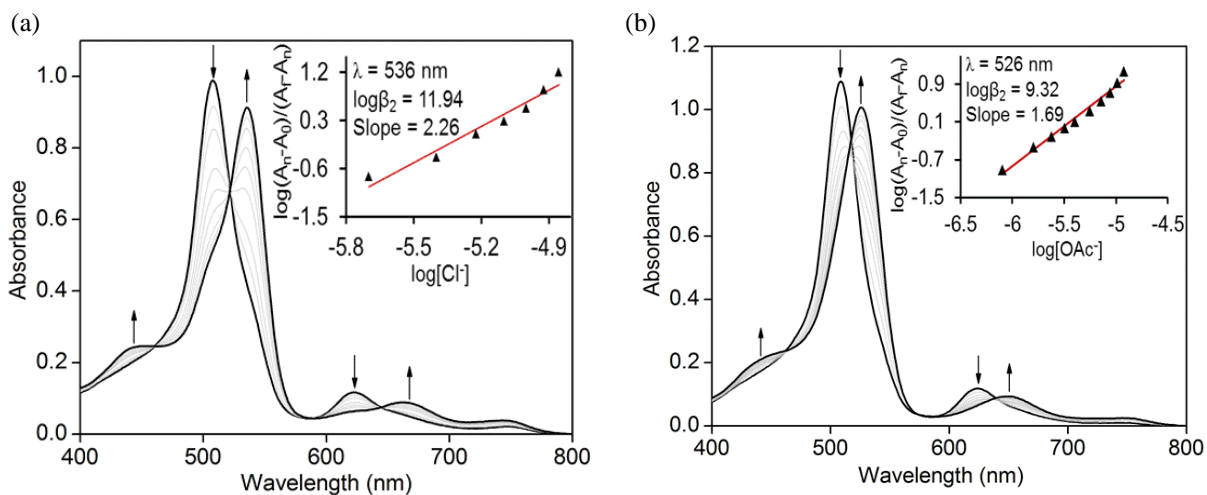|		
$H_2TPP(PE)_8$	507(5.41)	595(4.48), 672(3.96), 762(3.44)
F⁻	566(5.29	688(4.15) , 772(3.98)
CN⁻	566(5.04)	684(4.01), 770(3.87)
$ZnTPP(PE)_4$	458(5.48)	581(4.26), 630(4.68)
F⁻	480(5.47)	602(4.15), 652(4.62)
CN⁻	487(5.44)	660(4.46)
CH_3COO^-	464(5.24), 479(5.33)	651(4.46)
$H_2PO_4^-$	462(5.33)	633(4.43)
Cl⁻	483(5.39)	654(4.49)

Figure A25. UV-Visible titration of $ZnTPP(PE)_8$ with (a) Cl⁻ and (b) OAc⁻ ions in toluene at 298 K. Inset shows corresponding Hill plots.

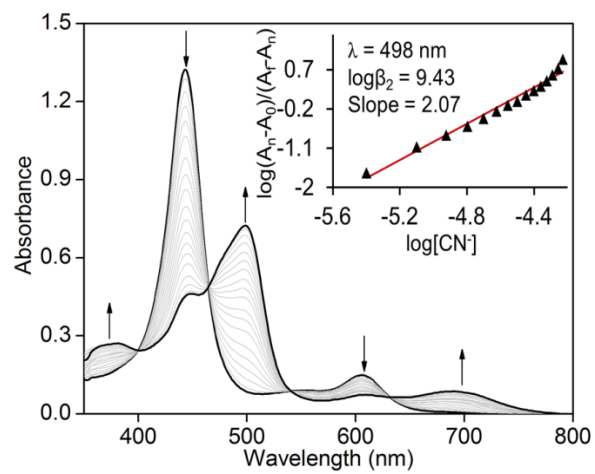**Figure A26.**UV-Visible titration of ZnTPP(PE)$_4$with CN$^-$ ion in toluene at 298 K. Inset shows Hill Plot.